GEOMAR REPORT

GEOMAR

Helmholtz-Zentrum für Ozeanforschung Kiel

The SUGAR Toolbox

A library of numerical algorithms and data
for modelling of gas hydrate systems
and marine environments

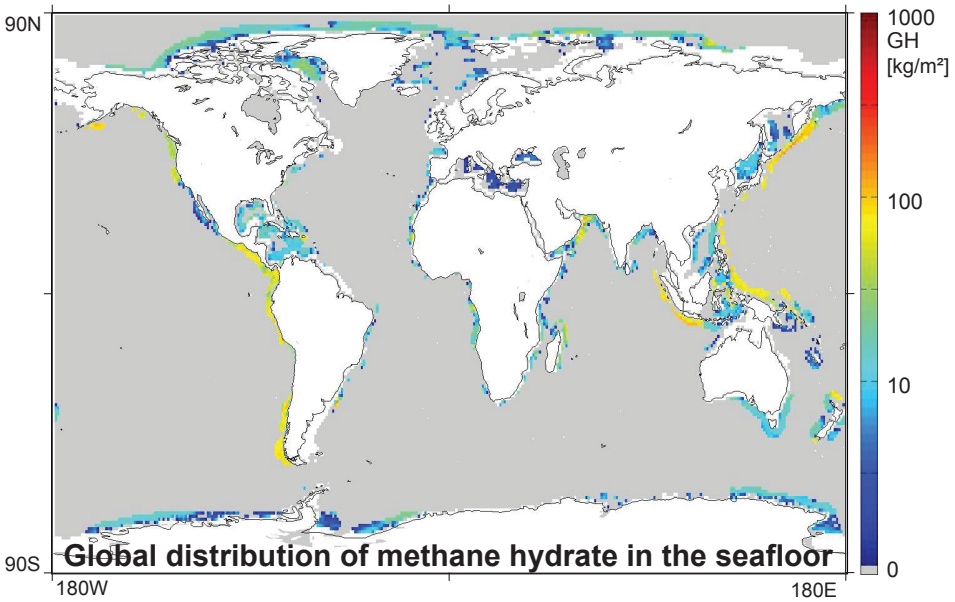

Global distribution of methane hydrate in the seafloor

Berichte aus dem GEOMAR
Helmholtz-Zentrum für Ozeanforschung Kiel

Nr. 8 (N. Ser.)

Juli 2013

GEOMAR

Helmholtz-Zentrum für Ozeanforschung Kiel

The SUGAR Toolbox

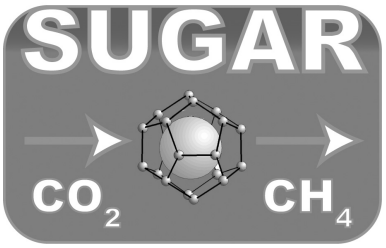

A library of numerical algorithms and data
for modelling of gas hydrate systems
and marine environments

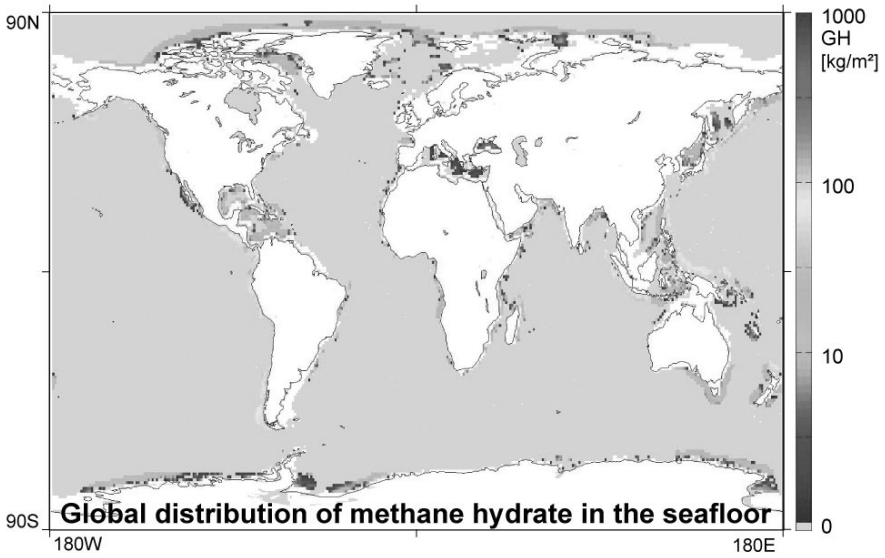

Berichte aus dem GEOMAR
Helmholtz-Zentrum für Ozeanforschung Kiel

Nr. 8 (N. Ser.)

Juli 2013

ISSN Nr.: 2193-8113

GEOMAR
Helmholtz-Zentrum für Ozeanforschung Kiel

Das GEOMAR Helmholtz-Zentrum für Ozeanforschung Kiel ist Mitglied der Helmholtz-Gemeinschaft Deutscher Forschungszentren e.V.

The GEOMAR Helmholtz Centre for Ocean Research Kiel is a member of the Helmholtz Association of German Research Centres

Herausgeber / Editor:
Elke Kossel, Nikolaus Bigalke, Elena Piñero, Matthias Haeckel

GEOMAR Report
ISSN Nr.: 2193-8113, DOI 10.3289/GEOMAR_REP_NS_8_2013

Helmholtz-Zentrum für Ozeanforschung Kiel / Helmholtz Centre for Ocean Research Kiel
GEOMAR
Dienstgebäude Westufer / West Shore Building
Düsternbrooker Weg 20
D-24105 Kiel
Germany

Helmholtz-Zentrum für Ozeanforschung Kiel / Helmholtz Centre for Ocean Research Kiel
GEOMAR
Dienstgebäude Ostufer / East Shore Building
Wischhofstr. 1-3
D-24148 Kiel
Germany

Tel.: +49 431 600-0
Fax: +49 431 600-2805
www.geomar.de

1. Introduction

The SUGAR Toolbox contains scripts for calculating various thermodynamic, kinetic, and geologic properties of substances occurring in the marine environment, particularly gas hydrate and seep systems. The algorithms have been programmed over the past fifteen years and have been updated, corrected and harmonized in the course of the German gas hydrate intiative SUGAR (2008-2014).

The scripts are coded as functions in the MATLAB environment and require the basic version as well as the “Optimization Toolbox”. From the latter the function ‘fsolve’ is used in several scripts. ‘fsolve’ can be replaced by ‘fzero’, if necessary, but this may lead to poor or no performance.

The scripts return ‘NaN’ output values for provided input values outside of the validity range of the respective underlying algorithm. A warning is issued as well. This check may be removed by the user at his/her own risk.

The scripts were checked against values reported in the cited references as much as possible, but no guarantee is given for correctness. If you, the user, find severe errors, we, the authors, would be grateful, if you would report them to us by sending an email to “mhaeckel@geomar.de”.

In addition to brief descriptions of the toolbox scripts and some notes on the underlying basic theory, this document also contains tables of property values where no algorithm for programming could be found. All of this is by no means a compendium covering the topics or provides a complete reference list, but, hopefully, assists in getting started in the fascinating world of marine biogeochemical modelling.

The SUGAR Toolbox can be downloaded from the PANGEA world database at “http://doi.pangaea.de/10.1594/PANGAEA.816333”.

Kiel, July 2013

Acknowledgements

Funding for this work was primarily provided through the SUGAR project by the German Federal Ministries of Economy (BMWi; grant nos. 03SX250 + 03SX320A) and Education & Research (BMBF; grant nos. 03G0687A + 03G0819A).

2. Thermodynamic properties

2.1. Phase diagrams of seawater and the binary systems CH_4–H_2O and CO_2–H_2O

The most commonly used model to predict gas hydrate equilibrium pressures and temperatures was developed by van der Waals and Platteeuw (1959) and extended by Parrish and Prausnitz (1972) to account for mixed gas hydrates. It is based on the equality of the chemical potential of water molecules in gas hydrate and in liquid water at equilibrium:

$$\Delta\mu_{\mathrm{W}}^{\mathrm{h}} = \Delta\mu_{\mathrm{W}}^{\mathrm{l}} \qquad \text{(Eq.2.1.1)}$$

where $\Delta\mu_{\mathrm{W}}^{\mathrm{h}}$ is the difference in chemical potential between water in the hypothetical empty gas hydrate lattice and in the real gas hydrate lattice filled with guest molecules, whereas $\Delta\mu_{\mathrm{W}}^{\mathrm{l}}$ is the difference in chemical potential between water in the hypothetical empty gas hydrate lattice and water in the liquid phase. At temperatures below the freezing point of water, the chemical potential difference to water in ice has to be taken instead.

$\Delta\mu_{\mathrm{W}}^{\mathrm{h}}$ can be calculated from:

$$\Delta\mu_{\mathrm{W}}^{\mathrm{h}} = -\mathrm{R}T\sum_{\mathrm{m}} v_{\mathrm{m}} \ln\left(1-\sum_{\mathrm{j}}\Theta_{\mathrm{m,j}}\right) \qquad \text{(Eq.2.1.2)}$$

where R is the gas constant, T is the temperature in Kelvin, m is the type of gas hydrate cage (large or small), v_{m} is the number of cages of type m per water molecule in the gas hydrate lattice, j is the type of guest molecule and $\Theta_{\mathrm{m,j}}$ is the cage occupancy of molecule j in cages of type m. For structure-I hydrate, v_{large} and v_{small} equal 6/46 and 2/46, respectively. The cage occupancy is given by a Langmuir adsorption relation:

$$\Theta_{\mathrm{m,j}} = \frac{\mathrm{C}_{\mathrm{mj}} f_{\mathrm{j}}}{1+\sum_{\mathrm{l}} \mathrm{C}_{\mathrm{ml}} f_{\mathrm{l}}} \qquad \text{(Eq.2.1.3)}$$

where f_{j} is the fugacity of the guest molecule j and the sum in the denominator is running over all types of guest molecules present in the hydrate lattice. The Langmuir constant C_{ml} is obtained by integrating the interaction potential between the guest molecule and the water in the hydrate lattice. In most publications, a Kihara-type cell potential is assumed and the integration space is confined to one lattice cell. An exception is the work of Duan and Sun (2005; 2006), who derive the Langmuir constants from *ab initio* intermolecular potentials. The calculated Langmuir constants depend on the parameters that are used for the Kihara potential, the distances

between the interacting molecules in the hydrate lattice and the size of the integration space which differ in publications from different research groups.

The difference in chemical potential between the empty hydrate lattice and water in the liquid phase is derived from:

$$\frac{\Delta\mu_{\mathrm{W}}^{\mathrm{l}}}{\mathrm{R}T} = \frac{\Delta\mu_{\mathrm{W}}^{\mathrm{l}_0}}{\mathrm{R}T_0} - \int_{T_0}^{T} \frac{\Delta H_{\mathrm{W_m}}^{\mathrm{l}}}{\mathrm{R}T^2} dT + \int_{p_0}^{p} \frac{\Delta V_{\mathrm{W}}^{\mathrm{l}}}{\mathrm{R}T} dp - \ln(a_{\mathrm{w}}) \qquad \text{(Eq.2.1.4)}$$

where $\Delta\mu_{\mathrm{W}}^{\mathrm{l}_0}$ is the chemical potential difference at reference pressure p_0 and reference temperature T_0, usually taken to be 0 MPa and 273.15 K, and a_{w} is the activity of water. The second term on the right hand side gives the temperature dependence at constant pressure, while the third term corrects for pressure effects. The expressions $\Delta H_{\mathrm{W_m}}^{\mathrm{l}}$ and $\Delta V_{\mathrm{W}}^{\mathrm{l}}$ are the molar enthalpy difference and the change in the partial molar volume of water between an empty gas hydrate and liquid phase, respectively.

In order to calculate the activity of water, interactions of water molecules with dissolved ions and molecules have to be taken into account. The Pitzer (1973) formalism is widely considered to be the standard model for calculating activities in seawater. According to this model, the activity coefficient γ_{i} for species i is calculated from

$$\ln\gamma_{\mathrm{i}} = \mathrm{DH} + \sum_{\mathrm{ij}} m_{\mathrm{i}} m_{\mathrm{j}} \mathrm{B}_{\mathrm{ij}}^{\gamma} + \sum_{\mathrm{ijk}} m_{\mathrm{i}} m_{\mathrm{j}} m_{\mathrm{k}} \mathrm{C}_{\mathrm{ijk}}^{\gamma} \,. \qquad \text{(Eq.2.1.5)}$$

DH is a Debye-Hückel limiting law, $\mathrm{B}_{\mathrm{ij}}^{\gamma}$ are interaction parameters for the binary interactions of species i and j, $\mathrm{C}_{\mathrm{ijk}}^{\gamma}$ are interaction parameters for the ternary interactions of species i, j and k and m is the concentration of the species in terms of molality. The activity coefficient is related to the activity by

$$a_{\mathrm{w}} = \gamma_{\mathrm{w}} m_{\mathrm{w}} \,. \qquad \text{(Eq.2.1.6)}$$

When all constants in Eq.2.1.2 and Eq.2.1.4 are known, Eq.2.1.1 can be solved for the equilibrium pressure at a given temperature by numerical iteration.

A slightly different approach to calculating gas hydrate equilibria is the fugacity model, where the equilibrium condition is given by

$$f_{\mathrm{W}}^{\mathrm{h}} = f_{\mathrm{W}}^{\mathrm{l}} \qquad \text{(Eq.2.1.7)}$$

with f_{W} being the fugacity of water in the hydrate or liquid phase (e.g. Klauda and Sandler, 2000; 2003; Ballard and Sloan, 2002; Jager et al., 2003).

A multiparametric equation for the direct calculation of methane and carbon dioxide hydrate equilibrium pressures as a function of temperature and salinity was developed by Tishchenko et al. (2005; 2009). In this approach, the equation for the dissociation pressure was derived by fitting of experimental phase boundary data.

SUGAR Toolbox:

Included programs for the calculation of phase boundaries are:

phase_co2h2o.m Phase boundaries of carbon dioxide with seawater
phase_ch4h2o.m Phase boundaries of methane with seawater
They are based on the multiparametric equations of Tishchenko et al. (2005; 2009).

phase_sw.m Phase boundaries of seawater
vlh_naclh2o.m Vapor/liquid/halite 3 phase equilibrium of NaCl solutions
These scripts are based on multiparametric equations as published by Driesner (2007). Driesner's equations were developed for NaCl solutions. Input for the script is salinity which is converted to a NaCl concentration of equivalent ionic strength using Millero's reference composition of seawater (Millero et al., 2008).

hydrate_phasediagram.m Plots the dissociation curves of CH_4- and CO_2-hydrates
sw_phasediagram.m Plots the phase diagram of seawater

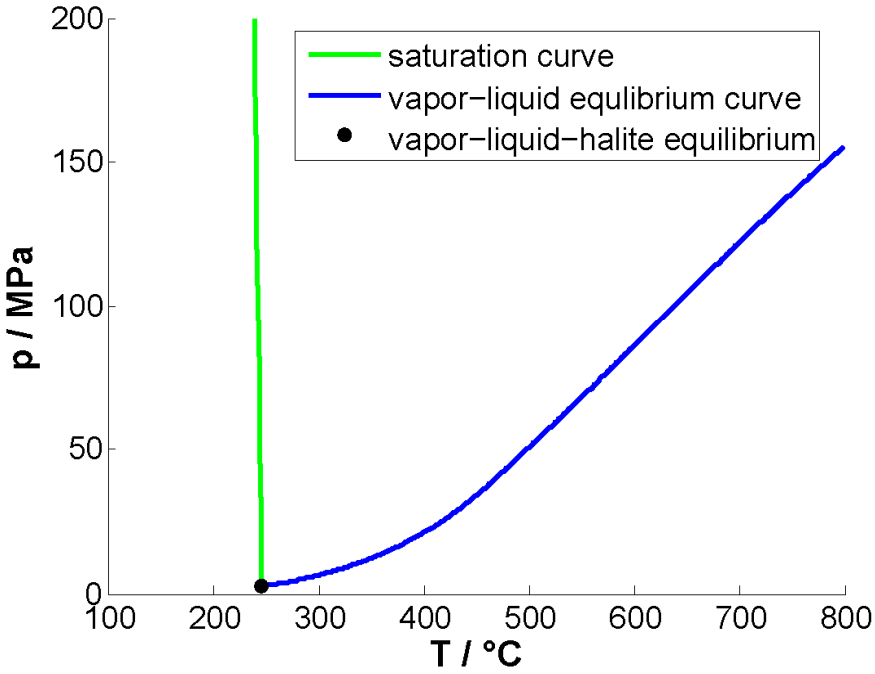

Figure 2.1: Vapor-liquid equilibrium curve and saturation curve of the system NaCl-H_2O. The NaCl concentration corresponds to S = 300 (see comments in toolbox script *phase_sw.m*).

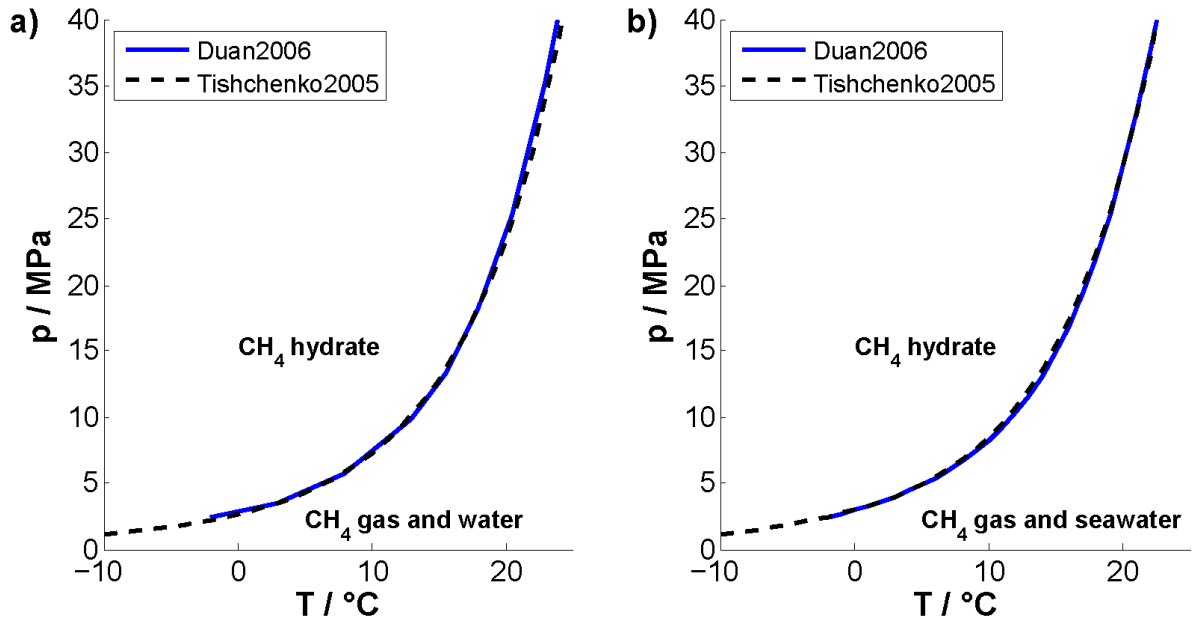

Figure 2.2: Phase diagrams of the system CH_4-H_2O: a) pure water (S=0), b) seawater (S=35).

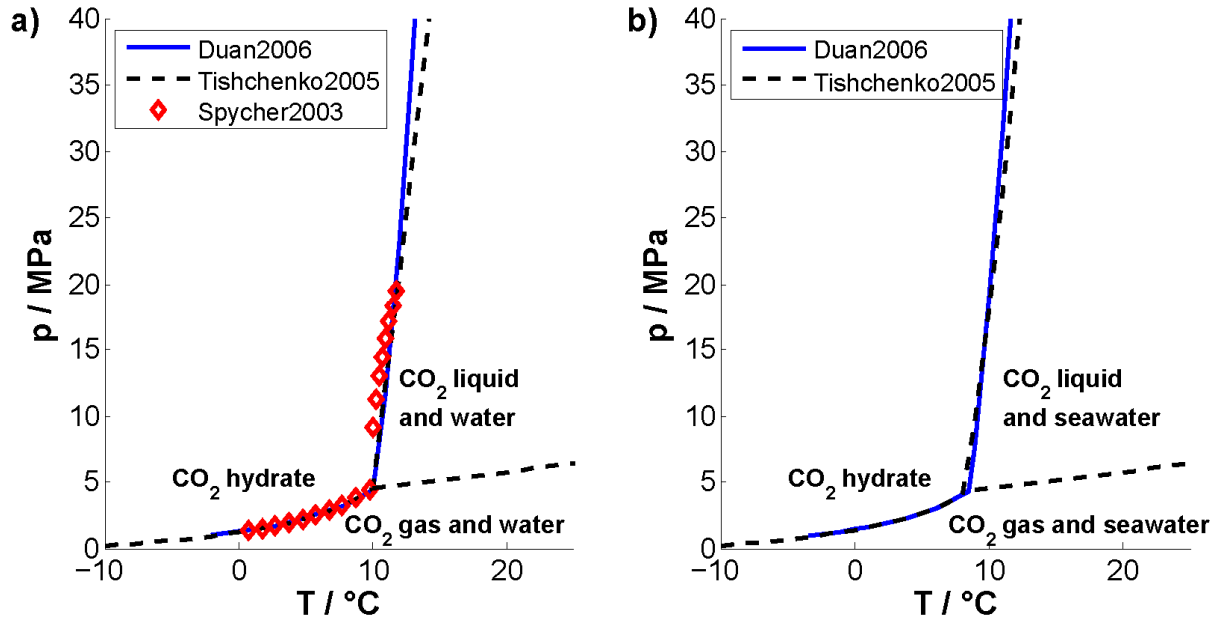

Figure 2.3: Phase diagrams of the system CO_2-H_2O: a) pure water (S=0), b) seawater (S=35).

2.2. Energies for phase transitions

When a thermodynamic system undergoes a phase transition, a change of enthalpy is observed. The enthalpy of vaporization is the energy that is required to transform a given quantity of a substance into a gas, while the enthalpy of fusion is the energy that is required to transform a solid into a liquid. The enthalpy of vaporization ΔH_{v} can be calculated from the Clapeyron equation:

$$\frac{\mathrm{d}p}{\mathrm{d}T} = \frac{\Delta H_{\mathrm{v}}}{\Delta V_{\mathrm{v}} T} \qquad \text{(Eq.2.2.1)}$$

where ΔV_{v} is the volume change during the phase transition.

For isobaric phase transitions, ΔH_{v} can also be derived from the volume change and the change of internal energy ΔU_{v}:

$$\Delta H_{\mathrm{v}} = \Delta U_{\mathrm{v}} + p\Delta V_{\mathrm{v}} \quad . \qquad \text{(Eq.2.2.2)}$$

SUGAR Toolbox:

The specific enthalpy of CH_4, CO_2, N_2, O_2 and (sea)water is an output parameter of the functions:
eos_ch4.m
eos_co2.m
eos_n2.m
eos_o2.m
eos_h2o.m
eos_sw.m
eos_swDriesner.m
Enthalpies for phase transitions can thus be calculated from the enthalpy change at the phase boundary.

In the pressure and temperature range of interest for hydrate formation, CH_4, N_2 and O_2 do not undergo a phase transition, whereas the liquid/gas phase boundary of CO_2 and the solid/liquid phase boundary of water intersect with this range. The equations used in *eos_sw.m* are valid for the liquid phase of seawater and the liquid and gas phase of pure water, only. Therefore, no enthalpies of fusion for can be derived from this function, while enthalpies of vaporization for pure water can be extracted from the output of *eos_h2o.m* and enthalpies of vaporization for saltwater can be extracted from *eos_swDriesner.m*. The enthalpy of vaporization for CO_2 can be calculated from the output of *eos_co2.m* by evaluating the enthalpy difference at conditions slightly above and below the phase transition curve.

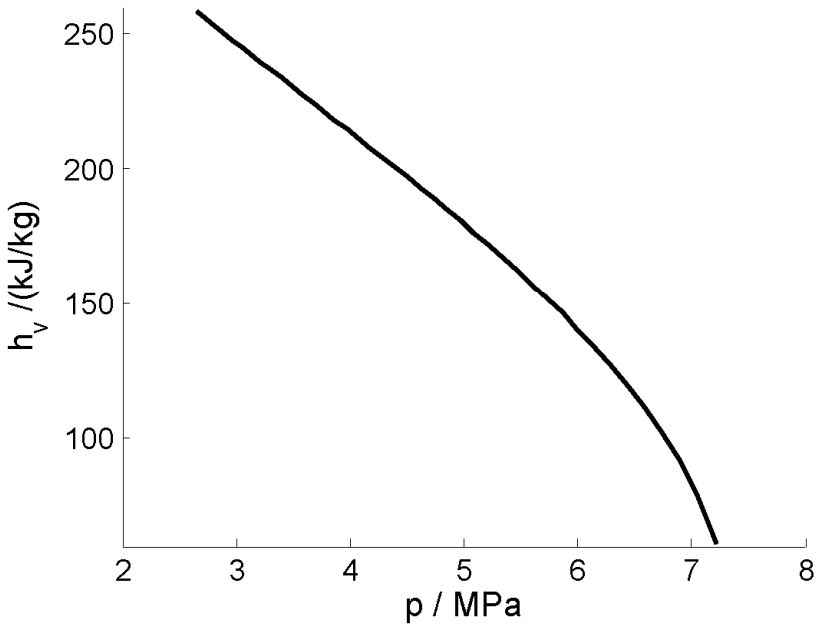

Figure 2.4: Specific enthalpy of vaporization for CO_2.

2.3. Heat capacities of H_2O, seawater, N_2, O_2, H_2S, CH_4, CO_2, CH_4 hydrate and CO_2 hydrate

The specific heat capacity c is the proportionality factor between the thermal energy Q that is absorbed by a substance of mass m and the generated change in temperature ΔT :

$$c = \frac{1}{m}\frac{\partial Q}{\partial T}. \qquad \text{(Eq.2.3.1)}$$

(Incompressible) liquids and solids have a single heat capacity value. For gases, two values are defined: The specific heat capacity at constant pressure (c_p) and the specific heat capacity at constant volume (c_V).

SUGAR Toolbox:

As for all thermodynamic properties, the heat capacity can be calculated from any fundamental thermodynamic potential. Based on this approach, it is an output parameter of the routines:

eos_h2o.m	for water
eos_sw.m	for seawater
eos_swDriesner	for seawater
eos_co2.m	for CO_2
eos_ch4.m	for CH_4
eos_n2.m	for N_2
eos_o2.m	for O_2

For the temperature dependence of the methane hydrate heat capacity, an empirical function has been developed by Gupta (2007). This function has been integrated into the routine:
heatcap_ch4gh.m.

No published data for the heat capacity of CO_2 hydrate could be found, but it is believed to show a similar behavior as methane hydrate.

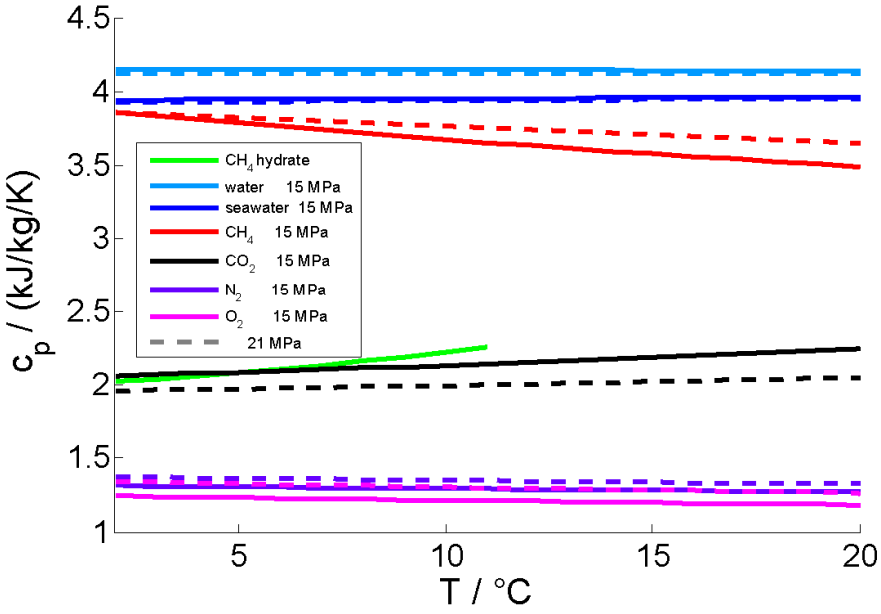

Figure 2.5: Specific heat capacity of seawater and isobaric heat capacities of (sea)water, CH_4, CO_2, N_2, O_2 and CH_4 hydrate as a function of temperature.

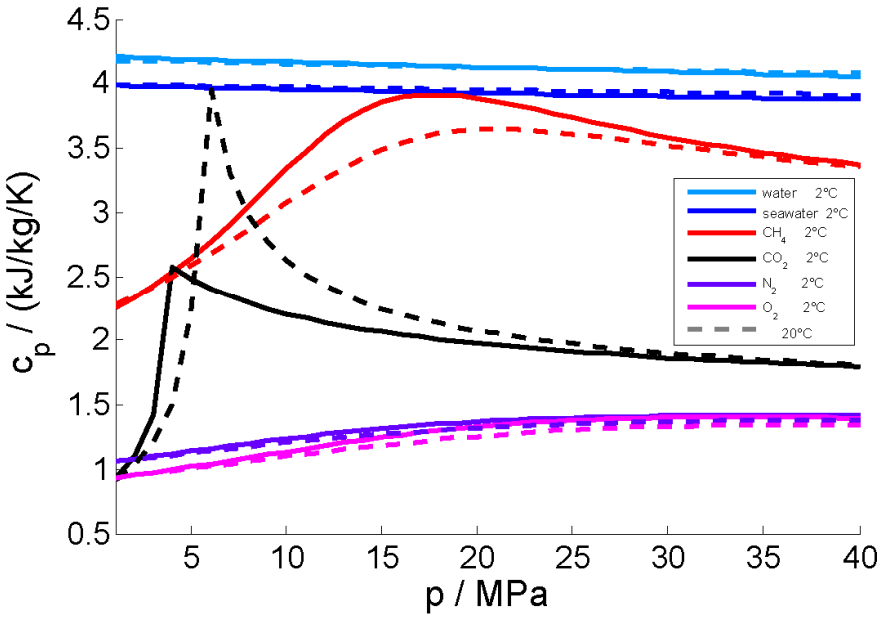

Figure 2.6: Specific heat capacity of seawater and isobaric heat capacities of (sea)water, CH_4, CO_2, N_2 and O_2 as a function of pressure. The phase transition from gaseous to liquid CO_2 is marked by a decrease of c_p.

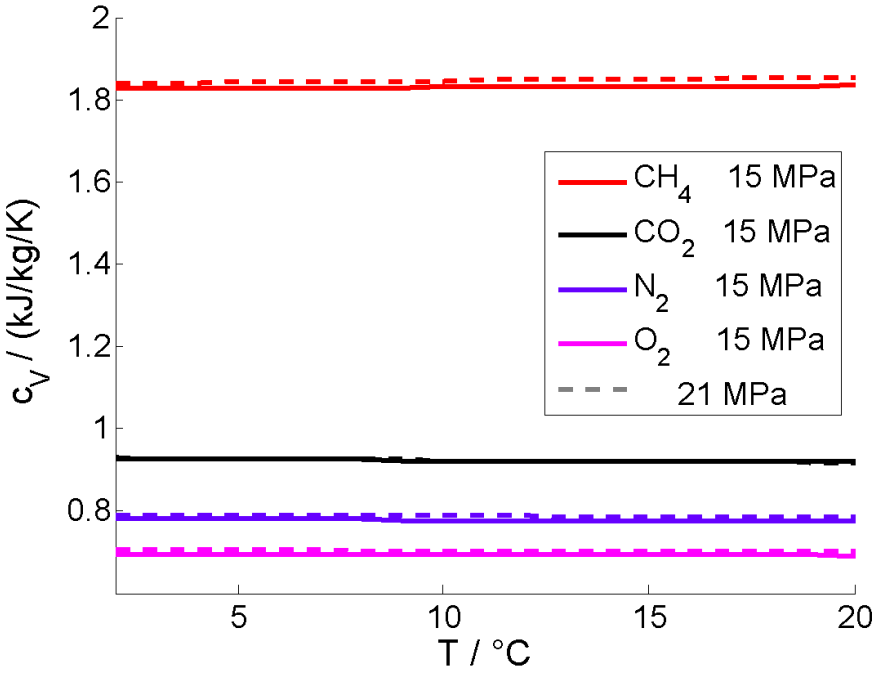

Figure 2.7: Specific heat capacities at constant volume of CH_4, CO_2, N_2 and O_2 as a function of temperature.

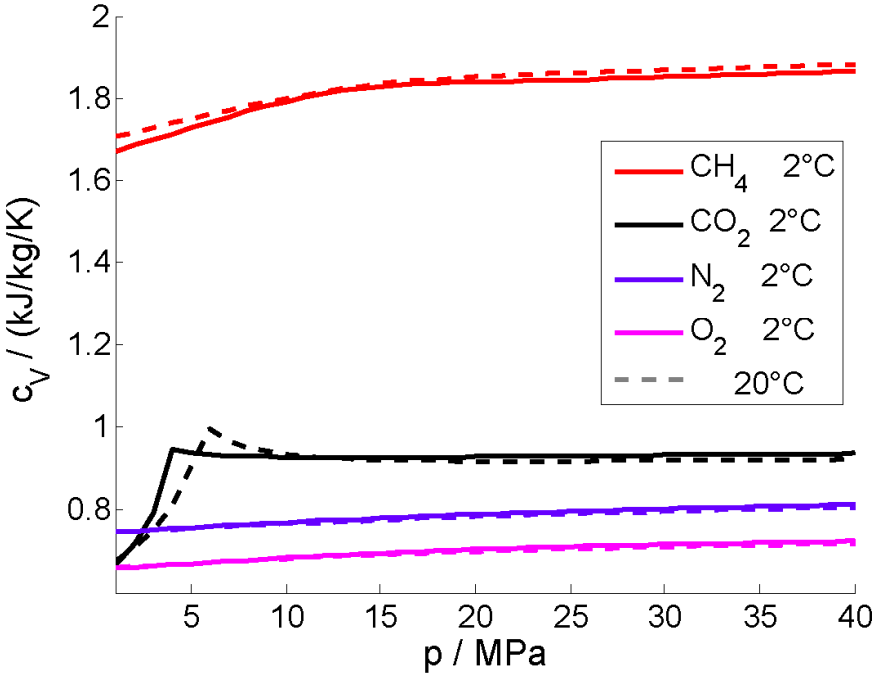

Figure 2.8: Specific heat capacities at constant volume of CH_4, CO_2, N_2 and O_2 as a function of pressure. The phase transition from gaseous to liquid CO_2 is marked by a decrease of c_V.

2.4 Equations of State for H_2O, seawater, CH_4, CO_2, N_2, O_2 and H_2S

From statistical mechanics, it is possible to derive an expansion of the ideal gas law which is known as the virial equation of state (virial EOS):

$$\frac{p}{\mathrm{k_B}T} = \rho + \sum_{\mathrm{n}=2}^{\mathrm{j}} \mathrm{B_n}\rho^{\mathrm{n}} \qquad \text{(Eq.2.4.1)}$$

where ρ is the density, $\mathrm{k_B}$ is the Boltzmann constant and $\mathrm{B_n}$ are the temperature dependent virial coefficients.

Although the virial EOS has a firm theoretical background, the derivation of the virial coefficients is not trivial. More applicable equations for an EOS are for example the Redlich-Kwong (Redlich and Kwong, 1949), Redlich-Kwong-Soave (Soave, 1972) and Peng-Robinson (Peng and Robinson, 1976) equations of state. These are cubic equations with respect to the molar volume V_m and have the general form:

$$p = \frac{\mathrm{R}T}{V_m - \mathrm{b}} + \mathrm{f}\left(V_m, T\right) \qquad \text{(Eq.2.4.2)}$$

where b is a constant that depends on the molecule of interest and $\mathrm{f}\left(V_m, T\right)$ is a function of molar volume and temperature.

Alternatively, the EOS can be derived from a thermodynamic potential. If a fundamental thermodynamic potential of a system is known, the complete thermodynamic representation of the system is available and all thermodynamic equilibrium properties can be calculated, including the EOS. Each thermodynamic potential has natural independent variables. Experimental data in marine sciences are typically measured as a function of pressure and temperature. The corresponding thermodynamic potential with pressure and temperature as natural variables is the Gibbs free energy G:

$$G(p,T) = U + pV - TS \qquad \text{(Eq.2.4.3)}$$

where U is the internal energy and S is the entropy of the system.

Unfortunately, the Gibbs function is ambiguous at phase boundaries. Therefore it cannot be used for the description of systems with phase transitions in the temperature and pressure range of interest. For these systems, the Helmholtz free energy A

$$A(\rho,T) = U - TS \qquad \text{(Eq.2.4.4)}$$

is used instead. Natural variables of the Helmholtz free energy are density and temperature. The density is calculated for given pressures by numerically solving the EOS.

SUGAR Toolbox:

The toolbox functions
eos_ch4.m
eos_co2.m
eos_n2.m
eos_o2.m
eos_h2o.m
use formulations for the thermodynamic properties of CH_4 (Setzmann and Wagner, 1991), CO_2 (Span and Wagner, 1996), N_2 (Span et al., 2000), O_2 (Schmidt and Wagner, 1985) and H_2O (Wagner and Pruß, 2002; with additional information from IAPWS, 1996, IAPWS, 2007, and Marcus, 2000) that have been derived from the Helmholtz energy formalism.

Some older publications use the (outdated) IAPS 1984 formulation (IAPS, 1984; Kestin, 1986; IAPWS, 2007; Marcus, 2000). The parameter-fits depend on water densities from IAPS84. Therefore, the IAPS84 formulation is also provided in the toolbox, but its use is not recommended.
eos_IAPS84.m

For seawater, a Gibbs energy formalism has been developed (Feistel, 2008; IAPWS, 2008), which corrects the values for pure water for salt effects. The pure water values are calculated with a formalsm based on the Helmholtz energy (Wagner and Pruß, 2002). Since the Gibbs energy formalism is inaccurate at phase boundaries, it is only valid for seawater in the liquid phase. The corresponding toolbox function is
eos_sw.m

Densities, enthalpies and heat capacities for NaCl solutions over an extended temperature and pressure range can be calculated with the formalism of Driesner and Heinrich (2007). Driesner (2007) and Driesner and Heinrich (2007) use the Wagner and Pruß (2002) EOS for pure water and substitute the input temperature by a “modified temperature” that depends on NaCl concentration. The toolbox implementation takes salinity as input parameter und converts it to a NaCl concentration of equivalent ionic strength.
eos_swDriesner.m

eos_h2s.m
calculates density and fugacity coefficient of H_2S (Duan et al., 2007; Reamer et al., 1950). It is based on an equation of state that is a higher order polynomial of the inverse molar volume.

2.5. Densities of H_2O, seawater, CH_4, CO_2, N_2, O_2, H_2S, CH_4-CO_2-N_2 mixtures, CH_4-rich and CO_2-rich seawater

The densities of the pure phases of CH_4, CO_2 N_2, O_2 and (sea)water can be obtained by numerically solving the equations of state at given pressure, temperature and in case of seawater also at given salinity (Setzmann and Wagner, 1991; Span and Wagner, 1996; Span et al., 2000; Schmidt and Wagner, 1985; Wagner and Pruß, 2002; Feistel, 2008). Less accurate, but faster in terms of computational cost, is the option to calculate densities from multiparametric equations such as the formulae published by the UNESCO Joint Panel on Oceanographic Tables and Standards (Fofonoff and Millard, 1983; Poisson et al., 1991; Sun et al., 2008; Spivey and McCain, 2004).

For solutions of gases in seawater, the density ρ_{sol} is given by:

$$\rho_{\mathrm{sol}} = \frac{\sum_{\mathrm{i}} x_{\mathrm{i}} M_{\mathrm{i}}}{x_{\mathrm{W}} V_{\mathrm{W}} + \sum_{\mathrm{i}\neq\mathrm{W}} x_{\mathrm{i}} V_{\mathrm{i}}} \qquad \text{(Eq.2.5.1)}$$

where x_{i} is the mole fraction of component i, M_{i} is the molar mass of component , V_{W} is the molar volume of pure water and $V_{\mathrm{i}\neq\mathrm{W}}$ is the apparent molar volume of solute i (ion or gas molecule) in water (Duan and Mao, 2006; Duan et al., 2008; Hu et al., 2007; Mao and Duan, 2006).

For the calculation of mixture densities, mixing rules have to be applied to the equation of state. As a consequence, the equation becomes more complex and is more difficult to solve. A relatively simple and robust equation of state is the cubic Peng-Robinson equation of state (PR-EOS) (Peng and Robinson, 1976):

$$Z^3 - (1-B)Z^{\ 2} + (A - 3B^2 - 2B)Z - (AB - B^2 - B^3) = 0 \qquad \text{(Eq.2.5.2)}$$

with

$$Z = \frac{PV_m}{RT} \qquad \text{(Eq.2.5.3)}$$

$$A = \frac{P}{R^2T^2}\sum_{i,j} x_i x_j a_{ij} \qquad \text{(Eq.2.5.4)}$$

$$B = \frac{P}{RT}\sum_{i} x_i b_i \qquad \text{(Eq.2.5.5)}$$

V_m is the molar volume, a is a parameter that describes the inter- and intra-molecular particle interactions, b is a parameter that is related to particle size and x_i is the mole fraction of component i in the mixture. The PR-EOS is known to produce good results for gas phases but is less accurate in the liquid phase.

SUGAR Toolbox:

The toolbox functions
density_ch4.m
density_co2.m
call the corresponding EOS to calculate the densities of CH_4 and CO_2.

The densities of N_2, O_2, H_2S, pure water and seawater are output parameters of the respective EOS scripts:
eos_n2.m
eos_o2.m
eos_h2s.m
eos_h2o.m
eos_sw.m

density_swSpivey.m
density_swSun.m
density_cacl2brine.m
calculate the density of seawater at elevated pressures and temperatures (Spivey and McCain, 2004; Sun et al., 2008) and $CaCl_2$ brines (Al Ghafri et al., 2012) from multiparametric equations. The equations of (Spivey and McCain, 2004) were derived for NaCl solutions. Hence, the input salinity is converted to a NaCl concentration of equivalent mass.

density_swUnesco.m
calculates the density of seawater based on the UNESCO formulations.

density_sw.m
checks the input pressure, temperature and salinity and calls the function matching the p-T-S range of validity best, i.e. *eos_sw.m*, *eos_swDriesner.m*, *density_swSpivey.m, density_swSun.m or density_swUnesco.m*. The choice of the functions can also be forced by an additional input parameter.

Eq. 2.5.1 for the densities of seawater with dissolved gases is integrated in
density_ch4sw.m
density_co2sw.m
density_n2sw.m

A Peng-Robinson equation of state is used to calculate the densities and composition of single-phase and two-phase mixtures of CH_4, CO_2 and N_2 (Risnes et al., 1981; Michelsen, 1982; Adewumi):
density_ch4co2n2.m

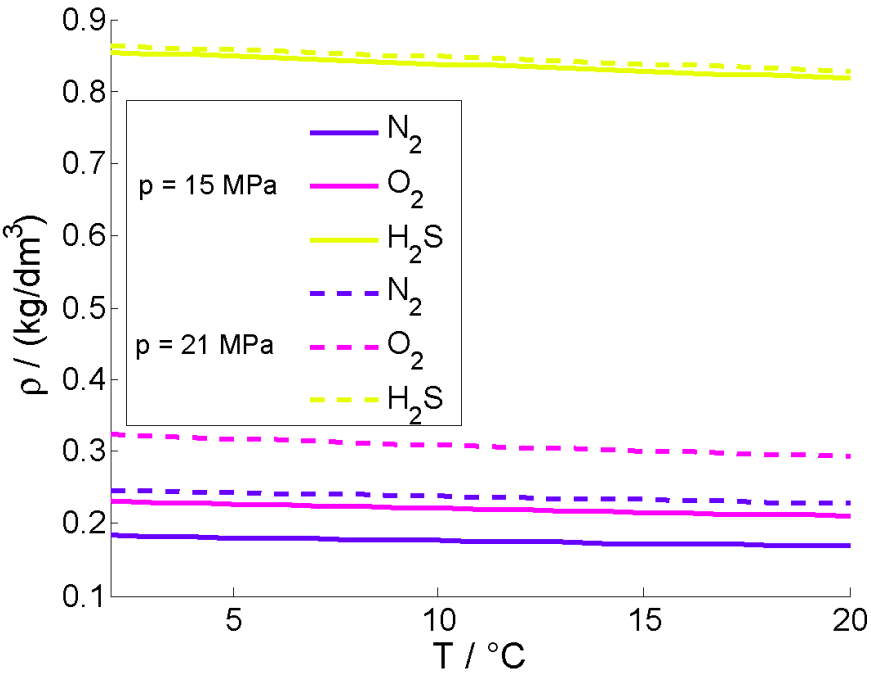

Figure 2.9: Densities of N_2, O_2 and H_2S as a function of temperature.

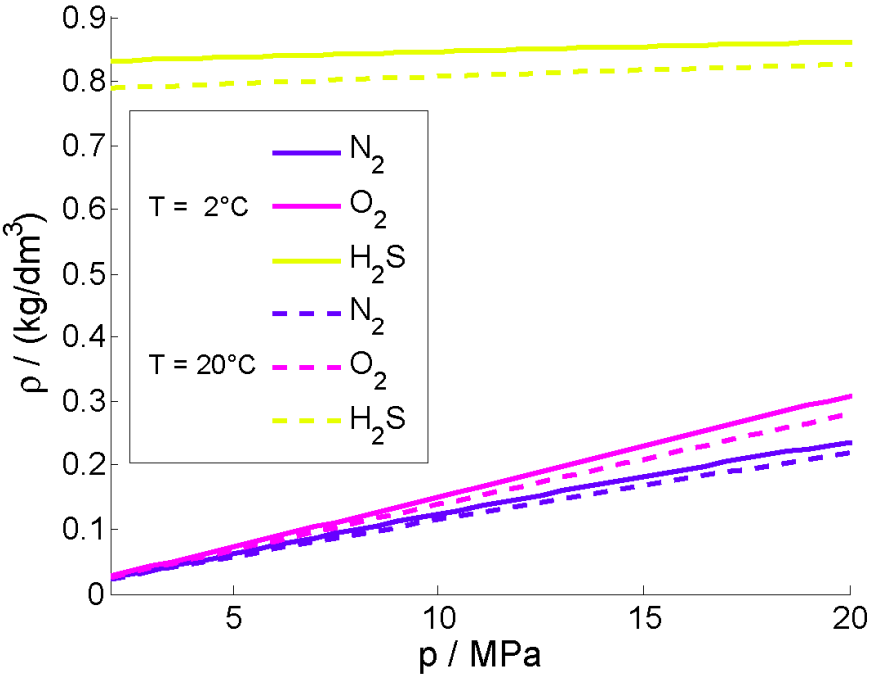

Figure 2.10: Densities of N_2, O_2 and H_2S as a function of pressure.

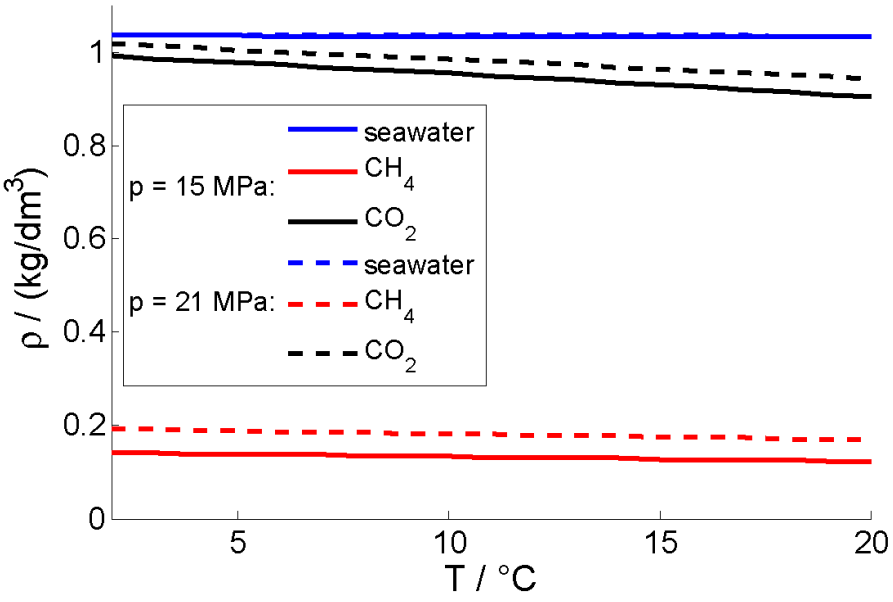

Figure 2.11: Densities of seawater, CH_4 and CO_2 as a function of temperature.

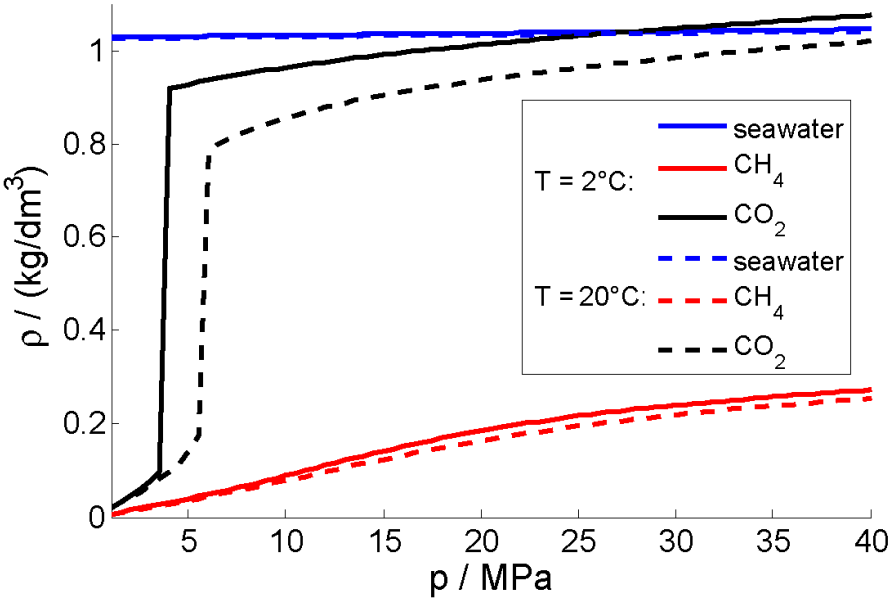

Figure 2.12: Densities of seawater, CH_4 and CO_2 as a function of pressure. The phase transition from gaseous to liquid CO_2 is marked by a steep increase in density.

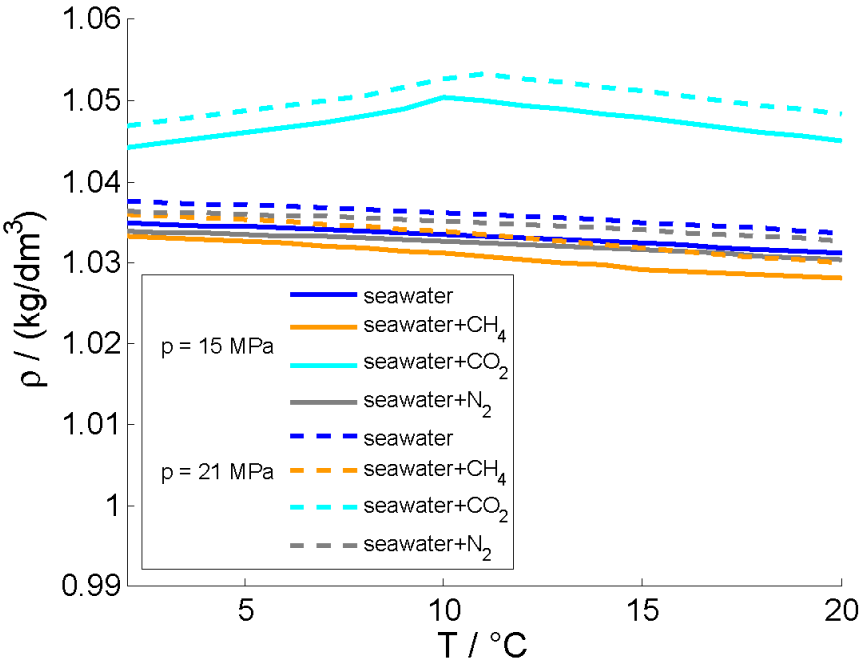

Figure 2.13: Densities of seawater and seawater saturated with CH_4, CO_2 or N_2 as a function of temperature**.** A distinct change in density is observed at the hydrate dissociation temperature.

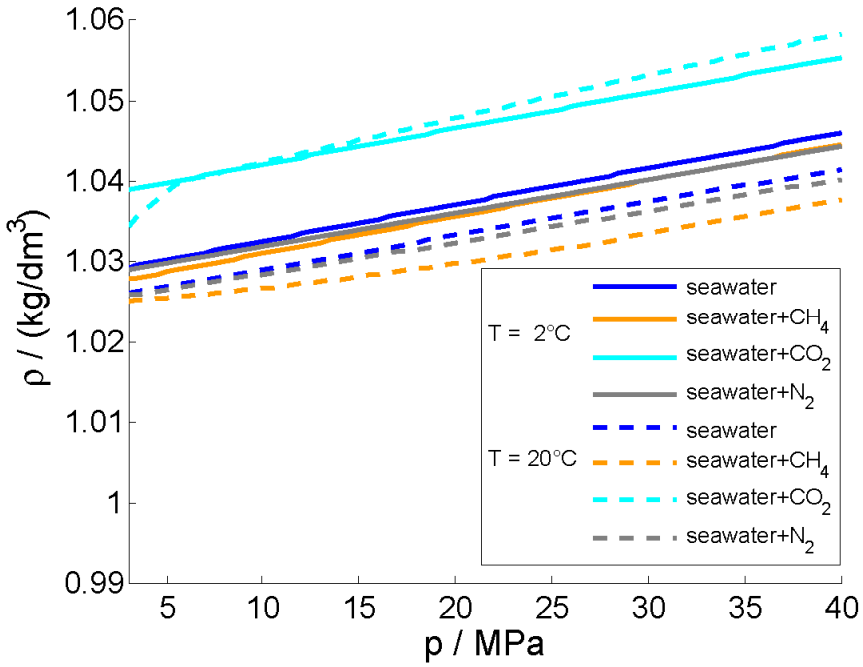

Figure 2.14: Densities of seawater and seawater saturated with CH_4, CO_2 or N_2 as a function of pressure. The phase transition of CO_2 hydrate is omitted for the curve at T = 2 ℃ because the calculated density shows an er ratic behavior at this point.

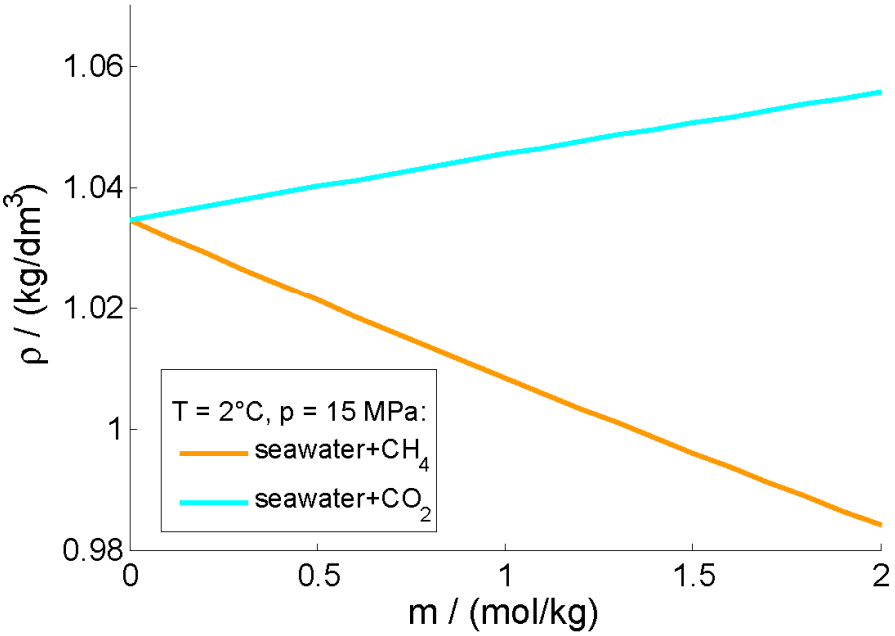

Figure 2.15: Densities of seawater as a function of dissolved CH_4 or CO_2 concentration.

2.6. Fugacities of CH_4, CO_2, N_2, O_2, H_2S and H_2O in all phases

The fugacity f is a measure of the effective partial pressure of a real gas. The fugacity coefficient ϕ describes the deviation from ideal gas behavior:

$$f = \phi \; p_{\mathrm{i}} \qquad \text{(Eq.2.6.1)}$$

For ideal gases, ϕ equals 1 and the fugacity equals the (partial) gas pressure p_{i}.
ϕ is related to the basic thermodynamic variables via

$$\ln(\phi) = \int_{p_0}^{p} \left(\frac{V_m}{RT} - \frac{1}{P} \right) dP \qquad \text{(Eq.2.6.2)}$$

By substituting Eq.2.6.2 into Eq.2.6.1 and introducing a reference state fugacity, f_0, the basic form of the fugacity equation becomes:

$$f = f_0 \exp\left(\frac{\Delta\mu}{RT} \right) \qquad \text{with} \qquad \Delta\mu = \int_{p_0}^{p} V_m \, dp \qquad \text{(Eq.2.6.3)}$$

where $\Delta\mu$ is the change of the chemical potential with respect to the reference state $p = p_0$, and V_{m} is the molar volume of the gas.

Strictly speaking, the fugacity is a property of the gas phase only. Nevertheless, Eq.2.6.3 can also be applied to calculate a pseudo fugacity for other phases, if the difference in chemical potential with respect to a gas state fugacity is known. The reference pressure for liquid phases is the saturation pressure p_{sat}:

$$f_{lq} = f_{p_{sat}} \exp \int_{p_{sat}}^{p} \left(\frac{V_m}{RT} \right) dp = f_{p_{sat}} \exp\left(\frac{\Delta\mu}{RT} \right) \qquad \text{(Eq.2.6.4)}$$

Klauda and Sandler (2000; 2003) compiled a set of equations for hydrate phase fugacities $f_{H_2O,H}$ (fugacity of water in gas hydrate) and $f_{j,H}$ (fugacity of a guest molecule of type j in gas hydrate):

$$f_{H_2O,H} = p_{sat,\beta} \exp\left(\frac{V_{sat,\beta}\left(p - p_{sat,\beta}\right)}{RT} \right) \exp\left(\frac{-\Delta\mu}{RT} \right) \qquad \text{(Eq.2.6.5)}$$

$$\Delta\mu = -RT \sum_i n_i \ln\left(1 - \sum_j \frac{C_{ij} f_{j,H}}{1 + \sum_j C_{ij} f_{j,H}} \right) \qquad \text{(Eq.2.6.6)}$$

Here, $p_{sat,\beta}$ is the saturation pressure of the hypothetical empty gas hydrate lattice, $V_{sat,\beta}$ is the molar volume of the hypothetical empty gas hydrate lattice, n_i is the number of cages of type i per water molecule in the hydrate lattice and C_{ij} is the Langmuir constant of a guest molecule of type j in a lattice cage of type i. Langmuir constants are coefficients that are related to cell potential parameters. Fugacities of dissolved gases can be calculated from Henry's law (Eq.2.7.1; Henry, 1803).

SUGAR Toolbox:

Fugacity coefficients of pure CO_2, CH_4, N_2, O_2, H_2S and water are output parameters of the functions:
eos_co2.m
eos_ch4.m
eos_n2.m
eos_o2.m
eos_h2s.m
eos_seawater.m

For seawater, the pure water fugacity is corrected for the presence of salt ions and dissolved methane and carbon dioxide by incorporating the corresponding activity coefficient (Jager et al., 2003):
fugacity_sw.m

The formalism of Klauda and Sandler (2000; 2003) and Cole and Goodwin (1990) is used to calculate the fugacities of H_2O in CH_4 hydrate (mh) and CO_2 hydrate (ch) as well as fugacities of the guest molecules CH_4 and CO_2 in gas hydrate (for the calculation of guest molecule fugacities, cage occupancies have to be known):
fugacity_h2omh.m
fugacity_h2och.m
fugacity_ch4gh.m
fugacity_co2gh.m

Fugacities of dissolved gases are calculated via Henry's law (see chapter 2.7):
fugacity_ch4sw.m
fugacity_co2sw.m
fugacity_n2sw.m
fugacity_o2sw.m
fugacity_h2ssw.m

Eq.2.1.7 states that hydrate formation is initiated, if the fugacity of a molecule in the aqueous phase equals its fugacity in the hydrate phase. Since only gas phase fugacities can be measured directly, only the equations for gas phase fugacities are validated by experimental data. All other equations for fugacities are based on the evaluation of related quantities, such as solubility or dissociation pressure, which depend on more than one parameter. The derived fugacity values, therefore, depend on the formulation of the additional parameters, which differ by authors. The functions for water fugacities in hydrate phases were fitted to match water phase fugacities at gas hydrate dissociation pressures.

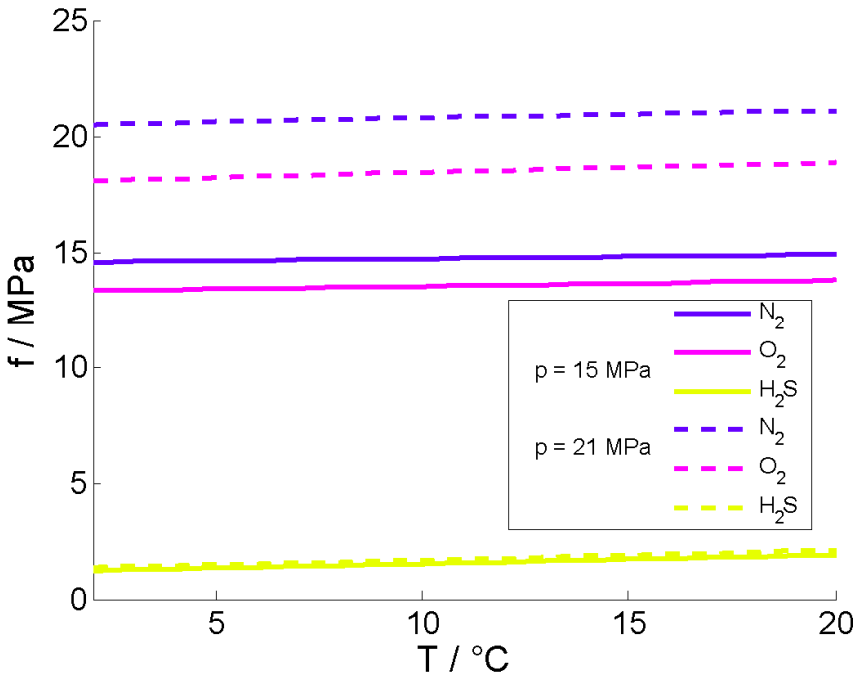

Figure 2.16: Fugacities of pure N_2, O_2 and H_2S as a function of temperature.

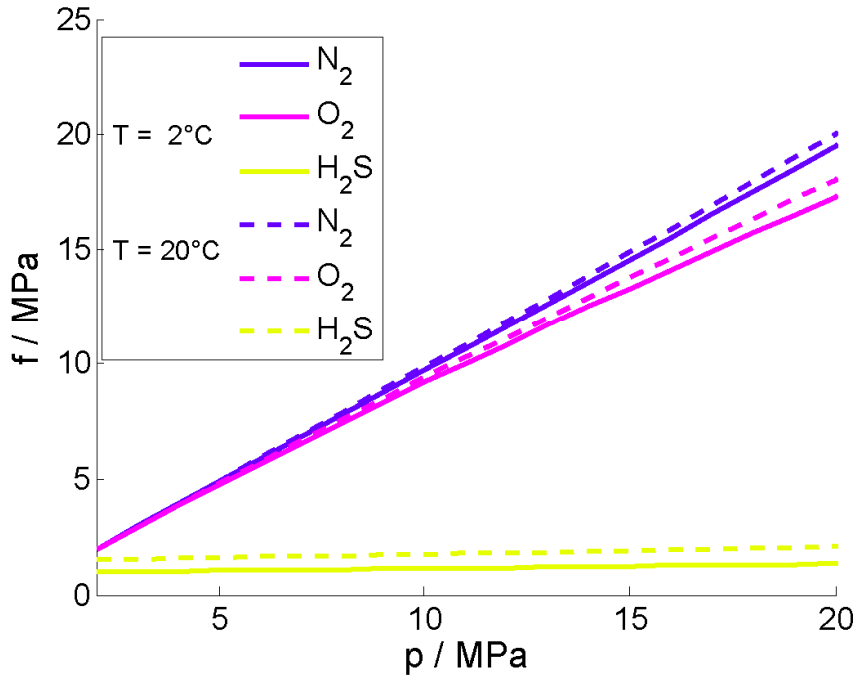

Figure 2.17: Fugacities of pure N_2, O_2 and H_2S as a function of pressure.

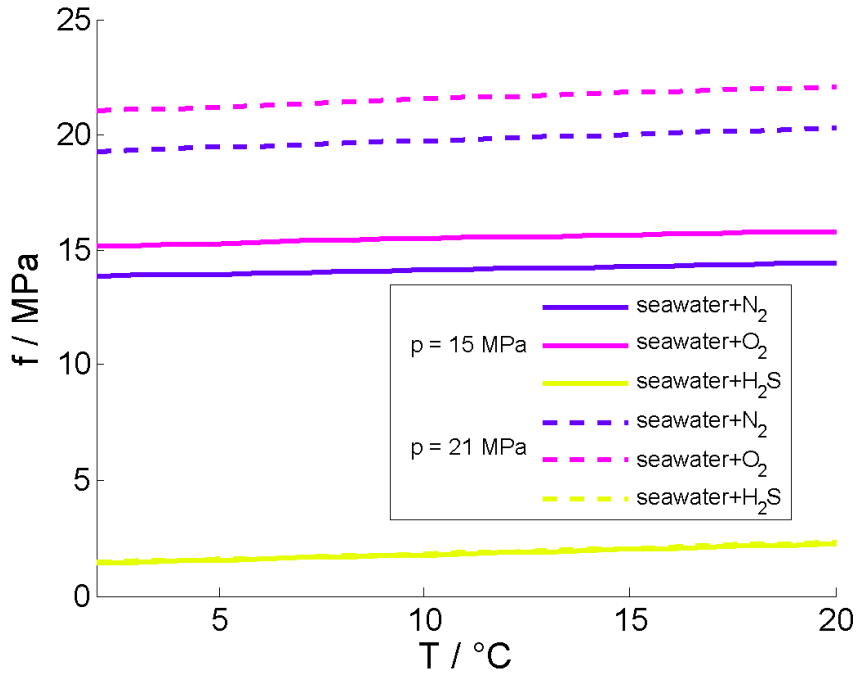

Figure 2.18: Fugacities of N_2, O_2 and H_2S dissolved in seawater at saturation as a function of temperature.

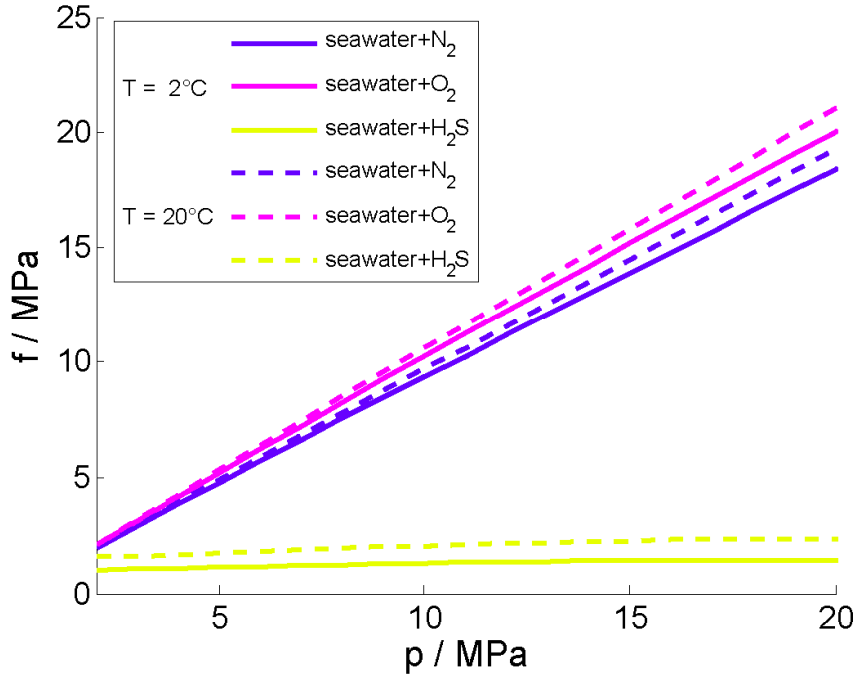

Figure 2.19: Fugacities of N_2, O_2 and H_2S dissolved in seawater at saturation as a function of pressure.

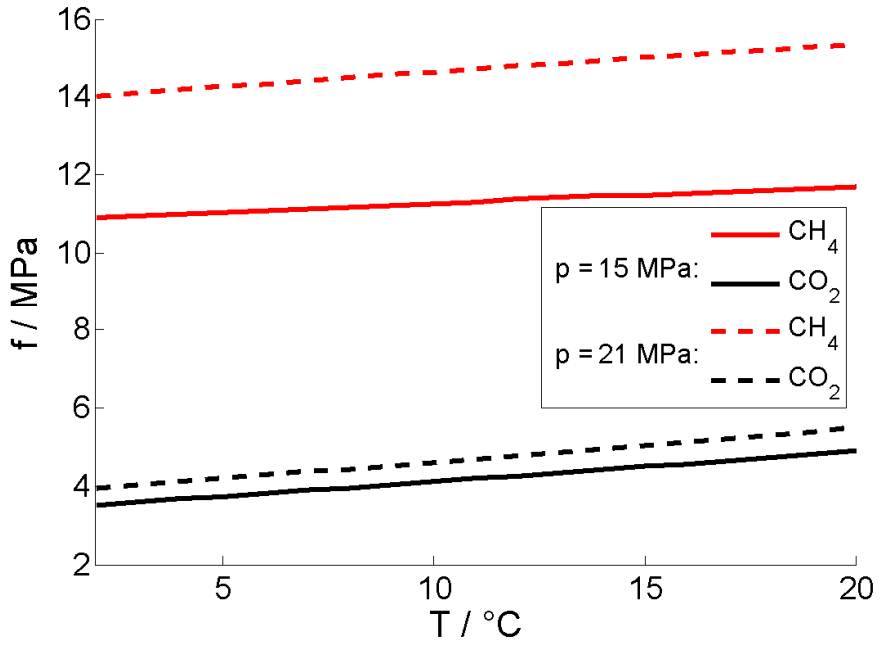

Figure 2.20: Fugacities of pure CH_4 and CO_2 as a function of temperature (no hydrate formation).

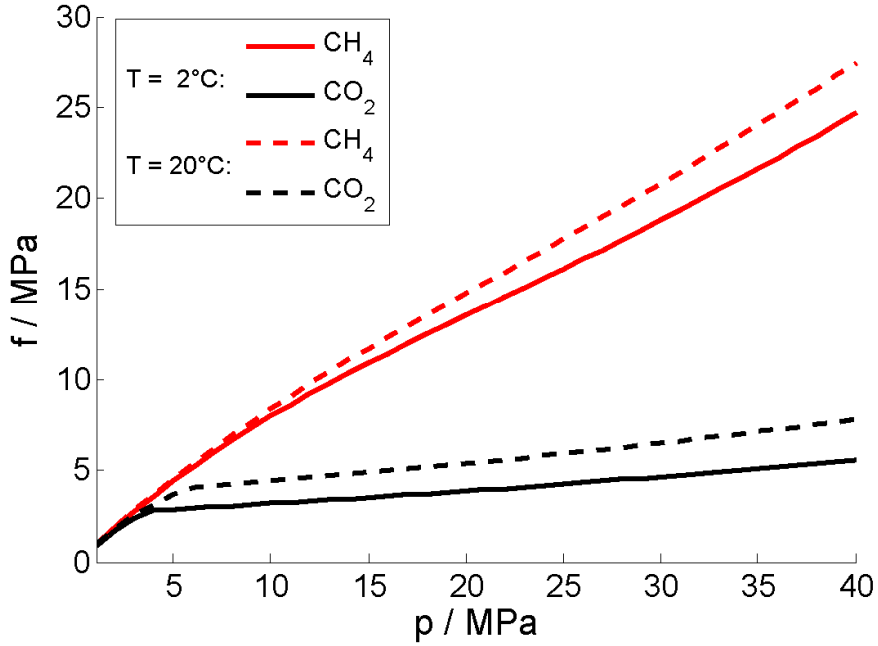

Figure 2.21: Fugacities of pure CH_4 and CO_2 as a function of pressure (no hydrate formation).

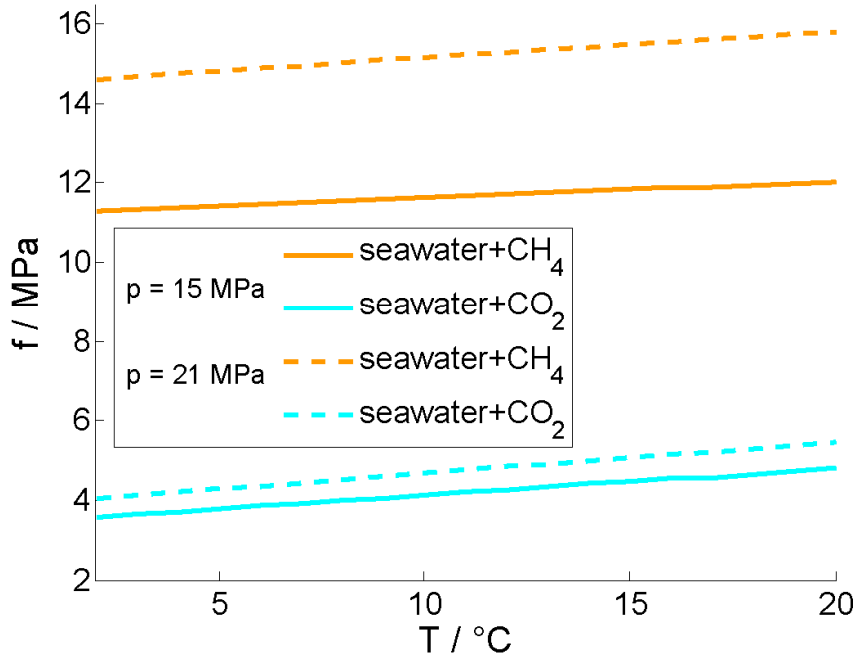

Figure 2.22: Fugacities of CH_4 and CO_2 dissolved in seawater at saturation as a function of temperature.

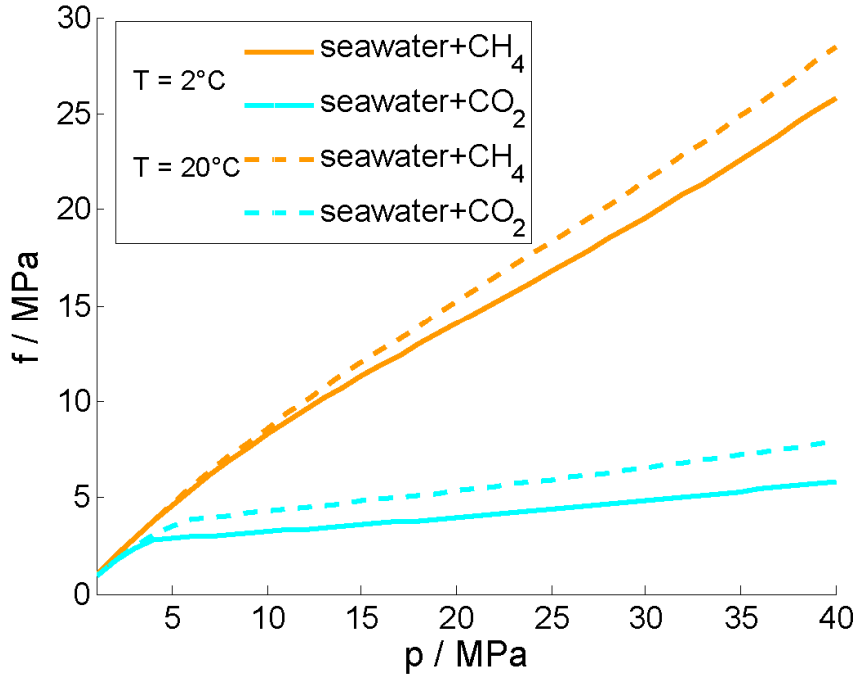

Figure 2.23: Fugacities of CH_4 and CO_2 dissolved in seawater at saturation as a function of pressure.

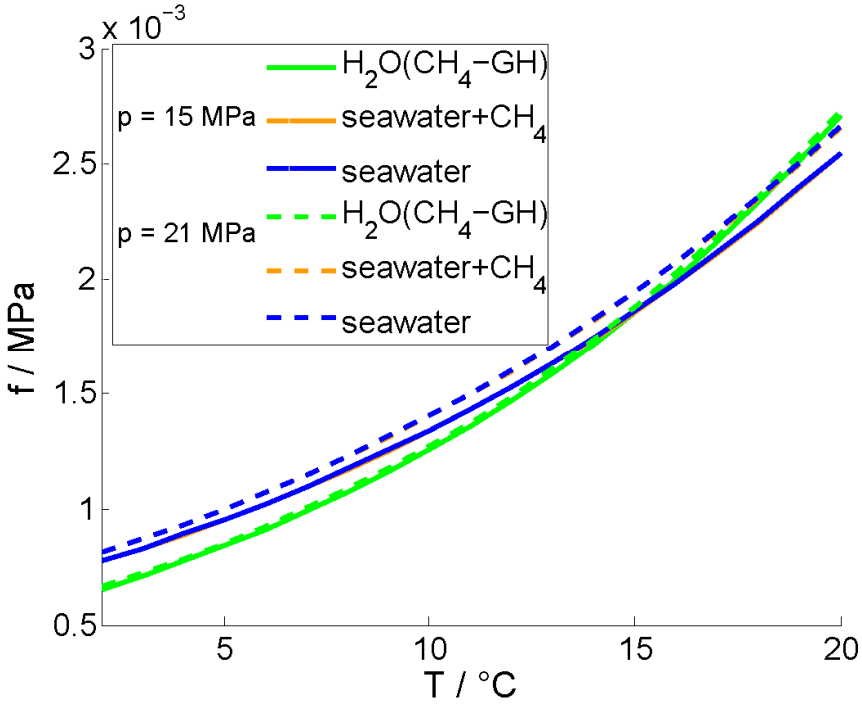

Figure 2.24: Fugacities of water in seawater, CH_4-saturated seawater and CH_4 gas hydrate as a function of temperature. The curves for seawater and CH_4-saturated seawater are almost identical and cannot be distinguished in this representation.

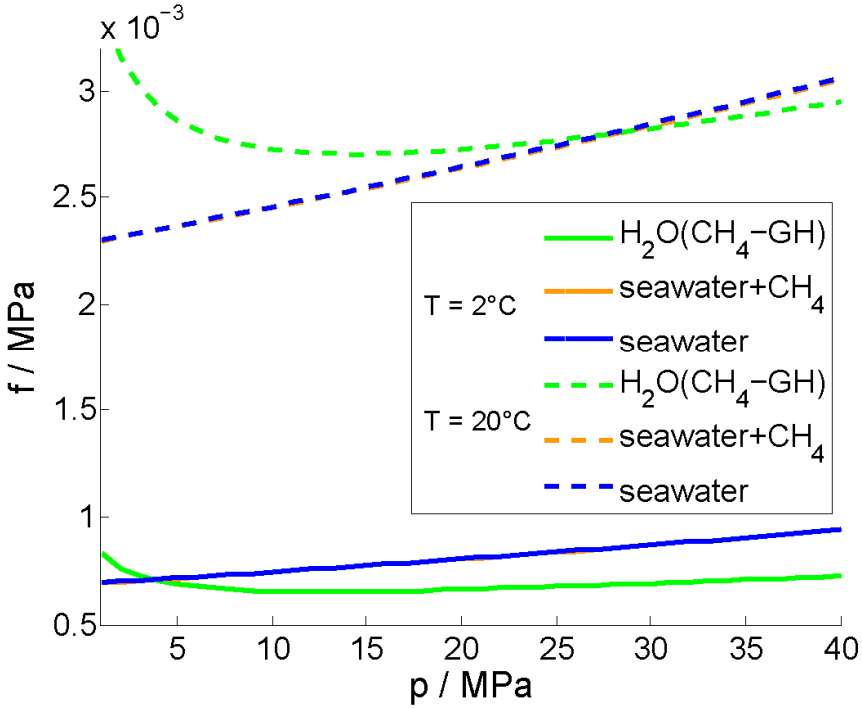

Figure 2.25: Fugacities of water in seawater, CH_4-saturated seawater and CH_4 gas hydrate as a function of pressure. The curves for seawater and CH_4-saturated seawater are almost identical and cannot be distinguished in this representation.

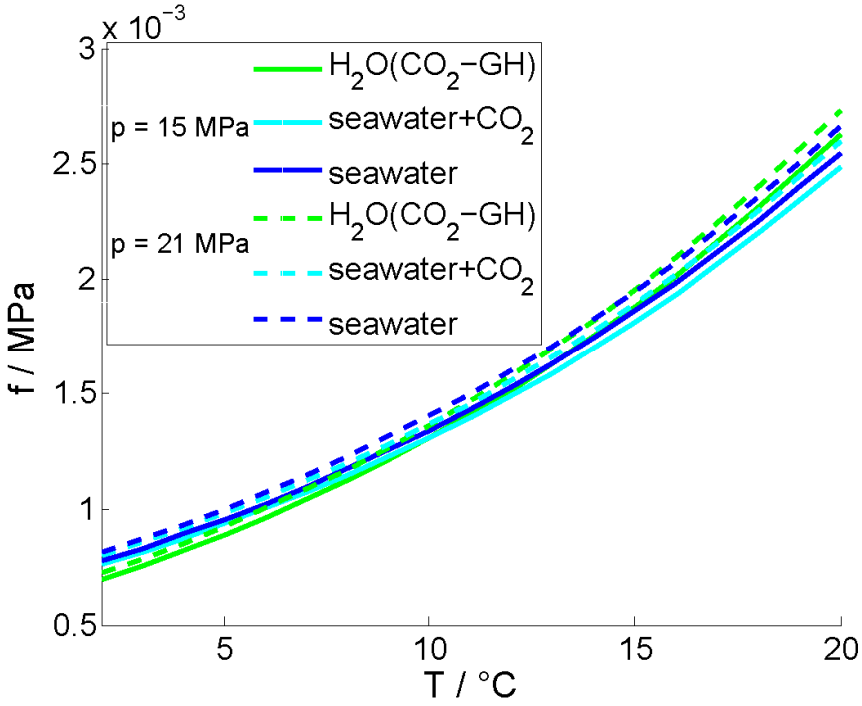

Figure 2.26: Fugacities of water in seawater, CO_2-saturated seawater and CO_2 gas hydrate as a function of temperature. The curves for seawater and CO_2-saturated seawater are almost identical.

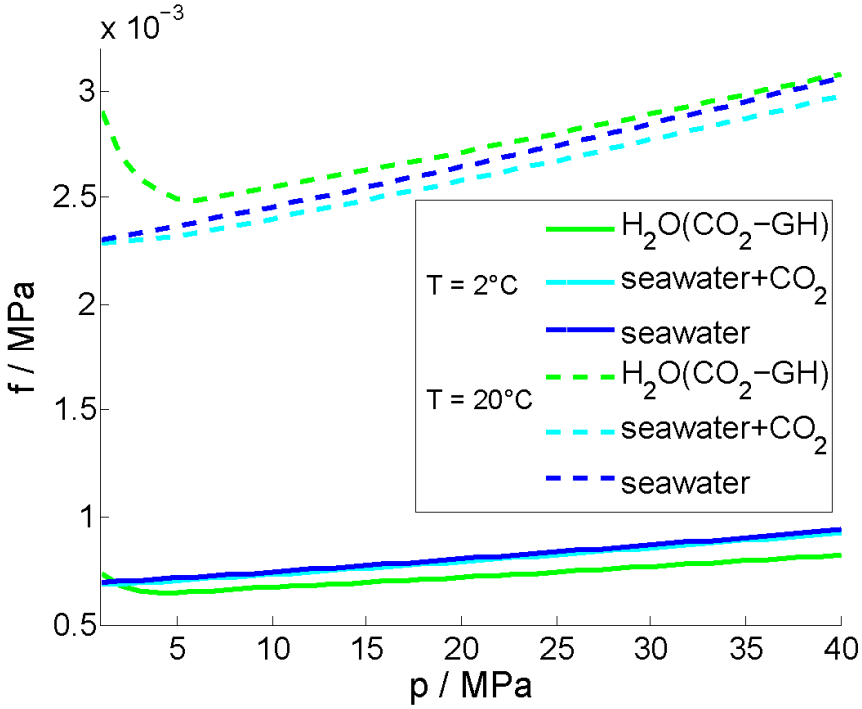

Figure 2.27: Fugacities of water in seawater, CO_2-saturated seawater and CO_2 gas hydrate as a function of pressure. The curves for seawater and CO_2-saturated seawater are almost identical.

2.7. Henry constants of CH_4, CO_2, N_2, O_2 and H_2S in H_2O and seawater

Henry's law describes the solubility of a gas in a liquid (Henry, 1803):

$$f = \frac{x}{K_H} \qquad \text{(Eq.2.7.1)}$$

where f is the fugacity of the gas, x is the mole fraction of the dissolved gas at saturation and K_H is Henry's constant, which is defined at infinite dilution:

$$K_H = \lim_{x \to 0} \frac{x}{f} \qquad \text{(Eq.2.7.2)}$$

A more elaborate form of Henry's law is

$$f = \gamma \frac{x}{K_H^0} \exp\left(\int_{p_0}^{p} \frac{V_\mathrm{m}}{\mathrm{R}T} dp \right) \qquad \text{(Eq.2.7.3)}$$

where K_H^0 is Henry's constant at a reference pressure. The exponential term defines the pressure dependency of the solubility. Salinity effects can be accounted for by a non-unity activity coefficient. For dilute solutions of weakly interacting molecules in water, Eq.2.7.3 reduces to the Krichevski-Kasarnovski equation (Krichevski and Kasarnovski, 1935):

$$f = \frac{\mathrm{x}}{\mathrm{K}_\mathrm{H}^0} \exp\left(\frac{V_m^\infty}{\mathrm{R}T} (p - p_0) \right) \; . \qquad \text{(Eq.2.7.4)}$$

However, this simplification is not applicable for dissolved gases in seawater at high pressures. Here, the common approach is a semi empirical formulation for K_H^0 with a pressure correction as given in Eq.2.7.4 and a salinity dependency in the form of a Setchenov equation (Setchenov, 1889):

$$\frac{x}{x^0} = \exp(\mathrm{k_S} c) \qquad \text{(Eq.2.7.5)}$$

where x^0 is the mole fraction at zero salinity, c is the concentration of the dissolved salt (or the salinity) and $\mathrm{k_S}$ is the Setchenov constant. Weiss (1974) calculates K_H^0 based on an integrated form of van't Hoff's equation (Eq.2.11.2), whereas Harvey (1996) uses a correlation with critical parameters of the solvent. The latter approach takes advantage of the fact, that Henry's constant shows a distinct behavior at the solvent's critical point. In general, Henry's law is most accurate at low pressures and for dilute solutions.

SUGAR Toolbox:

Within the SUGAR toolbox, pressure and salinity dependent Henry constants are calculated based on Harvey (1996) with partial molar volumes from Plyasunov et al. (2000) and activity corrections from Duan et al. (2006), Duan and Mao (2006), Mao and Duan (2006), Geng and Duan (2010), and Duan et al. (2007). Henry constants are converted to the unit mol/kg/MPa by assuming that seawater and the gas of interest are the only components of the system. Henry's law does not hold for total pressures above the vapor pressure of a solvent.

The following toolbox functions compute Henry constants as functions of pressure, temperature, salinity and partial gas pressure.Two Henry constants are calculated: KH_m (which has the unit mol/kg/MPa) and KH_x (which has the unit 1/MPa).

soluhenry_co2sw.m	for CO_2 in seawater
soluhenry_ch4sw.m	for CH_4 in seawater
soluhenry_n2sw.m	for N_2 in seawater
soluhenry_o2sw.m	for O_2 in seawater
soluhenry_h2ssw.m	for H_2S in seawater

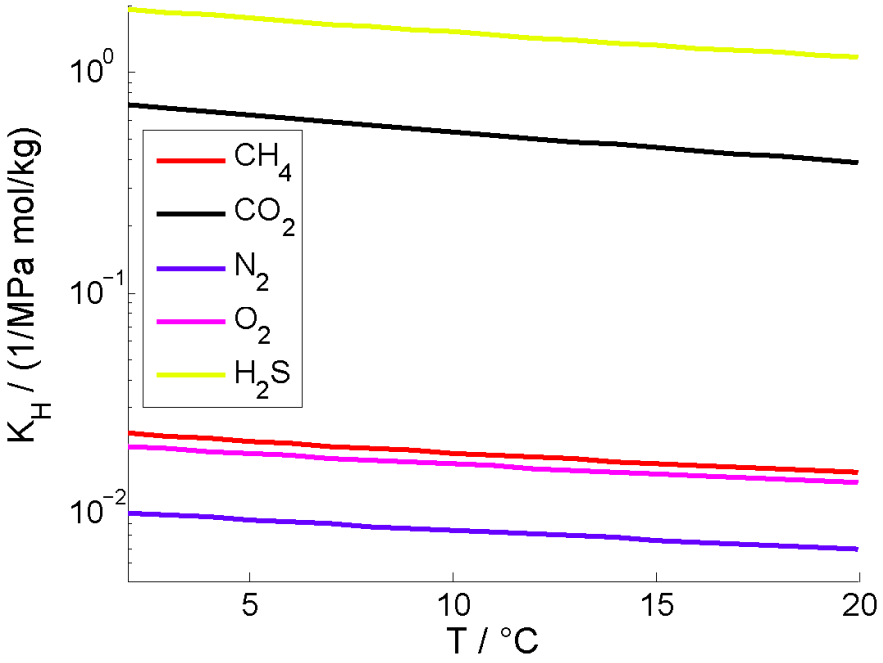

Figure 2.28: Henry constants for CO_2, CH_4, N_2, O_2 and H_2S at reference pressure (0.1 MPa) and zero salinity.

2.8. Solubilities of CH_4, CO_2, N_2, O_2 and H_2S, in H_2O and seawater

A more general equation to calculate the solubility of gases in liquids is based on the equality of the molecules' chemical potential in the vapor phase and in solution:

$$\mu_{\mathrm{G}}^{\mathrm{g}_0} + \mathrm{R}T\ln(f) = \mu_{\mathrm{G}}^{\mathrm{l}_0} + \mathrm{R}T\ln(a) \qquad \text{(Eq.2.8.1)}$$

where $\mu_{\mathrm{G}}^{\mathrm{g}_0}$ is the ideal gas chemical potential in the vapor phase at standard pressure, f is the fugacity in the vapor phase, $\mu_{\mathrm{G}}^{\mathrm{l}_0}$ is the chemical potential in a solution of unit molality and $a = \gamma\, m$ is the activity of the gas molecules in solution (Sun and Duan, 2005; Duan et al., 2006). For uncharged species N in dilute solutions with anions a and cations c, Eq.2.1.5 for the calculation of the activity coefficient γ can be simplified to

$$\ln\gamma_{\mathrm{N}} = 2\sum_{\mathrm{a}} m_{\mathrm{a}}\lambda_{\mathrm{Na}} + 2\sum_{\mathrm{c}} m_{\mathrm{c}}\lambda_{\mathrm{Nc}} + \sum_{\mathrm{ac}} m_{\mathrm{a}} m_{\mathrm{c}}\zeta_{\mathrm{Nac}} \qquad \text{(Eq.2.8.2)}$$

with interaction parameters $\lambda_{Na/c}$ and ζ_{Nac} (Millero, 2007) and molalities $m_{a/c}$.

SUGAR Toolbox:

Solubilities are calculated from multiparametric equations. With only two phases present (gas and liquid water), the equations of Duan et al. (1992; 1996; 2006; 2007), Duan and Sun (2003), Duan and Mao (2006), Mao and Duan (2006), and Geng and Duan (2010) with vapor pressures from (Wagner and Pruß (1993), Shibue (2003), and Velasco et al. (2008) are used:

solu_co2gl.m for CO_2 in seawater
solu_ch4gas.m for CH_4 in seawater
solu_n2sw.m for N_2 in seawater
solu_o2sw.m for O_2 in seawater
solu_h2ssw.m for H_2S in seawater

Solubilities as functions of the gas partial pressure can be derived from Henry's law (see chapter 2.7):

soluhenry_co2sw.m for CO_2 in seawater
soluhenry_ch4sw.m for CH_4 in seawater
soluhenry_n2sw.m for N_2 in seawater
soluhenry_o2sw.m for O_2 in seawater
soluhenry_h2ssw.m for H_2S in seawater

In the presence of gas hydrate, the formalism of Tishchenko et al. (2005; 2009) is employed:

solu_co2gh.m for CO_2 in seawater + hydrate
solu_ch4gh.m for CH_4 in seawater + hydrate

solu_co2.m
solu_ch4.m
call *solu_co2gl.m* and *solu_ch4gas.m*, respectively, if pressure and temperature conditions are outside the gas hydrate stability zone and they call *solu_co2gh.m* and *solu_ch4gh.m*, respectively, if pressure and temperature conditions are inside the respective gas hydrate stability zone. Due to the use of two different formulations, a slight mismatch of the solubilities at the hydrate dissociation pressure may occur.

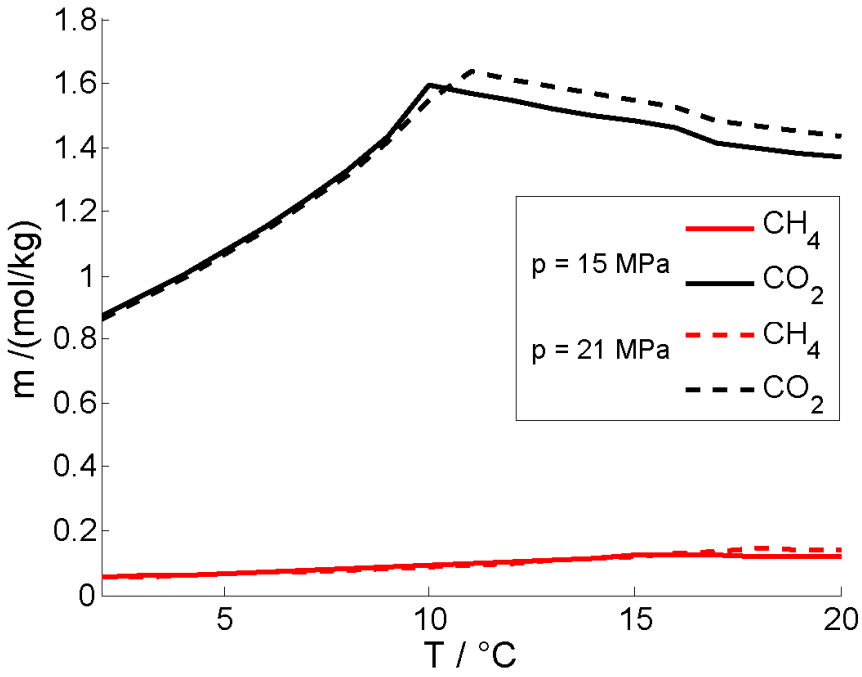

Figure 2.29: Solubilities of CO_2 and CH_4 in seawater as a function of temperature. A distinct change in solubility is observed at the gas hydrate dissociation temperature.

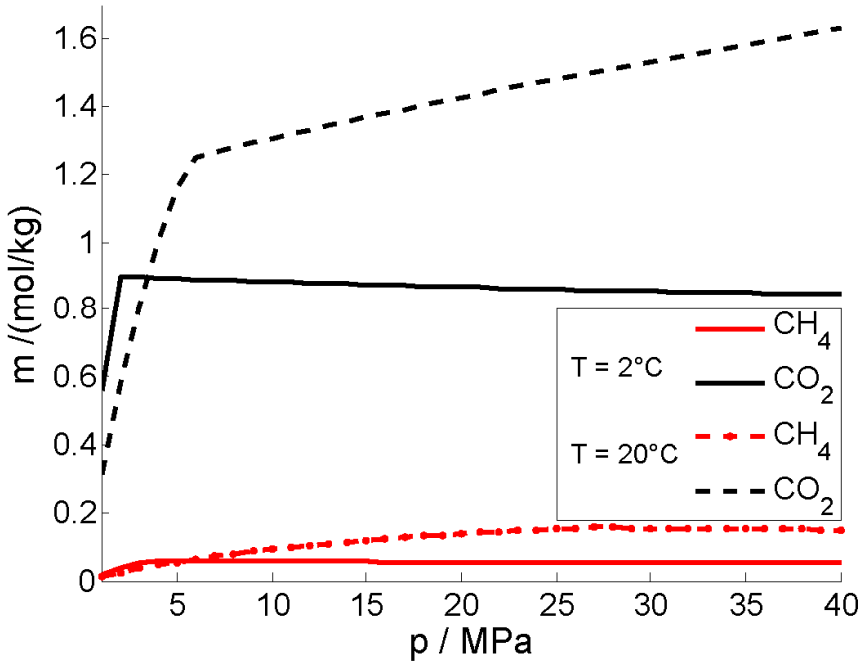

Figure 2.30: Solubilities of CO_2 and CH_4 in seawater as a function of pressure. A distinct change in solubility is observed at the gas/liquid phase transition of CO_2 (T = 20 ℃) and at the onset of gas hydrate formati on (T = 2 ℃).

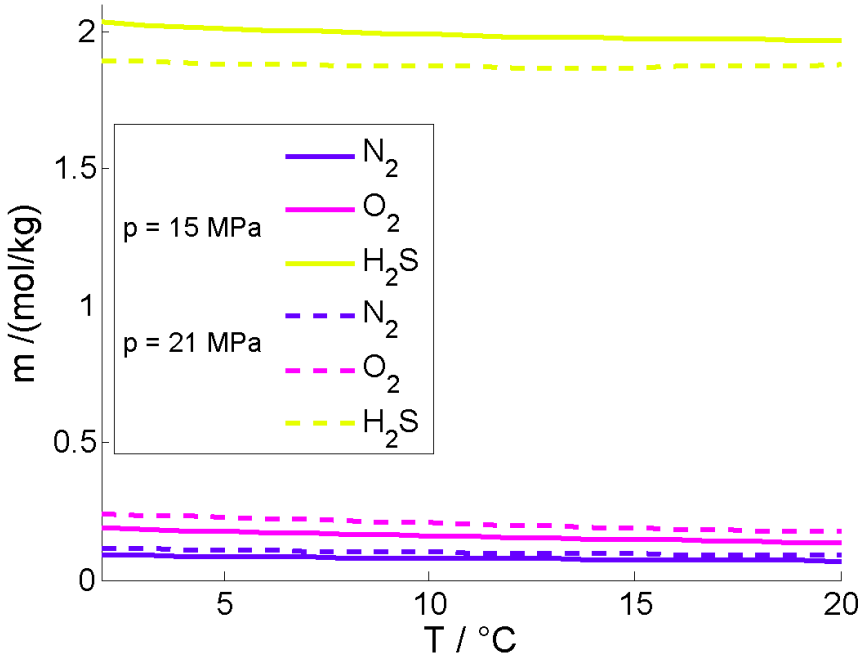

Figure 2.31: Solubilities of N_2, O_2 and H_2S in seawater as a function of temperature.

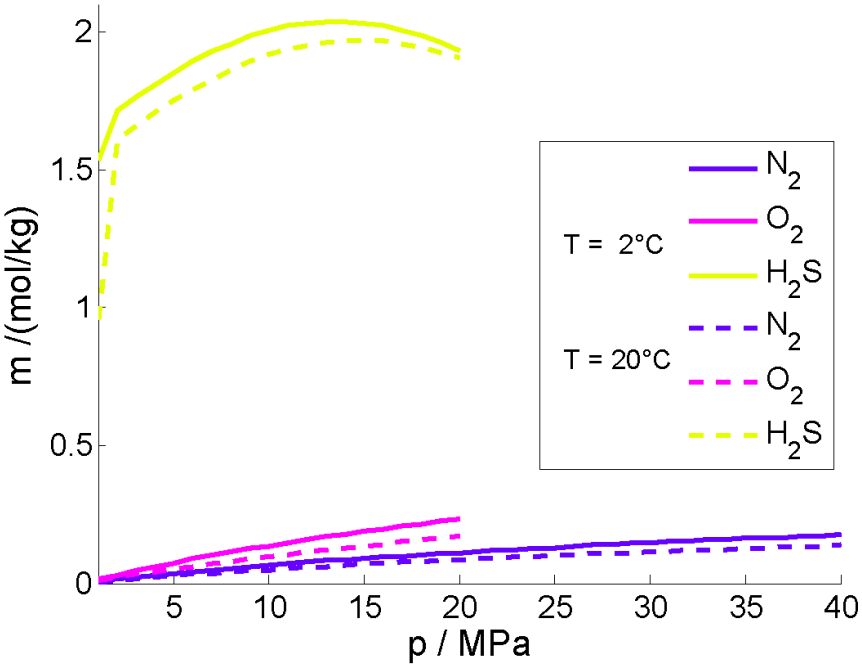

Figure 2.32: Solubilities of N_2, O_2 and H_2S in seawater as a function of pressure. A distinct change in solubility is observed at the H_2S gas/liquid phase transition.

2.9. Solubilities of H_2O, CH_4 and N_2 in CO_2 and of CO_2 in CH_4

To a small extent, water dissolves in liquid CO_2. The mole fraction of the dissolved water is in the order of a few tenth of a percent (Spycher et al., 2003). Equations for the calculation of the solubility of H_2O in CO_2 as a function of pressure, temperature and salinity have been derived by Spycher et al. (2003) and Tishchenko (unpublished).

Mole fractions of dissolved CH_4 and N_2 in liquid CO_2 can reach several tens of a percent (Al-Sahhaf et al., 1983). The standard approach for calculating solubilities in liquid CO_2 is by solving a multiphase equation of state with suitable interaction parameters.

SUGAR Toolbox:

Solubilities of water in CO_2 are calculated from Tishchenko's empirical equations in:
solu_swco2.m

Solubilities of CH_4 and N_2 in CO_2 are estimated from the multiphase Peng-Robinson equation of state that is utilized in the function *density_ch4co2n2.m* (see chapter 2.5): The gas concentration at which the phase separation (liquid → gas + liquid) occurs is returned as the solubility of the gas in liquid CO_2:
solu_ch4co2.m
solu_n2co2.m

solu_co2ch4.m
calculates the partial pressure of CO_2 in a CH_4 gas bubble from a Henry's law approach (Wong et al., 2005; Duan et al., 2008; Tishchenko, unpublished). The CO_2 concentration in the surrounding seawater is assumed to be the saturation concentration.

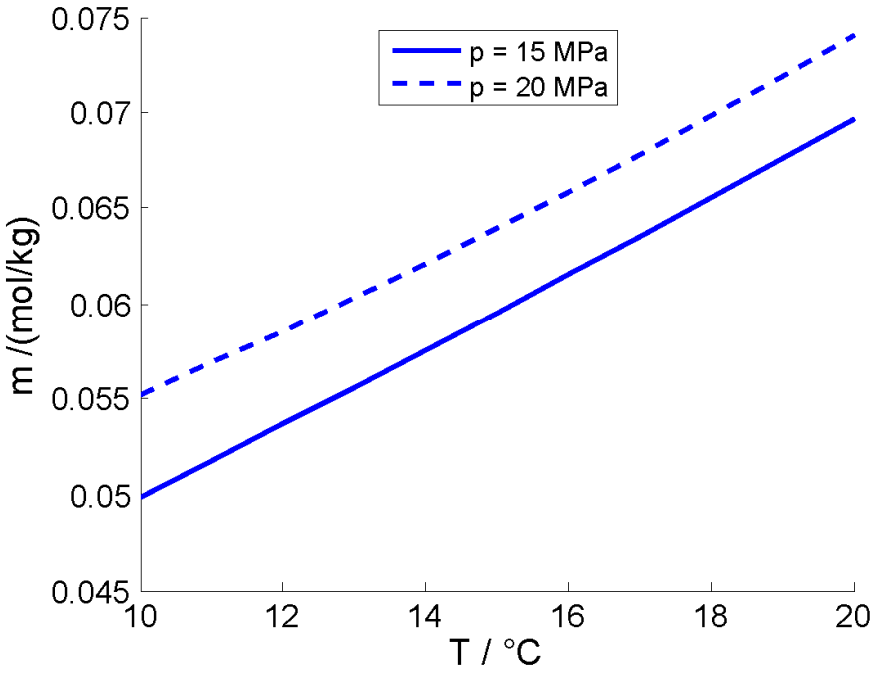

Figure 2.33: Solubility of H_2O in liquid CO_2 as a function of temperature.

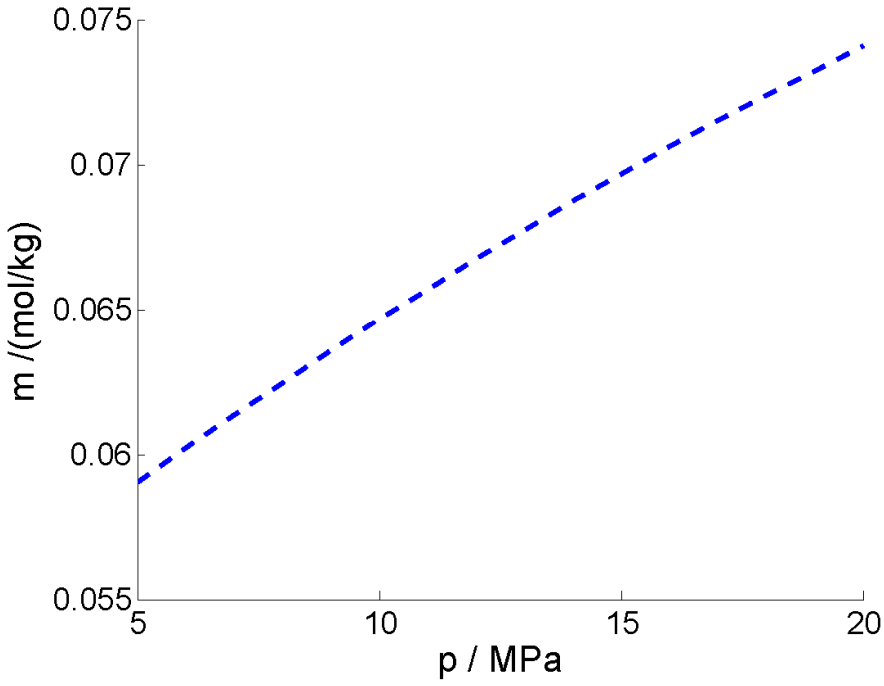

Figure 2.34: Solubility of H_2O in liquid CO_2 as a function of pressure at T = 20 ℃.

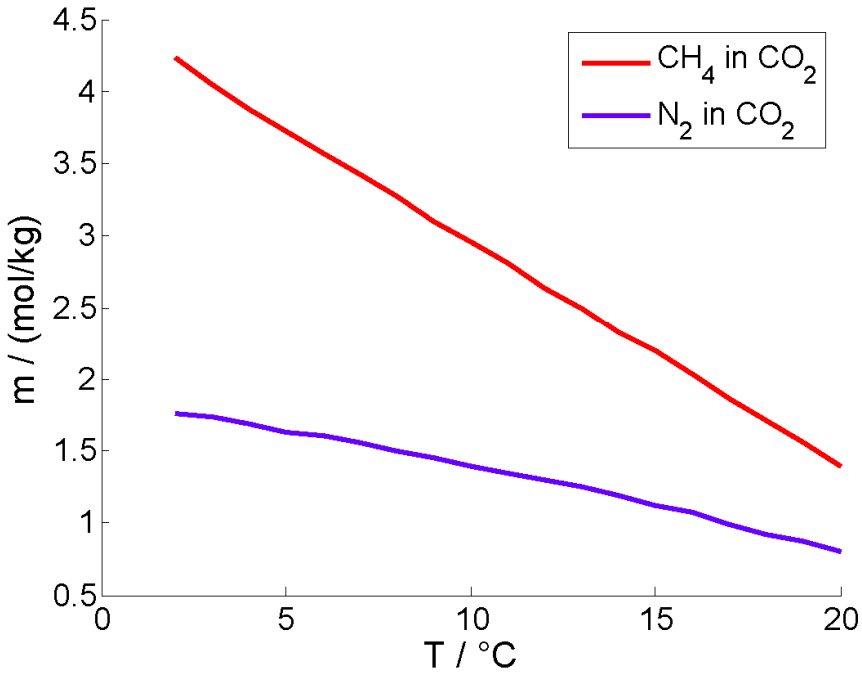

Figure 2.35: Solubilities of CH_4 and N_2 in liquid CO_2 as a function of temperature.

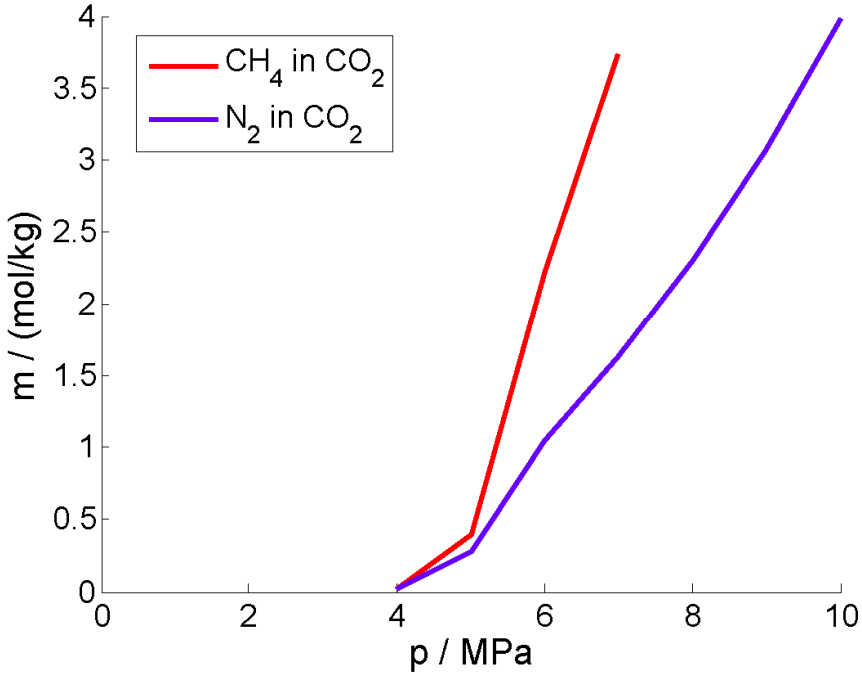

Figure 2.36: Solubilities of CH_4 and N_2 in liquid CO_2 as a function of pressure.

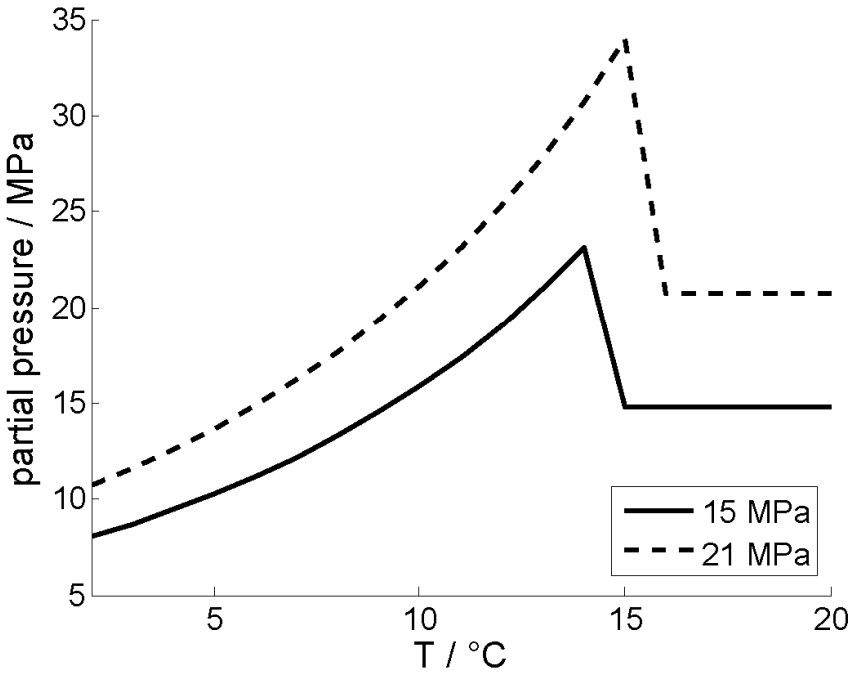

Figure 2.37: Partial pressure of CO_2 in CH_4 gas that is in equilibrium with CO_2-saturated seawater as a function of temperature. CO_2 hydrate formation causes a distinct change in solubility and thus in partial pressure.

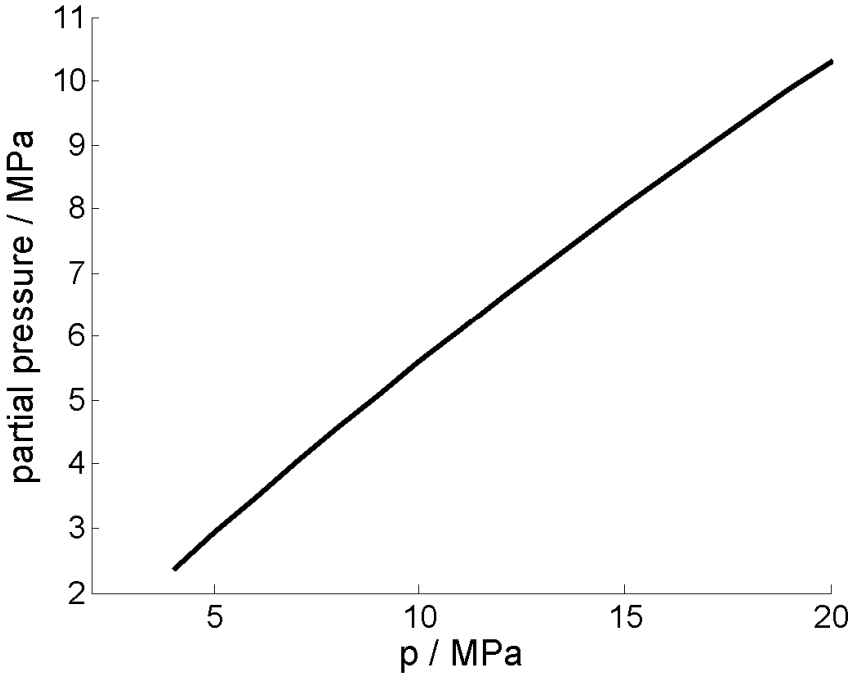

Figure 2.38: Partial pressure of CO_2 in CH_4 gas that is in equilibrium with CO_2-saturated seawater as a function of of pressure.

2.10. Solubilities of minerals in seawater

The solubility m of minerals in water depends on the activity coefficient of the dissolved mineral $\gamma_{\min}$ and the thermodynamic equilibrium constant for the dissolution process K (see chapter 2.11):

$$m = \frac{K}{\gamma_{\min}} \qquad \text{(Eq.2.10.1)}$$

K is determined by the change in Gibbs free energy ΔG during dissolution:

$$K = \exp\left(-\frac{\Delta G}{RT}\right) \qquad \text{(Eq.2.10.2)}$$

While the term for K dominates the temperature dependence of m, additional correction terms have to be included in Eq.2.10.2 to account for pressure-dependent variations. The basic equation for the pressure correction of K is:

$$RT\frac{\partial \ln K}{\partial p} = -\Delta V_m \qquad \text{(Eq.2.10.3)}$$

where ΔV_m is the change in partial molar volume of the reactants.
If the minerals are dissolved in an ionic solution such as seawater, the activity of the solvent a_W has to be explicitly included in Eq.2.10.1:

$$m = \frac{K\ a_W^n}{\gamma_{\min}} \qquad \text{(Eq.2.10.4)}$$

With n being the hydration number.

K is not to be confused with the solubility product K_L of a dissolution process:

$$K_L = \prod_{\mathrm{i}} a_{\mathrm{i}}{}^{\nu_{\mathrm{i}}} \qquad \text{(Eq.2.10.5)}$$

Here, a_i are the activities of the dissolved ions only and ν_i the stoichiometric coefficients.

SUGAR Toolbox:

The toolbox includes empirical multiparametric functions with pressure and salinity corrections for calculating the solubility product of $CaSO_4$ (gypsum, anhydrite and hemihydrate) (Marshall and Slusher, 1968; Blount and Dickson, 1973) and the solubilities of NaCl (Driesner, 2007; Driesner and Heinrich, 2007), opal (Fournier, 1983; Fournier and Marshall, 1983; Willey, 1974; Sun et al., 2008; Walther and Helgeson, 1977; Helgeson and Kirkham, 1974), and quartz (von Damm et al., 1991; Fournier, 1983) in (sea)water. For opal and quartz, two different functions are available covering different pressure, temperature and salinity ranges. The scripts *solu_opal.m* and *solu_quartz.m* choose the appropriate functions based on the input:

solu_caso4.m	solubility product of gypsum, anhydrite, hemihydrate
solu_nacl.m	solubility of NaCl
solu_opal.m	calling routine
solu_opalFournier.m	solubility of opal (Fournier and Marshall, 1983)
solu_opalWalther	solubility of opal (Walther and Helgeson, 1977)
solu_quartz	calling routine
solu_quartzFournier	solubility of quartz (Fournier, 1983)
solu_quartzDamm	solubility of quartz (von Damm et al., 1991)

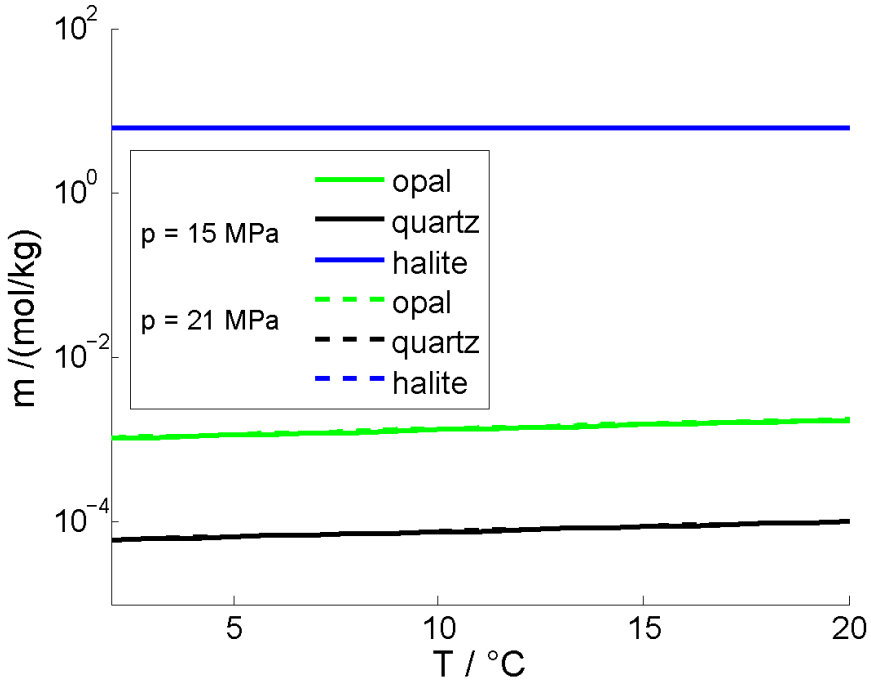

Figure 2.39: Solubilities of opal, quartz and halite as a function of temperature. Differences in solubility at different pressures are hardly visible in this representation.

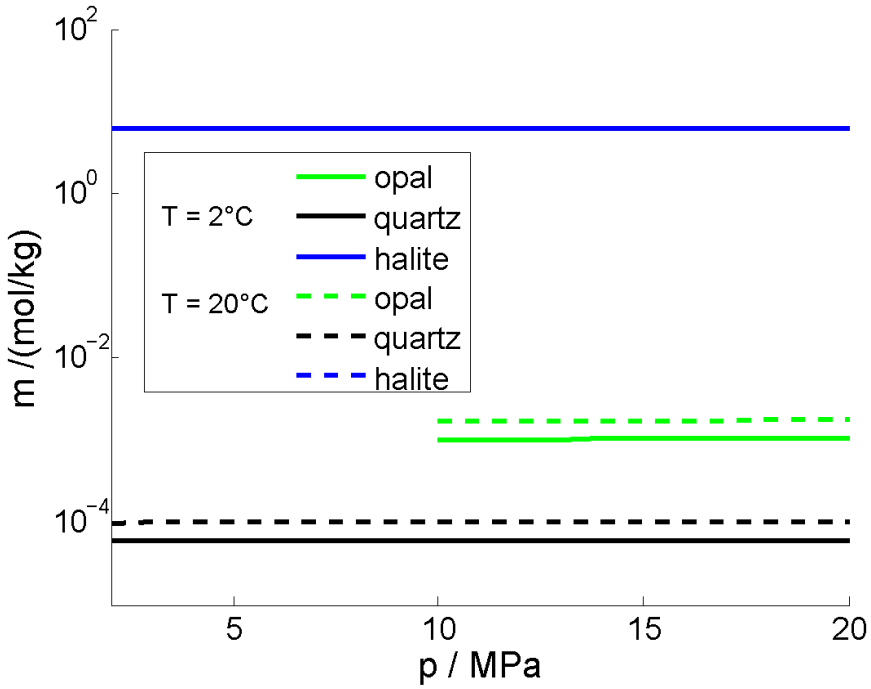

Figure 2.40: Solubilities of opal, quartz and halite as a function of pressure. Differences in halite solubility at different pressures are hardly visible in this representation.

2.11. Acid-base and mineral equilibria in seawater and CO_2-rich seawater

Equilibrium constants of chemical reactions in seawater are affected by temperature, pressure and salinity. The law of mass action relates the equilibrium constant K to the reactant's and product's activities a_i

$$K = \prod_i a_i^{\nu_i} \qquad \text{(Eq.2.11.1)}$$

where ν_i are the stoichiometric coefficients; $\nu_i < 0$ for educts and $\nu_i > 0$ for products.

As indicated by Eq.2.1.5, the presence of salt ions changes the activities of the reacting species. At high concentrations of CO_2, the calculation of the equilibrium constants must also include interactions between dissolved carbon dioxide molecules and between CO_2 and the salt components (Wong et al., 2005).

The temperature dependence of the equilibrium constants is described by van't Hoff's law:

$$\left(\frac{\mathrm{d}(\ln K)}{\mathrm{d}T}\right)_{p_0} = \frac{\Delta H^0}{RT^2} \qquad \text{(Eq.2.11.2)}$$

where ΔH^0 is the standard molar enthalpy change of the reaction. The temperature dependence of the enthalpy change is given by

$$\Delta H_{T_2}{}^0 - \Delta H_{T_1}{}^0 = \int_{T_1}^{T_2} C_{p_\mathrm{m}}\, dT \qquad \text{(Eq.2.11.3)}$$

where C_{p_m} is the molar isobaric heat capacity.

Equilibrium constants are often calculated from empirical functions of temperature and salinity at standard pressure and then explicitly corrected for pressure effects. The pressure correction accounts for the change in molar volume ΔV_m and the change in compressibility $\Delta\kappa$ with pressure and is an approximate solution of Eq.2.10.3:

$$\ln\left(K_p\right) = \ln\left(K_{p_0}\right) - \frac{\Delta V_\mathrm{m}}{RT}\, p + \mathrm{B}\Delta\kappa\frac{p^2}{2\mathrm{R}T} \qquad \text{(Eq.2.11.4)}$$

with B being an empirical constant.

Equilibrium constants for dissociation reactions of dissolved compounds and solubility products for minerals in water can be used to determine the ionic concentrations in the solution at equilibrium. The pH value of the solution is then defined as the negative decadal logarithm of the H^+ concentration.

SUGAR Toolbox:

Equilibrium constants and solubility products for various dissociation and dissolution reactions in seawater are calculated from empirical functions that depend on temperature and salinity. Pressure corrections are integrated in the form of Eq.2.11.4 (Boudreau, 1996; Clegg and Whitfield, 1995; Fofonoff and Millard, 1983; Luff et al., 2001; Millero, 1983; 1995; 2007; Millero et al., 2006; Stumm and Morgan, 1996; Van Cappellen and Wang, 1996; Zeebe and Wolf-Gladrow, 2001):

kequilib_sw.m	for reactions in seawater
kco2_sw.m	for carbonic acid dissociation in CO_2-rich seawater

ph_analyt.m
ph_model.m
access the above equilibrium constants to calculate the pH value and concentrations of dissociated species in mol/{kg H2O} of a user-defined system by either analytical solutions (less species) or numerical iteration.

References

Adewumi, M. (2013) *Phase Relations in Reservoir Engineering*. https://www.e-education.psu.edu/png520/resources/l1.html.

Al Ghafri, S., G. C. Maitland, et al. (2012). "Densities of aqueous $MgCl_2$(aq), $CaCl_2$(aq), KI(aq), NaCl(aq), KCl(aq), $AlCl_3$(aq), and (0.964 NaCl + 00136 KCl)(aq) at temperatures between (283 and 472) K, pressures up to 68.5 MPa, and molalities up to 6 mol.kg^{-1}." *Journal of Chemical and Engineering Data* **57**(4): 1288-1304.

Al-Sahhaf, T., A. Kidnay, et al. (1983). "Liquid + vapor equilibria in the N_2 + CO_2 + CH_4 system." *Industrial & Engineering Chemical Fundamentals* **22**: 372-380.

Ballard, A. L. and E. D. Sloan (2002). "The next generation of hydrate predicition. I. Hydrate standard states and incorporation of spectroscopy." *Fluid Phase Equilibria* **194-197**: 371-383.

Blount, C. and F. Dickson (1973). "Gypsum-anhydrite equilibria in systems $CaSO_4$-H_2O and $CaCO_3$-NaCl-H_2O." *American Mineralogist* **58**: 323-331.

Boudreau, B. P. (1996). "A method-of-lines code for carbon and nutrient diagenesis in aquatic sediments." *Computers & Geosciences* **22**(5): 479-496.

Clegg, S. L. and M. Whitfield (1995). "A chemical model of seawater including dissolved ammonia and the stoichiometric dissociation constant of ammonia in estuarine water and seawater from -2 to 40℃." *Geochimica et Cosmochimica Acta* **59**(12): 2403-2421.

Cole, W. and S. Goodwin (1990). "Flash calculations for gas hydrates: A rigorous approach." *Chemical Engineering Science* **45**(3): 569-573.

Driesner, T. and C. A. Heinrich (2007). "The system H_2O-NaCl. Part I: Correlation formulae for phase relations in temperature-pressure-composition space from 0 to 1000 ℃, 0 to 5000 bar, and 0 to 1 X-NaCl." *Geochimica et Cosmochimica Acta* **71**(20): 4880-4901.

Driesner, T. (2007). "The system H_2O-NaCl. Part II: Correlations for molar volume, enthalpy, and isobaric heat capacity from 0 to 1000 ℃, 1 to 5000 bar, and 0 to 1 X-NaCl." *Geochimica et Cosmochimica Acta* **71**(20): 4902-4919.

Duan, Z., N. Møller, et al. (1992). "An equation of state for the CH_4-CO_2-H_2O system: I. Pure systems from 50 to 1000℃ and 0 to 8000 bar." *Geochimica et Cosmochimica Acta* **56**: 2605-2617.

Duan, Z. H., N. Moller, et al. (1996). "Prediction of the solubility of H_2S in NaCl aqueous solution: An equation of state approach." *Chemical Geology* **130**(1-2): 15-20.

Duan, Z. H. and R. Sun (2003). "An improved model calculating CO_2 solubility in pure water and aqueous NaCl solutions from 273 to 533 K and from 0 to 2000 bar." *Chemical Geology* **193**(3-4): 257-271.

Duan, Z., R. Sun, et al. (2006). "An improved model for the calculation of CO_2 solubility in aqueous solutions containing Na^+, K^+, Ca^{2+}, Mg^{2+}, Cl^-, and SO_4^{2-}." *Marine Chemistry* **98**: 131-139.

Duan, Z. and R. Sun (2006). "A model to predict phase equilibrium of CH_4 and CO_2 clathrate hydrate in aqueous electrolyte solutions." *American Mineralogist* **91**: 1346-1354.

Duan, Z. and S. Mao (2006). "A thermodynamic model for calculating methane solubility, density and gas phase composition of methane-bearing aqueous fluids from 273 to 523 K and from 1 to 2000 bar." *Geochimica et Cosmochimica Acta* **70**: 3369-3386.

Duan, Z. H., R. Sun, et al. (2007). "Accurate thermodynamic model for the calculation of H_2S solubility in pure water and brines." *Energy & Fuels* **21**(4): 2056-2065.

Duan, Z., J. Hu, et al. (2008). "Densities of the CO_2–H_2O and CO_2–H_2O–NaCl systems up to 647 K and 100 MPa." *Energy & Fuels* **22**: 1666-1674.

Feistel, R. (2008). "A Gibbs function for seawater thermodynamics for -6 to 80 ℃ and salinity up to 1 20 g/kg." *Deep-Sea Research I* **55**: 1639-1671.

Fofonoff, N. C. and R. C. Millard (1983). "Algorithms for computation of fundamental properties of seawater." *Unesco Technical Papers in Marine Science* **44**: 1-53.

Fournier, R. (1983). "A method of calculating quartz solubilities in aqueous sodium chloride solutions." *Geochimica et Cosmochimica Acta* **47**: 579-586.

Fournier, R. and W. Marshall (1983). "Calculation of amorphous silica solubilities at 25℃ to 300℃ an d apparent cation hydration numbers in aqueous salt solutions using the concept of effective density of water." *Geochimica et Cosmochimica Acta* **47**: 587-596.

Geng, M. and Z. H. Duan (2010). "Prediction of oxygen solubility in pure water and brines up to high temperatures and pressures." *Geochimica et Cosmochimica Acta* **74**(19): 5631-5640.

Gupta, A. (2007). *Methane hydrate dissociation measurements and modelling: The role of heat transfer and reaction kinetics*. PhD Thesis Colorado School of Mines.

Harvey, A. (1996). "Semiempirical correlation for Henry's constant over large temperature ranges." *American Institute of Chemical Engineers Journal* **42**(5): 1491-1494.

Helgeson, H. and D. Kirkham (1974). "Theoretical prediction of the thermodynamic behavior of aqueous electrolytes at high pressure and temperatures: I. Summary of the thermodynamic/electrostatic properties of the solvent." *American Journal of Science* **274**: 1089-1198.

Henry, W. (1803). "Experiments on the quantity of gases absorbed by water at different temperatures and under different pressures*." Philosophical Transactions of the Royal Society of London* **93**: 29-42.

Hu, J. W., Z. H. Duan, et al. (2007). "PVTx properties of the CO_2-H_2O and CO_2-H_2O-NaCl systems below 647 K: Assessment of experimental data and thermodynamic models." *Chemical Geology* **238**(3-4): 249-267.

IAPS (1984). *IAPS Formulation 1984 for the Thermodynamic Properties of Ordinary Water Substance for Scientific and General Use*. http://iapws.org.

IAPWS (1992). *Revised supplementary release on saturation properties of ordinary water substance*. http://iapws.org.

IAPWS (1996). *Release on the IAPWS formulation 1995 for the thermodynamic properties of ordinary water substance for general and scientific use*. http://iapws.org.

IAPWS (2007). *Revised Release on the IAPWS Industrial Formulation 1997 for the Thermodynamic Properties of Water and Steam*. http://iapws.org.

IAPWS (2008). *Release on the IAPWS formulation 2008 for the thermodynamic properties of seawater*. http://iapws.org.

Jager, M. D., A. L. Ballard, et al. (2003). "The next generation of hydrate predicition. II. Dedicated aqueous phase fugacity model for hydrate prediction." *Fluid Phase Equilibria* **211**: 85-107.

Kestin, J. and J. V. Sengers (1986). "New international formulations for the thermodynamic properties of light and heavy water." *Journal of Physical and Chemical Reference Data* **15**(1): 305-320.

Klauda, J. and S. Sandler (2000). "A fugacity model for gas hydrate phase equilibria." *Industrial & Engineering Chemistry Research* **39**: 3377-3386.

Klauda, J. and S. Sandler (2003). "Phase behavior of clathrate hydrates: a model for single and multiple gas component hydrates." *Chemical Engineering Science* **58**: 27-41.

Krichevski, I. and J. Kasarnovski (1935). "Thermodynamical calculations of solubilities of nitrogen and hydrogen in water at high pressures." *Journal of the American Chemical Society* **57**: 2168-2172.

Luff, R., M. Haeckel, et al. (2001). "Robust and fast FORTRAN and MATLAB libraries to calculate pH distributions in a non-steady state model for aqueous systems." *Computers & Geosciences* **27**(2): 157-169.

Mao, S. D. and Z. H. Duan (2006). "A thermodynamic model for calculating nitrogen solubility, gas phase composition and density of the N-2-H2O-NaCl system." *Fluid Phase Equilibria* **248**(2): 103-114.

Marcus, Y. (2000). "Supercritical water: relationships of certain measured properties to the extent of hydrogen bonding obtained from a semi-empirical model." *Physical Chemistry Chemical Physics*

2(7): 1465-1472.

Marshall, W. and R. Slusher (1968). "Solubility to 200℃ of calcium sulfate and its hydrates in sea wa ter and saline water concentrates, and temperature-concentration limits." *Journal of Chemical and Engineering Data* **13**(1): 83-93.

Michelsen, M. L. (1982). "The isothermal flash problem. Part 1. Stability." *Fluid Phase Equilibria* **9**: 1-19.

Millero, F. J. (1983). “Influence of pressure on chemical processes in the sea.” In: *Chemical Oceanography* **Vol. 8** (eds.) J. P. Riley and R. Chester, Academic Press: 1-88.

Millero, F. J. (1995). "Thermodynamics of the carbon dioxode system in the oceans." *Geochimica et Cosmochimica Acta* **59**(4): 661-677.

Millero, F., T. Graham, et al. (2006). "Dissociation constants of carbonic acid in seawater as a function of salinity and temperature." *Marine Chemistry* **100**: 80-94.

Millero, F. J. (2007). "The marine inorganic carbon cycle." *Chemical Reviews* **107**: 308-341.

Millero, F. J., R. Feistel, et al. (2008). "The composition of standard seawater and the definition of the reference-composition salinity scale." *Deep-Sea Research I* **55**(1): 50-72.

Parrish, W. and J. Prausnitz (1972). "Dissociation pressures of gas hydrates formed by gas mixtures." *Industrial & Engineering Chemistry Process Design and Development* **11**: 26-35.

Peng, D. and D. Robinson (1976). "A new two-constant equation of state." *Industrial and Engineering Chemistry Fundamentals* **15**(1): 59-64.

Pitzer, K. (1973). "Thermodynamics of electrolytes. I. Theoretical basis and general equations." *Journal of Physical Chemistry* **77**(2): 268-277.

Plyasunov, A. V., J. P. O'Connell, et al. (2000). "Infinite dilution partial molar properties of aqueous solutions of nonelectrolytes. I. Equations for partial molar volumes at infinite dilution and standard thermodynamic functions of hydration of volatile nonelectrolytes over wide ranges of conditions." *Geochimica et Cosmochimica Acta* **64**(3): 495-512.

Poisson, A., M. Gadhoumi, et al. (1991). "Salinity and density of seawater: Tables for high salinities (42 to 50)." *Unesco Technical Papers in Marine Science* **62**.

Reamer, H. H., B. H. Sage, et al. (1950). "Volumetric behavior of hydrogen sulfide." *Industrial and Engineering Chemistry* **1**(1): 140-143.

Redlich, O. and J. Kwong (1949). "On the thermodynamics of solutions V: An equation of state. Fugacities of gaseous solutions." *Chemical Reviews* **44**: 233-244.

Risnes, R., V. Dalen, et al. (1981). "Phase equilibrium calculations in the near critical region." *Developments in Petroleum Science* **13**: 329-350.

Schmidt, R. and W. Wagner (1985). "A new form of the equation of state for pure substances and its application to oxygen." *Fluid Phase Equilibria* **19**: 175-200.

Setchenov, J. (1889). *Zeitschrift für Physikalische Chemie* **4**: 117-125.

Setzmann, U. and W. Wagner (1991). "A new equation of state and tables of thermodynamic properties for methane covering the range from the melting line to 625 K at pressures up to 1000 MPa." *Journal of Physical and Chemical Reference Data* **20**(6): 1061-1155.

Shibue, Y. (2003). "Vapor pressures of aqueous NaCl and $CaCl_2$ solutions at elevated temperatures." *Fluid Phase Equilibria* **213**(1-2): 39-51.

Sloan, E. D. and C. A. Koh (2008). *Clathrate Hydrates of Natural Gases*. Boca Raton, CRC Press.

Soave, G. (1972). "Equliibrium constants from a modified Redlich-Kwong equation of state." *Chemical Engineering Science* **27**(6): 1197-1340.

Span, R. and W. Wagner (1996). "A new equation of state for carbon dioxide covering the fluid region from the triple-point temperature to 1100 K at pressures up to 800 MPa." *Journal of Physical and Chemical Reference Data* **25**(6): 1509-1596.

Span, R., E. W. Lemmon, et al. (2000). "A reference equation of state for the thermodynamic properties

of nitrogen for temperatures from 63.151 to 1000 K and pressures to 2200 MPa." *Journal of Physical and Chemical Reference Data* **29**(6): 1361-1433.

Spivey, J. P. and W. D. McCain (2004). "Estimating density, formation volume factor, compressibility, methane solubility, and viscosity for oilfield brines at temperatures from 0 to 275 ℃, pressures to 200 MPa and salinities to 5.7 mol/kg." *Journal of Canadian Petroleum Technology* **43**(7): 52-61.

Spycher, N., K. Pruess, et al. (2003). "CO_2-H_2O mixtures in the geological sequestration of CO_2. I. Assessment and calculation of mutual solubilities from 12 to 100℃ and up to 600 bar." *Geochimica et Cosmochimica Acta* **67**(16): 3015-3031.

Stumm, W. and J. J. Morgan (1996). *Aquatic Chemistry*. New York, John Wiley & Sons.

Sun, R. and Z. Duan (2005). "Prediction of CH_4 and CO_2 hydrate phase equilibrium and cage occupancy from ab initio intermolecular potentials." *Geochimica et Cosmochimica Acta* **69**(18): 4411-4424.

Sun, H. B., R. Feistel, et al. (2008). "New equations for density, entropy, heat capacity, and potential temperature of a saline thermal fluid." *Deep-Sea Research I* **55**(10): 1304-1310.

Tishchenko, P., C. Hensen, et al. (2005). "Calculation of the stability and solubility of methane hydrate in seawater." *Chemical Geology* **219**: 37-52.

Tishchenko, P. Y., Wong, C. S., et al. (2009). “Stability and solubility of CO_2 hydrate in seawater.” *8th International Carbon Dioxide Conference*, Jena, Germany.

Van Cappellen, P. and Y. Wang (1996). "Cycling of iron and manganese in surface sediments: General theory for the coupled transport and reaction of carbon, oxygen, nitrogen, sulfur, iron, and manganese." *American Journal of Science* **296**: 197-243.

Van der Waals, J. H. and J. C. Plateeuw (1959). "Clathrate solutions." *Advances in Chemical Physics* **2**: 1-57.

Velasco, S., F. L. Roman, et al. (2008). "A predictive vapor-pressure equation." *Journal of Chemical Thermodynamics* **40**(5): 789-797.

Von Damm, K., J. Bischoff, et al. (1991). "Quartz solubility in hydrothermal seawater: an experimental study and equation describing quartz solubilities for up to 0.5 m NaCl solutions." *American Journal of Science* **291**: 977-1007.

Wagner, W. and A. Pruß (1993). "International equations for the saturation properties of ordinary water substance. Revised according to the International Temperature Scale of 1990." *Journal of Physical and Chemical Reference Data* **22**(3): 783-787.

Wagner, W. and A. Pruß (2002). "The IAPWS formulation 1995 for the thermodynamic properties of ordinary water substance for general and scientific use." *Journal of Physical and Chemical Reference Data* **31**(2): 387-535.

Walther, J. and H. Helgeson (1977). "Calculations of the thermodynamic properties of aqueous silica and the solubility of quartz and its polymorphs at high pressures and temperatures." *American Journal of Science* **277**: 1315-1351.

Weiss, R. (1974). "Carbon dioxide in water and seawater: The solubility of a non-ideal gas." *Marine Chemistry **2**: 2*03-215.

Willey, J. (1974). "The effect of pressure on the solubility of amorphous silica in seawater at 0℃." *Marine Chemistry* **2**: 239-250.

Wong, C. S., P. Y. Tishchenko, et al. (2005). "Effects of high CO_2 molality on the carbon dioxide equilibrium of seawater." *Journal of Chemical and Engineering Data* **50**: 822-831.

Zeebe, R. and D. Wolf-Gladrow (2001). *CO_2 in Seawater: Equilibrium, Kinetics, Isotopes*. Elsevier.

3. Properties for heat and mass transport

3.1. Viscosities of H_2O, seawater, CH_4, CO_2 and N_2

The dynamic viscosity η is a measure for the internal frictional forces of a liquid. In a first-order approximation, the viscosity is assumed to depend on temperature T only. For liquids, an Arrhenius-type expression can be used to describe the decrease in viscosity with increasing temperature:

$$\eta^{\mathrm{l}} = \mathrm{A}\exp\left(-\mathrm{B}T\right) \qquad \text{(Eq.3.1.1)}$$

where A and B are constants.

For gases, the viscosity increases with increasing temperature:

$$\eta^{\mathrm{g}} = \mathrm{D}\frac{T^{1.5}}{T+\mathrm{C}} \qquad \text{(Eq.3.1.2)}$$

Here, D and C are constants.

A more accurate procedure to calculate the viscosity of real gases and liquids is to use experimentally validated empirical functions to calculate the viscosity of the ideal gas and then to add one or more correction terms, that account for interactions in dense gases or liquids, as well as a critical enhancement term describing the change of the viscosity in the vicinity of the critical point (Hanley et al., 1977; Fenghour et al., 1998; Lemmon and Jacobsen, 2004; IAPWS, 2008). These terms are polynomial functions of density and temperature.

For seawater, a dense fluid, the standard approach is to use polynomial functions of pressure, temperature and salinity that were fitted to experimental data (Kestin et al., 1978; Kukulka et al., 1987; Spivey and McCain, 2004; Mao and Duan, 2009). Palliser and McKibbin (1998) use a slightly different strategy and combine the viscosities of pure water and pure NaCl to calculate brine viscosities.

Bando et al. (2004) deduced from the regression of experimental data that the viscosity of saltwater η_{SW} changes in the presence of dissolved CO_2 according to:

$$\eta_{\mathrm{CSW}} = \eta_{\mathrm{SW}}\left(1+\mathrm{f}(T)\frac{x_{\mathrm{C}}}{x_{\mathrm{SW}}}\right) \qquad \text{(Eq.3.1.3)}$$

where η_{CSW} is the viscosity of the CO_2-saltwater solution, x_{SW} and x_{C} are the mole fractions of saltwater and CO_2, respectively, and $\mathrm{f}(T)$ is a function of temperature.

No published data could be found for the viscosity of (sea)water with dissolved methane. Due to the small solubility of methane, the effect is assumed to be negligible.

SUGAR Toolbox:

The toolbox functions
visco_h2o.m
visco_co2.m
visco_ch4.m
visco_n2.m
use the empirical equations of IAPWS (2008), Fenghour et al. (1998), Hanley et al. (1977), and Lemmon and Jacobsen (2004) to calculate the viscosity of water, CO_2, CH_4 and N_2, respectively.

The toolbox includes several functions to calculate seawater viscosities covering different pressure, temperature and salinity ranges, including extreme conditions of high temperatures, pressures and salinities. The function
visco_sw.m
uses by default the formalism of Kukulka et al. (1987), which covers most of the pTS conditions in the open ocean. An additional flag can be set to call any of the following functions instead:
visco_swSpivey.m
visco_swMao.m
visco_swPalliser.m
These functions cover larger pTS ranges including hydrothermal brines. They can also be called directly.

The empirical equation of Bando et al. (2004) calculates the viscosity of seawater containing dissolved CO_2:
visco_co2sw.m

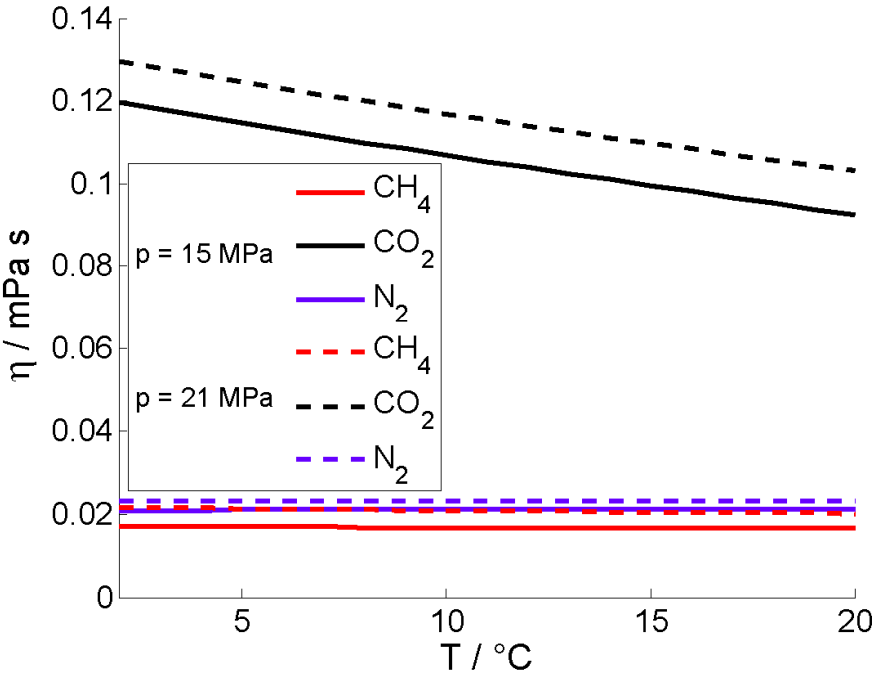

Figure 3.1: Viscosities of CH_4, CO_2 and N_2 as a function of temperature.

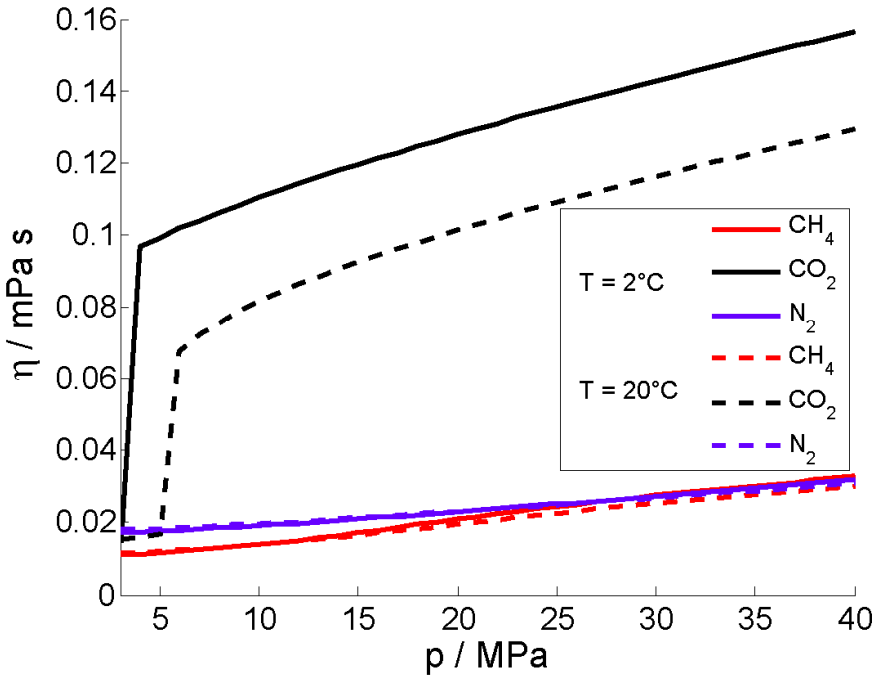

Figure 3.2: Viscosities of CH_4, CO_2 and N_2 as a function of pressure. A steep increase in viscosity results from the gas/liquid phase transition of CO_2.

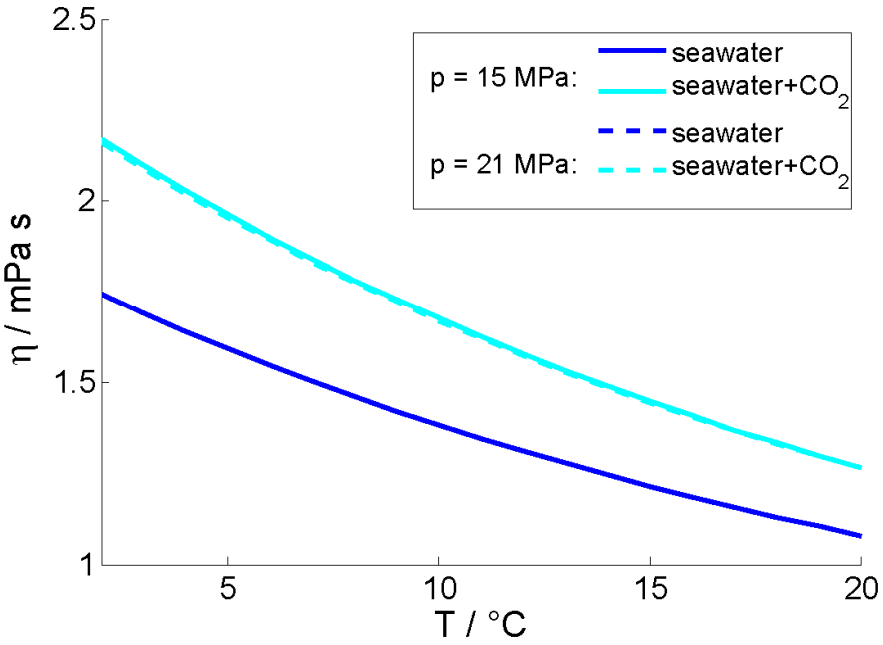

Figure 3.3: Viscosities of seawater and seawater saturated with CO_2 as a function of temperature. The curves at the two different pressures are almost identical.

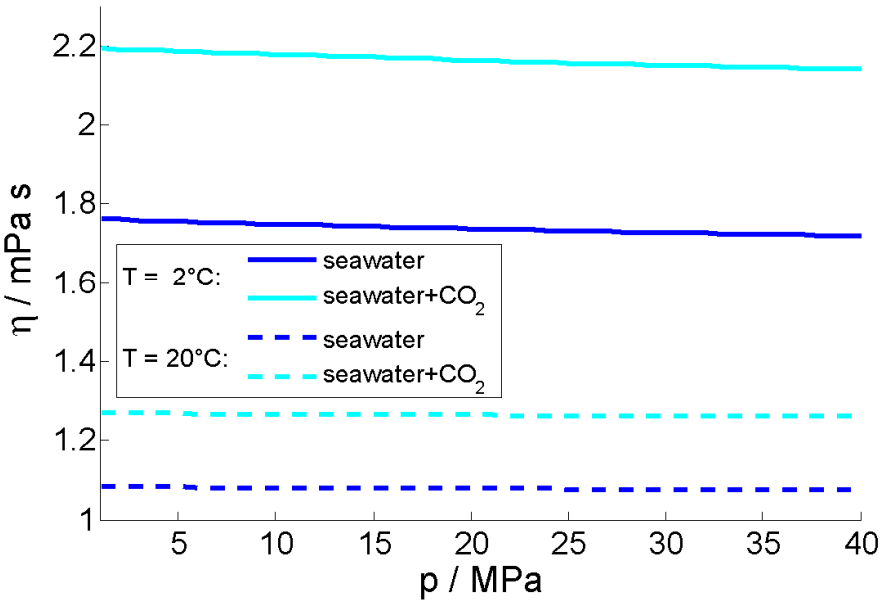

Figure 3.4: Viscosities of seawater and seawater saturated with CO_2 as a function of pressure.

3.2. Diffusion coefficients in seawater and sediment

Diffusion is caused by random motions of molecules and ions. The macroscopic result of this phenomenon is the transfer of solutes from areas of high concentrations to areas of low concentrations. The mass flux J is described by Fick's first law of diffusion:

$$\mathbf{J} = -D\nabla c \qquad \text{(Eq.3.2.1)}$$

where D is the diffusion coefficient , ∇ is the differential Nabla operator $\left(\frac{\partial}{\partial x}, \frac{\partial}{\partial y}, \frac{\partial}{\partial z}\right)$ and c is the concentration of the solute. The change in concentration over time is then described by Fick's second law:

$$\frac{\partial c}{\partial t} = \nabla \cdot (D\nabla c) \qquad \text{(Eq.3.2.2)}$$

The diffusion coefficient is a function of pressure, temperature and salinity. A first approximation for the diffusion of uncharged particles in liquids at infinite dilution is the Stokes-Einstein equation. It assumes spherical particles of radius r diffusing in a solvent with viscosity η that is composed of molecules which are much smaller than the molecules of the solute. The diffusion coefficient is then given by:

$$D = \frac{\mathrm{k_B} T}{6\pi \eta \mathrm{r}} \qquad \text{(Eq.3.2.3)}$$

with $\mathrm{k_B}$ being the Boltzmann constant. If charged particles are considered, the Nernst-Einstein equation has to be used instead:

$$D = \frac{\mathrm{R} T \Lambda}{(z\mathrm{F})^2} \qquad \text{(Eq.3.2.4)}$$

where F is the Faraday constant and Λ is the equivalent conductivity.

Theoretical expressions for diffusion coefficients need to idealize the shape and the interactions of solute and solvent molecules. Their accuracy is therefore limited. More reliable calculations are possible with empirical expressions. Most of them are low order polynomial functions or exponential functions with respect to temperature. An overview of different models for diffusion coefficients of molecules and ions in (sea)water is presented in Boudreau (1997). Effects of pressure and salinity on the diffusion coefficient are considered by taking into account the corresponding changes in viscosity. From the Stokes-Einstein equation at constant temperature, it follows that

$$D\eta\big|_{T=\mathrm{const}} = \mathrm{const} \qquad \text{(Eq.3.2.5)}$$

Hence, the molecular diffusion coefficient can be derived from the diffusion coefficient at reference pressure and salinity by multiplying with the respective relative viscosity change. Eq.3.2.3 can also be used for a temperature correction, if a more accurate equation is not available:

$$\left.\frac{D}{T}\right|_{\eta=\mathrm{const}} = \mathrm{const} \qquad \text{(Eq.3.2.6)}$$

In porous media, however, the actual path that a dissolved species moves along is longer than the direct distance between two points (Fig. 3.10). Hence, the molecular diffusion coefficient needs to be corrected for this effect. The tortuosity θ is the ratio of the average length of the shortest path between two points $\mathrm{d}L$ and their direct distance $\mathrm{d}x$:

$$\theta = \frac{\mathrm{d}L}{\mathrm{d}x} \qquad \text{(Eq.3.2.7)}$$

Boudreau (1997) lists a number of empirically or theoretically derived relations between the porosity ϕ, which is an measurable parameter, and the tortuosity (see chapter 3.5). A good fit to available data could be derived with the relation:

$$\theta^2 = 1 - 2\log(\phi) \qquad \text{(Eq.3.2.8)}$$

Once the tortuosity is known, the effective diffusion coefficient D_{eff} can be calculated from the molecular diffusion coefficient D:

$$D_{\mathrm{eff}} = \frac{D}{\theta^2} \qquad \text{(Eq.3.2.9)}$$

SUGAR Toolbox:

diffcoeff_sw.m
calculates the diffusion coefficients of the most relevant gases, moelcules and ions in seawater based on empirical equations (Hayduk and Laudie, 1974; Li and Gregory, 1974; Boudreau, 1997). The diffusion coefficients are functions of pressure, temperature and salinity. The influence of dissolved CO_2 is integrated by considering the corresponding change in viscosity.
Included species are: O_2, NO_3^-, Mn^{2+}, Fe^{2+}, SO_4^{2-}, CH_4, HS^-, H_2S, NH_4^+, NH_3, PO_4^{3-}, HPO_4^{2-}, $H_2PO_4^-$, H_2O, H^+, OH^-, CO_2, HCO_3^-, CO_3^{2-}, $B(OH)_3$, $B(OH)_4^-$, Mg^{2+}, Ca^{2+}, Ba^{2+}, Sr^{2+}, Cl^-, Br^-, Li^+, SiO_4^-, He, Ne, Ar, Kr, Xe, Rn, N_2

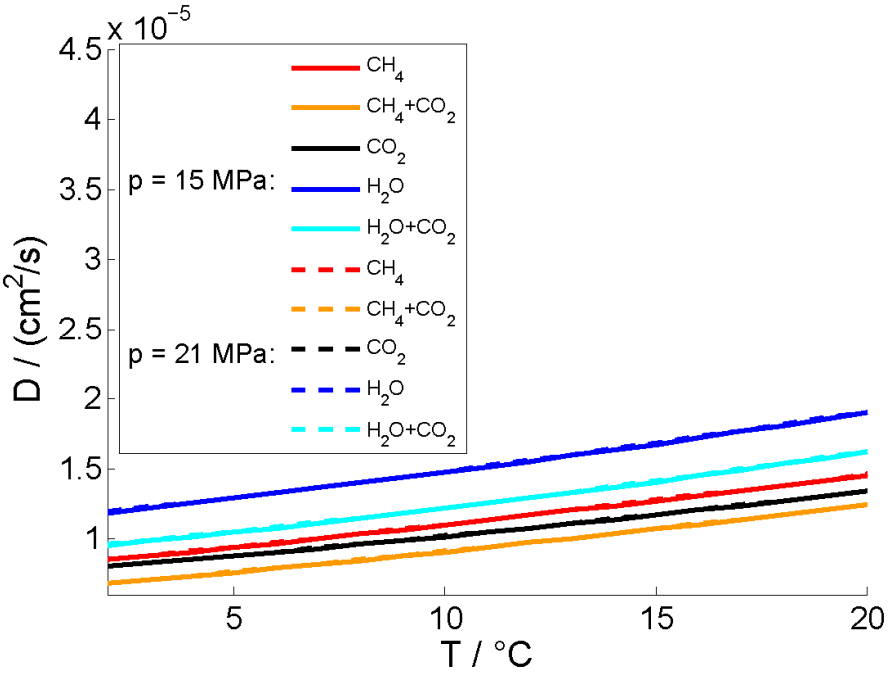

Figure 3.5: Diffusion coefficients for the molecules CH_4, CO_2 and H_2O in seawater and CO_2-saturated seawater (+CO_2) as a function of temperature. The curves for the two different pressures are almost identical.

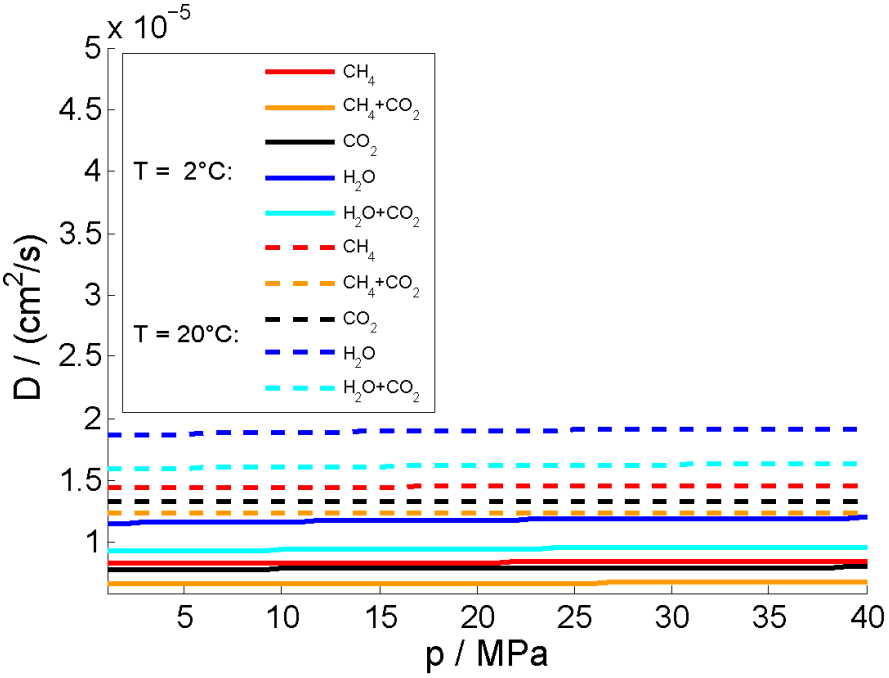

Figure 3.6: Diffusion coefficients for the molecules CH_4, CO_2 and H_2O in seawater and CO_2-saturated seawater (+CO_2) as a function of pressure.

3.3. Diffusion coefficients in CO_2

Supercritical CO_2 is an excellent solvent for lipophilic organic compounds. Almost all research that has been conducted on diffusion of molecules in CO_2 is related to this application. To our knowledge, the only publication that deals with the diffusion of water in liquid CO_2 is Xu et al. (2003). This paper presents experimental data, but does not include a theoretical model. Publications concerning the diffusion of salt ions or methane in liquid CO_2 could not be found.

SUGAR Toolbox:

diffcoeff_co2h2o.m
calculates the diffusion coefficient of water in liquid carbon dioxide from a function, that was fitted to the published data points of Xu et al. (2003).

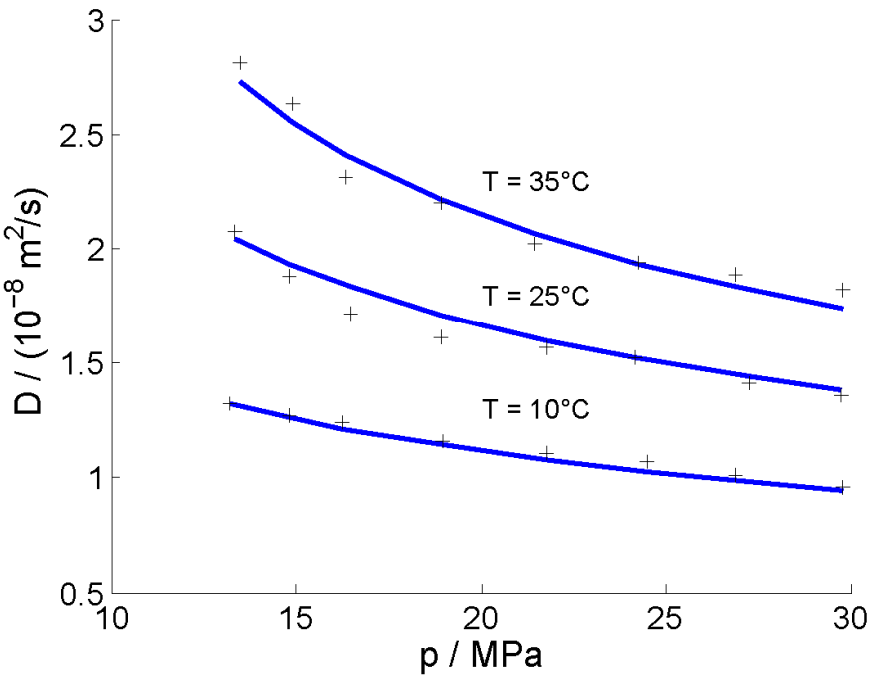

Figure 3.7: Diffusion coefficients of H_2O dissolved in liquid CO_2: Experimental data (crosses) from Xu et al. (2003) and fitted equation (lines).

3.4. Thermal conductivites of sediment, H_2O, seawater, gas hydrate, CO_2, CH_4 and N_2

Heat conduction is a transfer of thermal energy driven by a temperature gradient. The mathematical equations describing this process are similar to Fick's laws for diffusion: The heat flux J_q is derived from Fourier's first law:

$$\mathbf{J}_q = -\lambda \nabla T \qquad \text{(Eq.3.4.1)}$$

where λ is the thermal conductivity. Analogously, the temperature change over time is derived from Fourier's second law:

$$\frac{\partial T}{\partial t} = \nabla \cdot (\lambda \nabla T) \qquad \text{(Eq.3.4.2)}$$

The thermal conductivity for real gases and liquids is often calculated from the thermal conductivity of the ideal gas with one or more correction terms that account for interactions in dense gases or liquids and a critical enhancement term that describes the change of the thermal conductivity in the vicinity of the critical point (Scalabrin et al., 2007; Hanley et al., 1977; Lemmon and Jacobsen, 2004). These terms are polynomial functions of density and temperature.

Seawater is a dense matter that cannot be approximated by a dilute phase. Therefore, a single polynomial function of pressure, temperature and salinity is used to calculate its thermal conductivity (Caldwell, 1974).

Various authors have published values of the thermal conductivity of methane hydrate (see Appendix A.2). Sloan and Koh (2007) specify λ_{MH} to be 0.5 W/(m K), whereas more recent publications state slightly higher values of 0.62 W/(m K) (Waite et al., 2007) and 0.68 W/(m K) (Rosenbaum et al., 2007). The temperature and pressure dependencies of the published correlations are very small. In the pressure and temperature range of typical interest, they are within the range of uncertainty of the experimental data. Therefore, the thermal conductivity values of gas hydrates can be assumed independent of pressure and temperature. No published data could be found for the thermal conductivity of CO_2 hydrate, but its value is expected to be similar to that of methane hydrate (Mellon, 1996).

Large variations are reported for the thermal conductivity of the sediment matrix (see Appendix A.2). The value strongly depends on the composition of the sediment. Thermal conductivities for common sediment forming minerals are provided by Horai (1971). They range from 1.8 W/(m K) for illite to 19.2 W/(m K) for pyrite. As a consequence, the thermal conductivities of sedimentary rocks typically vary between 0.5 W/(m K) and 8.3 W/(m K) with mean values of 2-3 W/(m K) (Aplin et al., 1999).

Several models exist to derive the thermal conductivity of wet sediment from the thermal conductivity of the sedimentary rock λ_S and the thermal conductivity of the pore fluid λ_L. Among these models, three relatively simple relationships are most

commonly used: the arithmetic mean, the harmonic mean and the geometric mean (e.g., Aplin et al., 1999; Buntebarth and Schopper, 1998; Maxwell, 1873; Woodside and Messmer, 1961a+b). All of them are functions of porosity ϕ, which serves as a weighting factor for the two contributions.

(1) arithmetic mean: $$\lambda = \phi\lambda_{\mathrm{L}} + (1-\phi)\lambda_{\mathrm{S}} \quad \text{(Eq.3.4.4)}$$

(2) harmonic mean: $$\frac{1}{\lambda} = \frac{\phi}{\lambda_{\mathrm{L}}} + \frac{(1-\phi)}{\lambda_{\mathrm{S}}} \quad \text{(Eq.3.4.5)}$$

(3) geometric mean: $$\lambda = \lambda_{\mathrm{L}}{}^{\phi}\,\lambda_{\mathrm{S}}{}^{(1-\phi)} \quad \text{(Eq.3.4.6)}$$

Generally, the arithmetic mean defines an upper boundary for the value of the thermal conductivity of the wet sediment, whereas the lower boundary is given by the harmonic mean.

The above equations can be extendend for the calculation of thermal conductivities of hydrate-bearing sediments by simply adding a third term or factor for the gas hydrate weighting all the three contributions with their respective volume fraction.

For hydrate-bearing sediments, Moridis et al. (2008) propose a different model that they derived from matching laboratory data:

$$\lambda = \lambda_{\mathrm{S}} + \left(\sqrt{S_W} + \sqrt{S_H}\right)\left(\lambda_{\mathrm{bulk}} - \lambda_{\mathrm{S}}\right) \quad \text{(Eq.3.4.7)}$$

where λ_{bulk} is the thermal conductivity of the bulk (i.e. wet) sediment and S_W and S_H are the pore saturations of water and gas hydrate, respectively.

Other proposed models are summarized by Waite et al. (2009). Experimentally determined thermal conductivities for several types of sediments with different contents of hydrate and water were investigated by Martin (2004). The obtained values range from 0.5 W/(m K) to 3.5 W/(m K).

SUGAR Toolbox:

Included scripts for the calculation of thermal conductivities are

heatcond_sw.m	thermal conductivity of seawater
heatcond_co2.m	thermal conductivity of carbon dioxide
heatcond_ch4.m	thermal conductivity of methane
heatcond_n2.m	thermal conductivity of nitrogen

They are based on the empirical equations of Caldwell (1974), Scalabrin et al. (2007), Hanley et al. (1977), and Lemmon and Jacobsen (2004).

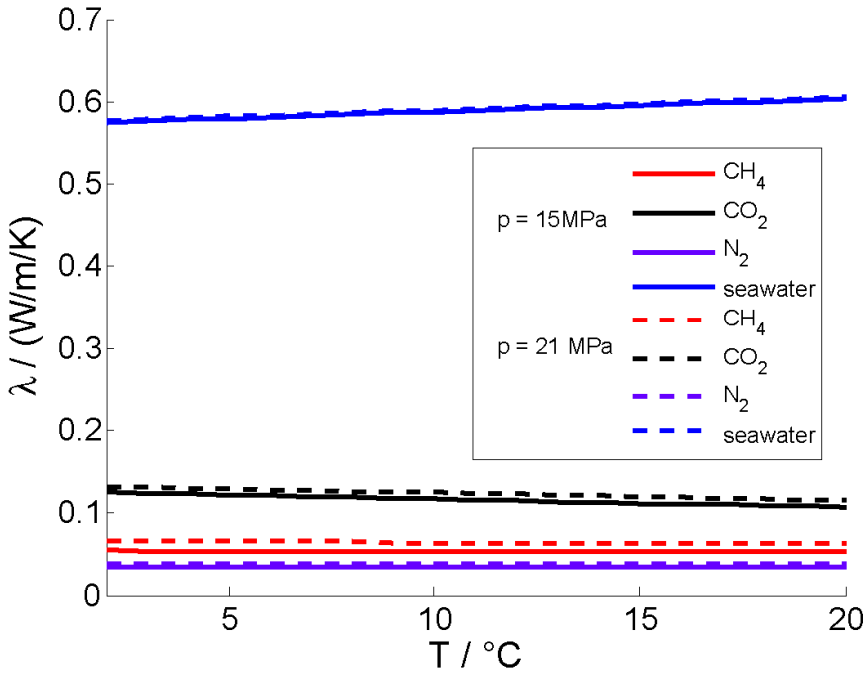

Figure 3.8: Thermal conductivities of seawater, CH_4, CO_2 and N_2 as a function of temperature.

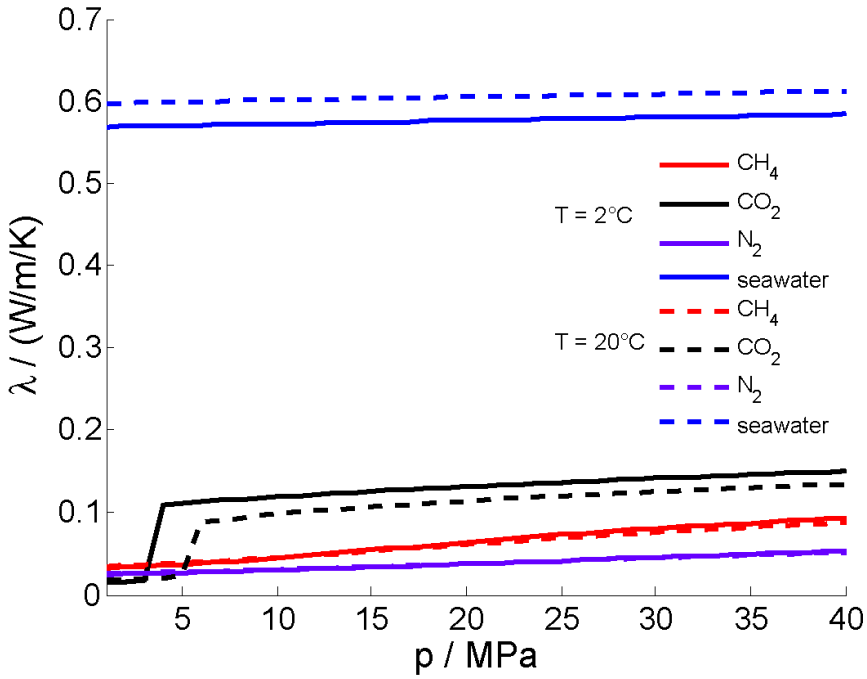

Figure 3.9: Thermal conductivities of seawater, CH_4, CO_2 and N_2 as a function of pressure. The steep increase in thermal conductivity results from the gas/liquid phase transition of CO_2.

3.5. Porosity, tortuosity and permeability

Porosity ϕ is a quantity that characterizes a porous medium. It is defined as the ratio of the void volume V_v and the total volume V or, in other words, the volume of the mobile phase divided by the total volume:

$$\phi = \frac{V_v}{V} \qquad \text{(Eq.3.5.1)}$$

Transport in porous media is restricted to the void volume and therefore depends on the porosity. It also depends on structural parameters of the pore space such as pore diameters and interconnectivity of the pores.

The tortuosity θ is defined as the ratio of the average length of the shortest path between two points $\mathrm{d}L$ and their direct distance $\mathrm{d}x$:

$$\theta = \frac{\mathrm{d}L}{\mathrm{d}x} \qquad \text{(Eq.3.5.2)}$$

Tortuosity is a concept that is, for example, used to calculate the effective diffusion coefficient D_{eff} in a porous medium, where molecular diffusion is slowed down due to tortuos connections within the pore space (Fig. 3.10):

$$D_{\mathrm{eff}} = \frac{D}{\theta^2} \qquad \text{(Eq.3.5.3)}$$

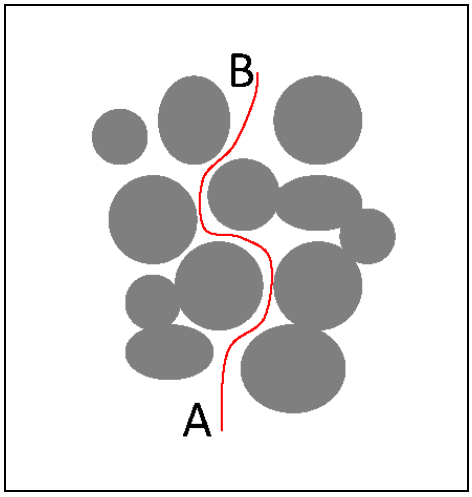

Figure 3.10: The concept of tortuosity: A particle travelling from A to B cannot take the direct, linear path, but must take a longer way around the sediment grains (red line).

Numerous equations, mostly empirical, relate the tortuosity θ to the porosity ϕ. Most of them contain adjustable parameters to account for the geometrical diversity among pore spaces. Examples for porosity-tortuosity relationships are (Boudreau, 1997):

$\theta^2 = 1 - a\ln(\phi)$	modified Weissberg equation	(Eq.3.5.4)
$\theta^2 = \phi^{(1-a)}$	Archie's law	(Eq.3.5.5)
$\theta^2 = \phi + a(1-\phi)$	Buerger-Friecke equation	(Eq.3.5.6)

where a represents an adjustable parameter.

In contrast to diffusion, which takes place in the entire (filled) pore space, fluid flow is restricted to the interconnected pore space. The permeability k is a measure characterizing the ability of a porous medium to establish a fluid flow v when exposed to a pressure difference $\frac{\partial p}{\partial x}$:

$$v = \frac{k}{\eta}\frac{\partial p}{\partial x} \qquad \text{(Eq.3.5.7)}$$

Here, η represents the dynamic viscosity of the pore fluid. The permeability is proportional to the hydraulic conductivity K of the system:

$$k = K\frac{\mu}{\rho\, g} \qquad \text{(Eq.3.5.8)}$$

with μ being the kinematic viscosity of the pore fluid, ρ being the fluid density and g being the gravitational acceleration.

Equation 3.5.8 is known as Darcy's law and is one of the central equations for fluid flow in porous media. It is valid for low to moderate Reynold's numbers.

Boudreau (1997) suggests the following (semi)theoretical equations to calculate the permeability of a porous system based on a known porosity value and the mean (sediment) particle diameter d_p:

$k = \frac{d_p^2}{180}\frac{\phi^3}{(1-\phi)^2}$	Carman-Kozeny	(Eq.3.5.9)
$k = \frac{d_p^2}{150}\frac{\phi^3}{(1-\phi)^2}$	Blake-Kozeny	(Eq.3.5.10)
$k = \frac{d_p^2\phi^{5.5}}{5.6}$	Rumpf-Gupte	(Eq.3.5.11)

These equations have been proven to work well for $\phi < 0.8$, i.e. small to moderate porosities. The Hsu-Cheng equation was developed for large porosities $\phi \to 1$

$$k = \frac{d_p^2 \phi^2}{18\,(1-\phi)}. \qquad \text{(Eq.3.5.12)}$$

and the blended Hsu-Cheng equation is a theoretical form that merges Eq. 3.5.9 with the Hsu-Cheng equation 3.5.12:

$$k = \frac{d_p^2 \phi^3}{180\,(1-\phi)^2}\left[1-\exp\left(-10\,\frac{1-\phi}{\phi}\right)\right] \qquad \text{(Eq.3.5.13)}$$

Adding gas hydrate to the sediment reduces the pore space available for the mobile phases, gas and water. Consequently, the permeability is drastically reduced by 3-5 orders of magnitude (Kurihara et al., 2005). Currently, no validated equations exist to predict the effect of hydrate saturation on absolute (or even relative) permeabilities. Some typically used equations can be found, for example, in Kurihara et al. (2005), Moridis et al. (2008), Nimblett and Ruppel (2003), Waite et al. (2009).

SUGAR Toolbox:

tortuos.m
calculates the tortuosity of a porous medium at a given porosity. The user can choose from the porosity-tortuosity relationships Eq. 3.5.4, Eq. 3.5.5 and Eq. 3.5.6. Default is a modified Weissberg equation with *a* = 2 proposed by Boudreau (1997) and tested by Boudreau and Meysman (2006).

permeab.m
predicts the permeability of a porous medium based on porosity and the mean particle diameter. The user can choose from the porosity-permeability relationships Eq. 3.5.9, Eq. 3.5.10, Eq. 3.5.11, Eq. 3.5.12 and Eq. 3.5.13. Default is the blended Hsu-Cheng equation and a mean particle diameter of 1 µm.

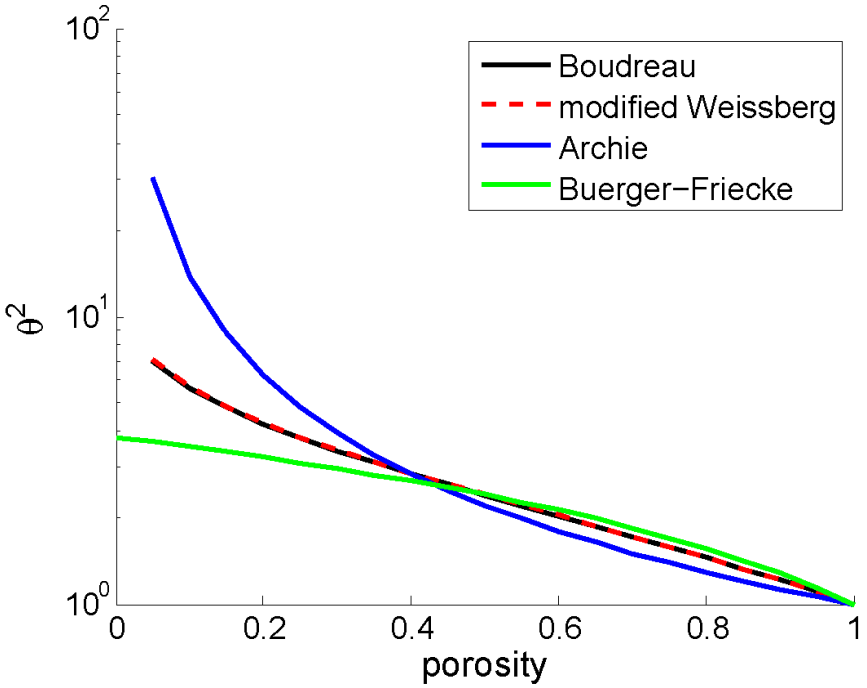

Figure 3.11: Comparison of different porosity-tortuosity relationships. “Boudreau” is a Weissberg equation with *a* = 2.

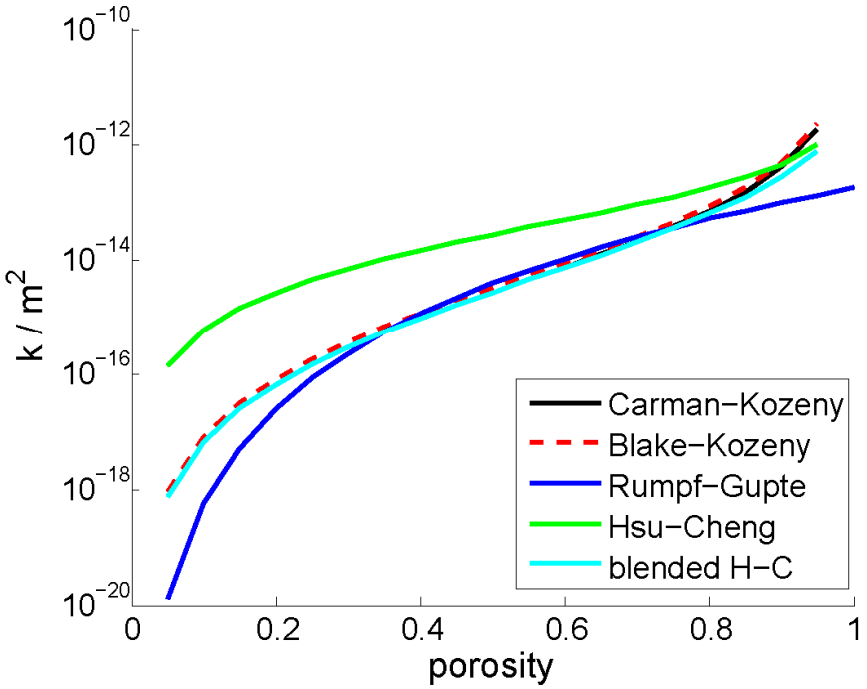

Figure 3.12: Comparison of different porosity-permeability relationships for a mean particle diameter of 1 µm.

References

Aplin, A., A. Fleet, et al. (1999). "Muds and mudstones: Physical and fluid flow properties." *Geological Society Special Publication No. 158*.

Bando, S., F. Takemura, et al. (2004). "Viscosity of aqueous NaCl solutions with dissolved CO_2 at (30 to 60) ℃ and (10 to 20) MPa." *Journal of Chemical and Engineering Data* **49**: 1328-1332.

Boudreau, B. P. (1997). *Diagenetic Models and Their Implementation: Modelling Transport and Reactions in Aquatic Sediments*. Berlin, Heidelberg, New York, Springer-Verlag.

Boudreau, B. P. and F. J. R. Meysman (2006). "Predicted tortuosity of muds." *Geology* **34**: 693-696.

Buntebarth, G. and J. R. Schopper (1998). "Experimental and theoretical investigations on the influence of fluids, solids and interactions between them on thermal properties of porous rocks." *Physics and Chemistry of the Earth* **23**: 1141-1146.

Caldwell, D. (1974). "Thermal conductivity of sea water." *Deep-Sea Research* **21**: 131-137.

Fenghour, A., W. A. Wakeham, et al. (1998). "The viscosity of carbon dioxide." *Journal of Physical and Chemical Reference Data* **27**(1): 31-44.

Hanley, H., W. Haynes, et al. (1977). "The viscosity and thermal conductivity coefficients for dense gaseous and liquid methane." *Journal of Physical and Chemical Reference Data* **6**(2): 597-609

Hayduk, W. and H. Laudie (1974). "Prediction of diffusion coefficients for nonelectrolytes in dilute aqueous solutions." *American Institute of Chemical Engineers Journal* **20**: 611-615.

Horai, K. (1971). "Thermal conductivity of rock-forming minerals." *Journal of Geophysical Research* **76**(5): 1278-1308.

IAPWS (2008). *Release on the IAWPS Formulation 2008 for the Viscosity of Ordinary Water Substance*. http://iapws.org.

Kestin, J., H. Khalifa, et al. (1978). "Effect of pressure on the viscosity of aqueous NaCl solutions in the temperature range 20-150 ℃." *Journal of Chemical and Engineering Data* **23**(4): 328-336.

Kukulka, D. J., B. Gebhart, et al. (1987). "Thermodynamic transport properties of pure and saline water." *Advances in Heat Transfer* **18**: 325-363.

Kurihara, M., H. Ouchi, et al. (2005). "Analysis of the JAPEX/JNOC/GSC et al. Mallik 5L-38 gas hydrate thermal-production test through numerical simulation." In: *Scientific Results from the Mallik 2002 Gas Hydrate Production Research Well Program, Mackenzie Delta, Northwest Territories, Canada*. S. Dallimore and T. Collett (eds.), *Geological Survey of Canada Bulletin* **585**.

Lemmon, E. W. and R. T. Jacobsen (2004). "Viscosity and thermal conductivity equations for nitrogen, oxygen, argon, and air." *International Journal of Thermophysics* **25**(1): 21-6

Li, Y. and S. Gregory (1974). "Diffusion of ions in seawater and in deep-sea sediments." *Geochimica et Cosmochimica Acta* **38**: 703-714.

Mao, S. D. and Z. H. Duan (2009). "The Viscosity of Aqueous Alkali-Chloride Solutions up to 623 K, 1,000 bar, and High Ionic Strength." *International Journal of Thermophysics* **30**(5): 1510-1523.

Martin, A. (2004). *Hydrate bearing sediments - thermal conductivity*. Master Thesis, Georgia Institute of Technology.

Maxwell, J. C. (1873). *A treatise on electricity and magnetism, Vol. 1*. Clarendon Press, Oxford.

Mellon, M. (1996). "Limits on the CO_2 content of the martian polar deposits." *ICARUS* **124**: 268-279.

Moridis, G. J., M. B. Kowalsky, et al. (2008). *TOUGH+Hydrate v1.0 User's Manual: A Code for the Simulation of System Behavior in Hydrate-Bearing Geologic Media*. Lawrence Berkeley National Laboratory.

Nimblett, J. and C. Ruppel (2003). "Permeability evolution during the formation of gas hydrates in marine sediments." *Journal of Geophysical Research* **108**(B9): doi:10.1029/2001JB001650.

Palliser, C. and R. McKibbin (1998). "A model for deep geothermal brines, III: Thermodynamic

properties - Enthalpy and viscosity." *Transport in Porous Media* **33**(1-2): 155-171.

Rosenbaum, E. J., N. J. English, et al. (2007). "Thermal conductivity of methane hydrate from experiment and molecular simulation." *Journal of Physical Chemistry B* **111**(46): 13194-13205.

Scalabrin, G., P. Marchi, et al. (2006). "A reference multiparameter thermal conductivity equation for carbon dioxide with a optimized functional form." *Journal of Physical and Chemical Reference Data* **35**(4): 1549-1575.

Sloan, E. D. and C. A. Koh (2008). *Clathrate Hydrates of Natural Gases*. Boca Raton, CRC Press.

Spivey, J. P. and W. D. McCain (2004). "Estimating density, formation volume factor, compressibility, methane solubility, and viscosity for oilfield brines at temperatures from 0 to 275 ℃, pressures to 200 MPa and salinities to 5.7 mole/kg." *Journal of Canadian Petroleum Technology* **43**(7): 52-61.

Waite, W. F., L. A. Stern, et al. (2007). "Simultaneous determination of thermal conductivity, thermal diffusivity and specific heat in sI methane hydrate." *Geophysical Journal International* **169**(2): 767-774.

Waite, W. F., J. C. Santamarina, et al. (2009). “Physical properties of hydrate-bearing sediments.” *Reviews of Geophysics* **47**: doi:10.1029/2008RG000279.

Woodside, W. and J. H. Messmer (1961a). “Thermal conductivity of porous media. I. Unconsolidated sands.” *Journal of Applied Physics* **32**: 1688-1699.

Woodside, W. and J. H. Messmer (1961b). “Thermal conductivity of porous media. II. Consolidated rocks.” *Journal of Applied Physics* **32**: 1699-1706.

Xu, B., K. Nagashimi, et al. (2003). "Diffusion of water in liquid and supercritical Carbon Dioxide: An NMR study." *The Journal of Physical Chemistry A* **107**(1): 1-3.

4. Kinetic expressions for gas hydrate and gas reactions

4.1. Gas hydrate formation process

This chapter gives a brief summary on the topic following Sloan and Koh (2008), where the reader can find more details.

Nucleation

Gas hydrate formation starts with a phase transition of water and a hydrate-forming gas into a crystalline solid. The transition occurs if this lowers the Gibbs free energy, ΔG, of the system considered. The solid-liquid interface between the solution and a newly created nucleus introduces a surface energy term, ΔG^{sfc}, to the energy state of the system. The change of ΔG, is thus

$$\Delta G = \Delta G^{sfc} + \Delta_B G^h \qquad \text{(Eq.4.1.1)}$$

where $\Delta_B G^h$ denotes the Gibbs free energy change associated with formation of gas hydrates. Note that the contribution from $\Delta_B G^h$ to ΔG is negative and proportional to r^3 of the nucleus whereas ΔG^{sfc} is positive and proportional to r^2. By stating that the absolute value of $\Delta_B G^h$ has to be large enough to over-compensate ΔG^{sfc} in order to lower ΔG, Eq.4.1.1 indicates that

(1) only super-saturated or sub-cooled solutions stabilize the nuclei and stimulate further growth;

(2) nuclei have to grow to a critical size in order to establish a balance between $\Delta_B G^h$ and ΔG^{sfc}.

Growth of hydrate clusters to a critical, stable size in a super-saturated solution is a statistical process. The time interval between the establishment of super-saturation and first formation of stable hydrate nuclei is called induction time, t_{ind}. It depends strongly on the abundance and surface properties of foreign particles that facilitate nucleation by offering stable solid-liquid interfaces for hydrate clusters to agglomerate on. Hence, the nucleation process can occur via two pathways:

(1) homogeneous nucleation: the system is devoid of seed sites requiring maximum levels of super-saturation;

(2) heterogeneous nucleation: pre-existing surfaces promote hydrate nucleation at lower degrees of super-saturation by reducing the Gibbs free energy increase associated with the appearance of a new phase.

The majority of natural gas hydrates forms deep within submarine sediments due to reaction of hydrocarbon gas with pore water. These gas hydrates are therefore very unlikely to have formed by homogeneous nucleation. Even in laboratory investigations, where hydrates have been crystallized from distilled water, growth frequently started

from two-phase interfaces (gas/water, container wall/water) to reveal, at least to some extent, heterogeneous nucleation behavior.

Skovborg and Rasmussen (1993) expressed the driving force for nucleation as the chemical potential difference of distilled water in the liquid and hydrate phases, $\Delta\mu_W^{l\text{-}h}$. The authors found t_{ind} to decrease exponentially with $\Delta\mu_W^{l\text{-}h}$ at large driving forces ($\Delta\mu_W^{l\text{-}h}$ > 80 J mol^{-1}).

Natarajan et al. (1994) expressed the driving force for hydrate nucleation at high thermodynamic driving forces using the fugacity difference between the guest molecule in the gas phase at measured conditions, f_j^g, and the hydrate phase at thermodynamic equilibrium, f_j^h:

$$t_{ind} = \xi_1 \left(\frac{f_j^g(p,T)}{f_j^h(p^{eq},T)} - 1 \right)^{-\xi_2} \qquad \text{(Eq.4.1.2)}$$

Here, ξ_1 and ξ_2 are guest-molecule-specific parameters. Experimental measurements on t_{ind} are usually obtained with large variability, particularly at low thermodynamic driving forces. To account for the more stochastic nature of t_{ind}, Takeya et al. (2000) expressed their measurements of carbon dioxide hydrate nucleation in terms of an exponential nucleation probability and time:

$$P(t) = 1 - e^{-J(t-t_{ind})} \qquad \text{(Eq.4.1.3)}$$

where J denotes the nucleation rate per second.

Experimental evidence that not only the driving force but also the thermal history of the water is important to t_{ind} was first proposed by Vysniauskas and Bishnoi (1983). These authors noticed that water from thawed ice or dissociated gas hydrate considerably sped up nucleation with respect to cold tap water. This phenomenon was termed the “memory effect”. It has been described in many studies since then (e.g., Parent and Bishnoi, 1996; Lee et al., 2005; Servio and Englezos, 2003; Linga et al., 2007) and has generally been interpreted as the persistence of hydrate-like microstructures of water molecules remaining in solution after dissociation of the hydrate phase. This hypothesis has been challenged by Buchanan et al. (2005), who found no evidence for the proposed microstructures in neutron diffraction experiments, and Wilson et al. (2008) carried out repeated dissociation/crystallization experiments without being able to confirm any “memory effect”.

Growth

Once stable gas hydrate nuclei are formed at t_{ind} further decrease in the Gibbs free energy may be accomplished by particle growth. The onset of this stage is characterized by a substantial increase of the gas consumption, the rate of which can be measured to find kinetic rate laws and constants for hydrate growth. The amount of hydrate-forming gas trapped in the hydrate cages may exceed the particular gas

solubility by several orders of magnitude. Therefore, the mass transport of the gas to the hydrate surface is of major importance to crystal growth. Additionally, since hydrate crystallization is an exothermic process (see Appendix A), heat transport away from the growth front can also control formation kinetics. In summary, hydrate growth can be considered to be limited by three factors:

(1) kinetics of crystal growth at the hydrate surface (intrinsic growth);

(2) mass transfer of components to the growth front;

(3) heat transfer away from the growth front.

First relevant experiments set up to investigate methane hydrate formation were carried out by Vysniauskas and Bishnoi (1983). Using a stirred tank reactor filled with water and methane gas, the authors measured the gas consumption and correlated the data to the hydrate growth via the following semi-empirical relationship:

$$\left(\frac{\mathrm{d}n}{\mathrm{d}t}\right) = FA^{\mathrm{if}} \exp\left(\frac{-E_{\mathrm{A}}}{RT}\right)\exp\left(\frac{-\xi_1}{(T^{\mathrm{eq}}-T)^{\xi_2}}\right)p^{\xi_3} \qquad \text{(Eq.4.1.4)}$$

where n is the gas consumption in moles, t is time, F is the pre-exponential factor, A^{if} is the area of the gas/liquid interface, E_{A} is the activation energy, R is the universal gas constant, T is temperature, T^{eq} is the equilibrium temperature for gas hydrate formation and $\xi_{1,2,3}$ are fitting parameters.

(a) Intrinsic growth

In a slightly modified version of the experimental apparatus of Vysniauskas and Bishnoi (1983), Englezos et al. (1987) conducted experiments with methane and distilled water. Ruling out the significance of gas dissolution to the rate of hydrate growth, the authors proposed a 2-step model:

(1) diffusive transport of the guest molecule from the bulk liquid to the hydrate-solution interface;

(2) reaction of water and guest molecules at the hydrate-solution interface.

The growth rate for a single stable hydrate nucleus was defined as

$$\left(\frac{\mathrm{d}n}{\mathrm{d}t}\right)^{\mathrm{P}} = k_{\mathrm{d+r}}A^{\mathrm{P}}(f_{\mathrm{j}}^{\mathrm{bulk}} - f_{\mathrm{j}}^{\mathrm{eq}}). \qquad \text{(Eq.4.1.5)}$$

Here, $k_{\mathrm{d+r}}$ is the combined rate constant for the diffusion and reaction steps involved in hydrate growth, A^{p} is the surface area of the hydrate particle, $f_{\mathrm{j}}^{\mathrm{bulk}}$ and $f_{\mathrm{j}}^{\mathrm{eq}}$ denote the

fugacities of the hydrate-forming gas dissolved in the water and at the three-phase equilibrium at operating temperature, respectively.

Due to the strong agitation of the water, mass and heat transfer limitations were reasoned to be insignificant to hydrate growth in the stirred tank, implying that growth was controlled by reaction only, i.e. $k_{d+r} = k_r$, (the latter being termed *intrinsic* growth rate). To determine k_r, Englezos et al. (1987) equaled the amount of gas consumed due to hydrate formation to the flux of methane across the gas-liquid interface, arguing that at steady state the amount of methane transferred during these two mechanisms has to balance, i.e. $f_j^{bulk} = f_j^g$ (where f_j^g denotes the fugacity of gas "j" in the vapour phase). The mass flux across the two-phase interface is equal to the gas consumption rate in the reactor and was calculated by employing a two-film theory:

$$\left(\frac{\mathrm{d}n}{\mathrm{d}t}\right) = -\frac{D\,c^{W0}}{K_H} A^{if} \left(\frac{\mathrm{d}f_j^{bulk}}{\mathrm{d}y}\right) \qquad \text{(Eq.4.1.6)}$$

where D is the diffusion coefficient of methane in water, c^{W0} is the initial concentration of methane in water, K_H is the Henry constant and y is an axial coordinate along a normal to the gas/water interface.

Assessing the overall gas consumption rate due to hydrate growth requires integration of Eq. 4.1.6 over the whole particle population in the system:

$$\left(\frac{\mathrm{d}n}{\mathrm{d}t}\right) = 4\pi \int_0^\infty k_r r^2 \left(f_j^{bulk} - f_j^{eq}\right) o(r,t) = 4\pi\, k_r\, \varphi(r,t) \left(f_j^{bulk} - f_j^{eq}\right) \qquad \text{(Eq.4.1.7)}$$

The particle size distribution $\varphi(r,t)$ was determined by including a population balance equation, which for lack of experimental data had to rely on a number of assumptions. The concept of (Englezos et al. (1987) was adopted in many following studies. Dholabhai et al. (1993) conducted experiments to estimate the intrinsic growth rate for methane hydrate in aqueous electrolyte solutions. While the fugacities had to be changed to include the effect of the electrolytes, Dholabhai et al. (1993) found that kinetic rate constants remained unaffected, verifying the values for k_r found by Englezos et al. (1987). First experimental data on carbon dioxide hydrate growth kinetics were gained using distilled water and gaseous carbon dioxide (Chun and Lee, 1996). Further data was provided by Malegaonkar et al. (1997) who used distilled water and liquid carbon dioxide as well as methane gas. The first attempts to measure the crystal size distribution *in situ* in order to turn $\varphi(r,t)$ into an input parameter were made by Herri et al. (1999) for methane and Clarke and Bishnoi (2005) for carbon dioxide. Using the experimental data, Clarke and Bishnoi (2005) calculate k_r values, which are about one order of magnitude higher than those obtained by Malegaonkar et al. (1997).

Bergeron and Servio (2008) and Bergeron et al. (2010) reported a rate law for methane and carbon dioxide hydrate formation, where they expressed the driving force in terms of mole fractions of the gas in the aqueous solution, x, instead of fugacities:

$$\left(\frac{\mathrm{d}n}{\mathrm{d}t}\right) = \frac{V_W \rho_W}{M_W} \pi\, k_\mathrm{r}\, \varphi(r,t)\left(x_\mathrm{j}^{\mathrm{bulk}} - x_\mathrm{j}^{\mathrm{eq}}\right) \qquad \text{(Eq.4.1.8)}$$

where V_W, ρ_W and M_W are the volume, the density and molar weight of water, respectively. From their experiments they could observe an Arrhenius-type increase of the kinetic rate constant with temperature, but they did not determine the activation energy.

(b) Mass transfer controlled growth

Reviewing the experimental data gained in the aforementioned stirred-tank experiments Skovborg and Rasmussen (1994) conclude that the monitored hydrate growth is limited by *mass transfer* of the gas from the gas/liquid interface to the bulk liquid, i.e. gas dissolution. This finding eliminates the need to determine the crystal size distribution in the solution. Accordingly, the global hydrate growth rate can be simplified to:

$$\left(\frac{\mathrm{d}n}{\mathrm{d}t}\right) = k_\mathrm{d} A^{\mathrm{if}} c^{\mathrm{W0}} (x_\mathrm{j}^{\mathrm{bulk}} - x_\mathrm{j}^{\mathrm{eq}}). \qquad \text{(Eq.4.1.9)}$$

where k_d is the mass transfer coefficient of the hydrate forming gas across the gas/liquid interface, A^{if} is the corresponding area, c^{W0} is the initial concentration of the gas dissolved in the liquid phase, $x_\mathrm{j}^{\mathrm{bulk}}$ is the mole fraction of the hydrate former in the liquid phase in equilibrium with the vapour, and $x_\mathrm{j}^{\mathrm{eq}}$ the mole fraction in equilibrium with the hydrate. Further experimental verification of the model was provided by Gaillard et al. (1999).

Although Herri et al. (1999) acknowledged the importance of mass transfer control across the gas/liquid interface to hydrate formation in the described stirred-tank reactors, the authors stressed the importance of crystal growth rates for models of gas hydrate formation and maintained the need to include a population balance equation. In a new set of stirred-tank experiments Herri et al. (1999) tracked particle sizes at various time steps and correlated the measured crystal growth to the stirring speed. Because of the strong dependence of the mean particle radius on the stirring speed hydrate growth was reasoned to be limited by the transfer of methane from the bulk liquid to the crystal surface rather than by the incorporation of gas and water into the crystal lattice. Accordingly, the driving force for particle growth could be expressed as a concentration difference between the 3-phase equilibrium ($c_\mathrm{j}^{\mathrm{eq}}$) and the bulk liquid phase ($c_\mathrm{j}^{\mathrm{bulk}}$):

$$\left(\frac{\mathrm{d}r}{\mathrm{d}t}\right) = k_\mathrm{d}\left(c_\mathrm{j}^{\mathrm{bulk}} - c_\mathrm{j}^{\mathrm{eq}}\right) \qquad \text{(Eq.4.1.10)}$$

Note that in the above equation particle growth is expressed in m s^{-1} and k_d in m^4 mol^{-1} s^{-1}.

(c) Heat transfer controlled growth

Uchida et al. (1999) measured the hydrate film growth across the surface of a carbon dioxide droplet. While the propagation rate was found to be temperature-dependent the authors showed that it was not controlled by thermal activation processes. Hence Uchida et al. (1999) concluded that hydrate film formation was mainly *heat transfer* controlled:

$$\rho^{\mathrm{H}} \Delta_{\mathrm{B}}^{\mathrm{H}} H \left(\frac{\mathrm{d}x}{\mathrm{d}t} \right) = \frac{\lambda_{\mathrm{W}}}{0.5\, z^{H}} \left(T^{eq} - T \right) \qquad \text{(Eq.4.1.11)}$$

where x is the lateral position of the hydrate film front, z^{H} is the hydrate film thickness, λ_{W} is the thermal conductivity of water, T^{eq} is the corresponding hydrate equilibrium temperature, and T is the temperature of the system.

Freer et al. (2001) presentend a similar expression:

$$\rho^{\mathrm{H}} \Delta_{\mathrm{B}}^{\mathrm{H}} H \left(\frac{\mathrm{d}x}{\mathrm{d}t} \right) = \frac{k_{d+r}\, h}{k_{d+r} + h} \left(T^{eq} - T \right) \qquad k_{\mathrm{d+r}} = k_0 \exp\left(\frac{-E_{\mathrm{A}}}{R T_{\mathrm{eq}}} \right) \qquad \text{(Eq.4.1.12)}$$

where k_{d+r} is the kinetic constant for gas hydrate formation (expressed by an Arrhenius-type equation) and h is the heat transfer coefficient.

The correlations derived by Uchida et al. (1999), Freer et al. (2001) and others were criticized by Mochizuki and Mori (2006) for physical weaknesses and/or oversimplifications in the formulation of the heat transfer from the film front. In a more realistic approach, using two-dimensional conductive heat transfer from the film front to water, guest fluid and hydrate phases, Mochizuki and Mori (2006) expressed the linear growth rate (dx/dt) as

$$\rho^{\mathrm{H}} \Delta_{\mathrm{B}}^{\mathrm{H}} H \left(\frac{\mathrm{d}x}{\mathrm{d}t} \right) = \int_0^{z^{\mathrm{H}}} \left(\lambda^{\mathrm{H}} \frac{\partial T}{\partial x^{\mathrm{H}}} - \lambda_{\mathrm{W}} \frac{\partial T}{\partial x_{\mathrm{W}}} \right) \mathrm{d}y \qquad \text{(Eq.4.1.13)}$$

Here, x is the lateral position of the hydrate film front, z^{H} is the hydrate film thickness, λ^{H} and λ_{W} are the thermal conductivity of hydrate and water, respectively, and $\partial T/\partial x$ is the temperature gradient at the hydrate and water side of the film, respectively.

Although an accurate prediction of the hydrate formation rate requires evaluation of all the rates of mass transfer, heat transfer and intrinsic formation rates, the role of intrinsic kinetics has been suggested in the recent literature to play a smaller role than mass or heat transfer effects (Sloan & Koh, 2008). However, the applicability of one of the above concepts depends on external factors such as hydrodynamic conditions, saturation state of the solvent or ambient pT-conditions. An example is the hydrate formation process under water flow, of which the flow rate is sufficiently high to ensure an adequate removal of heat released due to hydrate growth while at the same time keeping up the supply of reactants. In this case information of the intrinsic growth rate is essential for the prediction of hydrate formation.

4.2. Kinetic expressions of gas hydrate formation in numerical models

Mechanistically, gas hydrate formation is typically modelled as a two-step process via two possible pathways:

(1) Gas is dissolved in the water phase and after saturation with respect to the gas phase, hydrate precipitates from this solution because it is oversaturated with respect to the hydrate phase;

(2) Gas hydrates form directly from the gas phase and subsequently the water phase equilibrates with the hydrate phase, i.e. methane dissolves in the pore water.

The selection of the pathway usually depends on the available environmental or experimental data.

The rate of dissolution of a gas in pore water, R^{g}_{dis}, is conveniently expressed in terms of the change in dissolved gas concentration with time and is driven by the difference between the actual dissolved gas concentration and its theoretical solubility (e.g., Haeckel et al., 2004):

$$R^{g}_{dis} = \frac{d\ c_{\mathrm{j}}^{\mathrm{pw}}}{d\ t} = k^{g}_{dis}\ \left(c_{\mathrm{j}}^{\mathrm{eq(g)}} - c_{\mathrm{j}}^{\mathrm{pw}}\right) \qquad \text{for } c_{\mathrm{j}}^{\mathrm{pw}} \le c_{\mathrm{j}}^{\mathrm{eq(g)}} \qquad \text{(Eq.4.2.1)}$$

where k^{g}_{dis} is the dissolution rate constant, $c_{\mathrm{j}}^{\mathrm{pw}}$ is the concentration of the dissolved gas j in the pore water, $c_{\mathrm{j}}^{\mathrm{eq(g)}}$ is the concentration of the dissolved gas j in equilibrium with the gas phase. In Eq.4.2.1 the rate is defined positive for gas dissolution. The gas solubility is either calculated applying Henry's law or more sophisticated algorithms based on its chemical potential (see Chapter 2.8).

The rate of formation of gas hydrate, R^{h}_{form}, from the dissolved gas is typically expressed in terms of the fraction of pore volume occupied by gas hydrate, ϕ_h, and is driven by the oversaturation of the pore water with respect to the gas hydrate solubility (e.g., Haeckel et al., 2004; Hensen and Wallmann, 2005; Wallmann et al., 2006):

$$R^{h}_{form} = -\frac{M_h}{\rho_h}\frac{d\ c_{\mathrm{j}}^{\mathrm{pw}}}{d\ t} = \frac{d\ \phi_h}{d\ t} = k^{h}_{form}\left(\frac{c_{\mathrm{j}}^{\mathrm{pw}}}{c_{\mathrm{j}}^{\mathrm{eq(h)}}} - 1\right) \qquad \text{for } c_{\mathrm{j}}^{\mathrm{eq(h)}} \le c_{\mathrm{j}}^{\mathrm{pw}} \qquad \text{(Eq.4.2.2)}$$

Here, k^{h}_{form} is the rate constant for gas hydrate formation and $c_{\mathrm{j}}^{\mathrm{eq(h)}}$ is the concentration of dissolved gas j in equilibrium with the hydrate phase. In order to calculate the rate of consumption of dissolved gas in the pore water, $dc_{\mathrm{j}}^{\mathrm{pw}} \big/ dt$, R_h needs to be multiplied by

the density of the gas hydrate, ρ_h, and divided by its molar weight, M_h. In Eq.4.2.2 the rate is defined positive for gas hydrate being formed.

Davie and Buffett (2001) present an alternative formulation:

$$R^{h}_{form} = \frac{d\,\phi_h}{d\,t} = k_{d+r}\left(c_{\mathrm{j}}^{\mathrm{pw}} - c_{\mathrm{j}}^{\mathrm{eq(h)}}\right) \qquad \text{for } c_{\mathrm{j}}^{\mathrm{eq(h)}} \le c_{\mathrm{j}}^{\mathrm{pw}} \qquad \text{(Eq.4.2.3)}$$

In order to ensure that the rate of hydrate growth is not limited by its solubility, but by the transport of dissolved gas, Davie and Buffett (2001) progressively increase the kinetic constant, $k_{\mathrm{d+r}}$, in Eq.4.2.3 until the numerical solution becomes insensitive to further change. Changes in the concentration of methane in the equilibrium across the gas hydrate stability zone (GHSZ) as a function of temperature are expressed by a simple empirical relationship:

$$c^{\mathrm{eq}}(T) = c^{\mathrm{eq}}(T_3)\exp[(T - T_3)/\tau] \qquad \text{(Eq.4.2.4)}$$

where c^{eq} is the dissolved gas concentration at the equilibrium, $c^{\mathrm{eq}}(T_3)$ is the dissolved gas concentration at the phase boundary, i.e. at the base of the GHSZ and τ is ~ 10 ºC for mixtures of methane hydrate and seawater.

Cathles and Chen (2004) proposed a model, where gas hydrates crystallize directly from a gas stream following a first-order rate equation:

$$\frac{d\,m_{\mathrm{j}}}{d\,t} = -k_{\mathrm{d+r}}\Delta x_{\mathrm{j}}\exp\left[\frac{E_{\mathrm{A}}}{R}\left(\frac{1}{T^0} - \frac{1}{T}\right)\right] \qquad \text{(Eq.4.2.5)}$$

where m_{j} is the mass of the gas j that crystallizes as gas hydrate, Δx_{j} is the difference between the mass fraction in the gas stream and the fictive mass fraction in the gas that would be in equilibrium with the hydrate crystallising from this gas, and that can be calculated from a polynomial expansion in pressure and temperature (e.g. Sloan and Koh, 2008); E_{A} is the activation energy of the crystallization reaction, R is the gas constant, T is temperature and T^0 is 273.15 K.

Garg et al. (2008) present an alternative approach where thermodynamic equilibrium is assumed at all times. Hence, changes in gas concentration, pressure, temperature and fluid salinity are equilibrated instantaneously into all participating phases, i.e. gas hydrate, pore water, and gas. Kinetic phenomena are not taken into account, because they are assumed not to be important on geological time scales. Thus, only the respective mass balance equations and one energy balance equation are solved for the entire system.

The TOUGH+HYDRATE model (Moridis et al., 2008) considers either thermodynamic equilibrium or the kinetic hydration reactions to calculate dissociation and formation of gas hydrates. The kinetic behaviour of the gas hydrate follows the model of Kim et al. (1987):

$$\frac{d\,m}{d\,t} = -k_{\mathrm{r}}\,\exp\left(\frac{E_{\mathrm{A}}^{\mathrm{hyd}}}{RT}\right)F_{\mathrm{A}}A\left(f^{\mathrm{eq}} - f_{\mathrm{g}}\right) \qquad \text{(Eq.4.2.6)}$$

where m is the mass of the gas, k_{r} is the intrinsic hydration reaction constant, $E_{\mathrm{A}}^{\mathrm{hyd}}$ is the activation energy for gas hydrate formation, R is the gas constant, T is temperature of the system, F_{A} is an area adjustment factor, A is the surface area participating in the reaction, f_{g} and f^{eq} are the fugacities of the gas phase and at equilibrium at temperature T, respectively. The surface area is computed by assigning the hydrate saturation uniformly to the interstitial spaces of the porous medium. Fugacities are computed following a Peng-Robinson equation of state using the real-gas property package included in the model.

4.3. Gas hydrate decomposition

Since gas hydrate dissociation or dissolution can be understood as the formation reaction having the opposite sign. The concepts for gas hydrate decomposition are largely identical to those outlined above for hydrate formation. Bishnoi and coworkers conducted several stirred-tank experiments to measure intrinsic dissociation rates of methane hydrates. Kim et al. (1987) proposed a rate law based on the fugacity difference between the point at which dissociation takes place ($f_{\mathrm{j}}^{\mathrm{G}}$) and equilibrium conditions ($f_{\mathrm{j}}^{\mathrm{eq}}$):

$$-\left(\frac{\mathrm{d}n}{\mathrm{d}t}\right)^{\mathrm{P}} = k_{\mathrm{r}}A^{\mathrm{p}}\left(f_{\mathrm{j}}^{\mathrm{eq}} - f_{\mathrm{j}}^{\mathrm{G}}\right) \qquad \text{(Eq.4.3.1)}$$

The intrinsic rate constant k_{r} was determined by fitting an Arrhenius-type expression

$$k = k_{\mathrm{r}}\exp\left(-\frac{E_{\mathrm{A}}}{RT}\right) \qquad \text{(Eq.4.3.2)}$$

to the logarithmic values of the measured rate constant k versus $1/T$.

In order to improve the accuracy, the measurements were repeated by Clarke and Bishnoi (2001), who refined the experimental apparatus of Kim et al. (1987) by including a particle size analyzer. Measurements of intrinsic rate constants for the dissociation of carbon dioxide hydrate followed (Clarke and Bishnoi, 2004; 2005).

Sean et al. (2007a) argued that simple stirring might not suffice to eliminate heat and mass transfer resistances. In an effort to test the results published by the Bishnoi group, Sean et al. (2007a+b) measured the shrinkage rate of a methane hydrate

sphere dissociating in a flow of water. In step 1, dissolution was achieved by under-saturating the ambient water at pressures above the three-phase equilibrium line. The driving force for dissolution was expressed by the associated change of the Gibbs free energy. The latter was approximated by the difference in chemical potential of methane at equilibrium and in the ambient aqueous phases:

$$-\left(\frac{\mathrm{d}n}{\mathrm{d}t}\right) = k_\mathrm{r} A^\mathrm{p} RT \ln \frac{x_\mathrm{j}^\mathrm{eq}}{x_\mathrm{j}^\mathrm{sfc}}. \qquad \text{(Eq.4.3.3)}$$

where $x_\mathrm{j}^\mathrm{sfc}$ is the mole fraction of methane at the surface of the hydrate sphere and x_j^eq is the mole fraction of methane in water in equilibrium with gas hydrate. Note that in the above equation the sign was changed with respect to the original article by Sean et al. (2007a) in order to indicate a dissolution process.

The authors registered a homogeneous surface temperature around the dissolving gas hydrate sphere, which was identical to that of the ambient water. Furthermore, the obtained value for k_r was shown to be independent of the flow rate. Although admitting the narrow range of flow conditions, the observations led the authors to the conclusion that neither heat nor mass transfer effects were rate-determining factors during hydrate dissolution at *pT*-conditions within the gas hydrate stability field. The intrinsic rate constant found in step 1 was successfully tested in step 2 of the investigation, during which gas hydrate dissociation was induced by depressurization below the three-phase equilibrium line (Sean et al., 2007b).

The comparison of dissolution and dissociation rates observed by Sean et al. (2007a+b) and those by Kim et al. (1987) reveal a slight disagreement at low dissociation pressures: the discrepancy became smaller when the pressure approached the three-phase equilibrium pressure.

Rehder et al. (2004) studied the simultaneous dissolution of synthetic methane and carbon dioxide hydrate specimens in an ocean experiment. The samples were brought to a water depth of 1028 meters. Pressures at this depth exceeded the three-phase equilibrium and dissolution occurred due to an under-saturation of the ambient seawater in methane and carbon dioxide. The authors applied a diffusive boundary layer model to express the dissolution rates:

$$-\left(\frac{\mathrm{d}n}{\mathrm{d}t}\right) = A \frac{D_\mathrm{j}}{z^\mathrm{DBL}} c_\mathrm{j}^\mathrm{eq} \qquad \text{(Eq.4.3.4)}$$

where D_j is the diffusion coefficient of the gas species j and z^DBL is the thickness of the diffusive boundary layer.

Since the methane concentration measured in the ambient seawater was negligible, Rehder et al. (2004) reduced the driving force of dissolution to the methane solubility in seawater equilibrated with a hydrate phase. Since the gas hydrate specimens had identical sample geometry and were dissolved simultaneously, D_j, z^DBL and A were identical for the two hydrate species. By showing that the dissolution rate ratio of the

two hydrate species was identical to the ratio of the respective gas species, the authors identified a mass transfer limitation in the dissolution reaction, thereby verifying their prior assumption.

Bigalke et al. (2009) measured the dissolution rates of methane hydrate films due to under-saturation as a function of temperature and flow-induced shear stress. In the hydrodynamic and thermodynamic regime of their investigation, the authors proved dissolution to be mass transfer limited and present a correlation of the diffusive boundary layer thickness and shear stress.

4.4. Kinetic expressions of gas hydrate dissociation in numerical models

Gas hydrate dissociation is typically treated by the same 2-step formalism outlined above for gas hydrate formation. However, the rates for both processes observed in experiments and in the field are usually different and hence, separate rate laws are formulated for the dissociation and formation reaction in order to provide individual, adjustable kinetic constants.

Step 1: “Dissociation of gas hydrate”:

$$R_{dis}^{h} = \frac{M_h}{\rho_h}\frac{d\ c_{\mathrm{j}}^{\mathrm{pw}}}{d\ t} = -\frac{d\ \phi_h}{d\ t} = k_{dis}^{h}\left(1-\frac{c_{\mathrm{j}}^{\mathrm{pw}}}{c_{\mathrm{j}}^{\mathrm{eq(h)}}}\right) \qquad \text{for } c_{\mathrm{j}}^{\mathrm{eq(h)}} > c_{\mathrm{j}}^{\mathrm{pw}} \qquad \text{(Eq.4.4.1)}$$

where R_{dis}^{h} is the rate of gas hydrate dissociation, which is again expressed in terms of pore volume, and k_{dis}^{h} is the respective kinetic constant.

To avoid producing numerically negative gas hydrate saturations when the gas hydrate pool in the sediment has been depleted, Hensen and Wallmann (2005) and Wallmann et al. (2006) simply multiplied the rate of dissociation with the gas hydrate concentration, ϕ_h.

Step 2: “Formation of the gas phase”:

$$R_{vap}^{g} = -\frac{d\ c_{\mathrm{j}}^{\mathrm{pw}}}{d\ t} = k_{vap}^{g}\left(c_{\mathrm{j}}^{\mathrm{eq(g)}} - c_{\mathrm{j}}^{\mathrm{pw}}\right) \qquad \text{for } c_{\mathrm{j}}^{\mathrm{pw}} > c_{\mathrm{j}}^{\mathrm{eq(g)}} \qquad \text{(Eq.4.4.2)}$$

where R_{vap}^{g} is the rate of gas production and k_{vap}^{g} is the respective kinetic constant.

In many gas hydrate reservoir simulators, e.g. TOUGH+HYDRATE (Eq.4.2.6; Moridis et al., 2008) and MH-21 (Kurihara et al., 2005), the hydrate dissociation process, induced by either depressurization or adding heat, is typically modelled with a Kim-Bishnoi-type rate expression (Eq.4.3.1; Kim et al., 1987). Here, the driving force for

dissociation is the difference in gas fugacities between the vapour-hydrate-liquid (three-phase) equilibrium and the reservoir conditions. Typically, an energy conservation equation is also included to account for the uptake of heat during hydrate dissociation (~55 kJ/mol) and the corresponding significant cooling of the reservoir.

4.5. Gas bubble dissolution and formation

Gas bubble dissolution

At typical oceanic conditions methane or carbon dioxide are highly under-saturated in the water column (at least below the mixed layer). Methane-rich gas bubbles entering the open water column at deep-sea seep sites rapidly shrink as the gas dissolves. Growth due to adverse transfer of dissolved oxygen and nitrogen as well as decreasing hydrostatic pressure accompany the bubble ascent, but are small compared to the shrinkage caused by gas dissolution. The mass flux of any gas into or out of a bubble is given by

$$\pm\left(\frac{\mathrm{d}n}{\mathrm{d}t}\right) = k_{\mathrm{diss}}^{\mathrm{bub}}\ A^{\mathrm{bub}}\ \left(c_{\mathrm{j}}^{\mathrm{eq}} - c_{\mathrm{j}}^{\mathrm{bulk}}\right). \qquad \text{(Eq.4.5.1)}$$

Here, A^{bub} is the bubble surface area, $k_{\mathrm{diss}}^{\mathrm{bub}}$ is the bubble-specific mass transfer coefficient, $c_{\mathrm{j}}^{\mathrm{eq}}$ is the concentration of the gas species j at equilibrium, and $c_{\mathrm{j}}^{\mathrm{bulk}}$ is the concentration of j in the ambient seawater.

Important factors affecting $k_{\mathrm{diss}}^{\mathrm{bub}}$ are the molecular diffusivity D_j in the seawater and the flow field around the bubble. The latter in turn is influenced by seawater density and viscosity, bubble size, shape and density and surface mobility (Clift et al., 1978; Leifer and Patro, 2002). All of these factors are commonly expressed by the drag coefficient C_{d}.

Gas bubble and liquid droplet dissolution in general have been investigated in numerous experiments, many of which have been summarized in Clift et al. (1978). Without exception, these experiments have been performed at atmospheric pressures. While advancing the fundamental understanding of bubble/droplet propagation in a continuous medium the results are of limited applicability to oceanographic studies concerned with the lifetime of bubbles released at several hundreds of meters below sea level. Hydrostatic pressures and low temperatures in these cases may trigger hydrate formation around the bubble, which has been shown to significantly enhance bubble lifetimes due to attenuated dissolution (Rehder et al., 2002; Heeschen et al., 2004; Sauter et al., 2006; Greinert et al., 2007).

Technically challenging, laboratory simulations of the water column at near-seafloor conditions are still scarce. Thus parameterizations of $k_{\mathrm{diss}}^{\mathrm{bub}}$ use theoretical models of large bubbles exceeding 1 cm in radius and data for small bubbles of a size around r = 1 mm. In between, $k_{\mathrm{diss}}^{\mathrm{bub}}$ is parameterized as a monotonical function of r^{bub}. Useful

experiments on the lifetime of methane bubbles rising in a natural water column were carried out by Rehder et al. (2002). Methane bubbles were released into the ocean between 830 and 440 m water depth. Their rise was monitored for several hundred meters by piloting a ROV-mounted camera vertically upwards in the water column. Shrinkage rates of bubbles rising within the methane hydrate stability field regularly shifted from fast to slow several minutes after release. This shift was attributed to a sudden formation of a hydrate skin around the bubbles. These data were used, among others, to validate the model by McGinnis et al. (2006), who expressed $k_{\mathrm{diss}}^{\mathrm{bub}}$ via:

$$k_{\mathrm{diss}}^{\mathrm{bub}} = 1.13\left(\frac{u_{\mathrm{t}}^{\mathrm{bub}}}{0.45 + 0.4r^{\mathrm{bub}}}\right)^{0.5} D_{\mathrm{j}}^{\mathrm{n}} \qquad \text{for } 0 < r^{\mathrm{bub}} < 0.25 \text{ cm} \qquad \text{(Eq.4.5.2)}$$

$$k_{\mathrm{diss}}^{\mathrm{bub}} = 6.5 D_{\mathrm{j}}^{\mathrm{n}} \qquad \text{for } 0.25 < r^{\mathrm{bub}} < 0.65 \text{ cm} \qquad \text{(Eq.4.5.3)}$$

$$k_{\mathrm{diss}}^{\mathrm{bub}} = 6.94\left(2r^{\mathrm{bub}}\right)^{-0.25} \qquad \text{for } r^{\mathrm{bub}} > 0.65 \text{ cm} \qquad \text{(Eq.4.5.4)}$$

In the above equations $u_{\mathrm{t}}^{\mathrm{bub}}$ is the steady-state rise velocity of a gas bubble, and *n* is a diffusion exponent that varies from 1/2 to 2/3 for clean and dirty bubbles, respectively.

For bubbles smaller than r^{bub} = 0.13 cm, the rise velocity was defined by

$$u_{\mathrm{t}}^{\mathrm{bub}} = \sqrt{\frac{8rg}{3C_{\mathrm{d}}}\left(1 - \frac{\rho_{\mathrm{j}}^{\mathrm{bub}}}{\rho_{\mathrm{SW}}}\right)} \qquad \text{(Eq.4.5.5)}$$

where $\rho_{\mathrm{j}}^{\mathrm{bub}}$ is the bubble density, ρ_{SW} is the seawater density, g is the gravitational acceleration, and C_{d} is defined as

$$C_{\mathrm{d}} = \frac{24}{\mathrm{Re}} + \frac{3}{\sqrt{\mathrm{Re}}} + 0.34 \qquad \mathrm{Re} = \frac{2\, r^{bub}\, u_t^{bub}}{\nu_{SW}} \qquad \text{(Eq.4.5.6)}$$

where Re is the Reynolds number and v_{SW} denotes the kinematic viscosity of seawater.

The terminal rise velocity of larger bubbles (r^{bub} > 0.13 cm) was defined by

$$u_{\mathrm{t}}^{\mathrm{bub}} = \sqrt{\frac{\sigma_{\mathrm{j}}}{r^{\mathrm{bub}}(\rho_{\mathrm{SW}} + \rho_{\mathrm{j}}^{\mathrm{bub}})} + gr^{\mathrm{bub}}}\,, \qquad \text{(Eq.4.5.7)}$$

where σ_{j} is the surface tension of the compressed gas j.

The model was adjusted empirically to account for a delayed mass transfer of gas across the hydrate-shielded bubble surface. This was criticized by Rehder et al. (2009), who showed that the observed delay in dissolution could be explained by

depth-dependent thermodynamic parameters alone and did not require empirical adjustments. The authors used a model by Leifer and Patro (2002), where $k_{\mathrm{diss}}^{\mathrm{bub}}$ is defined as:

$$k_{\mathrm{diss}}^{\mathrm{bub}} = \left(0.212 \frac{D u_{\mathrm{t}}^{\mathrm{bub}}}{r^{\mathrm{bub}}} \right)^{0.5} \quad \text{(for hydrate-free bubbles at Re<70)} \quad \text{(Eq.4.5.8)}$$

$$k_{\mathrm{diss}}^{\mathrm{bub}} = \left(\frac{2}{\pi} \left(1 - 2.89 \mathrm{Re}^{-0.5} \right) \frac{D u_{\mathrm{t}}^{\mathrm{bub}}}{r^{\mathrm{bub}}} \right)^{0.5} \quad \text{(for hydrate-free bubbles at Re>70)} \quad \text{(Eq.4.5.9)}$$

$$k_{\mathrm{diss}}^{\mathrm{bub}} = 0.42 g^{0.3} \left(\frac{D}{\upsilon_{\mathrm{SW}}} \right)^{-2/3} \upsilon_{\mathrm{SW}}^{0.4} r^{\mathrm{bub}\,-0.1} \quad \text{(for hydrate-coated bubbles)} \quad \text{(Eq.4.5.10)}$$

and $u_{\mathrm{t}}^{\mathrm{bub}}$ is parameterized as:

$$u_{\mathrm{t}}^{\mathrm{bub}} = \frac{2}{3} \frac{g r^{\mathrm{bub}\,2} \left(\rho_{\mathrm{SW}} - \rho_{\mathrm{j}}^{\mathrm{bub}} \right)}{\upsilon_{\mathrm{SW}} \rho_{\mathrm{SW}}} \left(\frac{1+\kappa}{2+3\kappa} \right) \quad \text{(Eq.4.5.11)}$$

with $\kappa = 0$ for hydrate-free and $\kappa = \infty$ for hydrate-coated bubbles.

Liquid droplet dissolution

Aya et al. (1993) studied the dissolution behavior of liquid carbon dioxide droplets in pressurized water and seawater. The driving force for dissolution was expressed in terms of a concentration difference between the measured bulk concentration and the saturation value. Dissolution was found to be significantly delayed if the droplets developed a hydrate skin on their surfaces. This effect was attributed to the lower equilibrium solubility inside the hydrate stability field with respect to higher values in metastable absence of hydrates at identical *pT*-conditions. While Aya et al. (1993) showed that dissolution in flowing water proceeded faster than in stagnant water, the first quantitative treatment of flow was a numerical simulation study by Haugan et al. (1995). However, in this study, the effect of gas hydrate formation around the droplets was left unconsidered. First experimental results on the dissolution of hydrate-skinned carbon dioxide droplets were reported by Hirai et al. (1996). Supported by a metal ring, the droplets were exposed to a controlled flow of under-saturated water. The dissolution behavior was expressed as

$$-\left(\frac{\mathrm{d}m}{\mathrm{d}t} \right) = k_{\mathrm{diss}}^{\mathrm{drop}} A^{drop} \left(c_{\mathrm{j}}^{\mathrm{eq}} - c_{\mathrm{j}}^{\mathrm{bulk}} \right) \quad \text{(Eq.4.5.12)}$$

Note that here dissolution is expressed in kg s^{-1} and, consequently, *c* in kg m^{-3}. The authors found $k_{\mathrm{diss}}^{\mathrm{drop}}$ to satisfy the equation

$$k_{\mathrm{diss}}^{\mathrm{drop}} = -0.5\gamma \frac{\rho_{\mathrm{j}}^{\mathrm{drop}}}{c_{\mathrm{j}}^{\mathrm{eq}} \sqrt{2r^{\mathrm{drop}}}}. \qquad \text{(Eq.4.5.13)}$$

Here, γ is a fitting parameter.

Although Hirai et al. (1996) also detected delayed dissolution once a hydrate skin formed at the droplet surface, the effect of the hydrate on dissolution rates was not explicitly stated. This was resolved in a following study by the group (Hirai et al., 1997), where the fitting parameter γ was defined as

$$\gamma = \frac{-1.504 c_{\mathrm{j}}^{\mathrm{eq}}}{\rho_{\mathrm{j}}^{\mathrm{drop}} D^{-2/3} \upsilon^{0.139} u_{\mathrm{t}}^{\mathrm{drop}\,-0.472}} \qquad \text{(Eq.4.5.14)}$$

$u_{\mathrm{t}}^{\mathrm{drop}}$ was calculated analogously to Eq.4.5.5, in which C_{d} takes the form

$$C_{\mathrm{d}} = 24\,\frac{1+0.125\,\mathrm{Re}^{0.72}}{\mathrm{Re}} \qquad \text{(for Re < 1000)} \qquad \text{(Eq.4.5.15)}$$

$$C_{\mathrm{d}} = \left(0.55 + \frac{4.8}{\mathrm{Re}^{0.5}}\right)^2 \qquad \text{(for Re > 1000)} \qquad \text{(Eq.4.5.16)}$$

Pressurized-tank experiments by Ozaki et al. (2001) revealed that these relationships produced significant errors for droplets exceeding a radius of 4.5 mm. For droplet radii in the range of 1-11 mm they proposed the improved relationship

$$C_{\mathrm{d}} = 24\,\frac{1+0.125\,\mathrm{Re}^{0.75}}{\mathrm{Re}} + \frac{\mathrm{Re}^3}{2.2*10^9} \qquad \text{(Eq.4.5.17)}$$

Brewer et al. (2002) used a similar technique as Rehder et al. (2002) to track the rise of single carbon dioxide droplets released in 800 m water depth in Monterey Bay, California. The ascent of the droplets was followed until the liquid had evaporated after crossing the gas-liquid phase boundary for carbon dioxide in 400 m water depth. A thin hydrate layer was observed to surround the droplet during its rise. Droplet size and rise velocity were reported for five experiments. From these data the authors deduced a constant dissolution flux of 3 µmol cm^{-2} s^{-1}. $u_{\mathrm{t}}^{\mathrm{drop}}$ was observed to increase from initially 10.2 cm s^{-1} at 800 m water depth to 14.9 cm s^{-1} at 400 m water depth. The acceleration of the droplets during their transit through the water column was attributed to the increasing density difference between carbon dioxide and seawater with diminishing seawater depth (see also Fig. 2.12). Using Eq.4.5.5 with $C_{\mathrm{d}} = \rho_{\mathrm{j}}^{\mathrm{bub}} / \rho_{\mathrm{SW}}$, the authors managed to reproduce the rise history of the droplets. The match of the rise rates calculated with this definition of C_{d} with observed $u_{\mathrm{t}}^{\mathrm{drop}}$ was criticized as “fortuitous” by Zhang (2005), but was supported in a response by Alendal et al. (2006).

Gangstø et al. (2005) re-interpreted the data of Brewer et al. (2002), adopting Eq.4.5.12 for the mass transfer and the u_t^{drop} parameterization of Bozzano and Dente (2001), which is based on observed shapes of air bubbles rising in a variety of liquids at atmospheric pressures. They achieved a good agreement, however, the model fails to reproduce observations by Bigalke et al. (2008), who simulated oceanic conditions up to a water depth of 2000 m in order to provide a reference data set for u_t^{drop} for carbon dioxide droplets with a radius of 1-12 mm. The study of Bigalke et al. (2008) confirmed the C_d-parameterization of Chen et al. (2003):

$$C_d = 24 \frac{1 + 0.125 \mathrm{Re}^{0.72}}{\mathrm{Re}} \frac{xy}{r^{drop\,2}} \qquad \text{(Eq.4.5.18)}$$

where

$$\frac{xy}{r^{drop\,2}} = 1.0 + 5.6419 \cdot 10^{-4}\ \mathrm{Re} - 8.3484 \cdot 10^{-7}\ \mathrm{Re}^2 + 1.4596 \cdot 10^{-9}\ \mathrm{Re}^3 \qquad \text{(Eq.4.5.19)}$$

is a factor correcting for the deviation of the droplet shape from being a perfect sphere.

Gas bubble growth

Gas bubble nucleation and growth follow generally the same basic principles as gas hydrate nucleation and growth, which are outlined in Chapter 4.1.

Boudreau et al. (2001) applied a diffusion-reaction model to determine the controls on bubble growth rate considering the dynamics of methane formation, diffusion and its incorporation into a bubble

$$r^{bub}(t) = \sqrt{\frac{\phi D_{eff}}{2 c_j^{bub}} \left(\frac{R_{t,j} d^2}{3 D_{eff}} + (c_j^{pw} - c_j^{pw,d}) \right) t + r_0^2} \qquad \text{(Eq.4.5.20)}$$

where d^{bub} is the bubble diameter; ϕ is the porosity; D_{eff} is the diffusion coefficient corrected for tortuosity; c_j^{bub} is the concentration of gas j in the bubble; $R_{t,j}$ is the rate of production of j (methanogenesis in this case) near the bubble; d is the half-separation distance between bubbles; c_j^{pw} is the ambient concentration of the gas j in the pore water; $c_j^{pw,d}$ is the concentration of the gas j in pore water at the position d; t is time; r_0 is the initial bubble radius.

References

Alendal, G., P. M. Haugan, et al. (2006). “Comment on "Fate of rising CO_2 droplets in seawater".” *Environmental Science & Technology* **40**: 3653-3654.

Aya, I., K. Yamane, et al. (1993). ”Effect of CO_2 concentration in water on the dissolution rate of its clathrate.” *International Symposium on CO_2 Fixation & Efficient Utilization of Energy*. Tokyo Institute of Technology, Tokyo, Japan.

Bergeron, S. and P. Servio (2008). "Reaction rate constant of CO_2 hydrate formation and verification of old premises pertaining to hydrate growth kinetics." *American Institute of Chemical Engineers Journal* **54**(11): 2964-2970.

Bergeron, S., J. Beltran, et al. (2010). "Reaction rate constant of methane clathrate formation." *Fuel* **89**(2): 294-301.

Bigalke, N. K., G. Rehder, et al. (2008). “Experimental investigation of the rising behavior of CO_2 droplets in seawater under hydrate-forming conditions.” *Environmental Science & Technology* **42**: 5241-5246.

Bigalke, N. K., G. Rehder, et al. (2009). “Methane hydrate dissolution rates in undersaturated seawater under controlled hydrodynamic forcing.” *Marine Chemistry* **115**: 226-234.

Boudreau, B. P., B. S. Gardiner, et al. (2001). "Rate of growth of isolated bubbles in sediments with a diagenetic source of methane." *Limnology and Oceanography* **46**(3): 616-622.

Bozzano, G. and M. Dente (2001). “Shape and terminal velocity of single bubble motion: a novel approach.” *Computers and Chemical Engineering* **25**: 571-576.

Brewer, P. G., E. T. Peltzer, et al. (2002). “Experimental determination of the fate of rising CO_2 droplets in seawater.” *Environmental Science & Technology* **36**: 5441-5446.

Buchanan, P., A. K. Soper, et al. (2005). “Search for memory effects in methane hydrate: Structure of water before hydrate formation and after hydrate decomposition”. *Journal of Chemical Physics* **123**.

Cathles, L. M. and D. F. Chen (2004). "A compositional kinetic model of hydrate crystallization and dissolution." *Journal of Geophysical Research* **109**(B08102): doi:10.1029/2003JB002910.

Chen, B. X., Y. Song, et al. (2003). “Large-eddy simulation of double-plume formation induced by CO_2 dissolution in the ocean.” *Tellus* **55**: 723-730.

Chun, M. K. and H. Lee (1996). “Kinetics of formation of carbon dioxide clathrate hydrates.” *Korean Journal of Chemical Engineering* **13**: 620-626.

Clarke, M. and P. R. Bishnoi (2001). “Determination of the activation energy and intrinsic rate constant of methane gas hydrate decomposition.” *Canadian Journal of Chemical Engineering* **79**: 143-147.

Clarke, M. A. and P. R. Bishnoi (2004). “Determination of the intrinsic rate constant and activation energy of CO_2 gas hydrate decomposition using in-situ particle size analysis.” *Chemical Engineering Science* **59**: 2983-2993.

Clarke, M. A. and P. R. Bishnoi (2005). “Determination of the intrinsic kinetics of CO_2 gas hydrate formation using in situ particle size analysis.” *Chemical Engineering Science* **60**: 695-709.

Clift, R., J. R. Grace, et al. (1978). *Bubbles, Drops, and Particles.* Academic Press New York.

Davie, M. K. and B. A. Buffett (2001). "A numerical model for the formation of gas hydrate below the seafloor." *Journal of Geophysical Research* **106**(B1): 497-514.

Davie, M. K., O. Y. Zatsepina, et al. (2004). "Methane solubility in marine hydrate environments." *Marine Geology* **203**(1-2): 177-184.

Dholabhai, P. D., N. Kalogerakis, et al. (1993). “Kinetics of methane hydrate formation in aqueous-electrolyte solutions.” *Canadian Journal of Chemical Engineering* **71**: 68-74.

Englezos, P., N. Kalogerakis, et al. (1987). “Kinetics of formation of methane and ethane gas hydrates.” *Chemical Engineering Science* **42**: 2647-2658.

Freer, E. M., M. S. Selim, et al. (2001). “Methane hydrate film growth kinetics”. *Fluid Phase Equilibria* **185**(1-2): 65-75.

Gaillard, C., J. P. Monfort, et al. (1999). “Investigation of methane hydrate formation in a recirculating flow loop: Modeling of the kinetics and tests of efficiency of chemical additives on hydrate inhibition.” *Oil & Gas Science and Technology* **54**: 365-374.

Gangstø, R., P. M. Haugan, et al. (2005). “Parameterization of drag and dissolution of rising CO_2 drops in seawater.” *Geophysical Research Letters* **32**: doi:10.1029/2005GL022637.

Garg, S. K., J. W. Pritchett, et al. (2008). "A mathematical model for the formation and dissociation of methane hydrates in the marine environment." *Journal of Geophysical Research* **113**(B01201): doi:10.1029/2006JB004768.

Greinert, J., Y. Artemov, et al. (2006). “1300-m-high rising bubbles from mud volcanoes at 2080m in the Black Sea: Hydroacoustic characteristics and temporal variability.” *Earth and Planetary Science Letters* **244**, 1-15.

Haeckel, M., E. Suess, et al. (2004). "Rising methane gas-bubbles form massive hydrate layers at the seafloor." *Geochimica et Cosmochimica Acta* **68**(21): 4335-4345.

Haugan, P., F. Thorkildsen, et al. (1995). “Dissolution of CO_2 in the ocean.” *Energy Conversion and Management* **36**: 461-466.

Heeschen, K. U., R. S. Keir, et al. (2004). “Methane dynamics in the Weddell Sea determined via stable isotope ratios and CFC-11.” *Global Biogeochemical Cycles* **19**.

Hensen, C. and K. Wallmann (2005). "Methane formation at Costa Rica continental margin - constraints for gas hydrate inventories and cross-décollement fluid flow." *Earth and Planetary Science Letters* **236**: 41-60.

Herri, J. M., J. S. Pic, et al. (1999). “Methane hydrate crystallization mechanism from in-situ particle sizing.” *American Institute of Chemical Engineers Journal* **45**: 590-602.

Hirai, S., K. Okazaki, et al. (1996). “Transport phenomena of liquid CO_2 in pressurized water flow with clathrate-hydrate at the interface.” *Energy Conversion and Management* **37**: 1073-1078.

Hirai, S., K. Okazaki, et al. (1997). “Dissolution rate of liquid CO_2 in pressurized water flows and the effect of clathrate films.” *Energy* **22**: 285-293.

Kim, H. C., P. R. Bishnoi, et al. (1987). “Kinetics of methane hydrate decomposition.” *Chemical Engineering Science* **42**: 1645-1653.

Kurihara, M., H. Ouchi, et al. (2005). “Analysis of the JAPEX/JNOC/GSC et al. Mallik 5L-38 gas hydrate thermal-production test through numerical simulation.” In: *Scientific Results from the Mallik 2002 Gas Hydrate Production Research Well Program, Mackenzie Delta, Northwest Territories, Canada*. S. Dallimore and T. Collett (eds.), *Geological Survey of Canada Bulletin* **585**.

Lee, J. D., R. Susilo, et al. (2005). “Methane-ethane and methane-propane hydrate formation and decomposition on water droplets.” *Chemical Engineering Science* **60**: 4203-4212.

Leifer, I. and R. K. Patro (2002). “The bubble mechanism for methane transport from the shallow sea bed to the surface: A review and sensitivity study.” *Continental Shelf Research* **22**: 2409-2428.

Linga, P., R. N. Kumar, et al. (2007). “Gas hydrate formation from hydrogen/carbon dioxide and nitrogen/carbon dioxide gas mixtures.” *Chemical Engineering Science* **62**: 4268-4276.

Malegaonkar, M. B., P. D. Dholabhai, et al. (1997). “Kinetics of carbon dioxide and methane hydrate formation.” *Canadian Journal of Chemical Engineering* **75**: 1090-1099.

McGinnis, D. F., J. Greinert, et al. (2006). “Fate of rising methane bubbles in stratified waters: How much methane reaches the atmosphere?” *Journal of Geophysical Research* **111**: doi:10.1029/2005JC003183.

Mochizuki, T. and Y. H. Mori (2006). “Clathrate-hydrate film growth along water/hydrate-former phase

boundaries - numerical heat-transfer study." *Journal of Crystal Growth* **290**: 642-652.

Moridis, G. J., M. B. Kowalsky, et al. (2008). *TOUGH+Hydrate v1.0 User's Manual: A Code for the Simulation of System Behavior in Hydrate-Bearing Geologic Media*. Lawrence Berkeley National Laboratory.

Natarajan, V., P. R. Bishnoi, et al. (1994). "Induction phenomena in gas hydrate nucleation." *Chemical Engineering Science* **49**: 2075-2087.

Ozaki, M., J. Minamiura, et al. (2001). „CO_2 sequestration by moving ships." *Journal of Marine Science and Technology* **6**: 51-58.

Parent, J. S. and P. R. Bishnoi (1996). "Investigations into the nucleation behaviour of methane gas hydrates." *Chemical Engineering Communications* **144**: 51-64.

Rehder, G., P. W. Brewer, et al. (2002). "Enhanced lifetime of methane bubble streams within the deep ocean." *Geophysical Research Letters* **29**: doi:10.1029/2001GL013966.

Rehder, G., S. H. Kirby, et al. (2004). "Dissolution rates of pure methane hydrate and carbon-dioxide hydrate in undersaturated seawater at 1000-m depth." *Geochimica et Cosmochimica Acta* **68**: 285-292.

Rehder, G., I. Leifer, et al. (2009). "Controls on methane bubble dissolution inside and outside the hydrate stability field from open ocean field experiments and numerical modeling." *Marine Chemistry* **114**: 19-30.

Sauter, E. J., S. I. Muyakshin, et al. (2006). "Methane discharge from a deep-sea submarine mud volcano into the upper water column by gas hydrate-coated methane bubbles." *Earth and Planetary Science Letters* **243**: 354-365.

Sean, W. Y., T. Sato, et al. (2007a). "CFD and experimental study on methane hydrate dissociation Part I. Dissociation under water flow." *American Institute of Chemical Engineers Journal* **53**, 262-274.

Sean, W. Y., T. Sato, et al. (2007b). "CFD and experimental study on methane hydrate dissociation. Part II. General cases." *American Institute of Chemical Engineers Journal* **53**, 2148-2160.

Servio, P. and P. Englezos (2003). "Morphology of methane and carbon dioxide hydrates formed from water droplets." *American Institute of Chemical Engineers Journal* **49**, 269-276.

Skovborg, P., H. J. Ng, et al. (1993). "Measurement of induction times for the formation of methane and ethane gas hydrates. *Chemical Engineering Science* **48**: 445-453.

Skovborg, P. and P. Rasmussen (1994). "A mass-transport limited model for the growth of methane and ethane gas hydrates." *Chemical Engineering Science* **49**: 1131-1143.

Sloan, E. D. and C. A. Koh (2008). *Clathrate Hydrates of Natural Gases.* Boca Raton, CRC Press.

Takeya, S., A. Hori, et al. (2000). "Freezing-memory effect of water on nucleation of CO_2 hydrate crystals." *Journal of Physical Chemistry B* **104**: 4164-4168.

Uchida, T., T. Ebinuma, et al. (1999). "Microscopic observations of formation processes of clathrate-hydrate films at an interface between water and carbon dioxide." *Journal of Crystal Growth* **204**: 348-356.

Vysniauskas, A. and P. R. Bishnoi (1983). "A kinetic study of methane hydrate formation." *Chemical Engineering Science* **38**: 1061-1072.

Wallmann, K., G. Aloisi, et al. (2006). "Kinetics of organic matter degradation, microbial methane generation, and gas hydrate formation in anoxic marine sediments." *Geochimica et Cosmochimica Acta* **70**: 3905-3927.

Wilson, P. W., A. D. Haymet, et al. (2008). "Nucleation of clathrates from supercooled THF/water mixtures shows that no memory effect exists." *6th International Conference on Gas Hydrates (ICGH 2008)*, Vancouver, Canada.

Zhang, Y. X. (2005). "Fate of rising CO_2 droplets in seawater." *Environmental Science & Technology* **39**: 7719-7724.

Appendix A: Thermodynamic and kinetic properties of gas hydrate systems

A.1 Gas hydrate formation and dissociation process

A.1.1 Enthalpy of CH_4 hydrate dissociation: s-I CH_4 hydrate - - -> CH_4 + H_2O(l)

ΔH [kJ/mol]	p [MPa]	T [K]	Equation	Reference
Experiment				
52.0-51.6		273-298	ΔH = 13521 – 4.02*T/K [cal/mol]	Kamath (1984)
3.6-13.7		248-273	ΔH = 6543 – 11.97*T/K [cal/mol]	
54.19	1	160-210		Handa (1986)
52.8-57.7		278 -283		Lievois (1987)
56.84	0.1-0.3	273		Kang & Lee (2001)
51.4-54.9	2.9-214.4	274-314	Eq.2.2.1	Gupta (2007)
Modelling				
53.8				Garg et al. (2008)
52.0	water	273.15	ΔH = 56518 – 16.72*T/K [J/mol]	Kurihara et al. (2005)
13.6	Ice	273.15	ΔH = 27312 – 50.16*T/K [J/mol]	
ΔH = -R * d ln(f)/d (1/T); R=82.055 cm^3*atm/mol/K; ln(f/atm) = -6705/T + 27.73 + 3.0/(R*T)*exp(6705/T+27.73)				Smith et al. (2001)

A.1.2 Enthalpy of CO_2 hydrate dissociation: s-I CO_2 hydrate - - -> CO_2 + H_2O(l)

ΔH [kJ/mol]	p [MPa]	T [K]	Equation	Reference
Experiment				
80.38		273-298	ΔH = 19199 - 14.95*T/K [cal/mol]	Kamath (1984)
82	1.4-3.3	274-281		Clarke & Bishnoi (2004)
65.22	0.1 - 0.3	273		Kang & Lee (2001)
62.5	1.377	274	ΔH = 62.9 - 0.53*(T/K - 273.15)	Anderson (2003)
Modelling				
71.82		274	Monte Carlo simulation	Ota & Ferdows (2005)
ΔH = -R * d ln(f)/d (1/T); R=82.055 cm^3*atm/mol/K; ln(f/atm) = -8482/T + 33.43 + 3.0/(R*T)*exp(8482/T+33.43)				Smith et al. (2001)

A.1.3 Gibbs energy of CH_4->CO_2 hydrate conversion

Description	ΔG [kJ/mol]	p [MPa]	T [K]	Reference
s-I: [8 CH4(S+L) + 6 CO2 -> [2 CH4(S), 6 CO2(L)] + 6 CH4	-14.6	30	275	Dornan et al. (2007)
s-I: [8 CH4(S+L) + 6 CO2 + 2 N2 -> [2 N2(S), 6 CO2(L)] + 8 CH4	-5.4	30	275	
s-II: [24 CH4(S+L) + 24 CO2 -> [24 CO2(S+L)] + 24 CH4	-53.2	30	275	

A.1.4 Kinetics of CH_4 hydrate dissociation

E_A [kJ/mol]	k_0 [mol/(m^2 Pa s)]	p [MPa]	T [K]	Equation	Reference
78.3	$1.24x10^5$	0-7	274-283	Eq.4.3.1 + Eq.4.3.2	Kim et al. (1987)
81	$3.6x10^4$	3.1-6.1	275-281		Clarke & Bishnoi (2001)

A.1.5 Kinetics CO_2 hydrate dissociation

E_A [kJ/mol]	k_0 [mol/(m^2 s Pa)]	p [MPa]	T [K]	Equation	Reference
102.9	$1.83x10^8$	1.4-3.3	274-281	Eq.4.3.1 + Eq.4.3.2	Clarke & Bishnoi (2004)

A.1.6 Kinetics of CH_4 hydrate formation

Parameter [unit]	p [MPa]	T [K]	Equation	Reference
Intrinsic hydrate growth from gas consumption				
k = 0.55-0.65 [mol/(m^2 Pa s)]	0.6-8.9	274-282	Eq.4.1.5	Englezos et al. (1987)
k = 8.3-61.5 x 10^{-8} [m/s]		275-279	Eq.4.1.8	Bergeron et al. (2010)
Mass transfer contolled hydrate growth				
k = 4.08 x 10^{-5} [m/s]			Eq.4.1.9	Skovberg & Rasmussen (1994)
Heat transfer controlled hydrate growth				
k_0 = 1.61 x 10^{36} [W/m^2 K] E_A = 20599 [kJ/mol] h = 42326 [W/m^2 K]	3.6-9.1	273-275	Eq. 4.1.12	Freer et al. (2001)

A.1.7 Kinetics of CO_2 hydrate formation

Parameter [unit]	p [MPa]	T [K]	Equation	Reference
Intrinsic hydrate growth from gas consumption				
k = 3.2-6.4x10^{-3} [mol/(m^2 Pa s)]	1.6-3.0	274-279	Eq.4.1.5	Clarke & Bishnoi (2005)
k = 1.9-4.9x10^{-4} [mol/(m^2 Pa s)]		274-278		Malegoankar et al. (1997)
k = 1.8-18 x 10^{-8} [m/s]	2-3	276-279	Eq.4.1.8	Bergeron & Servio (2008)

A.1.8 Activation energy of CH_4 -> CO_2 gas hydrate conversion

E_A [kJ/mol]	k_0 [mol/(m^2 s Pa)]	p [MPa]	T [K]	Equation	Reference
14.5	2.4-2.6x10^8	3.25	271-275	Eq.4.3.1 (CH_4 hydrate decomposition)	Ota et al. (2005)
73.3	2.4-3.8x10^8			Eq.4.1.5 (CO_2 hydrate formation)	

A.1.9 Diffusion of CO_2 and CH_4 in the hydrate phase (percolation, hole-in-the-cage)

E_A [kJ/mol]	D_{ref} [m^2/s]	p [MPa]	T [K]	Comment	Reference
Experiment					
61.5		6.9	253-273	CH_4 hydrate from ice	Wang et al. (2002)
52.1	4.1×10^{-16}	6.0	263	CH_4 hydrate from ice	Kuhs et al. (2006)
27.2		6.2	230-263	CO_2 hydrate from ice	Henning et al. (2000)
54.6	1.8×10^{-15}	2.0	272	CO_2 hydrate from ice	Genov et al. (2006)
46	2×10^{-16}	1.0	253	CO_2 hydrate from ice	Falenty et al. (2013)
E_A [kJ/mol]	D_{ref} [m^2/s]	p [MPa]	T [K]	Comment	Reference
Modelling					
	$7 \times 10^{-15} * X$ (#)		250	CH_4 in hydrate	Peters et al. (2008)
	1×10^{-12}		273	CO_2 in hydrate	Demurov et al. (2008)

(#) X = fraction of unoccupied cages

A.1.10 CH_4 gas dissolution / exsolution step during hydrate formation / dissociation

Dissolution k_1 [1/s]	Exsolution k_{-1} [1/s]	p [MPa]	T [K]	Equation	Reference
$2.7\text{-}3.2 \times 10^{-4}$	$8.2\text{-}10.5 \times 10^{-3}$		284-298	$\ln\left(\frac{CH_4 - CH_4^{\infty}}{CH_4^{0} - CH_4^{\infty}}\right) = -(k_1 + k_{-1})\, t$	Lekvam & Ruoff (1993)

A.2 Thermal properties

A.2.1 Thermal conductivity of CH_4 hydrate

λ [W/m/K]	p [MPa]	T [K]	Equation	Reference
0.564-0.587	2.0	263-278		Huang & Fan (2004)
~0.68	2.5-14.7	261-277	λ = -1.99E-4*T/℃ + 0.682	Rosenbaum et al. (2007)
0.62-0.63	31.5	253-290	λ = -2.78E-4*T/℃ + 0.624	Waite et al. (2007)
0.50-0.58				Sloan & Koh (2008)

A.2.2 Thermal conductivity of some sediments and rocks

Sediment type	λ [W/m/K]	Comment	Reference
sandstone	1.46-4.27		Clark (1966)
	0.9-5.17		Schön (1996)
	3.4-8		Aplin et al. (1999)
sandy siltstone	2.49		Aplin et al. (1999)
shaly sandstone	2.66		Aplin et al. (1999)
muddy sandstone	3.2		Aplin et al. (1999)
siltstone	2.47-2.84		Schön (1996)
	3.2		Aplin et al. (1999)
mudstone-siltstone	2.5		Aplin et al. (1999)
clay-siltstone	1.7-3.4		Schön (1996)
claystone	0.6-4		Schön (1996)
	1.5-3		Aplin et al. (1999)
clay	1.2-1.4		Aplin et al. (1999)
sandy shale	2.1		Aplin et al. (1999)
shale	1.17-2.87		Clark (1966)
	0.55-4.25		Schön (1996)
	1.9-2.35		Aplin et al. (1999)
carbonate	3-3.24		Aplin et al. (1999)
limestone	3.2-3.6		Aplin et al. (1999)
167 North Sea wells	0.8-8.3		Aplin et al. (1999)
Gulf of Mexico	2.02		Aplin et al. (1999)
sedimentary rock	1.7-4.2		Aplin et al. (1999)

A.2.3 Thermal conductivity of some natural (water-saturated) marine sediments

Sediment type	λ [W/m/K]	Comment	Reference
Black Sea	0.6-1.3	water content: 70-30%	Petrunin et al. (2008)
Juan de Fuca Ridge	0.8-1.8		Goto & Matsubayashi (2008)
Chile, ODP sites 860 + 863	1.0-2.5	porosity: 0.6-0.2	Revil (2000)
Eastern Equatorial Pacific	0.6-1.0		Matsuda & von Herzen (1986)

A.2.4 Thermal conductivity of hydrate-bearing sediments

λ [W/m/K]	Comment	Reference
~1	λ = -3.2E-3*T/℃ + 1.04; quartz sand, Φ=0.4 (pores filled with gas); S_h=0.49 (volume expansion during hydrate formation)	Waite et al. (2002)
0.82-0.87	λ = -2.3E-3*T/℃ + 0.867; quartz sand, Φ=0.4 (pores filled with gas); S_h=1.14 (volume expansion during hydrate formation)	
~1	quartz sand, Φ=0.47, S_h=?; pores filled with gas+water	Huang & Fan (2005)
2.35-2.77	Mallik-sand; Φ=0.3, S_h=0.9; calculated from regional heat flow and core log data using mixing laws	Henninges et al. (2005)

A.2.5 Specific heat capacity of some minerals and non-porous rocks (at 20 ℃; Waples & Waples (2004a+b)

Mineral	c_p [J/kg/K]	Non-porous Rock	c_p [J/kg/K]
average	660 +/- 235	Average	938
Hematite	620	Plagioclases	711-837
Magnetite	586	Feldspars	628-800
Manganite	765	Olivines	576-840
Quartz	740	Pyroxenes	670-831
Opal	725	Basalt	898
Aragonite	785	Clay	860
Calcite	815	Limestone	680-880
Dolomite	870	Sandstone	775
Barite	540	Siltstone	910
Anhydrite	585	Tuff	795-1090
Gypsum	1070	Serpentinite	730-1005
Halite	216	Schist	790-1096
Pyrite	510		

A.2.6 Specific heat capacity of some natural (water-saturated) marine sediments

Sediment type	c_p [J/kg/K]	Comment	Reference
Black Sea	1580-3260	water content: 70-30%	Petrunin et al. (2008)

A.3 Kinetic parametrizations from a few modelling studies of natural gas hydrate and seep systems

Kinetic constant	Modelled Setting	Equation	Reference
k_{dis}^{G}	CH4 gas dissolution		
1.4-8.5 x 10^{-5} s^{-1}	Hydrate Ridge cold vent + hydrate	Eq. 4.2.1	Haeckel et al. (2004)
9.5 x 10^{-9} s^{-1}	Black Sea gas seep + hydrate	Eq. 4.2.1	Haeckel et al. (2008)
3.1 x 10^{-8} M^{-1} s^{-1}	Aarhus Bay gas seep	Eq. 4.2.1 * gas conc.	Dale et al. (2008)
k_{fm}^{H}	CH4 hydrate formation		
1 x 10^{-8} s^{-1}	Blake Ridge hydrate reservoir	Eq. 4.2.3	Davie & Buffett (2001)
9.4-32 x 10^{-6} s^{-1}	Hydrate Ridge cold vent + hydrate	Eq. 4.2.2	Haeckel et al. (2004)
6.3 x10^{-8} wt% s^{-1}	Blake Ridge hydrate reservoir	Eq. 4.2.2	Wallmann et al. (2006)
1.6 x 10^{-10} s^{-1}	Black Sea gas seep + hydrate	Eq. 4.2.2	Haeckel et al. (2008)
1 x 10^{-5} a^{-1}	Costa Rica margin subduction zone	Eq. 4.2.2	Hensen et al. (2005)
6.5 x 10^{-14} M/s	Bush Hill cold vent + hydrate	Eq. 4.2.5 (M_{GH}=122 g/mol)	Cathles & Chen (2004)
k_{fm}^{G}	CH4 gas bubble formation		
3.1 x 10^{-1} M^{-1} s^{-1}	Namibia Shelf gas seep	Eq. 4.4.2 * gas conc.	Dale et al. (2009)
1.6 x 10^{-9} m/s	Eckernförde Bay gas seep	Eq. 4.5.1	Mogollon et al. (2009)
1 x 10^{-8} s^{-1}	Blake Ridge hydrate reservoir	Eq. 4.4.2	Davie & Buffett (2001)
k_{dis}^{H}	CH4 hydrate dissociation		
6.3 x10^{-8} wt% s^{-1}	Blake Ridge hydrate reservoir	Eq. 4.4.1 * hydrate conc.	Wallmann et al. (2006)
3 x 10^{-12} s^{-1}	Costa Rica subduction zone	Eq. 4.4.1 * hydrate conc.	Hensen et al. (2005)

References

Anderson, G. (2003). "Enthalpy of dissociation and hydration number of carbon dioxide hydrate from the Clapeyron equation." *Journal of Chemical Thermodynamics* **35**: 1171-1183.

Aplin, A., A. Fleet, et al. (1999). "Muds and mudstones: Physical and fluid flow properties." *The Geological Society of London Special Publication **158**.*

Bergeron, S. and P. Servio (2008). "Reaction rate constant of CO_2 hydrate formation and verification of old premises pertaining to hydrate growth kinetics." *American Institute of Chemical Engineers Journal* **54**(11): 2964-2970.

Bergeron, S., J. Beltran, et al. (2010). "Reaction rate constant of methane clathrate formation." *Fuel* **89**(2): 294-301.

Cathles, L. M. and D. F. Chen (2004). "A compositional kinetic model of hydrate crystallization and dissolution." *Journal of Geophysical Research* **109**(B08102): doi:10.1029/2003JB002910.

Clark, S. (1966). *Handbook of Physical Constants*. Geological Society of America.

Clarke, M. and P. Bishnoi (2001). "Determination of the activation energy and intrinsic rate constant of methane gas hydrate decomposition." *The Canadian Journal of Chemical Engineering* **79**(1): 143-147.

Clarke, M. and P. Bishnoi (2004). "Determination of the intrinsic rate constant and activation energy of CO2 gas hydrate decomposition using in-situ particle size analysis." *Chemical Engineering Science* **59**(14): 2983-2993.

Clarke, M. A. and P. R. Bishnoi (2005). "Determination of the intrinsic kinetics of CO_2 gas hydrate formation using in situ particle size analysis." *Chemical Engineering Science* **60**(3): 695-709.

Dale, A. W., D. R. Aguilera, et al. (2008). "Seasonal dynamics of the depth and rate of anaerobic oxidation of methane in Aarhus Bay (Denmark) sediments." *Journal of Marine Research* **66**(1): 127-155.

Dale, A. W., V. Brüchert, et al. (2009). "An integrated sulfur isotope model for Namibian shelf sediments." *Geochimica et Cosmochimica Acta* **73**(7): 1924-1944.

Davie, M. K. and B. A. Buffett (2001). "A numerical model for the formation of gas hydrate below the seafloor." *Journal of Geophysical Research* **106**(B1): 497-514.

Demurov, A., R. Radhakrishnan, R., et al. (2002). "Computations of diffusivities in ice and CO_2 clathrate hydrates via molecular dynamics and Monte Carlo simulations." *Journal of Chemical Physics* **116**: 702-709.

Dornan, P., S. Alavi, et al. (2007). "Free energies of carbon dioxide sequestration and methane recovery in clathrate hydrates." *The Journal of Chemical Physics* **127**: 124510.

Englezos, P., N. Kalogerakis, et al. (1987). "Kinetics of formation of methane and ethane gas hydrates." *Chemical Engineering Science* **42**(11): 2647-2658.

Falenty, A., A. N. Salamatin, et al. (2013). "Kinetics of CO_2-hydrate formation from ice powders: data summary and modeling extended to low temperatures." *Journal of Physical Chemistry C* **117**: 8443-8457.

Freer, E. M., M. S. Selim, et al. (2001). “Methane hydrate film growth kinetics”. *Fluid Phase Equilibria* **185**(1-2): 65-75.

Garg, S. K., J. W. Pritchett, et al. (2008). "A mathematical model for the formation and dissociation of methane hydrates in the marine environment." *Journal of Geophysical Research* **113**: doi:10.1029/2006JB004768.

Genov, G., W. Kuhs, et al. (2004). "Experimental studies on the formation of porous gas hydrates." *American Mineralogist* **89**: 1228-1239.

Goto, S. and O. Matsubayashi (2008). "Inversion of needle-probe data for sediment thermal properties

of the eastern flank of the Juan de Fuca Ridge." *Journal of Geophysical Research* **113**(B08105): doi: 10.1029/2007JB005119.

Gupta, A. (2007). *Methane hydrate dissociation measurements and modelling: The role of heat transfer and reaction kinetics*. PhD Thesis, Colorado School of Mines.

Haeckel, M., A. Reitz, et al. (2008). “Methane budget of a large gas hydrate province offshore Georgia, Black Sea”. *6th International Conference on Gas Hydrates (ICGH 2008)*, Vancouver, Canada.

Haeckel, M., E. Suess, et al. (2004). "Rising methane gas-bubbles form massive hydrate layers at the seafloor." *Geochimica et Cosmochimica Acta* **68**(21): 4335-4345.

Handa, Y. (1986). "Compositions, enthalpies of dissociation and heat cpacities in the range 85 to 270 K for clathrate hydrates of methane, ethane and propane and enthalpy of dissociation of isobutane hydrate , as determined by a heat-flow calorimeter." *Journal of Chemical Thermodynamics* **18**: 915-921.

Henning, R. W., A. J. Schultz, et al. (2000). "Neutron diffraction studies of CO_2 clathrate hydrate: Formation from deuterated ice." *Journal of Physical Chemistry A* **104**: 5066-5071.

Hensen, C. and K. Wallmann (2005). "Methane formation at Costa Rica continental margin - constraints for gas hydrate inventories and cross-décollement fluid flow." *Earth and Planetary Science Letters* **236**: 41-60.

Huang, D. and S. Fan (2004). "Thermal conductivity of methane hydrate formed from sodium dodecyl sulfate solution." *Journal of Chemical Engineering Data* **49**: 1479-1482.

Kamath, V. (1984). *A study of heat transfer characteristics during dissociation of gas hydrates.* PhD Thesis, University of Pittsburgh.

Kang, S. and H. Lee (2001). "Enthalpies of dissociation of clathrate hydrates of carbon dioxide, nitrogen, (carbon dioxide + nitrogen), and (carbon dioxide + nitrogen + tetrahydrofuran)." *Journal of Chemical Thermodynamics* **33**: 513-521.

Kim, H. C., P. R. Bishnoi, et al. (1987). "Kinetics of methane hydrate decomposition." *Chemical Engineering Science* **42**(7): 1645-1653.

Kuhs, W., D. Staykova, et al. (2006). "Formation of methane hydrate from polydisperse ice powders." *Journal of Physical Chemistry B* **110**: 13283-13295.

Kurihara, M., H. Ouchi, et al. (2005). “Analysis of the JAPEX/JNOC/GSC et al. Mallik 5L-38 gas hydrate thermal-production test through numerical simulation.” In: *Scientific Results from the Mallik 2002 Gas Hydrate Production Research Well Program, Mackenzie Delta, Northwest Territories, Canada*. S. Dallimore and T. Collett (eds.), *Geological Survey of Canada Bulletin* **585**.

Lekvam, K. and P. Ruoff (1993). "A reaction kinetic mechanism for methane hydrate formation in liquid water." *Journal of the American Chemical Society* **115**(19): 8565-8569.

Lievois, J. (1987). *Development of an automated, high pressure heat flux calorimeter and its application to measure the heat of dissociation of methane hydrate*. PhD Thesis, Rice University.

Malegoankar, M. B., P. D. Dholabhai, et al. (1997). "Kinetics of carbon dioxide and methane hydrate formation." *Canadian Journal of Chemical Engineering* **75**(6): 1090-1099.

Matsuda, J. and R. von Herzen (1986). "Thermal conductivity variation in a deep-sea sediment core and its relation to H_2O, Ca and Si content." *Deep-Sea Research* **33**(2): 165-175.

McGinnis, D. F., J. Greinert, et al. (2006). "Fate of rising methane bubbles in stratified waters: How much methane reaches the atmosphere?" *Journal of Geophysical Research* **111**(C09007): doi:10.1029/2005JC003183.

Mogollón, J. M., I. L'Heureux, I., et al. (2009). “Methane gas-phase dynamics in marine sediments: A model study.” *American Journal of Science* **309**: 189-220.

Mori, Y. (2001). "Estimating the thickness of hydrate films from their lateral growth rates: application of a simplified heat transfer model." *Journal of Crystal Growth* **223**(1-2): 206-212.

Ota, M., Y. Abe, et al. (2005). "Methane recovery from methane hydrate using pressurized CO_2." *Fluid*

Phase Equilibria **228-229**: 553-559.

Ota, M. and M. Ferdows (2005). "Monte Carlo approach to structure and thermodynamic property of CO_2 hydrate " *Japan Society of Mechanical Engineers International Journal Series B* **48**(4): 802-810.

Peters, B., N. E. R. Zimmermann, et al. (2008). "Path sampling calculation of methane diffusivity in natural gas hydrates from a water-vacancy assisted mechanism." *Journal of the American Chemical Society* **130**, 17342-17350.

Petrunin, G., V. Popov, et al. (2008). "Thermal Properties of the Bottom Sediments of the Black Sea." *Moscow University Physics Bulletin* **63**(1): 61-66.

Revil, A. (2000). "Thermal conductivity of unconsolidated sediments with geophysical applications." *Journal of Geophysical Research* **105**(B7): 16749-16768.

Rosenbaum, E. J., N. J. English, et al. (2007). "Thermal conductivity of methane hydrate from experiment and molecular simulation." *Journal of Physical Chemistry B* **111**(46): 13194-13205.

Schön, J. (1996). "Physical propertues of rocks: fundamentals and principles of petrophysics." *Seismic Exploration* **18**, Elsevier, Oxford.

Skovborg, P. and P. Rasmussen (1994). "A Mass-Transport Limited Model for the Growth of Methane and Ethane Gas Hydrates." *Chemical Engineering Science* **49**(8): 1131-1143.

Sloan, E. D. and C. A. Koh (2008). *Clathrate Hydrates of Natural Gases*. Boca Raton, CRC Press.

Smith, D., K. Seshadri, et al. (2001). "Assessing the thermodynamic feasibility of the conversion of methane hydrate into carbon dioxide hydrate in porous media." *First National Conference on Carbon Sequestration, National Energy Technology Laboratory*.

Staykova, D., W. Kuhs, et al. (2003). "Formation of Porous Gas Hydrates from Ice Powders: Diffraction Experiments and Multistage Model." *Journal of Physical Chemistry B* **107**: 10299-10311.

Uchida, T., T. Ebinuma, et al. (1999). "Microscopic observations of formation processes of clathrate-hydrate films at an interface between water and carbon dioxide." *Journal of Crystal Growth* **204**(3): 348-356.

Vysniauskas, A. and P. R. Bishnoi (1983). "A kinetic study of methane hydrate formation." *Chemical Engineering Science* **38**(7): 1061-1072.

Waite, W., L. Gilbert, et al. (2005). "Thermal property measurements in Tetrahydrofuran (THF) hydrate and hydrate-bearing sediment between -25 and +4°C, and their application to methane hydrate." *Proceedings of the Fifth International Conference on Gas Hydrates*.

Waite, W., L. Stern, et al. (2007). "Simultaneous determination of thermal conductivity, thermal diffusivity and specific heat in sI methane hydrate." *Geophysical Journal International* **169**: 767-774.

Wallmann, K., G. Aloisi, et al. (2006). "Kinetics of organic matter degradation, microbial methane generation, and gas hydrate formation in anoxic marine sediments." *Geochimica et Cosmochimica Acta* **70**: 3905-3927.

Wang, X., A. Schultz, et al. (2002). "Kinetics of methane hydrate formation from polycrystalline deuterated ice." *Journal of Physical Chemistry A* **106**: 7304-7309.

Waples, D. W. and J. S. Waples (2004a). “A review and evaluation of specific heat capacities of rocks, minerals, and subsurface fluids. Part 1: Minerals and nonporous rocks.” *Natural Resources Research* **13**: 97-122.

Waples, D. W. and J. S. Waples (2004b). “A review and evaluation of specific heat capacities of rocks, minerals, and subsurface fluids. Part 2: Fluids and porous rocks.” *Natural Resources Research* **13**: 123-130.

Appendix B: Application example of a hypothetical gas hydrate reservoir

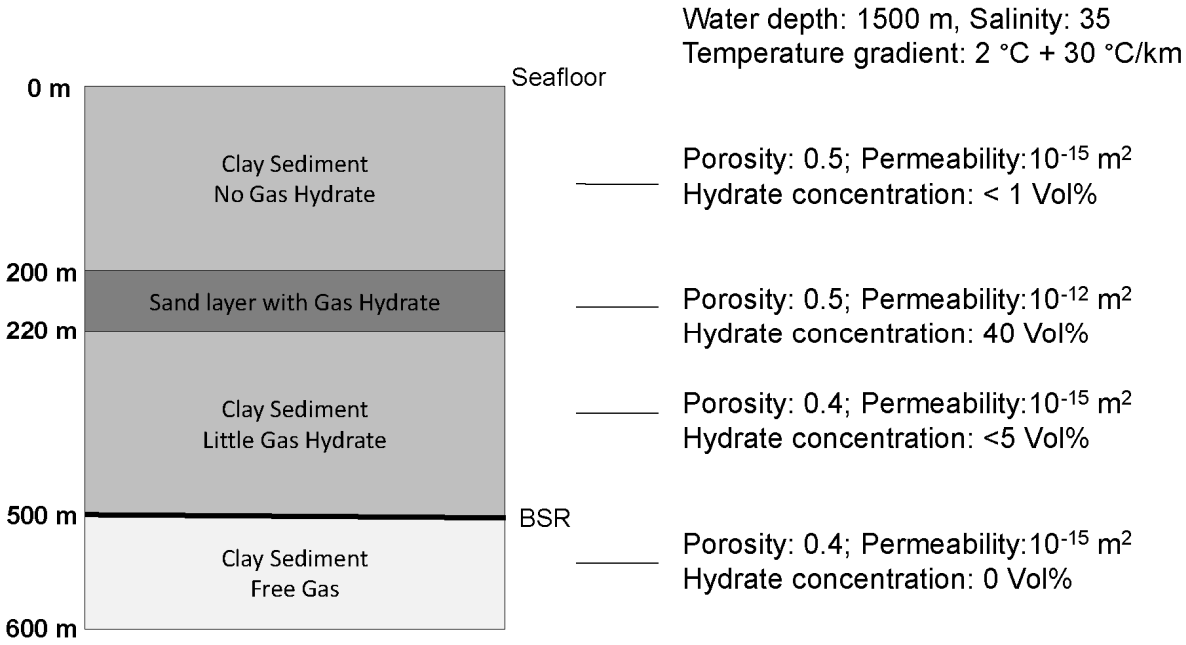

Figure B.1: Geological setting of the hypothetical gas hydrate reservoir.

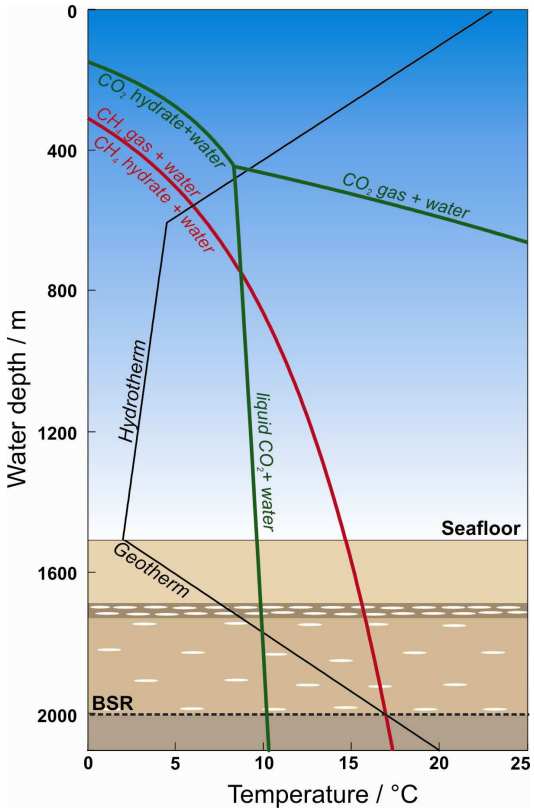

Figure B.2: Phase boundaries for methane (red) and carbon dioxide (green) gas hydrates for the imposed temperature profiles in the water column (hydrotherm) and sediment (geotherm).

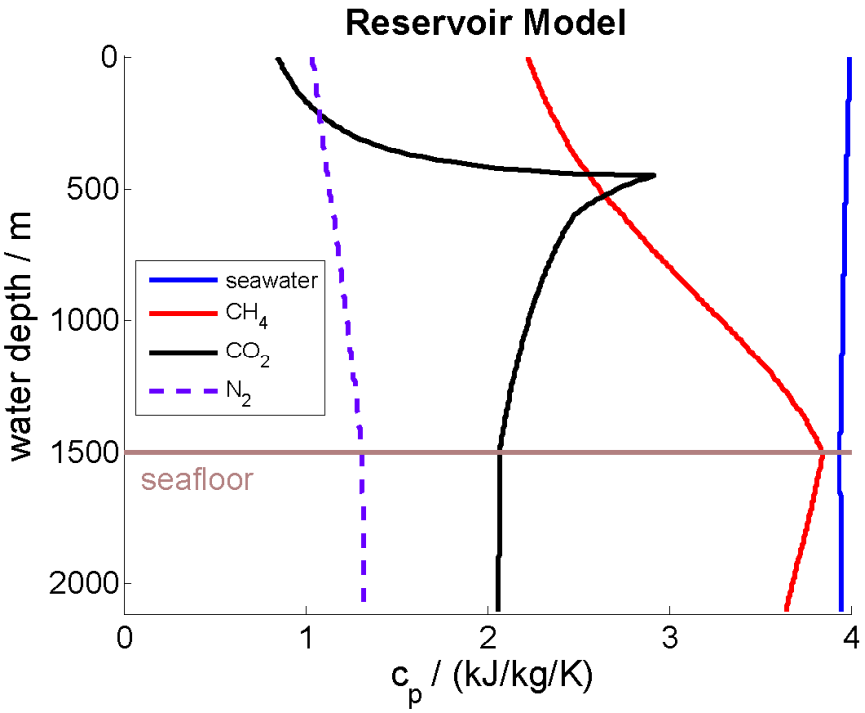

Figure B.3: Profiles of (isobaric) specific heat capacities. The steep decrease in heat capacity results from the gas/liquid phase transition of CO_2.

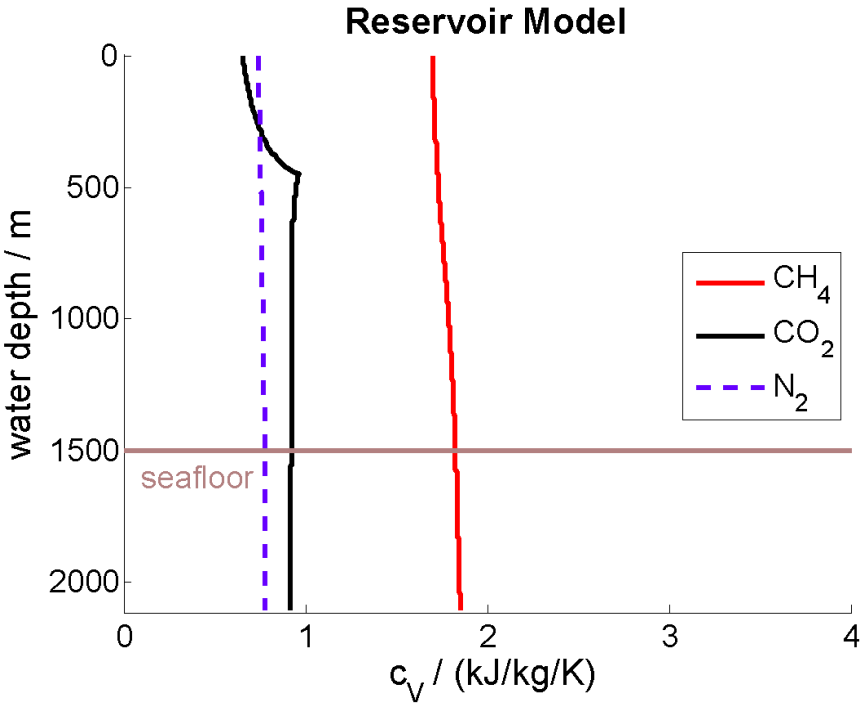

Figure B.4: Profiles of specific heat capacities at constant volume. The decrease in heat capacity results from the gas/liquid phase transition of CO_2.

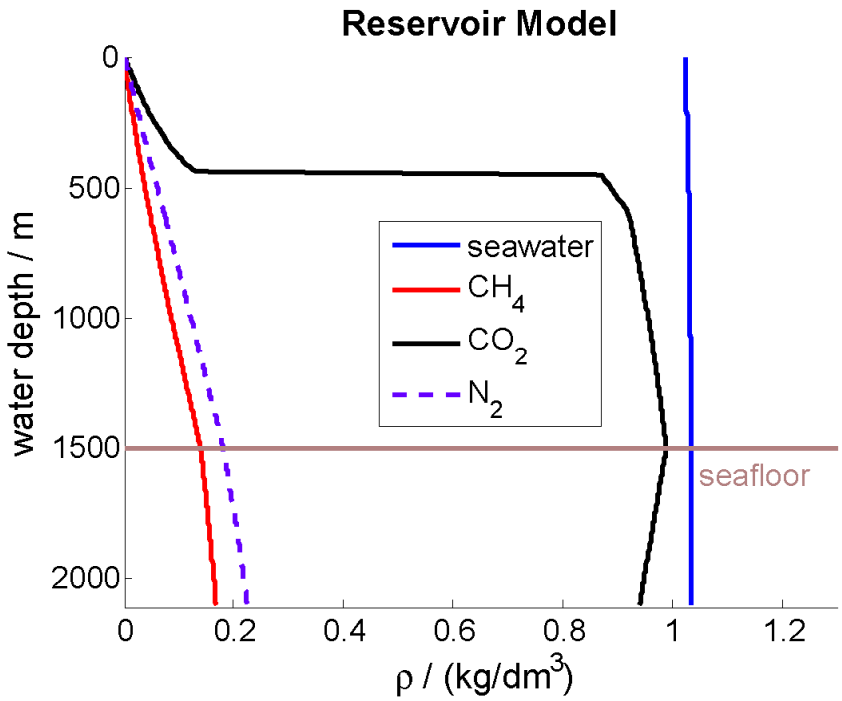

Figure B.5: Density profiles for pure seawater, CH_4, CO_2 and N_2. The steep increase in density results from the gas/liquid phase transition of CO_2.

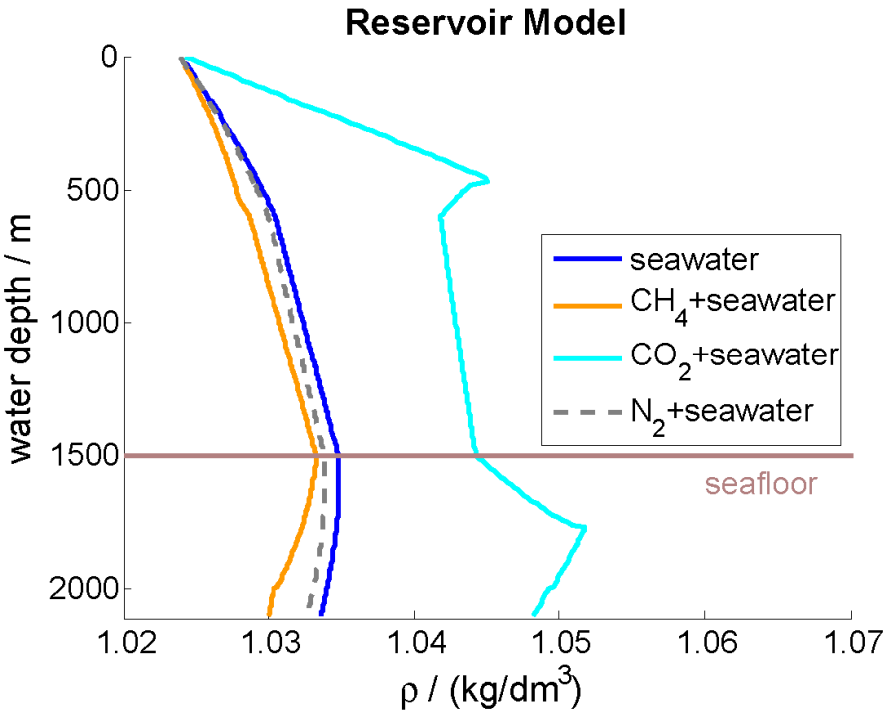

Figure B.6: Density profiles for pure seawater and seawater saturated with CH_4, CO_2 or N_2. Sudden density changes are associated with hydrate formation and hydrate dissociation.

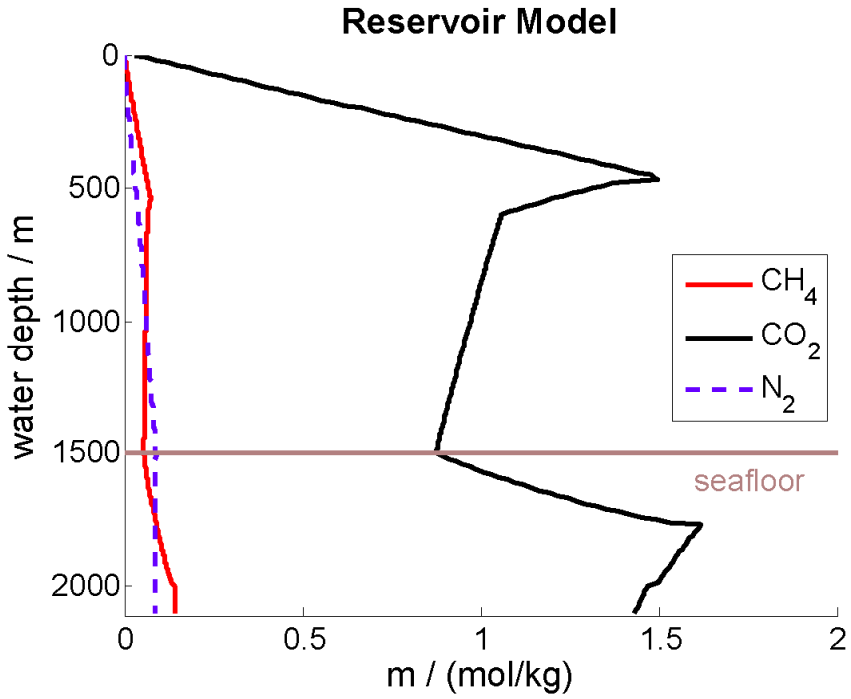

Figure B.7: Solubility profiles for CH_4, CO_2 and N_2 in seawater. Sudden solubility changes are associated with hydrate formation, hydrate dissociation, phase transitions and changes in the temperature gradient.

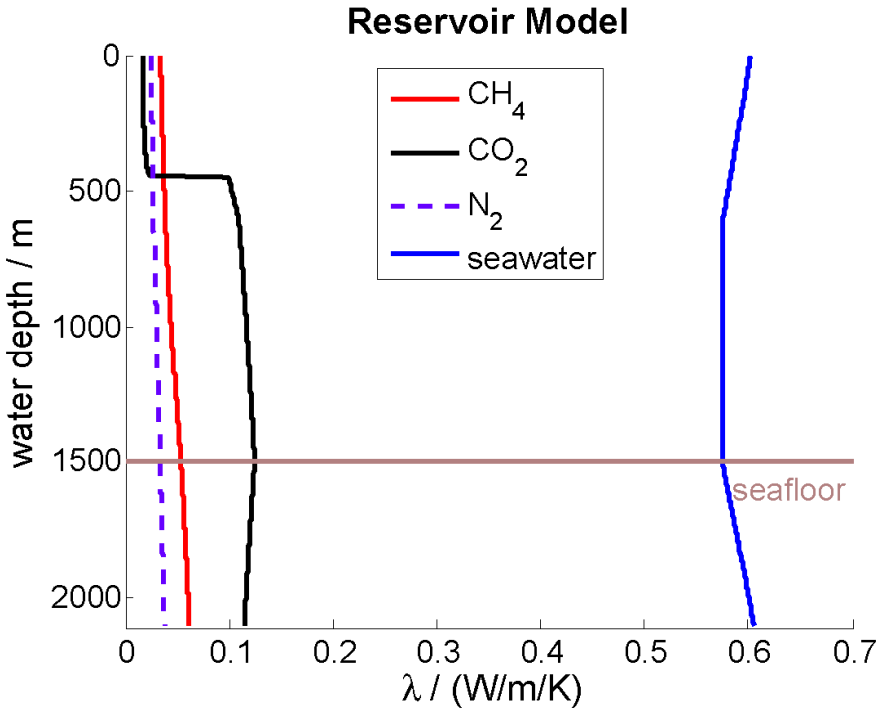

Figure B.8: Thermal conductivity profiles for CH_4, CO_2, N_2 and seawater. The steep increase in thermal conductivity results from the gas/liquid phase transition of CO_2.

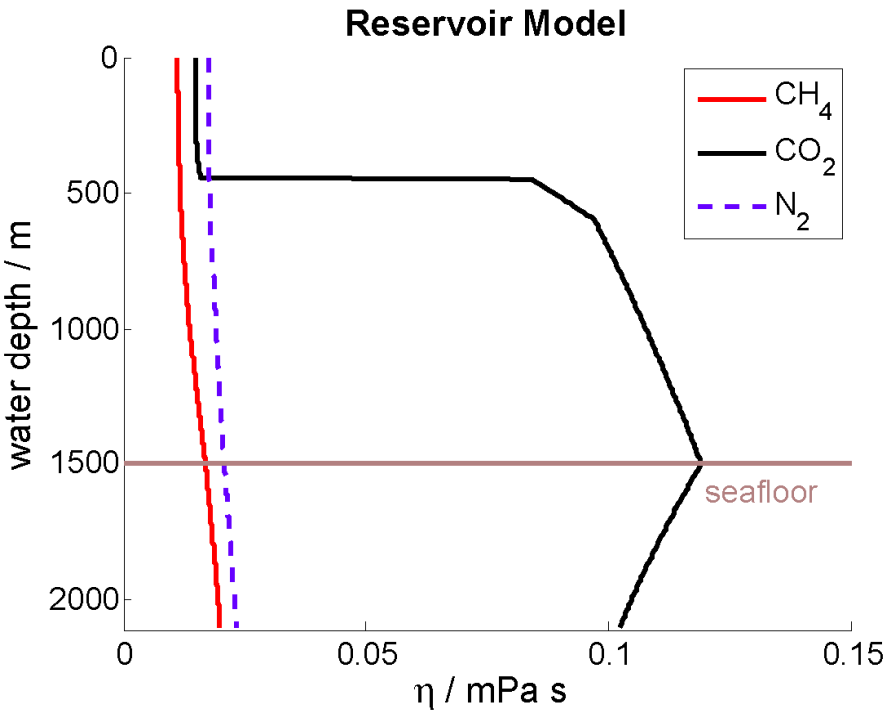

Figure B.9: Viscosity profiles for CH_4, CO_2 and N_2. The steep increase in viscosity results from the gas/liquid phase transition of CO_2.

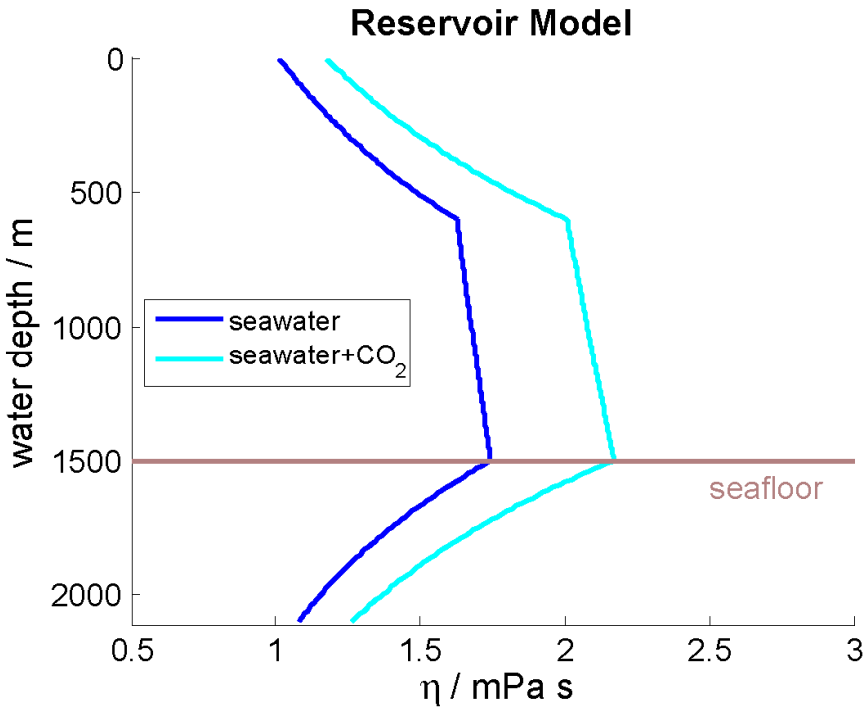

Figure B.10: Viscosity profiles seawater and CO_2-saturated seawater. Sudden viscosity changes are associated with abrupt changes of the temperature gradient.

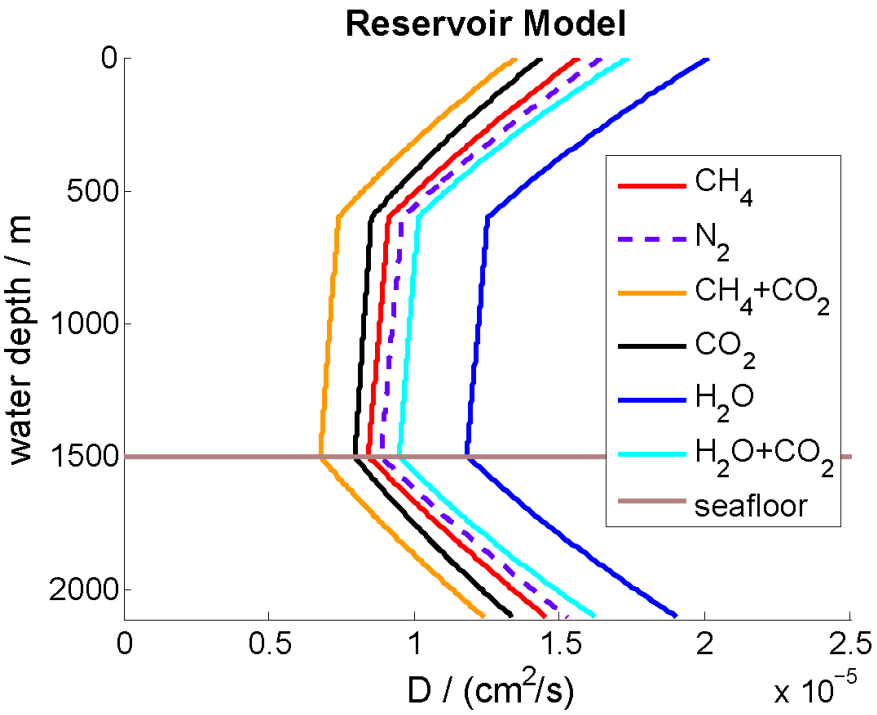

Figure B.11: Profiles of the molecular diffusion coefficients for CH_4, CO_2, N_2 and H_2O in seawater and CO_2-saturated seawater (+CO_2).

Table B.1: Thermodynamic, kinetic, and transport properties at the model boundaries (x = 0 m: sediment-water interface; x = 600 m: 100 m below gas hydrate stability zone)

	x = 0 p = 15 MPa, T = 2 ℃, S = 35	**x = 600 p = 21 MPa, T = 20 ℃, S = 35**
pure CH_4		
density [kg/m^3]	141.165	169.443
heat capacity cp [J/(kg K)]	3857.100	3645.000
fugacity coefficient	0.726	0.731
viscosity [mPa s]	0.017	0.020
thermal conductivity [W/m/K]	0.054	0.062
pure CO_2		
density [kg/m^3]	990.790	942.686
heat capacity cp [J/(kg K)]	2064.600	2050.700
fugacity coefficient	0.235	0.262
viscosity [mPa s]	0.120	0.103
thermal conductivity [W/m/K]	0.125	0.115
pure N_2		
density [kg/m^3]	182.946	227.856
heat capacity cp [J/(kg K)]	1314.400	1325.400
fugacity coefficient	0.969	1.004
viscosity [mPa s]	0.021	0.023
thermal conductivity [W/m/K]	0.036	0.038
pure seawater		
density [kg/m^3]	1034.900	1033.700
heat capacity cp [J/(kg K)]	3941.100	3949.600
fugacity coefficient	5.166E-05	1.286E-04
viscosity [mPa s]	1.744	1.078
thermal conductivity [W/m/K]	0.575	0.606
saturated CH_4-seawater solution		
density [kg/m^3]	1033.400	1030.100
solubility of CH_4 sw (+hydrate) [mol/kg]	0.056	0.142
diffusion coefficient of CH_4 [m^2/s]	8.438E-10	1.454E-09
fugacity coefficient of water at saturation	5.150E-05	1.265E-04
Henry constant [1/MPa*mol/kg]	0.0141	0.0089
fugacity of dissolved gas [MPa]	11.3	15.86

	x = 0 p = 15 MPa, T = 2 ℃, S = 35	**x = 600 p = 21 MPa, T = 20 ℃, S = 35**
saturated CO_2-seawater solution		
density [kg/m^3]	1044.300	1048.400
solubility of CO_2 in sw (+hydrate) [mol/kg]	0.875	1.440
viscosity [mPa s]	2.171	1.264
fugacity coefficient of water at saturation	5.086E-05	1.237E-04
diffusion coefficient of CO_2 [m^2/s] at saturation	7.957E-10	1.337E-09
Henry constant [MPa*kg/mol]	0.517	0.261
fugacity of dissolved gas [MPa]	3.598	5.459
saturated N_2-seawater solution		
density [kg/m^3]	1033.9	1032.8
solubility of N_2 in seawater [mol/kg]	0.090	0.088
diffusion coefficient of N_2 [m^2/s]	8.868E-10	1.528E-09
Henry constant [MPa*kg/mol]	0.0065	0.0043
fugacity of dissolved gas [MPa]	1.387E+01	2.027E+01
water dissolved in liquid CO_2		
solubility of water [mol/kg]	Eq. not applicable	0.075
diffusion coefficient of water [m^2/s]	9.894E-09	1.430E-08
CH_4 dissolved in liquid CO_2		
solubility [mol/kg]	Inf	Inf
N_2 dissolved in liquid CO_2		
solubility of water [mol/kg]	Inf	Inf
CH_4 hydrate		
fugacity of water in hydrate [Pa]	654.760	2733.200
heat capacity [J/kg/K]	2023.400	Eq. not applicable
CO_2 hydrate		
fugacity of water in hydrate [Pa]	695.660	2700.000
CH_4 + CO_2 in seawater		
partial pressure of CO_2 in CH_4 gas bubbles for CO_2 saturated seawater [MPa]	8.049	20.766

Appendix C: Scripts for unit conversion and auxiliary functions

Calculation of standard seawater composition (molalities):

seasalt.m
calculates the molalities of the major sea salt components from salinity, *S*, according to the standard seawater composition in Millero et al. (2008).

Calculation of standard seawater composition (molarities):

seasalt_molarity.m
calculates the molarities of the major sea salt components from the pressure and temperature dependent seawater density, ρ , and salinity, *S*.

Calculation of salinity from Cl^- ion concentration:

cl2salin.m
calculates the practical salinity, *S*, from the concentration of Cl^- ions, *m_Cl*, assuming standard seawater composition :

$$S = m\_Cl \frac{35}{0.5657647} \qquad \text{(Eq.C.1)}$$

Ionic strength of seawater:

i_sw.m
calculates the ionic strength, *I,* of seawater from ion concentrations, *m*, and ion charge numbers, *z*, at a given salinity, *S:*

$$I = 0.5 \sum_{ions} z_{ion}^2 \; m_{ion} \qquad \text{(Eq.C.2)}$$

Conversion from seawater molarity to seawater molality:

molar2molal_sw.m
calculates molalities, *m*, from molarities, *c*, salinity, *S* and seawater density, ρ :

$$m = \frac{c}{(1 - 0.0001005S)\rho} \qquad \text{(Eq.C.3)}$$

Conversion from seawater molality to seawater molarity:

molal2molar_sw.m
calculates molarities, *c*, from molalities, *m*, salinity, *S* and seawater density, ρ :

$$c = m(1 - 0.0001005\,S)\rho \qquad \text{(Eq.C.4)}$$

Conversion from seawater mol/kg{H_2O} to seawater mol/kg{solution}:

mkgh2o2mkgsol.m
calculates concentrations, *k*, in mol/kg{solution} from concentrations, *m*, given in mol/kg{H_2O} and salinity, *S*:

$$k = m(1 - 0.0001005\,S) \qquad \text{(Eq.C.5)}$$

Conversion from seawater mol/kg{solution} to seawater mol/kg{H_2O}:

mkgsol2mkgh2o.m
calculates concentrations, *m*, in mol/kg{H_2O} from concentrations, *k*, given in mol/kg{solution} and salinity, *S*:

$$m = \frac{k}{1 - 0.0001005\,S} \qquad \text{(Eq.C.6)}$$

Conversion from CH_4 partial pressure to CH_4 partial molar volume:

pp2pv_ch4.m, pp2pv_co2.m, pp2pv_n2.m, pp2pv_o2.m, pp2pv_h2s.m
calculate the partial molar gas volume of a gas, V_m, from partial pressure *pp*, total pressure *p* and temperature *T*:

$$V_m = \frac{\rho(pp, T)}{\rho(p, T)} \qquad \text{(Eq.C.7)}$$

Calculation of partial presure from gas solubility in seawater:

mol2pp_ch4.m, mol2pp_co2.m, mol2pp_n2.m, mol2pp_o2.m, mol2pp_h2s.m
calculate the partial pressure of a gas, *pp*, at given molal concentration in the aqueous phase, total pressure and temperature from Henry's law with Poynting correction for pressure effects and seawater activity factors.

References

Millero, F. J., R. Feistel, et al. (20080. "The composition of Standard Seawater and the definition of the Reference-Composition Salinity Scale." *Deep-Sea Research I* **55**: 50-72.

Appendix D: List of SUGAR Toolbox scripts and valid pTS ranges

Script name	Application	Pressure range	Temperature range	Salinity range
Equations of State				
eos_ch4	Thermodynamic properties of CH4: density, specific heat capacities, specific entropy, specific internal energy, specific enthalpy, fugacity coefficient, Joule-Thomson coefficient, vapor pressure	0.012 - 1000 MPa	-183 - 347 ℃	
eos_co2	Thermodynamic properties of CO2: density, specific heat capacities, specific entropy,specific internal energy, specific enthalpy, fugacity coefficient, Joule-Thomson coefficient, vapor pressure	0 - 800 MPa	0 - 827 ℃	
eos_n2	Thermodynamic properties of N2: density, specific heat capacities, specific entropy, specific internal energy, specific enthalpy, fugacity coefficient	0 - 1000 MPa	-73 - 727 ℃	
eos_o2	Thermodynamic properties of O2: density, specific heat capacities, specific entropy, specific internal energy, specific enthalpy, fugacity coefficient, Joule-Thomson coefficient	0 - 818 MPa	-219 - 127 ℃	
eos_h2s	density and fugacity coefficient of H2S	0.1 - 35 MPa	0 - 137.7 ℃	

Script name	Application	Pressure range	Temperature range	Salinity range
eos_h2o	Thermodynamic properties of pure water: density, specific heat capacities, specific entropy, specific internal energy, specific enthalpy, isentropic temperatuer-pressure coefficient, fugacity coefficient, Joule-Thomson coefficient	0 - 167.5 MPa	0 - 1000 ℃ (not valid for ice phase)	
eos_sw	Thermodynamic properties of seawater: density, specific heat capacities, specific entropy, specific internal energy, specific enthalpy, fugacity coefficient, chemical potential of water, chemical potential of salt, thermal expansion coefficient, isentropic temperature pressure coefficient, compressibilities, haline contraction coefficient, fugacity coefficient (pure water)	0 - 100 MPa	0 - 80 ℃	0 - 120
eos_IAPS84	outdated formulation for the density of pure water, may be used for eos_swDriesner around the critical point of water.	0 - 500 MPa	0 - 1000 ℃ (not valid for ice phase)	
eos_swDriesner	density, specific enthalpy and specific isobaric heat capacity for NaCl solutions, valid for an extended pressure and temperature range	0.1 - 167.5 MPa	0 - 600 ℃	up to NaCl saturation
Densities				
density_ch4	density of pure CH4	0.012 - 1000 MPa	-183 - 347 ℃	
density_ch4sw	density of CH4-seawater solution (mch4 is set to saturation concentration, if not provided)	0.1 - 200 MPa	0 - 250 ℃	0 - 350

Script name	Application	Pressure range	Temperature range	Salinity range
density_co2	density of pure CO2	0 - 800 MPa	0 - 827 ℃	
density_co2sw	density of CO2-seawater solution (mco2 is set to saturation concentration, if not provided)	0.1 - 100 MPa	0 - 200 ℃	0 - 350
density_n2sw	density of N2-seawater solution	0.1 - 60 MPa	0 - 127 ℃	0 - 350
density_sw	Checks pTS range and calls the appopriate function to calculate seawater density. User can decide by setting the input variable "choice" (default is ‘eos_sw’).			
density_swUnesco	UNESCO formulation for density of seawater	0.1 - 100 MPa	0 - 40 ℃	0.5 - 50
density_swSpivey	density of seawater for high pTS values	0- 200 MPa	0 - 275 ℃	0 - 216
density_swSun	density of seawater for high pTS values	0.1- 100 MPa	0 - 374 ℃	0 - 80
density_ch4co2n2	density for mixtures of CH4, CO2 and N2, mole fractions in liquid and vapor, vapor phase fraction	1-? MPa		
density_cacl2brine	density of CaCl2-water solutions	0.1- 68.5 MPa	10 - 199 ℃	0 - 86
Phase boundaries				
hydrate_phasediagram	plots the phasediagrams of the sytems seawater-CH4 and seawater-CO2			

Script name	Application	Pressure range	Temperature range	Salinity range
phase_ch4sw	dissociation pressure of CH4-hydrate in water, seawater and porewater	0.012 - 1000 MPa	- 10 - 30 ℃	0 - 70
phase_co2sw	Melting, sublimation, and vapor pressure of CO2, dissociation pressure of CO2-hydrate in seawater	0 - 800 MPa	0 - 827 ℃	0 - 40
phase_sw	phase boundaries and critical properties of the system water – salt		0 - 1000 ℃	0 - 1000
sw_phasediagram	plots the phasediagram of saltwater			
vlh_naclh2o	3-phase (vapor-liquid-halite) equilibrium		0 - 1000 ℃	
Fugacities				
fugacity_ch4gh	fugacity of CH4 in hydrate			
fugacity_ch4sw	fugacity of CH4 dissolved in seawater	0.1 - 200 MPa	0 - 250 ℃	0 - 350
fugacity_co2gh	fugacity of CO2 in hydrate			
fugacity_co2sw	fugacity of CO2 dissolved in seawater	0.1-35 MPa	0-162 ℃	0-263
fugacity_h2och	fugacity of water and fractional cage occupancies in CO2-hydrate		-133 - 57 ℃	

Script name	Application	Pressure range	Temperature range	Salinity range
fugacity_h2omh	fugacity of water and fractional cage occupancies in CH4-hydrate		-133 - 57 ℃	
fugacity_sw	fugacity of water in solutions with dissolved salt, CH4 and CO2	0.1 - 400 MPa		0 - 350
fugacity_h2ssw	fugacity of H2S dissolved in seawater	0.1 - 20 MPa	0 - 127 ℃	0 - 350
fugacity_n2sw	fugacity of N2 dissolved in seawater	0.1-35 MPa	0-317 ℃	0-350
fugacity_o2sw	fugacity of O2 dissolved in seawater	0.1 - 20 MPa	0 - 127 ℃	0 - 350
Solubilities				
solu_ch4	Checks pTS range and calls the appopriate function to calculate solubility of CH4 in seawater (‘solu_ch4gas’ or ‘solu_ch4gh’)			
solu_ch4gas	solubility of CH4 in seawater in equilibrium with gas phase and mole fraction of water in CH4 gas phase	0.1 - 200 MPa	0 - 250 ℃	0 - 350
solu_ch4gh	solubility of CH4 in seawater and SO4-free porewater in equilibrium with hydrate phase	0.1 - 50 MPa	0 - 20 ℃	0 - 70
solu_co2	Checks pTS range and calls the appopriate function to calculate solubility of CO2 in seawater (‘solu_co2gl’ or ‘solu_co2gh’)			

Script name	Application	Pressure range	Temperature range	Salinity range
solu_co2gl	solubility of CO2 in seawater in equilibrium with gas or liquid phase	0.1- 100 MPa	0 - 162℃	0 - 263
solu_co2gh	solubility of CO2 in seawater or SO4-free porewater in equilibrium with hydrate phase	0.1 - 50 MPa	0 - 12 ℃	0 - 40
solu_h2ssw	solubility of H2S in seawater	0.1 - 20 MPa	0 - 127 ℃	0 - 350
solu_n2sw	solubility of nitrogen in seawater	0.1 - 60 MPa	0 - 317 ℃	0 - 350
solu_o2sw	solubility of O2 in seawater	0.1 - 20 MPa	0 - 127 ℃	0 - 350
solu_co2ch4	partial pressure of CO2 in CH4-gas	3.5 - 50 MPa	0 - 25 ℃	0 - 40
solu_ch4co2	solubility of CH4 in liquid CO2			
solu_n2co2	solubility of N2 in liquid CO2			
solu_swco2	solubility of H2O in liquid CO2	5 - 20 MPa	10 - 40 ℃	0 - 40
solu_nacl	solubility of NaCl	0-500 MPa	0-1000 ℃	
solu_caso4	solubility product of anhydrite, gypsum and CaSO4 hemihydrate	0.1 - 100 MPa	30 - 300 ℃	0 – 250

Script name	Application	Pressure range	Temperature range	Salinity range
solu_opal	calls ‘solu_opalWalther’ or ‘solu_opalFournier’ to calculate the solubility of opal in seawater (default is ‘solu_opalWalther’)			
solu_opalFournier	solubility of opal in seawater	10 - 120 MPa	150 - 350 ℃	0 - 80
solu_opalWalther	solubility of opal in seawater	10 - 120 MPa	0 - 350 ℃	0 - 80
solu_quartz	Checks pTS range and calls appopriate function to calculate solubility of quartz in seawater. User can decide by setting input variable "choice" (default is ‘solu_quartzFournier’).			
solu_quartzDamm	solubility of quartz in seawater	0.1 - 986 MPa	45 - 900 ℃	0 - 80
solu_quartzFournier	solubility of quartz in seawater	0.1 - 100 MPa	0 - 350 ℃	0 - 80
soluhenry_ch4sw	solubility of CH4 in seawater calculated from pS-corrected Henry constant + Henry constant	0.1 - 200 MPa	0 - 250 ℃	0 - 350
soluhenry_co2sw	solubility of CO2 in seawater calculated from pS-corrected Henry constant + Henry constant	0.1-35 MPa	0-162 ℃	0-263
soluhenry_h2ssw	solubility of H2S in seawater calculated from pS-corrected Henry constant + Henry constant	0.1 - 20 MPa	0 - 127 ℃	0 - 350

Script name	Application	Pressure range	Temperature range	Salinity range
soluhenry_n2sw	solubility of N2 in seawater calculated from pS-corrected Henry constant + Henry constant	0.1-35 MPa	0-317 ℃	0-350
soluhenry_o2sw	solubility of O2 in seawater calculated from pS-corrected Henry constant + Henry constant	0.1 - 20 MPa	0 - 127 ℃	0 - 350
Viscosities				
visco_ch4	viscosity of pure CH4	0 - 50 MPa	- 178 - 227 ℃	
visco_co2	viscosity of pure CO2	0.1 - 300 MPa	- 56 - 827 ℃	
visco_h2o	viscosity of water (not suitable for pT conditions close to the critical point)	0.1 - 167.5 MPa	0 - 80 ℃	
visco_n2	viscosity of N2	0.1 - 100 MPa	(-120)- 727 ℃	
visco_sw	checks the pTS range and calls appopriate function to calculate solubility of quartz in seawater. User can decide by setting input variable "choice" (default is Kukulka's equation).	0- 100 MPa (Kukulka)	0 - 30 ℃ (Kukulka)	0 - 36.1 (Kukulka)
visco_swSpivey	viscosity of seawater for high pTS values	0- 200 MPa	0 - 275 ℃	0 - 290
visco_swMao	viscosity of seawater	0.1 - 100 MPa	0 - 350 ℃	0 - 300
visco_swPalliser	viscosity of seawater	0.1 - ? MPa	0.1 - 727 ℃	0 - 1000 (?)

Script name	Application	Pressure range	Temperature range	Salinity range
visco_co2sw	viscosity of CO2-seawater (mco2 is set to saturation concentration, if not provided)	(1-20 MPa)	(30-60℃)	(0 - 30)
Thermal properties				
heatcap_ch4gh	heat capacity of CH4-hydrate		-25 - 11 ℃	
heatcond_ch4	thermal conductivity of pure CH4	0 - 50 MPa	-5 - 227 ℃	
heatcond_co2	thermal conductivity of pure CO2	0.1 - 200 MPa	-48 - 727 ℃	
heatcond_n2	thermal conductivity of N2	0.1 -100 MPa	(-120)- 727 ℃	
hetacond_sw	thermal conductivity of seawater	0 -1 40 MPa	0 - 60 ℃	0 - 45
Diffusion coefficients				
diffcoeff_h2oco2	diffusion coefficient of H2O in liquid CO2	(13 - 30 MPa)	(10 - 35 ℃)	
diffcoeff_sw	diffusion coefficients of various solutes in seawater and CO2-rich seawater	variable (see script)	variable (see script)	variable (see script)
Acid-Base and Mineral Equilibria				
kco2_sw	equilibrium constants of carbonic acid dissociation in CO2-rich seawater	0.1 -100 MPa	0 - 45 ℃	0 - 45

Script name	Application	Pressure range	Temperature range	Salinity range
kequilib_sw	equilibrium constants of various solute dissociation and mineral dissolution reactions in seawater	0.1 -100 MPa	0 - 45 ℃	0 - 45
ph_analyt	Analytical solution of seawater pH and equilibrium concentrations of H+, CO2, HCO3-, CO32-, B(OH)4-, B(OH)3, H2S, HS- based on total concentrations and total alkalinity			
ph_model	Numerical solution of seawater pH, equilibrium concentrations of acid-base species, total alkalinity and total concentrations based on variable input			
Unit conversions				
cl2salin	converts Cl- molality to practical salinity			
molal2molar_sw	converts mol/kg to mol/l for seasalt components			
molar2molal_sw	converts mol/l to mol/kg for seasalt components			
molkgh2o2molkgsol	converts mol/kg{H2O} to mol/kg{solution}			
molkgsol2molkgh2o	converts mol/kg{solution} to mol/kg{H2O}			
mol2pp_ch4	converts molality of CH4 to partial pressure	0.1 - 200 MPa	0 - 250 ℃	0 - 350

Script name	Application	Pressure range	Temperature range	Salinity range
mol2pp_co2	converts molality of CO2 partial pressure	0.1-35 MPa	0-162 ℃	0-263
mol2pp_h2s	converts molality of H2S partial pressure	0.1 - 20 MPa	0 - 127 ℃	0 - 350
mol2pp_n2	converts molality of N2 partial pressure	0.1-35 MPa	0-317 ℃	0-350
mol2pp_o2	converts molality of O2 partial pressure	0.1 - 20 MPa	0 - 127 ℃	0 - 350
pp2pv_ch4	converts CH4 partial pressure to partial volume	0.012-1000 MPa	-183-347 ℃	
pp2pv_co2	converts CO2 partial pressure to partial volume	0.1-800 MPa	-57-827 ℃	
pp2pv_h2s	converts H2S partial pressure to partial volume	0.1-35 MPa	0-137.5 ℃	
pp2pv_n2	converts N2 partial pressure to partial volume	0.1-1000 MPa	-73-727 ℃	
pp2pv_o2	converts O2 partial pressure to partial volume	0-81.8 MPa	-219-127 ℃	
Auxiliary functions				
i_sw	ionic strength of seawater			
permeab	sediment permeability			
seasalt	Molalities of major salts based on seawater salinity			

Script name	Application	Pressure range	Temperature range	Salinity range
seasalt_molarity	Molarities of major salts based on seawater salinity			
tortuos	tortuosity correction for diffusion coefficients in sediments			

Appendix E: Header information of the SUGAR Toolbox scripts

SUGAR_TOOLBOX

Equations of state

eos_ch4	- calculates thermodynamic properties of CH4
eos_co2	- calculates thermodynamic properties of CO2
eos_n2	- calculates thermodynamic properties of N2
eos_o2	- calculates thermodynamic properties of O2
eos_h2s	- calculates density and fugacity coefficient of H2S
eos_h2o	- calculates thermodynamic properties of pure water
eos_sw	- calculates thermodynamic properties of seawater
eos_IAPS84	- outdated formulation to calculate thermodynamic properties of seawater
eos_swDriesner	- calculates thermodynamic properties of seawater for extreme conditions

Densities

density_ch4	- calculates the density of CH4 (calls eos_ch4)
density_ch4sw	- calculates the density of a CH4-seawater solution
density_co2	- calculates the density of CO2 (calls eos_co2)
density_co2sw	- calculates the density of a CO2-seawater solution
density_n2sw	- calculates the density of a N2-seawater solution
density_sw	- calculates the density of seawater (calls function with matching pTS range)
density_swUnesco	- UNESCO formulation to calculate the density of seawater
density_swSpivey	- calculates the density of seawater for high p-T conditions
density_swSun	- calculates the density of seawater for high p-T conditions
density_ch4co2n2	- calculates the density and phase composition of CH4-CO2-N2 mixtures
density_cacl2brine	- calculates the density of a CaCl2-water solution

Phase boundaries

hydrate_phasediagram	- plots the phase diagrams of CH4 and CO2 hydrates in seawater
phase_ch4sw	- calculates the phase boundaries of the system CH4-seawater
phase_co2sw	- calculates the phase boundaries of the system CO2-seawater
phase_sw	- calculates the phase boundaries of seawater
sw_phasediagram	- plots the phase diagram of seawater
vlh_naclh2o	- calculates the 3-phase (vapor-liquid-halite) coexistence of the system NaCl-H2O

Fugacities

fugacity_ch4gh	- calculates the fugacity of CH4 in CH4-hydrate
fugacity_ch4sw	- calculates the fugacity of CH4 dissolved in seawater
fugacity_co2gh	- calculates the fugacity of CO2 in CO2-hydrate
fugacity_co2sw	- calculates the fugacity of CO2 dissolved in seawater
fugacity_h2och	- calculates the fugacity of water in CO2 SI-hydrate
fugacity_h2omh	- calculates the fugacity of water in CH4 SI-hydrate
fugacity_sw	- calculates the fugacity of water in solutions with dissolved salts, CH4 and CO2
fugacity_h2ssw	- calculates the fugacity of H2S dissolved in seawater
fugacity_n2sw	- calculates the fugacity of N2 dissolved in seawater
fugacity_o2sw	- calculates the fugacity of O2 dissolved in seawater

Solubilities

solu_ch4	- calculates the solubility of CH4 in seawater (calls function with matching pTS range)
solu_ch4gas	- calculates the 2-phase (gas-water) equilibrium concentration of CH4 in seawater
solu_ch4gh	- calculates the 3-phase (gas-water-hydrate) equilibrium concentration of CH4 in seawater

solu_co2	- calculates the solubility of CO2 in seawater (calls function with matching pTS range)
solu_co2gl	- calculates the 2-phase (gas/liquid-water) equilibrium concentration of CO2 in seawater
solu_co2gh	- calculates the 3-phase (gas/liquid-water-hydrate) equilibrium concentration of CO2 in seawater
solu_h2ssw	- calculates the solubility of H2S in seawater
solu_n2sw	- calculates the solubility of N2 in seawater
solu_o2sw	- calculates the solubility of O2 in seawater
solu_co2ch4	- calculates the partial pressure of CO2 in methane gas
solu_ch4co2	- calculates the solubility of CH4 in CO2
solu_n2co2	- calculates the solubility of N2 in CO2
solu_swco2	- calculates the solubility of water in liquid CO2
solu_nacl	- calculates the solubility of NaCl in water
solu_caso4	- calculates the solubility of CaSO4 in seawater
solu_opal	- calculates the solubility of opal in seawater (calls function with matching pTS range)
solu_opalFournier	- calculates the solubility of opal in seawater
solu_opalWalther	- calculates the solubility of opal in seawater
solu_quartz	- calculates the solubility of quartz in seawater (calls function with matching pTS range)
solu_quartzDamm	- calculates the solubility of quartz in seawater for hydrothermal conditions
solu_quartzFournier	- calculates the solubility of quartz in seawater
soluhenry_ch4sw	- calculates the solubility and Henry constant of CH4 in seawater
soluhenry_co2sw	- calculates the solubility and Henry constant of CO2 in seawater
soluhenry_h2ssw	- calculates the solubility and Henry constant of H2S in seawater
soluhenry_n2sw	- calculates the solubility and Henry constant of N2 in seawater
soluhenry_o2sw	- calculates the solubility and Henry constant of O2 in seawater

Viscosities

visco_ch4	- calculates the dynamic viscosity of CH4
visco_co2	- calculates the dynamic viscosity of CO2
visco_h2o	- calculates the dynamic viscosity of pure water
visco_n2	- calculates the dynamic viscosity of N2
visco_sw	- calculates the dynamic viscosity of seawater (calls function with matching pTS range)
visco_swSpivey	- calculates the dynamic viscosity of seawater
visco_swMao	- calculates the dynamic viscosity of seawater
visco_swPalliser	- calculates the dynamic viscosity of seawater
visco_co2sw	- calculates the dynamic viscosity of CO2-seawater solutions

Thermal Properties

heatcap_ch4gh	- calculates the heat capacity of CH4 hydrate
heatcond_ch4	- calculates the thermal conductivity of CH4
heatcond_co2	- calculates the thermal conductivity of CO2
heatcond_n2	- calculates the thermal conductivity of N2
heatcond_sw	- calculates the thermal conductivity of seawater

Diffusion Coefficients

diffcoeff_h2oco2	- calculates the diffusion coefficient of water in liquid CO2
diffcoeff_sw	- calculates the diffusion coefficients of dissolved species in seawater

Acid-Base and Mineral Equilibria

kco2_sw	- calculates equilibrium constants for the carbonic acid system in seawater
kequilib_sw	- calculates stoichiometric equilibrium constants and solubility products
ph_analyt	- calculates pH-system in seawater analytically from given TAlk, TCO2, TH2S, TBOH4
ph_model	- calculates pH-system in seawater numerically from variable input combinations

Unit Conversions

cl2salin	- converts seawater chloride concentration to salinity
molal2molar_sw	- converts molal concentrations to molar concentrations for seawater salts
molar2molal_sw	- converts molar concentrations to molal concentrations for seawater salts
mkgh2o2mkgsol	- converts mol/kg{H2O} to mol/kg{solution}
mkgsol2mkgh2o	- converts mol/kg{solution} to mol/kg{H2O}
mol2pp_ch4	- calculates the CH4 partial pressure from its molal concentration in seawater
mol2pp_co2	- calculates the CO2 partial pressure from its molal concentration in seawater
mol2pp_h2s	- calculates the H2S partial pressure from its molal concentration in seawater
mol2pp_n2	- calculates the N2 partial pressure from its molal concentration in seawater
mol2pp_o2	- calculates the O2 partial pressure from its molal concentration in seawater
pp2pv_ch4	- converts CH4 partial pressure to partial volume
pp2pv_co2	- converts CO2 partial pressure to partial volume
pp2pv_h2s	- converts H2S partial pressure to partial volume
pp2pv_n2	- converts N2 partial pressure to partial volume
pp2pv_o2	- converts O2 partial pressure to partial volume

Auxiliary Functions

i_sw	- calculates the ionic strength of seawater
permeab	- estimates the permeability of the sediment from porosity and grain size
seasalt	- calculates the molal concentrations of major salts in seawater
seasalt_molarity	- calculates the molar concentrations of major salts in seawater
tortuous	- calculates the tortuosity correction for diffusion coefficients

E.1. Equations of State (EOS)

eos_ch4 - calculates thermodynamic properties of CH4 based on an equation of state

Usage: [rho cv cp s u h f JT pv cs] = eos_ch4(p,T)

Input parameters (scalars or vectors):
- p - pressure [MPa] (0.012 < p < 1000)
- T - temperature [degC] (-183< T < 347)

Output parameters:
- rho - density [kg/m^3]
- cv - specific isochoric heat capacity [J/(kg K)]
- cp - specific isobaric heat capacity [J/(kg K)]
- s - specific entropy [J/(kg K)]
- u - specific internal energy [J/kg]
- h - specific enthalpy [J/kg]
- f - fugacity coefficient
- JT - Joule-Thomson coefficient [K/MPa]
- pv - vapor pressure [MPa] (only for T < T_critical)
- cs - saturated liquid heat capacity [J/kg/K] (only for T < T_critical)

All thermodynamic properties (except for pv) are calculated from the dimensionless Helmholtz energy Phi = A/(RT)
(A(rho,T) = h_0(T)-R*T-T*s_0(rho,T)) and its derivatives with respect to p and T.

References:
Setzmann & Wagner (1991) J. Phys. Chem. Ref. Data 20, 1061-1155.

eos_co2 - calculates thermodynamic properties of CO2 based on an equation of state

Usage: [rho cv cp s u h f JT pv cs] = eos_co2(p,T)

Input parameters (scalars or vectors):
p - pressure [MPa] (0 < p < 800)
T - temperature [degC] (-57 (0)< T < 827)

Output parameters:
rho - density [kg/m^3]
cv - specific isochoric heat capacity [J/(kg K)]
cp - specific isobaric heat capacity [J/(kg K)]
s - specific entropy [J/(kg K)]
u - specific internal energy [J/kg]
h - specific enthalpy [J/kg]
f - fugacity coefficient
JT - Joule-Thomson coefficient [K/MPa]
pv - vapor pressure [MPa]
cs - saturated liquid heat capacity [J/kg/K]

All thermodynamic properties (except for pv) are calculated from the dimensionless Helmholtz energy Phi = A/(RT)
(A(rho,T) = h_0(T)-R*T-T*s_0(rho,T)) and its derivatives with respect to p and T.
The reduced Helmholtz energy is split into an ideal gas part (PHI_0) and a residual part (PHI_r):
A/(R*T) = PHI(del,tau) = PHI_0 + PHI_r
with del = RHO/RHOc and tau = Tc/T
The pressure is related to the Helmholtz energy by:
P(RHO,T) = -(dA/dV)_T
and thus to the reduced Helmholtz energy PHI by:
P(del,tau)/(RHO*R*T) = 1 + del*(dPHI_r/ddel)_tau
Rearranging gives:
RHO = P / (R*T*(1+del*(dPHI_r/ddel)_tau))
Since the density is part of both sides of the above equation, RHO is determined iteratively by minimizing the following expression:
0 = RHO - RHOeos

References:
Span & Wagner (1996) J. Phys. Chem. Ref. Data 25, 1509-1597.

Comments:
Caution should be taken because although the paper states that the equations are valid for temperatures between -57 degC and 827 degC, the curves show singularities at temperatures below 0 degC. The exact positions depend on p and occur mainly, but not exclusively, at temperatures below -20 degC.

eos_n2 - calculates thermodynamic properties of gaseous (supercritical) N2 based on an EOS

Usage: [rho cv cp s u h f] = eos_n2(p,T)

Input parameters (scalars or vectors):
p - pressure [MPa] (0 < p < 1000)
T - temperature [degC] (-73 (0)< T < 727)

Output parameters:
rho - density [kg/m^3]
cv - specific isochoric heat capacity [J/(kg K)]
cp - specific isobaric heat capacity [J/(kg K)]
s - specific entropy [J/(kg K)]

u - specific internal energy [J/kg]
h - specific enthalpy [J/kg]
f - fugacity coefficient

All thermodynamic properties (except for pv) are calculated from the dimensionless Helmholtz energy PHI = A/(RT)
(A(rho,T) = h_0(T)-R*T-T*s_0(rho,T)) and its derivatives with respect to p and T.
The reduced Helmholtz energy is split into an ideal gas part (PHI_0) and a residual part (PHI_r):
A/(R*T) = PHI(del,tau) = PHI_0 + PHI_r
with del = RHO/RHOc and tau = Tc/T
The pressure is related to the Helmholtz energy by:
P(RHO,T) = -(dA/dV)_T
and thus to the reduced Helmholtz energy PHI by:
P(del,tau)/(RHO*R*T) = 1 + del*(dPHI_r/ddel)_tau
Rearranging gives:
RHO = P / (R*T*(1+del*(dPHI_r/ddel)_tau))
Since the density is part of both sides of the above equation, RHO is determined iteratively by minimizing the following expression:
0 = RHO - RHOeos

Reference:
Span et al. (2000) J. Phys. Chem. Ref. Data 29, 1361-1433.

Comments:
For (supercritical) gas phase only (to keep things simple).

eos_o2 - calculates thermodynamic properties of O2 based on an equation of state

Usage: [rho cv cp s u h f JT] = eos_o2(p,T)

Input parameters (scalars or vectors):
p - pressure [MPa] (0 < p < 81.8)
T - temperature [degC] (-219 < T < 127)

Output parameters:
rho - density [kg/m^3]
cv - specific isochoric heat capacity [J/(kg K)]
cp - specific isobaric heat capacity [J/(kg K)]
s - specific entropy [J/(kg K)]
u - specific internal energy [J/kg]
h - specific enthalpy [J/kg]
f - fugacity coefficient
JT - Joule-Thomson coefficient [K/MPa]

All thermodynamic properties (except for pv) are calculated from the dimensionless Helmholtz energy Phi = A /(RT)
(A(rho,T) = h_0(T)-R*T-T*s_0(rho,T)) and its derivatives with respect to p and T.

Reference:
Schmidt & Wagner (1985) Fluid Phase Equilibria 19, 175-200.

eos_h2s - calculates the density and fugacity coefficient of H2S from a cubic equation of state

Usage: [rho phi] = eos_h2s(p,T)
Input parameters (scalars or vectors):
p - pressure [MPa] (0.1 < p < 35)
T - temperature [degC] (0 < T < 137.7)

Output parameters:
rho - density [kg/m3]
phi - fugacity coefficient

References:
Duan et al. (2007) Energy & Fuels 21, 2056-2065.
Reamer et al. (1950) Ind. Eng. Chem. 1, 140-143. (lookup table)

eos_h2o - calculates thermodynamic properties of pure water based on an equation of state

Usage: [rho cp cv s u h beta f JT] = eos_h2o(p,T)

Input parameters (scalars or vectors):
p - pressure [MPa] (0 < p < 167.5)
T - temperature [degC] (0 < T < 1000)

Output parameters:
rho - density [kg/m^3]
cp - specific isobaric heat capacity [J/(kg K)]
cv - specific isobaric heat capacity [J/(kg K)]
s - specific entropy [J/(kg K)]
u - specific internal energy [J/kg]
h - specific enthalpy [J/kg]
beta - isentropic temperature-pressure coefficient [K/Pa]
f - fugacity coefficient
JT - Joule-Thomson coefficient [K/MPa]

All thermodynamic properties are calculated from the Gibbs energy
(g = u + pV - Ts) and its derivatives with respect to p and T.

References:
IAPSW (1996) The IAPWS formlation 1995 for the thermodynamic
properties of ordinary water substance for general and scientific
use. www.iapws.org
Wagner & Pruss (2002) J.Phys.Chem.Ref.Data 31, 387-535.
IAPSW (2007) Revised release for the IAPWS industrial formlation 1997
for the thermodynamic properties of water and steam. www.iapws.org
Marcus (2000) Phys Chem Chem Phys 2, 1465-1472.

Comments:
Not valid for ice phase! (No check for ice phase implemented)

The deviation from the tabulated density values of Wagner and Pruss is less than 1%.

The formulation of IAPWS (2007) and equations from Marcus (2000) are used to calculate a start value for the iteration of the density.
The IAPWS (2007) formalism is valid for T=0-800 degC and p=0-100 MPa. Since the calculated density is only considered as a start value and only needs to be approximated but not exact, the formulation might be used for T=0-1000 degC and p<167.5 MPa or T=0-227 degC and p<225 MPa.

The formalism can be extended to the full range of IAPWS (0 < T < 1000 degC and p < 1000 MPa), if good starting values for the density calculations can be provided. A lookup-table could be implemented from table 13.2 in Wagner & Pruss (2002).

eos_sw - calculates thermodynamic properties of seawater based on an equation of state

Usage: [rho cp s u h phi mu_sw mu_ss alpha beta kappaT kappaS beta_hal fw] = eos_sw(p,T,S)

Input parameters (scalars or vectors):
- p - pressure [MPa] (0 < p < 100),
- T - temperature [degC] (-12 (0)< T < 80),
- S - practical salinity (0 < S < 120)

Output parameters:
- rho - Density [kg/m^3]
- cp - Specific isobaric heat capacity [J/(kg K)]
- s - Specific entropy [J/(kg K)]
- u - Specific internal energy [J/kg]
- h - Specific enthalpy [J/kg]
- phi - Specific Helmholtz energy [J/kg]
- mu_sw - Relative chemical potential of seawater [J/kg]
- mu_ss - Chemical potential of sea salt [J/kg]
- alpha - Thermal expansion coefficient [1/K]
- beta - Isentropic temperature-pressure coefficient [K/Pa]
- kappaT - Isothermal compressibility [1/Pa]
- kappaS - Isentropic compressibility [1/Pa]
- beta_hal - Haline contraction coefficient [kg/kg]
- fw - fugacity coefficient of pure(!) water

All thermodynamic properties are calculated from the Gibbs energy (g = u + pV - Ts) and its derivatives with respect to p, T and S.
The Gibbs energy of seawater is taken as the sum of the Gibbs energy of pure water and the Gibbs energy of the saline part. The pure water properties are first calculated from a formalism based on the Helmholtz energy (a = u - Ts) as given in IAPWS (1995).
The Gibbs energy of pure water and its derivatives are then derived from those calculated thermodynamic potentials. The saline contribution to the Gibbs energy is directly calculated from the formalism given in IAPWS (2008).

References:
IAPSW (1996) The IAPWS formulation 1995 for the thermodynamic properties of ordinary water substance for general and scientific use. www.iapws.org
Wagner & Pruss (2002) J.Phys.Chem.Ref.Data 31, 387-535.
IAPSW (2008) Release on the IAPWS formulation 2008 for the thermodynamic properties of seawater. www.iapws.org
Feistel (2008) DSR I 55, 1639–1671.

Comments: Not valid for ice phase!

eos_IAPS84 - calculates thermodynamic properties of pure water based on an equation of state from the outdated IAPS-84 formulation

Usage: rho = eos_IAPS84(p,T)

Input parameters (scalars or vectors):
- p - pressure [MPa] (0 < p < 500)
- T - temperature [degC] (0 < T < 1000)

Output parameters:
- rho - density of pure water [kg/m^3]

All thermodynamic properties are calculated from the Gibbs energy (g = u + pV - Ts) and its derivatives with respect to p and T.

References:
IAPS Formulation 1984 for the Thermodynamic Properties of Ordinary Water Substance for Scientific and General Use. http://iapws.org.
Kestin & Sengers (1986) J.Phys.Chem.Ref.Data 15, 305-320.
IAPSW (2007) Revised release for the IAPWS industrial formlation 1997 for the thermodynamic properties of water and steam. www.iapws.org
Marcus (2000) Phys Chem Chem Phys 2, 1465-1472.

Comments:
Not valid for ice phase! (No check for ice phase implemented)

The formalism is outdated and for an accurate calculation, the MATLAB script eos_h2o should be used. IAPS-84 might be needed for the function eos_swDriesner. Driesner did use the IAPS84 formulation to derive his density formalism. The deviations of IAPS84 from the actual formulation are small except in the vicinityof the critical point of water. For density calculations with eos_swDriesner close to the critical point, eos_swDriesner might be edited to use IAPS84 instead of eos_h2o.

eos_swDriesner - calculates the density, enthalpy and isobaric heat capacity of the system H2O-NaCl based on multiparametric equations

Usage: [rho h cp] = eos_swDriesner(p,T,S)

Input parameters (vectors or scalars, S: scalar):
p - pressure [MPa] (0.1 < P < 167.5)
T - temperature [degC] (0 < T < 600)
S - salinity (see comments)

Output parameters:
rho - density [kg/m^3]
h - specific enthalpy [J/kg]
cp - specific isobaric heat capacity [J/kg/K]

The densities, enthalpies and heat capacities are calculated from equations for pure water at a modified temperature that balances out the deviations caused by salinities.

References:
Driesner & Heinrich (2007) GCA 71, 4902-4919.

Comments:
Currently, the EOS for pure water based on the IAPWS formulation (eos_h2o), which is called by this routine, is not implemented for its full pT range. It holds for T < 1000 degC and p < 167.5 MPa and some more extended ranges. For details, see comments in eos_h2o.

The second extrapolation function of Driesner's formalism for T >= 600 degC, p <= 350 bar and high salinities (close to saturation) is not implemented. As a comsequence, the temperature range of this script is reduced to 0 < T < 600 degC.

This implemetation of Driesner's formalism calls the IAPS95 formulation for the calculation of pure water densities. Driesner developed his formalism based on the IAPS84 formulation. The two formulations differ mainly in the vicinity of the critical point of water. For calculations close to this point, it is recommended to edit this script to call the IAPS84 formulation.

Although Driesner's paper states that the formulation is valid for mole fractions of up to 100% NaCl, the calculated densities for 100% NaCl do not approach the pure NaCl densities properly, except for conditions with high saturation concentrations. It seems that the formulation is only meant for NaCl concentrations up to saturation. Since the curve for the density as a function of NaCl concentration progresses smoothly after exceeding the saturation concentration by some 10%, this script will allow

for the calculation of oversaturated solutions up to mole fraction values of 0.2 above the saturation mole fraction. If this value is exceeded, a warning will be issued.

E.2. Densities

density_ch4 - calculates the density of CH4 based on an EOS
The toolbox script EOS_CH4 is called.

Usage: rho = density_ch4(p,T)

Input parameters (scalars or vectors):
p - pressure [MPa] (0.012 < p < 1000)
T - temperature [degC] (-183< T < 347)

Output parameter:
rho - density of CH4 [kg/m^3]

References:
Setzmann & Wagner (1991) J. Phys. Chem. Ref. Data 20, 1061-1155.

density_ch4sw - calculates the density of a solution of CH4 in seawater

Usage: rho = density_ch4sw(p,T,S,m)

Input parameters (scalars or vectors):
p - pressure [MPa] (0.1 < p < 200),
T - temperature [degC] (0 < T < 250),
S - practical salinity (0 < S < 350)
m - molality of dissolved CH4 [mol/kg]
(default value is saturation concentration)
(input as scalar or p x T x S matrix)

Output parameter:
rho - density of CH4-rich seawater [kg/m^3]

References:
Duan et al. (2006) GCA 70, 3369-3386.

Comments:
The validity range for salinity is not specified and the limit for NaCl is taken instead.

density_co2 - calculates the density of CO2 based on an EOS
The toolbox script EOS_CO2 is called.

Usage: rho = density_co2(p,T)

Input parameters (scalars or vectors):
p - pressure [MPa] (0 < p < 800)
T - temperature [degC] (-57 (0)< T < 827)

Output parameter:
rho - density of CO2 [kg/m^3]

References:
Span & Wagner (1996) J.Phys.Chem.Ref.Data 25(6), 1509-1596.

density_co2sw - calculates the density of a solution of CO2 in seawater

Usage: rho = density_co2sw(p,T,S,m)

Input parameters (p,T,S: scalars or vectors):
p - pressure [MPa] (0.1 < p < 100),
T - temperature [degC] (0 < T < 200),
S - practical salinity (0 < S < 350)
m - molality of dissolved CO2 [mol/kg]
(default value is saturation concentration)
(input as scalar or p x T x S matrix)

Output parameter:
rho - density of CO2-rich seawater [kg/m^3]

References:
Duan et al. (2008) Energy & Fuels 22, 1666-1674.
Hu et al. (2007) Chemical Geology 238, 249-267.
Duan et al. (2006) GCA 70, 3369-3386.

Comments:
The validity range for salinity is not specified and the NaCl limit is taken instead. The formalism follows in part the Duan 2006 publication on density of CH4-seawater solutions.

density_n2sw - calculates the density of a N2-seawater solution

Usage: rho = density_n2sw(p,T,S,m)

Input parameters (scalars or vectors):
p - pressure [MPa] (0.1 < p < 60),
T - temperature [degC] (0 < T < 127),
S - practical salinity (0 < S < 350)
m - molality of dissolved N2 [mol/kg]
(default value is saturation concentration)
(input as scalar or p x T x S matrix)

Output parameter:
rho - density of N2-rich seawater [kg/m^3]

References:
Mao & Duan (2006) Fluid Phase Equilibria 248, 103-114.

Comments:
The validity range for salinity is not specified and the limit for NaCl is taken instead.

density_sw - calculates the density of seawater or saline brines
The user can choose 5 formalisms for different pTS ranges.
If no choice is specified, the formalism is chosen depending on the pTS input.

Usage: rho = density_sw(p,T,S,c)

Input parameters (scalars or vectors):
p - pressure [MPa],
T - temperature [degC]
S - practical salinity
c - user choice of algorithm (default is 'EOS')
'EOS': IAPSW seawater EOS (eos_sw)

'UNESCO': Unesco formulae (density_swUnesco)
'TEMP': for high T (density_swSun)
'BRINE': for high p,T,S (density_swSpivey)
'DRIESNER': for large p,T,S range (eos_swDriesner)

Output parameters:
rho - density of seawater [kg/m^3]

density_swUnesco - calculates the density of seawater using the UNESCO formulae from 1983 and 1991

Usage: rho = density_swUnesco(p,T,S)

Input parameters (scalars or vectors):
p - pressure [MPa],
T - temperature [degC]
S - salinity [g/kg]

Output parameters:
rho - density of seawater [kg/m^3]

References:
Fofonoff & Millard (1983) Unesco Technical Papers in Marine Science 44.
Poisson et al. (1991) Unesco Technical Papers in Marine Science 62.

density_swSpivey - calculates the density of seawater at elevated temperatures and NaCl concentrations

Usage: rho = density_swSpivey(p,T,S)

Input parameters (scalars or vectors):
p - pressure [MPa] (0 < p < 200)
T - temperature [degC] (0 < T < 275)
S - practical salinity (0 < S < 216)

Output parameter:
rho - density of seawater [kg/m^3]

References:
Spivey & McCain (2004) J.Can.Petrol.Tech 43, 52-61.

density_swSun - calculates the density of seawater at higher temperatures

Usage: rho = density_swSun(p,T,S)

Input parameters (scalars or vectors):
p - pressure [MPa] (0.1 < p < 100)
T - temperature [degC] (0 < T < 374)
S - practical salinity (0 < S < 80)

Output parameter:
rho - density of seawater [kg/m^3]

References:
Sun et al. (2008) DSR I 55, 1304-1310.

Comment:
Equations are valid in the liquid phase only.

density_ch4co2n2 - calculates the density of a mixture of CH4, CO2 and N2 and returns the phase composition (mixture might separate into a liquid and a vapor phase) and the vapor phase fraction. Calculations are based on the Peng-Robinson EOS.

Usage: [rho x y V exitflag] = density_ch4co2n2(p,T,mn2,mco2,mch4)

Input parameters (scalars!):
p - pressure [MPa] (p > 1 MPa)
T - temperature [degC]
mn2 - total amount of N2 in mixture [mol]
mco2 - total amount of CO2 in mixture [mol]
mch4 - total amount of CH4 in mixture [mol]

Output parameters:
rho - density of mixture [mol/kg]
(scalar for single phase; 2-component vector, if mixture consists of liquid and vapor phase)
x - mole fractions of N2, CO2, CH4 in liquid phase
(3-component vector)
y - mole fractions of N2, CO2, CH4 in vapor phase
(3-component vector)
V - vapor phase fraction
exitflag - exitflag of solver (to check the goodness of the numerical solution):
=999 if solver has not been used

References:
Peng & Robinson (1976) Ind. Eng. Chem. Fund. 15, 59-64.
Risnes et al. (1981) Developments in Petroleum Science 13, 329-350.
Michelsen (1982) Fluid Phase Equilibria 9, 1-19.

The calculation of the multi phase system follows the procedure outlined in the course documentation of M. Adewumi "Phase relations in reservoir engineering", Penn State College of Earth and Mineral Sciences, www.e-education.psu.edu/png520/m17_p4.html

Comments:
1. Only scalar input!
2. Results for pure fluids deviate from results of the Span & Wagner EOS by about 10% at 10 MPa. The deviation increases with increasing pressure.
3. V is set to NaN, if only 1 phase exists, but it is unknown if the phase is liquid or vapor
4. This script can be used to calculate solubilities of CH4 and N2 in liquid CO2: Vary the amount of CH4 or N2 until the 1-phase solution becomes a 2-phase solution: The highest amount with a 1-phase solution is the maximum amount that can be dissolved in the given amount of CO2 (see code example following this header, calculation is time consuming). Obtained values for solubility of CH4 in CO2 are smaller than those calculated from the toolbox script solu_ch4co2.

density_cacl2brine - calculates the density of aqueous CaCl2 solutions

Usage: rho = density_cacl2brine(p,T,m)

Input parameters (scalars or vectors):
p - pressure [MPa] (0.1 < p < 68.5)
T - temperature [degC] (10 < T < 199)
m - molality of CaCl2 [mol/kg] (0 < m < 6)

Output parameter:
rho - density of CaCl2 solution [kg/m^3]

References:
Al-Ghafri et al. (2012) J. Chem. Eng. Data 57, 1288-1304.

E.3. Phase Boundaries

hydrate_phasediagram - plots the phasediagrams of the binary systems CH4-H2O and CO2-H2O

Usage: hydrate_phasediagram(S,t1,t2,p2)

Input parameters (scalar!):
S - practical salinity (default: 35)
t1 - start of temperature axis [degC] (default: -10)
t2 - end of temperature axis [degC] (default: 35)
p2 - end of pressure axis [m water depth] (default: 2500) (starting pressure is 0)

References:
Tishchenko et al. (2005) Chem. Geol. 219, 35-52.
Tishchenko et al. (2009) 8th International CO2 Conference, Jena.

phase_ch4sw - calculates the phase boundaries of the binary system CH4-H2O

Usage: [pdisw,pdissw,pdispw] = phase_ch4sw(T,S)

Input parameters:
T - temperature [degC] (-10 < T < 30)
S - practical salinity (0 < S < 70)

Output parameters:
pdisw - hydrate dissociation pressure for pure water [MPa]
pdissw - hydrate dissociation pressure for seawater [MPa]
pdispw - hydrate dissociation pressure for SO4-free porewater [MPa]

References:
Tishchenko et al. (2005) Chem.Geol. 219, 35-52.

phase_co2sw - calculates the phase boundaries of the binary system CO2-H2O

Usage: [pm,ps,pv,pgh] = phase_co2sw(T,S)

Input parameters (scalars or vectors):
T - temperature [degC]
S - practical salinity (0 < S < 40)

Output parameters:
Pm - CO2 melting pressure [MPa]
Ps - CO2 sublimation pressure [MPa]
Pv - CO2 vapor pressure [MPa]
Pgh - CO2 hydrate pressure [MPa]

References:
Tishchenko et al. (2009) 8th International CO2 Conference, Jena.
Span & Wagner (1994) J.Phys.Chem.Ref.Data 25, 1509-1597.

phase_sw - calculates the phase boundaries of the system H2O-NaCl based on multiparametric equations (also valid for hydrothermal systems)

Usage:
[P_sat P_VL Tcrit Pcrit T_VLH P_VLH x_vap PmNaCl PsNaCl PbNaCl] = phase_sw(T,S)

Input parameters (T is scalar or vector; S is scalar):
T - temperature [degC] (0 < T < 1000)
S - practical salinity (0 < S < 1000)

Output parameter:
P_sat - saturation pressure [MPa] at given temperature + NaCl concentration (liquid-halite coexistence line)
P_VL - liquid-vapor coexistence pressure [MPa] at given temperature and NaCl concentration
Tcrit - critical temperature [degC] at given NaCl concentration
Pcrit - critical pressure [MPa] at given NaCl concentration
T_VLH - temperature [degC] at liquid-vapor-halite coexistence for given NaCl concentration
P_VLH - pressure [MPa] at liquid-vapor-halite coexistence for given NaCl concentration
xvap - mole fraction of NaCl in the vapor phase at liquid-vapor coexistence
PmNaCl - melting pressure [MPa] of NaCl at given temperatures
PsNaCl - sublimation pressure [MPa] of NaCl at given temperatures
PbNaCl - boiling pressure [MPa] of NaCl at given temperatures

References:
Driesner & Heinrich (2007) GCA 71, 4880-4901.
IAPWS (1992) Revised supplementary release on saturation properties of ordinary water substance. http://iapws.org

Comments:
The vapor-liquid coexistence line is calculated only for temperatures below the triple point temperature of NaCl (800.7 degC).

sw_phasediagram - plots the phasediagrams of the binary system NaCl-H2O for salinities up to 1000 g/kg, temperatures up to 1000 degC, and pressures of >500 MPa as calculated by phase_sw.

Usage: sw_phasediagram(S,T1,T2)

Input parameters (scalar):
S - practical salinity (default: 300)
T1 - start of temperature range [degC] (default is 0 degC)
T2 - end of temperature range [degC] (default is 800 degC)

References:
Driesner & Heinrich (2007) GCA 71, 4880-4901.

vlh_naclh2o - calculates the vapor-liquid-halite (VLH) coexistence point for a given temperature from a multiparametric equation

Usage: [p_vlh,mnacl] = vlh_naclh2o(T)

Input parameter (vector or scalar):
T - temperature [degC] (0 < T < 1000)

Output parameter:
p_vlh - VLH coexistence pressure [MPa]
mnacl - molality of NaCl at saturation [mol/kg]

References:
Driesner & Heinrich (2007) GCA 71, 4880-4901.

E.4. Fugacities

fugacity_ch4gh - calculates the fugacity of CH4 in CH4-hydrate

Usage: f = fugacity_ch4gh(T,N)

Input parameters (scalars or vectors):
T - temperature [degC]
N - moles of CH4 per mole of water in hydrate phase (0 < N < 4/23)

Output parameter:
f - fugacity of CH4 in CH4_hydrate [MPa]

References:
Cole & Goodwin (1990) Chem. Eng. Sci. 45, 569-573.
Klauda & Sandler (2003) Chem. Eng. Sci. 58, 27-41. (Langmuir constants)

Comments:
Function returns NaN, if no solution for f exists. This happens if N is too large (100% cage occupancy does not occur).

An approximate N can be derived from the output of the toolbox function fugacity_h2omh:
N = 1/23 * theta_s + 3/23 * theta_l

fugacity_ch4sw - calculates the fugacity of dissolved CH4 gas in equilibrium with seawater

Usage: f = fugacity_ch4sw(p,T,S,m)

Input parameters (scalars or vectors):
p - pressure [MPa] (0.1 < p < 200)
T - temperature [degC] (0 < T < 250)
S - practical salinity (S < 350)
m - molality of dissolved CH4 in seawater [mol/kg], default is saturation concentration

Output parameters:
f - fugacity of CH4 in seawater [MPa]

References:
Harvey (1996) AIChE 42, 1491-1494. (Henry constant)
Duan & Mao (2006) GCA 70, 3369-3386. (term gamma)
Duan et al. (2008) Energy & Fuels 22, 1666-1674. (molar volume of CH4)

fugacity_co2gh - calculates the fugacity of CO2 in CO2-hydrate

Usage: f = fugacity_co2gh(T,N)

Input parameters (scalars or vectors):
T - temperature [degC]
N - moles of CO2 per mole of water in hydrate phase (0 < N < 4/23)

Output parameter:
f - fugacity of CO2 in CO2_hydrate [MPa]

References:
Cole & Goodwin (1990) Chem. Eng. Sci. 45, 569-573.
Klauda $ Sandler (2003) Chem. Eng. Sci. 58, 27-41 (Langmuir constants)

Comments:
This algorithm is entirely based on a theoretical equation
- no validation by experimental data conducted.

An approximate N can be derived from the output of the toolbox function fugacity_h2och:
N = 1/23 * theta_s + 3/23 * theta_l

At hydrate dissociation pressure, the match between gas phase fugacity of CO2 and hydrate phase fugacity of CO2 is not satisfying.
N (as calculated from the output of fugacity_h2och) is decreased by about 2%.

fugacity_co2sw - calculates the fugacity of dissolved CO2 gas in equilibrium with seawater

Usage: f = fugacity_co2sw(p,T,S,m)

Input parameters (scalars or vectors, m: scalar/matrix of size pxtxS):
p - pressure [MPa] (0.1 < p < 35 or gas/liquid phase boundary)
T - temperature [degC] (0 < T < 162)
S - practical salinity (S < 263)
m - molality of dissolved CO2 in seawater [mol/kg],
default is saturation concentration

Output parameters:
f - fugacity of CO2 in seawater [MPa]

References:
Harvey (1996) AIChE 42, 1491-1494.
Wagner & Pruss (2002) J.Phys.Chem.Ref.Data 31, 387-535. (vapor pressure of water)
Duan et al. (2006) Mar.Chem. 98, 131-139. (term gamma)
Plyasunov et al. (2000) GCA 64, 495-512. (partial molar volume of CO2)

Comments:
Formalism is not valid for pT conditions where pure CO2 is liquid.

fugacity_h2och - calculates the fugacity of water in CO2 SI-hydrate

Usage: [f theta_s, theta_l] = fugacity_h2och(p,T)

Input parameters (scalars or vectors):
p - pressure [MPa]
T - temperature [degC] (-133 < T < 57)

Output parameter:
f - fugacity of water in CO2 SI-hydrate [MPa]
theta_s - fractional occupancy of small hydrate cages
theta_l - fractional occupancy of large hydrate cages

References:
Klauda & Sandler (2003) Chem. Eng. Sci. 58, 27-41.
Klauda & Sandler (2000) Ind. Eng. Chem. Res. 39, 3377-3386.

Comments:
Coefficients A-D for the vapor pressure of the empty hydrate lattice are derived from a fit to match the liquid water fugacity as provided by the toolbox function fugacity_sw to the water fugacity as calculated by the Klauda & Sandler formalism at the hydrate phase boundary (calculated by phase_co2sw).

Fugacities of CO2 in the hydrate phase are approximated as fugacities of gas phase CO2. For the calculation of hydrate phase fugacities, the total mount of CO2 in the hydrate phase has to be known.

fugacity_h2omh - calculates the fugacity of water in CH4 SI-hydrate

Usage: [f theta_s theta_l] = fugacity_h2omh(p,T)

Input parameters (scalars or vectors):
p - pressure [MPa]
T - temperature [degC] (-133 < T < 57)

Output parameter:
f - fugacity of water in CH4 SI-hydrate [MPa]
theta_s - fractional occupancy of small hydrate cages
theta_l - fractional occupancy of large hydrate cages

References:
Klauda & Sandler (2003) Chem. Eng. Sci. 58, 27-41.
Klauda & Sandler (2000) Ind. Eng. Chem. Res. 39, 3377-3386.

Comments:
Coefficients A-D for the vapor pressure of the empty hydrate lattice are derived from a fit to match the liquid water fugacity as provided by the toolbox function fugacity_sw to the water fugacity as calculated by the Klauda & Sandler formalism at the hydrate phase boundary (calculated by phase_ch4sw).

Fugacities of CH4 in the hydrate phase are approximated as fugacities of gas phase CH4. For the calculation of hydrate phase fugacities, the total mount of CH4 in the hydrate phase has to be known.

fugacity_sw - calculates the fugacity of water in solutions with dissolved salts, CH4 and CO2

Usage: f = fugacity_sw(p,T,S,mch4,mco2)

Input parameters (scalars or vectors):
p - pressure [MPa] (0.1 < p < 400)
T - temperature [degC]
S - practical salinity (0 < S < 350)
mch4 - molality of dissolved CH4 [mol/kg]
mco2 - molality of dissolved CO2 [mol/kg]

Output parameter:
f - fugacity of water in seawater with CO2 and CH4 [MPa]

References:
Jager et al. (2003) Fluid Phase Equilibria 211, 85-107.

Comments:
Pressure range reduced from 5000 bar to 4000 bar to avoid handling of different cases during integration. The activity of the solvent water is calculated and used to modify the pure water

fugacity as derived from the Wagner & Pruss EOS.

fugacity_h2ssw - calculates the fugacity of dissolved H2S gas in equilibrium with seawater

Usage: f = fugacity_h2ssw(p,T,S,m)

Input parameters (scalars or vectors, m: scalar/matrix of size pxtxS):
p - pressure [MPa] (0.1 < p < 20)
T - temperature [degC] (0 < T < 127)
S - practical salinity (0 < S < 350)
m - molality of dissolved H2S in seawater [mol/kg],
default is saturation concentration

Output parameter:
f - fugacity of H2S in seawater [MPa]

References:
Harvey (1996) AIChE 42, 1491-1494. (Henry constant)
Plyasunov et al. (2000) GCA 64, 2779-2795. (partial molar volume of H2S)
Duan et al (2007) Energy & Fuels 21, 2056-2065. (gamma term)

Comments:
Formalism is not valid for pT conditions where pure H2S is liquid.

fugacity_n2sw - calculates the fugacity of dissolved N2 gas in equilibrium with seawater

Usage: f = fugacity_n2sw(p,T,S,m)

Input parameters (scalars or vectors, m: scalar/matrix of size pxtxS):
p - pressure [MPa] (0.1 < p < 35)
T - temperature [degC] (0 < T < 317)
S - practical salinity (S < 350)
m - molality of dissolved N2 in seawater [mol/kg],
default is saturation concentration

Output parameters:
f - fugacity of N2 in seawater [MPa]

References:
Harvey (1996) AIChE 42, 1491-1494. (Henry constant)
Plyasunov et al. (2000) GCA 64, 495-512. (partial molar volume of N2)
Mao & Duan (2006) Fluid Phase Equilibria 248, 103-114.

fugacity_o2sw - calculates the fugacity of dissolved O2 gas in equilibrium with seawater

Usage: f = fugacity_o2sw(p,T,S,m)

Input parameters (scalars or vectors, m: scalar/matrix of size pxTxS):
p - pressure [MPa] (0.1 < P <20)
T - temperature [degC] (0 < T < 127)
S - practical salinity (0 < S < 350)
m - molality of dissolved O2 in seawater [mol/kg],
default is saturation concentration

Output parameters:
f - fugacity of O2 in seawater [MPa]

References:
Harvey (1996) AIChE 42, 1491-1494. (Henry constant)
Plyasunov et al. (2000) GCA 64, 495-512. (partial molar volume of O2)
Geng & Duan (2010) GCA 74, 5631-5640. (for gamma term)

E.5. Solubilities

solu_ch4 - calculates the equilibrium concentration of CH4 in seawater with a gas phase or hydrate phase. The phase at given parameters p,T,S is determined and the appropriate function for the calculation of the solubility is called.

Usage: m = solu_ch4(p,T,S)

Input parameters (scalars or vectors):
p - pressure [MPa],
T - temperature [degC]
S - practical salinity

Output parameter:
m - molality of CH4 in seawater [mol/kg]

solu_ch4gas - calculates the equilibrium concentration of CH4 in seawater with respect to the gas phase as well as the resulting mole fraction of water in the CH4 gas phase

Usage: [mCH4sw xsw] = solu_ch4gas(p,T,S)

Input parameters (scalars or vectors):
p - pressure [MPa] (0.1 < P < 200)
T - temperature [degC] (0 < T < 250)
S - practical salinity (S < 350)

Output parameter:
mCH4sw - molality of CH4 in seawater [mol/kg]
xsw - mole fraction of H2O in gas phase

References:
Duan & Mao(2006) GCA 70, 3369-3386.
Duan et al. (1992) GCA 56, 2605-2617.
Wagner & Pruss (1993) J.Phys.Chem.Ref.Data 22,783-787
Shibue (2003) Fluid Phase Equilibria 213, 39-51.

Comments:
This script does not check, if the pressure and temperature conditions are within the hydrate stability zone. Use solu_ch4 to discriminate between 2 phase and 3 phase solubilities.
No solubility for gaseous CH4 in SO4-free porewater available so far.

solu_ch4gh - calculates the solubility of CH4 in seawater and SO4-free porewater in equilibrium with methane hydrate (no gas phase)

Usage: [mch4sw,mch4pw] = solu_ch4gh(p,T,S)

Input parameters (scalars or vectors):

p - pressure [MPa] (0.1 < P < 50)
T - temperature [degC] (0 < T < 20)
S - practical salinity (S < 70)

Output parameter:
mch4sw - molality of CH4 in seawater [mol/kg]
mch4pw - molality of CH4 in SO4-free porewater [mol/kg]

References:
Tishchenko et al. (2005) Chem. Geol. 219, 35-52.

Comments:
This script does not check, if the pressure and temperature conditions are outside the hydrate stability zone. Use solu_ch4 to discriminate between 2-phase and 3-phase solubilities.

solu_co2 - calculates the CO2 equilibrium concentration in seawater with respect to gas phase, liquid phase or hydrate phase. The phase at given parameters p,T,S is determined and the appropriate function for the calculation of the solubility is called.

Usage: m = solu_co2(p,T,S)

Input parameters (scalars or vectors):
p - pressure [MPa]
T - temperature [degC]
S - practical salinity

Output parameter:
m - molality of CO2 in seawater [mol/kg]

solu_co2gl - calculates the CO2 equilibrium concentration in seawater with respect to gas and liquid phase

Usage: m = solu_co2gl(p,T,S)

Input parameters (scalars or vectors):
p - pressure [MPa] (0.1 < P < 100)
T - temperature [degC] (0 < T < 162)
S - practical salinity (S < 263)

Output parameter:
m - molality of CO2 in seawater [mol/kg]

References:
Duan & Sun (2003) Chemical Geology 193, 257-271.
Duan et al. (2006) Marine Chemistry 98, 131-139.

Comments:
This script does not check, if the pressure and temperature conditions are inside the hydrate stability zone. Use solu_co2 to discriminate between 2-phase and 3-phase solubilities.

Deviation of solubility values from those of Wong et al. (2005) (J.Chem.Eng.Data 50, 822-831) is <5% for pressures up to 250 bar.

No dissociation pressure for pore water available so far.
No solubility of liquid/gaseous CO2 in SO4-free porewater available so far.

solu_co2gh - calculates the solubility of CO2 in seawater and SO4-free porewater in equilibrium with CO2 hydrate (no gas phase).

Usage: [mco2pw,mco2sw] = solu_co2gh(p,T,S,pgh)

Input parameters (scalars or vectors):
p - pressure [MPa] (0.1 < P < 50)
T - temperature [degC] (0 < T < 12)
S - practical salinity (S < 40)

Output parameter:
mco2sw - molality of CO2 in seawater [mol/kg]
mco2pw - molality of CO2 in SO4-free porewater [mol/kg]

References:
Tishchenko et al. (2009) 8th International CO2 Conference, Jena.

Comments:
This script does not check, if the pressure and temperature conditions are outside the hydrate stability zone. Use solu_co2 to discriminate between 2-phase and 3-phase solubilities.
The equations are valid up to 10 degC. Extrapolation to 12 degC has been allowed to cover the full parameter range of the hydrate model.

solu_h2ssw - calculates the equilibrium concentration of H2S in seawater

Usage: m = solu_h2ssw(p,T,S)

Input parameters (scalars or vectors):
p - pressure [MPa] (0.1 < P < 20)
T - temperature [degC] (0 < T < 127)
S - practical salinity (S < 350)

Output parameter:
m - molality of H2S in seawater [mol/kg]

References:
Duan et al. (2007) Energy & Fuels 21, 2056-2065.
Duan et al. (1996) Chemical Geology 130, 15-20. (H2S-EOS)
Shibue (2003) Fluid Phase Equilibria 213, 39-51. (water saturation pressure)
Velasco et al. (2008) J.Chem.Thermo. 40, 789-797. (H2S vapor pressure)

solu_n2sw - calculates the equilibrium concentration of N2 in seawater

Usage: m = solu_n2sw(p,T,S)

Input parameters (scalars or vectors):
p - pressure [MPa] (0.1 < P < 60)
T - temperature [degC] (0 < T < 317)
S - practical salinity (S < 350)

Output parameter:
m - molality of N2 in seawater [mol/kg]

References:
Mao & Duan (2006) Fluid Phase Equilibria 248, 103-114.
Shibue (2003) Fluid Phase Equilibria 213, 39-51.

Comments:
The mole fraction of N2 in gas phase is set to 1.
At high temperatures and low pressures, the equation to calculate the H2O mole fraction in the vapor phase as given by Duan results in fractions >1. The formalism to calculate yH2O is still implemented, but has been marked as comment.

solu_o2sw - calculates the equilibrium concentration of O2 in seawater

Usage: m = solu_o2sw(p,T,S)

Input parameters (scalars or vectors):
p - pressure [MPa] (0.1 < P < 20)
T - temperature [degC] (0 < T < 127)
S - practical salinity (S < 350)

Output parameter:
m - molality of O2 in seawater [mol/kg]

References:
Geng & Duan (2010) GCA 74, 5631-5640.
Shibue (2003) Fluid Phase Equilibria 213, 39-51.

solu_co2ch4 - calculates the partial pressure of CO2 in a methane gas bubble in seawater

Usage: pp = solu_co2ch4(p,T,S)

Input parameters (scalars or vectors):
p - pressure [MPa] (3.5 < P < 50)
T - temperature [degC] (0 < T < 25)
S - practical salinity (S < 40)

Output parameter:
pp - partial pressure of CO2 in CH4-dominated gas [MPa]

References:
Wong et al. (2005) J.Chem.Eng.Data 50, 822-831.
Tishchenko et al. (2009) 8th International CO2 Conference, Jena.
Duan et al. (2008) Energy & Fuels 22, 1666-1674.
Comments:
If the pTS values are within the range of gaseous CO2, the function output is set to NaN.

solu_ch4co2 - calculates the solubility of CH4 in (liquid) CO2 by a "brute force" strategy (slow!). The feed composition is varied until the density as calculated by a Peng Robinson EOS is returned as a 2-component vector indicating a 2-phase system.

Usage: m = solu_ch4co2(p,T)

Input parameters (scalars!):
p - pressure [MPa]
T - temperature [degC]

Output parameter:
m - solubility of CH4 in liquid CO2 [mol/kg]

References:
Al-Sahhaf et al. (1983) Ind.Eng.Chem.Fund. 22, 372-380.

solu_n2co2 - calculates the solubility of N2 in (liquid) CO2 by a "brute force" strategy (slow!). The feed composition is varied until the density as calculated by a Peng Robinson EOS is returned as a 2-component vector indicating a 2-phase system.

Usage: m = solu_n2co2(p,T)

Input parameters (scalars!):
p - pressure [MPa]
T - temperature [degC]

Output parameter:
m - solubility of N2 in liquid CO2 [mol/kg]

References:
Al-Sahhaf et al. (1983) Ind.Eng.Chem.Fund. 22, 372-380.

solu_swco2 - calculates the solubility of water in liquid CO2 as a function of pressure, temperature and salinity from a multiparameter equation.

Usage: [cw xw] = solu_swco2(p,T,S)

Input parameters (scalars or vectors):
p - pressure [MPa] (5 < p < 20)
T - temperature [degC] (10 < T < 40)
S - practical salinity (0 < S < 40)

Output parameters:
cw - molality of H2O dissolved in CO2 [mol/kg{solution}]
xw - mole fraction of H2O in liquid CO2

References:
Tishchenko et al. (unpublished).

solu_nacl - calculates the saturation concentration of NaCl in seawater from a multiparametric equation

Usage: m = solu_nacl(p,T)

Input parameters (vectors or scalars):
p - pressure [MPa] (0 < P < 500)
T - temperature [degC] (0 < T < 1000)

Output parameter:
m - molality of NaCl at saturation [mol/kg]

References:
Driesner & Heinrich (2007) GCA 71, 4880-4901.

solu_caso4 - calculates the solubility product Ksp = m_Ca * m_SO4 for gypsum (CaSO4*2H2O), anhydrite (CaSO4), ad hemihydrate (CaSO4*0.5H2O) in seawater

Usage: [ka kg kh] = solu_caso4(p,T,sal)

Input parameters (scalars or vectors):
p - pressure [MPa] (0.1 < p < 100)
T - temperature [degC] (30 < T < 300)

S - practical salinity (0 < S < 250) (see comments!)

Output parameter:
ka - solubility product of anhydrite
kg - solubility product of gypsum
kh - solubility product of hemihydrate

References:
Marshall & Slusher (1968) J.Chem.Eng.Data 13, 83-93. (solubility at constant pressure)
Blount & Dickson (1973) Amer.Mineral. 58, 323-331. (pressure correction)

Comments:
Ionic strength refers to NaCl in NaCl solutions.
For seawater, the solubility product is assumed to equal the solubility product in NaCl solutions of the same ionic strength. However, this is true only for moderate temperatures (T < 100 degC) and low or moderate ionic strengths.
Equations are valid for:
p = 0.1 - 100 MPa
T = 60 - 95 degC (Gypsum)
T = 100 - 200 degC (Anhydrite)
S = 0 - 250 (==> I = 0 - 5 mol/kg)

solu_opal - calculates the solubility of opal in seawater
The user can choose 2 formalisms for different temperature ranges.

Usage: m = solu_opal(p,T,S,c)

Input parameters (scalars or vectors):
p - pressure [MPa] (10 < p < 120)
T - temperature [degC]
S - practical salinity (0 < S < 80)
c - choice of algorithm
'WALTHER' (default) (0 < T < 350)
'FOURNIER' (150 < T < 350)
Output parameters:
m - solubility of opal [mol/kg]

solu_opalFournier - calculates the solubility of amorphous silica in seawater

Usage: m = solu_opalFournier(p,T,S)

Input parameters (scalars or vectors):
p - pressure [MPa] (10 < p < 120)
T - temperature [degC] (150 < T < 350)
S - practical salinity (0 < S < 80)

Output parameter:
m - solubility of silica [mol/kg]

References:
Fournier & Marshall (1983) GCA 47, 587-596. (solubility at p=1000 bar)
Willey (1974) Mar.Chem. 2, 239-250. (pressure correction)
Fournier (1983) GCA 47, 579-586. (salinity correction of m)
Sun et al. (2008) DSR I 55, 1304-1310. (salinity correction density)

Comments:
The temperature dependency has been evaluated by Fournier & Marshall for data in the range of

150-350 degC at 1000 bar.
The pressure dependency has been evaluated by Willey for data in the range of 100-200 atm at 0 degC.
A salinity correction for the solubility as proposed for the solubility of quarz by Fournier (1983) is implemented, assuming that hydration numbers for quartz and amorphous silica are identical.

solu_opalWalther - calculates the solubility of amorphous slica in seawater

Usage: m = solu_opalWalther(p,T,S)

Input parameters (scalars or vectors):
p - pressure [MPa] (10 < p < 120)
T - temperature [degC] (0 < T < 350)
S - practical salinity (0 < S < 80)

Output parameter:
m - solubility of silica [mol/kg]

References:
Walther & Helgeson (1977) AJS 277, 1315-1351.
Helgeson & Kirkham (1974) AJS 274, 1089-1198.
Fournier & Marshall (1983) GCA 47, 579-586. (salinity correction m)
Sun et al. (2008) DSR I 55, 1304-1310. (salinity correction density)

Comments:
The regression in the paper was done on data from T=0-350 degC and p=100-1200 bar. A salinity correction for the solubility as proposed for the solubility of quarz by Fournier (1983) is implemented, assuming that hydration numbers for quartz and amorphous silica are identical.

solu_quartz - calculates the solubility of quartz in seawater
The user can choose 2 formalisms for different pTS conditions.

Usage: m = solu_quartz(p,T,S,c)
Input parameters (scalars or vectors):
p - pressure [MPa]
T - temperature [degC]
S - practical salinity
c - choice of algorithm
'FOURNIER' (default) (T=0-350 degC, p=0.1-100 MPa)
'DAMM' (for higher pT)

Output parameters:
m - solubility of quartz [mol/kg]

solu_quartzDamm - calculates the solubility of quartz in seawater for hydrothermal conditions

Usage: m = solu_quartzDamm(p,T,S)

Input parameters (scalars or vectors):
p - pressure [MPa] (0.1 < p < 986)
T - temperature [degC] (45 < T < 900)
S - practical salinity (0 < S < 80)

Output parameter:
m - solubility of quartz [mol/kg]

References:
von Damm et al. (1991) AJS 291, 977-1007.
Sun et al. (2008) DSR I 55, 1304-1310. (salinity correction density)

Comments:
The equation does not include salinity effects. Von Damm et al. state that salinity effects are within the range of uncertainty for moderate pressures and temperatures. For high p and T, non-neglible salinity effects are expected. According to Newton & Manning (2000) GCA 64, 2993-3005, the salinity dependence of the solubility at high pressures (> 10000 bar) is an exponential function, but they do not provide an equation. Von Damm et al. suggest to correct parameter 'a' in their equation for the amount of water that is immobilzed as a hydration layer around the salt ions.
The salinity correction for the density is valid in the liquid phase only for 0.1 < p < 100, 0 < T < 374, 0 < S < 40 (Von Damm et al. state that extrapolation up to S = 80 is ok).
The calculated density values for T < 350 degC compare well with the data from Fontaine et al. (2007) EPSL 275, 132-145. Data deviate for higher temperatures.

solu_quartzFournier - calculates the solubility of quartz in seawater

Usage: m = solu_quartzFournier(p,T,S)

Input parameters (scalars or vectors):
p - pressure [MPa] (0.1 < p < 100)
T - temperature [degC] (0 < T < 350)
S - practical salinity (0 < S < 80)

Output parameter:
m - solubility of quartz [mol/kg]

References:
Fournier (1983) GCA 47, 579-586. (solubility)
Sun et al. (2008) DSR I 55, 1304-1310. (salinity correction density)

Comments:
The solubility is derived from the general formula
log(m)= log(K) + n log(rho_e) - log(gamma) + log (Gamma)
with the last two terms set to zero.
rho_e is the density of free water, defined as
rho_e = rho F (1 - (h m(NaCl))/55.51).
The hydration number h of NaCl in solution is unknown, therefore Rho_e is approximated by
rho_e = rho F
with F being the weight fraction of water. Log(K) and n are calculated from multi-parameter equations.
The equation is valid for T = 350 degC. There is only a weak pressure dependency (in the density) and a weak dependency on salt concentration (in density and F). The salinity correction for the density is valid in the liquid phase only for 0.1 < p < 100, 0 < T < 374, 0 < S < 40 (authors state, that extrapolation up to S=80 is ok). The calculated density values for T < 350 degC compare well with the data from Fontaine et al. (2007) EPSL 275, 132-145. Data deviate for higher temperatures.
Calculation of rho_e requires the hydration number of NaCl ions. Fournier sets the hydration number to zero and states that this is a good approximation for temperatures > 200 degC. Therefore, equations may be less accurate for lower temperatures.

soluhenry_ch4sw - calculates the equilibrium concentration of CH4 in seawater from Henry's law

Usage: [m KH KHx] = soluhenry_ch4sw(p,T,S,pp)

Input parameters (scalars or vectors, pp: scalar or matrix of size p x T x S):
p - overall pressure [MPa] (0.1 < p < 200)

T - temperature [degC] (0 < T < 250)
S - practical salinity (S < 350)
pp - partial pressure of CH4 [MPa] (pp < p)
pp is set to p if no input value is provided

Output parameter:
m - molality of CH4 in seawater [mol/kg]
KH - pressure and salinity corrected Henry constant [mol/kg/MPa]
KHx - pressure and salinity corrected Henry constant [1/MPa]

References:
Harvey (1996) AIChE 42, 1491-1494. (Henry constant)
Plyasunov et al. (2000) GCA 64, 495-512. (partial molar volume of CH4)
Duan & Mao (2006) GCA 70, 3369-3386. (gamma term)

Comments:
Henry's law is not well suited for high pressures and should be used with care at high pressures:
Keep in mind that results are expected to be inaccurate.

soluhenry_co2sw - calculates the equilibrium concentration of CO2 in seawater from Henry's law

Usage: [m KH KHx] = soluhenry_co2sw(p,T,S,pp)

Input parameters (scalars or vectors, pp: scalar or matrix of size p x T x S):
p - overall pressure [MPa] (0.1 < p < 35 or gas/liquid phase boundary)
T - temperature [degC] (0 < T < 162)
S - practical salinity (S < 263)
pp - partial pressure of CO2 [MPa] (pp < p)
pp is set to p if no input value is provided

Output parameter:
m - molality of CO2 in seawater [mol/kg]
KH - pressure and salinity corrected Henry constant [mol/kg/MPa]
KHx - pressure and salinity corrected Henry constant [1/MPa]

References:
Harvey (1996) AIChE 42, 1491-1494. (Henry constant)
Wagner & Pruss (2002) J.Phys.Chem.Ref.Data 31, 387-535. (vapor pressure of water)
Duan et al. (2006) Mar.Chem. 98, 131-139. (gamma term)
Plyasunov et al. (2000) GCA 64, 495-512. (partial molar volume of CO2)

Comments:
The solubility of CO2 in (sea)water as function of pressure, temperature and salinity is related to Henry's constant KH by the equation:
m = f*KH0(T)/(gamma(S,T)*exp(integral(V_mol(P,T)/R/T) dP)))
f: fugacity
gamma: activity coefficient,
V_mol: apparent molar volume of dissolved gas

Henry's law is not well suited for high pressures and should be used with care at high pressures:
Keep in mind that results are expected to be inaccurate.

soluhenry_h2ssw - calculates the equilibrium concentration of H2S in seawater from Henry's law

Usage: [m KH KHx] = soluhenry_h2ssw(p,T,S,pp)

Input parameters (scalars or vectors, pp: scalar or matrix of size p x T x S):
p - overall pressure [MPa] (0.1 < p < 20)
T - temperature [degC] (0 < T < 127)
S - practical salinity (0 < S < 350)
pp - partial pressure of H2S [MPa] (pp < p)
pp is set to p if no input value is provided

Output parameter:
m - molality of H2S in seawater [mol/kg]
KH - pressure and salinity corrected Henry constant [mol/kg/MPa]
KHx - pressure and salinity corrected Henry constant [1/MPa]

References:
Harvey (1996) AIChE 42, 1491-1494. (Henry constant)
Plyasunov et al. (2000) GCA 64, 2779-2795 (partial molar volume of H2S)
Duan et al. (2007) Energy & Fuels 21, 2056-2065. (gamma term)

Comments:
Henry's law is not well suited for high pressures and should be used with care at high pressures:
Keep in mind that results are expected to be inaccurate.

soluhenry_n2sw - calculates the equilibrium concentration of N2 in seawater from Henry's law

Usage: [m KH KHx] = soluhenry_n2sw(p,T,S,pp)

Input parameters (scalars or vectors, pp: scalar or matrix of size p x T x S):
p - overall pressure [MPa] (0.1 < p < 35)
T - temperature [degC] (0 < T < 317)
S - practical salinity (S < 350)
pp - partial pressure of N2 [MPa] (pp < p)
pp is set to p if no input value is provided

Output parameter:
m - molality of N2 in seawater [mol/kg]
KH - pressure and salinity corrected Henry constant [mol/kg/MPa]
KHx - pressure and salinity corrected Henry constant [1/MPa]

References:
Harvey (1996) AIChE 42, 1491-1494. (Henry constant)
Plyasunov et al. (2000) GCA 64, 495-512. (partial molar volume of N2)
Mao & Duan (2006) Fluid Phase Equilib. 248, 103-114. (gamma term)

Comments:
Henry's law is not well suited for high pressures and should be used with care at high pressures:
Keep in mind that results are expected to be inaccurate.

soluhenry_o2sw - calculates the equilibrium concentration of O2 in seawater from Henry's law

Usage: [m KH KHx] = soluhenry_o2sw(p,T,S,pp)

Input parameters (scalars or vectors, pp: scalar or matrix of size p x T x S):
p - overall pressure [MPa] (0.1 < P <20)
T - temperature [degC] (0 < T < 127)
S - practical salinity (0 < S < 350)
pp - partial pressure of O2 [MPa] (pp < p)

pp is set to p if no input value is provided

Output parameter:
m - molality of O2 in seawater [mol/kg]
KH - pressure and salinity corrected Henry constant [mol/kg/MPa]
KHx - pressure and salinity corrected Henry constant [1/MPa]

References:
Harvey (1996) AIChE 42, 1491-1494. (Henry constant)
Plyasunov et al. (2000) GCA 64, 495-512. (partial molar volume of O2)
Geng & Duan (2010) GCA 74, 5631-5640. (gamma term)

Comments:
Henry's law is not well suited for high pressures and should be used with care at high pressures:
Keep in mind that results are expected to be inaccurate.

E.6. Viscosities

visco_ch4 - calculates the viscosity of pure CH4 from a multiparametric equation, including real gas effects

Usage: eta = visco_ch4(p,T)

Input parameters (scalars or vectors):
p - pressure [MPa] (0 < P < 50)
T - temperature [degC] (-178 < T < 227)

Output parameter:
eta - viscosity of methane [Pa*s]

References:
Hanley et al. (1977) J.Phys.Chem.Ref.Data 6, 597-609.

Comments:
The equation for eta_r was corrected for a misplaced paranthesis (see deviation between Eq. 4 in the paper and the corresponding equation in Hanley et al. (1975) Cryogenics).

visco_co2 - calculates the dynamic viscosity of CO2 from a multiparametric equation

Usage: eta = visco_co2(p,T)

Input parameters (scalars or vectors):
p - pressure [MPa] (0.1-300 MPa),
T - temperature [degC] ((-56) - 827 degC)

Output parameter:
eta - dynamic viscosity [Pa*s]

References:
Fenghour et al. (1998) J.Phys.Chem.Ref.Data 27(1), 31-44.

visco_h2o - calculates the viscosity of pure water as function of pressure and temperature based on a multiparametric equation

Usage: eta = visco_h2o(p,T)

Input parameters (scalars or vectors):
p - pressure [MPa] (0.1 < p < 167.5)
T - temperature [degC] (0.1 < T < 800)

Output parameter:
eta - dynamic viscosity [Pa*s]

Range of validity in the original paper:
for p <= 300 MPa and T <= 900 degC
for 300 MPa < p <= 350 MPa and T <= 600 degC
for 350 MPa < p <= 500 MPa and T <= 160 degC
for 500 MPa < p <=1000 MPa and T <= 100 degC
The calculation of the viscosity requires the density of H2O. Since the current script for density calculation is valid only up to 167.5 MPa, the range of validity for the viscosity calculation is reduced to 167.5 MPa.

Equations are not valid for ice phase (at temperatures below the melting point temperature).

References:
Release on the IAWPS Formulation 2008 for the Viscosity of Ordinary Water Substance.
http://iapws.org

Comments:
The critical enhancement close to the critical point (645.91 < T < 650.77 [K], 245.8 < rho < 405.3 [kg/m^3]) is omitted to save computation time. For calculations close to the critical point the viscosity shows a singularity and the critical enhancement term as given in the reference has to be considered.

visco_n2 - calculates the dynamic viscosity of N2 from a multiparametric equation

Usage: eta = visco_n2(p,T)

Input parameters (scalars or vectors):
p - pressure [MPa] (0.1-100 MPa),
T - temperature [degC] ((-120) - 727 degC)

Output parameter:
eta - dynamic viscosity [Pa*s]
References:
Lemmon & Jacobsen (2004) Int.J.Thermophys 25(1), 21-69.

visco_sw - calculates the dynamic viscosity of seawater
The user can choose from 4 formalisms for different pTS ranges. If no choice is given, the formalism is chosen based on pTS input.

Usage: eta = visco_sw(p,T,S,c)

Input parameters (scalars or vectors):
p - pressure [MPa] (0 < p < 100)
T - temperature [degC] (0 < T < 30)
S - practical salinity (0 < S < 36.1)
c - user choice for algorithm

'KUKULKA' (default)
'SPIVEY'
'MAO'
'PALLISER'

Output parameter:
eta - dynamic viscosity [Pa*s]

References:
Kukulka et al. (1987) Adv. Heat Transfer 18, 325-363.
Spivey & McCain (2004) J.Can.Petrol.Tech. 43, 52-61.
Mao & Duan (2009) Int.J.Thermophys. 30, 1510-1523.
Palliser & McKibbin (1998) Transport in Porous Media 33, 155-171.

visco_swSpivey - calculates the dynamic viscosity of seawater at elevated pressure, temperature, and salinity

Usage: eta = visco_swSpivey(p,T,S)

Input parameters (scalars or vectors):
p - pressure [MPa] (0 < p < 200)
T - temperature [degC] (0 < T < 275)
S - practical salinity (0 < S < 290)

Output parameter:
eta - dynamic viscosity [Pa*s]

References:
Spivey & McCain (2004) J.Can.Petrol.Tech. 43, 52-61.
Kestin et al. (1978) J.Chem.Eng.Data 23, 328-336.

visco_swMao - calculates the dynamic viscosity of seawater at elevated (pressure), temperature, and salinity based on a parametric equation

Usage: eta = visco_swMao(p,T,S)

Input parameters (scalars or vectors):
p - pressure [MPa] (0.1 < p < 100)
T - temperature [degC] (0 < T < 350)
S - practical salinity (0 < S < 300)

Output parameter:
eta - dynamic viscosity [Pa*s]

References:
Mao & Duan (2009) Int.J.Thermophys. 30, 1510-1523.

visco_swPalliser - calculates the dynamic viscosity of NaCl as function of pressure temperature and salinity based on a parametric equation.
The equations were fit to few available experimental data and include several assumptions and extrapolations. The accuracy might be limited, but no other paper on viscosity of brine in the supercritical region could be found.

Usage: eta = visco_swPalliser(p,T,S)

Input parameters (scalars or vectors):
p - pressure [MPa] (0.1 < p < ?)
T - temperature [degC] (0.1 < T < 727)
S - practical salinity (0 < S < 1000(?))

Output parameter:
eta - dynamic viscosity [Pa*s]

References:
Palliser & McKibbin (1998) Transport in Porous Media 33, 155-171.

visco_co2sw - calculates the dynamic viscosity of CO2-seawater solutions

Usage: eta = visco_co2_sw(p,T,S)

Input parameters
scalars or vectors:
p - pressure [MPa] (10 < p < 20)
T - temperature [degC] (20 < T < 60)
S - practical salinity
scalar or matrix of size p x T x S
mco2 - molality of CO2 in solution [mol/kg] (CO2 saturation is assumed if no value is provided)

Output parameter:
eta - dynamic viscosity [Pa*s]

References:
Bando et al. (2004) J. Chem. Eng. Data 49, 1328-1332.

Comments:
The valid parameter range is very restricted (p=10-20 MPa, T=30-60 degC, NaCl mass fractions of 0-0.03 and mole fractions of CO2 < 0.02), hence exclusion of pTS values outside this range is not feasible.
Experimental data of Kumagi & Yokoyama (1998) (Int.J.Thermophys. 19, 1315-1323) show a deviation of up to 10% for temperatures of 0-5 degC compared to values calculated with this script.

E.7. Thermal Properties

heatcap_ch4gh - calculates the heat capacity of CH4 hydrate

Usage: cp = heatcap_ch4gh(T)

Input parameter (scalar or vector):
T - temperature [degC] (-25 < T < 11)

Output parameter:
cp - heat capacity of methane hydrate [J/kg/K]

The heat capacity of methane hydrate is calculated from an empirical equation as function of temperature. The effect of pressure is assumed negligible (see e.g. the heat capacity of ice tabulated in Feistel & Wagner(2006) J.Phys.Chem.Ref.Data 35, 1021–1047.
Heat capacities for hydrates and ice are generally believed to be similar in values.

References:
Gupta (2007) PhD thesis, Colorado School of Mines.

Comments:
The calculated values seem to deviate from the experimental values of Gupta for temperatures above 11 degC.

heatcond_ch4 - calculates the thermal conductivity of pure CH4

The thermal conductivity of methane is calculated from a multi-parametric equation, including real gas effects.

Usage: lambda = heatcond_ch4(p,T)

Input parameters (scalars or vectors):
p - pressure [MPa] (0 < p < 50)
T - temperature [degC] (-5 < T < 227)

Output parameter:
lambda - thermal conductivity of CH4 [W/m/K]

References:
Hanley et al. (1977) J.Phys.Chem.Ref.Data 6, 597-609.

Comments:
The critical term delta_lambda_c is not specified in the paper and is therefore missing in the calculation of this script.
The error is largest close to the critical point of methane and is about 1-2% at temperatures above -5 degC. This error is not much larger then the error of the equation itself. As a consequence, the valid parameter range, that originally spanned the temperature range from -178 to 227 degC, was restricted.

heatcond_co2 - calculates the thermal conductivity of CO2 from a multiparameter equation

Usage: lambda = heatcond_co2(p,T)

Input parameters (scalars or vectors):
p - pressure [MPa] (0.1 < p < 200)
T - temperature [degC] (-48 < T < 727)

Output parameter:
lambda - thermal conductivity [W/m/K]

References:
Scalabrin et al. (2006) J.Phys.Chem.Ref.Data 35, 1549-1575.

heatcond_n2 - calculates the thermal conductivity of N2 from a multiparametric equation

Usage: lambda = heatcond_n2(p,T)

Input parameters (scalars or vectors):
p - pressure [MPa] (0.1 < p < 100),
T - temperature [degC] (-120 < T < 727)

Output parameter:
lambda - thermal conductivity [W/m/K]

References:
Lemmon & Jacobsen (2004) Int.J.Thermophys 25(1), 21-69.

heatcond_sw - calculates the thermal conductivity of seawater from a multiparameter equation

Usage: lambda = heatcond_sw(p,T,S)

Input parameters (scalars or vectors):
p - pressure [MPa] (0 < p < 140)
T - temperature [degC] (0 < T < 60)
S - practical salinity (0 < S < 45)

Output parameter:
lambda - thermal conductivity [W/m/K]

Reference:
Caldwell (1974) Deep Sea Research 21, 131-137.

Comments:
The estimated accuracy for the equation is 0-5%.
The authors recommend their equation for salinities from 25-45, but the calculated values for pure water are well within the accuracy.
pure water @ 1 bar / 20 degC:
lambda_calc = 0.604 [W/m/K]
lambda_ref = 0.598 [W/m/K] (tabulated reference value)

E.8. Diffusion Coefficients

diffcoeff_h2oco2 - calculates the diffusion coefficients of water molecules dissolved in liquid CO2

Usage: D = diffcoeff_h2oco2(P,T)

Input parameters (p,T: scalars or vectors):
p - pressure [MPa] (13.2 < P < 29.8)
T - temperature [degC] (10 < T < 35)

Output parameter:
D - diffusion coefficient [m^2/s]
References:
Xu et al. (2003) J. Phys. Chem. A 107, 1-3.

Comments:
The empirical function for the diffusion coefficient was derived by a fit of the data published by Xu et al. (2003). It is based on the form [D = (a + bT)*mu_0/mu] with an addiditional presure-dependent term. The parameter range specified above corresponds to the parameter range of the experimental data.

diffcoeff_sw - calculates the diffusion coefficients of dissolved species (ions, gases, etc.) in seawater or seawater with dissolved CO2

The correction for CO2-rich seawater is implemented via the respective viscosity. No validation by experimental data exists.

Usage: D = diffcoeff_sw(p,T,S,'species',mco2)

Input parameters (p,T,S: scalars or vectors, species: string,
mco2: scalar or matrix of size p x T x S):
p - pressure [MPa]
T - temperature [degC]

S - practical salinity
mco2 - molality of dissolved CO2 [mol/kg] (default: mco2=0)
'species'- choice of chemical substance for which the diffusion coefficient is calculated:

1	O2	'o2'
2	NO3-	'no3'
3	Mn2+	'mn'
4	Fe2+	'fe'
5	SO42-	'so4'
6	CH4	'ch4'
7	HS-	'hs'
8	H2S	'h2s'
9	NH4+	'nh4'
10	NH3	'nh3'
11	PO43-	'po4'
12	HPO42-	'hpo4'
13	H2PO4-	'h2po4'
14	H3PO4	'h3po4'
15	H2O	'h2o'
16	H+	'hp'
17	OH-	'oh'
18	CO2	'co2'
19	HCO3-	'hco3'
20	CO32-	'co3'
21	B(OH)3	'boh3'
22	B(OH)4-	'boh4'
23	Mg2+	'mg'
24	Ca2+	'ca'
25	Ba2+	'ba'
26	Sr2+	'sr'
27	Cl-	'cl'
28	Br-	'br'
29	Li+	'li'
30	SiO44-	'sio4'
31	He	'he'
32	Ne	'ne'
33	Ar	'ar'
34	Kr	'kr'
35	Xe	'xe'
36	Rn	'rn'
37	N2	'n2'

Output parameter:
D - diffusion coefficient [m^2/s]

References:
Li & Gregory (1974) GCA 38, 703-714.
Hayduk & Laudie (1974) Amer.Inst.Chem.Eng.J. 20(3), 611-615.
Boudreau (1997) Diagenetic Models and Their Implementation, Springer Verlag.

E.9. Acid-Base and Mineral Equilibria

kco2_sw - calculates the equilibrium constants of the carbonic acid system at high CO2 concentrations

Usage: keq = kco2_sw(p,T,S,species,mco2)

Input parameters (p,T,S:scalars or vectors, species: string,

mco2: scalar or matrix of size p x T x S):
p - pressure [MPa] (0.1-100)
T - temperature [degC] (0-45)
S - practical salinity (0-45)
mco2 - concentration of dissolved CO2 [mol/kg]
species - choice of chemical substance for which the equilibrium constant is calculated:

1 'co2' CO2 + H2O <--> H+ + HCO3- [mol/kg]
2 'hco3' HCO3- <--> H+ + CO32- [mol/kg]
3 'h2o' H20 <--> H+ + OH- [(mol/kg)^2]
4 'so4' HSO4- <--> H+ + SO4-- [mol/kg]
5 'hf' HF <--> H+ + F- [mol/kg]

Output parameter:
keq - equilibrium constant [mol/kg] or [mol/kg^2]

Default: Default value for mco2 is saturation concentration

References:
Wong et al. (2005), J. Chem. Eng. Data 50, 822-831.
Tishchenko, personal communication. (for kw)

kequilib_sw - calculates the stoichiometric equilibrium constants of various equilibrium reactions in seawater
The constants are calculated with respect to seawater pH scale.
The constants assume concentrations in molality.

Usage: keq = kequilib_sw(P,T,S,'species')

Input parameters (scalars or vectors):
p - pressure [MPa] (0.1-100 MPa),
T - temperature [degC] (0-45 ℃)
S - salinity [g/kg] (0-45 g/kg)
'species' - choice of the chemical substance for which the equilibrium constant is calculated:

1 'h2o' H2O <--> H+ + OH-
2 'co2' CO2 + H2O <--> H+ + HCO3-
3 'hco3' HCO3- <--> H+ + CO32-
4 'boh4' [B(OH)4]- <--> H+ + B(OH)3
5 'h3po4' H3PO4 <--> H+ + H2PO4-
6 'h2po4' H2PO4- <--> H+ + HPO42-
7 'hpo4' HPO42- <--> H+ + PO43-
8 'hno3' HNO3 <--> H+ + NO3-
9 'nh4' NH4+ <--> H+ + NH3
10 'h2s' H2S <--> H+ + HS-
11 'arag' aragonite: CaCO3 <--> Ca2+ + CO32-
12 'calc' calcite: CaCO3 <--> Ca2+ + CO32-
13 'mnco3' MnCO3 <--> Mn2+ + CO32-
14 'feco3' FeCO3 <--> Fe2+ + CO32-
15 'baso4' barite: BaSO4 <--> Ba2+ + SO42-
16 'srso4' celestite: SrSO4 <--> Sr2+ + SO42-
17 'so4' HSO4- <--> H+ + SO4--
18 'hf' HF <--> H+ + F-
19 'sio2' H4SiO4 <--> H+ + H3SiO4-

Output parameter:
keq - equilibrium constant [mol/kg(H2O)] or [(mol/kg(H2O))^2]

References:
Boudreau (1996) Computers & Geosciences 22, 479-496.

Clegg & Whitfield (1995) GCA 59(12), 2403-2421.
Fofonoff & Millard (1983) UNESCO Technical Paper in Marine Science 44.
Luff et al. (2001) Computers & Geosciences 27, 157-169.
Millero (1983) In: Ripley & Chester (eds.) Chemical Oceanography Vol.8, Academic Press, p.1-88.
Millero (1995) GCA 59(4), 661-677.
Millero et al. (2006) Mar. Chem. 100, 80-94.
Millero (2007) Chem. Rev. 107, 308-341.
Stumm & Morgan (1996) Aquatic Chemistry, Wiley&Sons.
Van Cappellen & Wang (1996) Amer. J. Sci. 296, 197-243.
Zeebe & Wolf-Gladrow (2001) CO2 in seawater: Equilibrium, kinetics, isotopes, Elsevier.

ph_analyt - calculates the pH of seawater and the equilibrium concentrations of the species H+, CO2, HCO3-, CO32-, B(OH)4-, B(OH)3, H2S, and HS- based on their total concentrations (DIC, TBOH4, TH2S) and the total alkalinity TALK.

The concentrations of dissolved ammonium, phosphate, silicate, sulfate, and fluoride species are only calculated from this pH. To assess their influence on the pH compare with the numerical result from the routine PH_MODEL.

Usage: [eqsys] = ph_analyt(p,T,S,TA,DIC,TBOH4,TH2S,TNH4,TPO4,TSi,TSO4,TF)

Input parameters (scalars only):
- p - pressure [MPa],
- T - temperature [degC]
- S - salinity [g/kg]
- TALK - total alkalinity [eq/kg]
- DIC - total dissolved inorganic carbon [mol/kg]
- TB - total dissolved bor [mol/kg]
- TH2S - total dissolved sulfide [mol/kg]
- TNH4 - total dissolved ammonium [mol/kg]
- TPO4 - total dissolved phosphate [mol/kg]
- TSi - total dissolved silicate [mol/kg]
- TSO4 - total dissolved sulfate [mol/kg]
- TF - total dissolved fluoride [mol/kg]

Output parameter:
- eqsys - structure array of pH and species equilibrium concentrations [mol/kg]
  of the form ('name1',value1,'name2',value2,...)

The analytical solution for the pH is based on the mass action laws of:

$CO_2 + H_2O \leftrightarrow H^+ + HCO_3^-$ $K_{c1} = H * HCO_3 / CO_2$

$HCO_3^- \leftrightarrow H^+ + CO_3^{2-}$ $K_{c2} = H * CO_3 / HCO_3$

$B(OH)_3 + H_2O \leftrightarrow H^+ + B(OH)_4^-$ $K_b = H * BOH_4 / BOH_3$

$H_2S \leftrightarrow H^+ + HS^-$ $K_s = H * HS / H_2S$

and the corresponding equations for alkalinity and mass conservation:

$TALK = HCO_3 + 2*CO_3 + BOH_4 + HS$

$DIC = CO_2 + HCO_3 + CO_3$

$TBOH_4 = BOH_4 + BOH_3$

$TH_2S = H_2S + HS$

The definition of TALK is a simplified form only considering the major contributing species that allows for analytical solutions.

Equilibrium constants are calculated with KEQUILIB_SW and if the CO2 concentration exceeds 0.01 mol/kg KCO2_SW is used.

Note: The analytical solution of the 4th order polynomial produces complex conjugate results and thus is solved using FZERO of MATLAB.
The analytical solution of the cubic or quadratic polynomials, i.e. for TBOH4 = 0 and/or TH2S = 0, are solved according to the recipe given in Bronstein & Semendjajew (1989) Taschenbuch der Mathematik.

Further speciations are calculated from:

H2O <--> H+ + OH-	Kw = H * OH
NH4+ <--> H+ + NH3	Kn = H * NH3 / NH4
H3PO4 <--> H+ + H2PO4-	Kp1 = H * H2PO4 / H3PO4
H2PO4- <--> H+ + HPO42-	Kp2 = H * HPO4 / H2PO4
HPO42- <--> H+ + PO43-	Kp3 = H * PO4 / HPO4
H4SiO4 <--> H+ + H3SiO4-	Ksi = H * H3SiO4 / H4SiO4
HSO4- <--> H+ + SO42-	Kso = H * SO4 / HSO4
HF <--> H+ + F-	Kf = H * F / HF

TNH4 = NH4 + NH3
TPO4 = H3PO4 + H2PO4 + HPO4 + PO4
TSi = H4SiO4 + H3SiO4
TSO4 = HSO4 + SO4
TF = HF + F

ph_model - calculates the pH and equilibrium concentrations of the acid-base species in seawater as well as their total concentrations and the total alkalinity.

Usage: eqsys = ph_model(p,T,S,'species1',conc1,'species2',conc2,...)

Input parameters (scalars):
- p - pressure [MPa],
- T - temperature [degC]
- S - salinity [g/kg]
- 'species' - input species name
- conc - species concentrations [mol/kg]

Output parameter:
- eqsys - structure array of pH and species equilibrium concentrations [mol/kg] of the form ('species1',conc1,'species2',conc2,...)

To allow for good solver performance it is desirable to provide one species out of each of the following groups, respectively conservation equations:
'pH','H','OH','TAlk'
'DIC','CO2','HCO3','CO3'
'TBOH4','BOH4','BOH3'
'TH2S','H2S','HS'
'TNH4','NH4','NH3',
'TPO4','H3PO4','H2PO4','HPO4','PO4'
'TSi','H4SiO4','H3SiO3'
'TSO4','HSO4','SO4'
'TF','HF','F'
Note: The above spelling of species names must be used for the input.

To exclude a group of species from the pH calculation the respective total concentration, i.e. DIC, TBOH4, TH2S, TNH4, TPO4, TSi, TSO4, TF, must be set explicitely to zero, e.g. 'TF',0.
Default values set for unspecified species groups are:
TA = 2.3e-3 eq/kg; DIC = 2.0e-3 mol/kg
TBOH4, TSO4, TF are calculated from salinity using the function SEASALT
TH2S, TNH4, TPO4, TSi are set to zero

Depending on the supplied input array the 21 equations solved are:
a) 12 mass-action laws

0 = Kw - H * OH	H2O <--> H+ + OH-
0 = Kc1 * CO2 - H * HCO3	CO2 + H2O <--> H+ + HCO3-
0 = Kc2 * HCO3 - H * CO3	HCO3- <--> H+ + CO32-
0 = Kb * BOH3 - H * BOH4	B(OH)3 + H2O <--> H+ + B(OH)4-
0 = Ks * H2S - H * HS	H2S <--> H+ + HS-
0 = Kn * NH4 - H * NH3	NH4+ <--> H+ + NH3
0 = Kp1 * H3PO4 - H * H2PO4	H3PO4 <--> H+ + H2PO4-
0 = Kp2 * H2PO4 - H * HPO4	H2PO4- <--> H+ + HPO42-
0 = Kp3 * HPO4 - H * PO4	HPO42- <--> H+ + PO43-
0 = Ksi * H4SiO4 - H * H3SiO4	H4SiO4 <--> H+ + H3SiO4-
0 = Kso * HSO4 - H * SO4	HSO4- <--> H+ + SO42-
0 = Kf * HF - H * F	HF <--> H+ + F-

b) 8 mass conservation and 1 alkalinity conservation equation

```
0 = TALK - HCO3 - 2*CO3 - BOH4 - HS - NH3 - HPO4 - 2*PO4 - H3SiO4
      - OH + H + H3PO4 + HSO4 + HF
0 = DIC - CO2 - HCO3 - CO3
0 = TBOH4 - BOH4 - BOH3
0 = TH2S - H2S - HS
0 = TNH4 - NH4 - NH3
0 = TPO4 - H3PO4 - H2PO4 - HPO4 - PO4
0 = TSi - H4SiO4 - H3SiO4
0 = TSO4 - HSO4 - SO4
0 = TF - HF - F
```

The definition of TALK follows that of Dickson (1981) DSR 28A, 609–623.
See also discussion in Wolf-Gladrow et al. (2007) Mar.Chem.106, 287-300.
Equilibrium constants are calculated with KEQUILIB_SW and if the CO2 concentration exceeds 0.01 mol/kg KCO2_SW is used.

E.10. Unit Conversions

cl2salin - calculates seawater salinity based on known Cl concentration

Usage: S = cl2salin(mCl)

Input parameters (scalar,vector or matrix):
mCl - chloride concentration in seawater [mol/kg]

Output parameter:
S - practical salinity

Comments:
This script takes the true Cl-ion concentration as input.
To calculate practical salinity from chlorinity use: S = Cl*1.80655

molal2molar_sw - converts solute concentration in molalities [mol/kg] into molarities [mol/l] for standard seawater composition

usage: c = molal2molar_sw(p,T,S,m)

Input parameters (scalars or vectors):
p - pressure [MPa]
T - temperature [degC]

S - practical salinity
m - molal concentration of salt component [mol/kg]

Output parameter:
c - molar concentration of salt component [mol/l]

molar2molal_sw - converts solute concentration in molarities [mol/l] into molalities [mol/kg] for standard seawater composition

Usage: m = molar2molal_sw(p,T,S,c)

Input parameters (scalars or vectors):
p - pressure [MPa]
T - temperature [degC]
S - practical salinity
c - molar concentration of salt component [mol/l]

Output parameter:
m - molal concentration of salt component [mol/kg]

mkgh2o2mkgsol - converts equilibrium constants or concentrations from mol/kg{H2O} to mol/kg{solution}

Usage: k2 = mkgh2o2mkgsol(k1,S)

Input parameters (scalars, vectors or matrices of SAME size):
k1 - equlilibrium constant or concentration [mol/kg{H2O}]
S - practical salinity

Output parameter:
k2 - equlilibrium constant or concentration [mol/kg{solution}]

mkgsol2mkgh2o - converts equilibrium constants or concentrations from mol/kg{solution} to mol/kg{H2O}

Usage: k1 = mkgsol2mkgh2o(k2,S)
Input parameters (scalars, vectors or matrices of SAME size):
k2 - equlilibrium constant or concentration [mol/kg{solution}]
S - practical salinity

Output parameter:
k1 - equlilibrium constant or concentration [mol/kg{H2O}]

mol2pp_ch4 - calculates the partial pressure of CH4 for a given CH4 concentration in aqueous solution using Henry's law.
The Henry constant for CH4 gas in water is calculated as a function of pressure, temperature and salinity from a multiparametric equation.

Usage: pp = mol2pp_ch4(p,T,S,m)

Input parameters (p,T,S: scalars or vectors; m: scalar/matrix of size P x T x S):
p - pressure [MPa] (0.1 < p < 200)
T - temperature [degC] (0 < T < 250)
S - practical salinity (S < 350)
m - molal concentration of CH4 [mol/kg]

Output parameter:
pp - partial pressure of CH4 [MPa]

References:
Harvey (1996) AIChE 42, 1491-1494.
Wagner & Pruss (2002) J.Phys.Chem.Ref.Data 31, 387-535. (water vapor pressure)
Plyasunov et al. (2000) GCA 64, 2779-2795. (Poynting-pressure correction)
Duan & Sun (2003) Chem. Geol. 193, 257-271. (Pitzer-type salinity correction)

Comments:
No interactions with molecules other than CH4 in the gas phase are considered, because no reliable interaction parameters were found.
Change of phase boundary with pressure is not considered in calculation of partial molar volume.

mol2pp_co2 - calculates the partial pressure of CO2 for a given CO2 concentration in aqueous solution using Henry's law
The Henry constant for CO2 gas in water is calculated as a function of pressure, temperature and salinity from a multiparametric equation.

Usage: pp = mol2pp_co2((p,T,S,m)

Input parameters (p,T,S: scalars or vectors; m: scalar/matrix of size(p x T x S)):
p - pressure [MPa] (0.1 < p < 35 or gas/liquid phase boundary)
T - temperature [degC] (0 < T < 162)
S - practical salinity (S < 263)
m - molal concentration of CO2 [mol/kg]

Output parameter:
pp - partial pressure of CO2 [MPa]

References:
Harvey (1996) AIChE 42, 1491-1494.
Wagner & Pruss (2002) J.Phys.Chem.Ref.Data 31, 387-535. (water vapor pressure)
Plyasunov et al. (2000) GCA 64, 2779-2795. (Poynting-pressure correction)
Duan & Sun (2003) Chem. Geol. 193, 257-271. (Pitzer-type salinity correction)

Comments:
No interactions with molecules other than CO2 in the gas phase are considered, because no reliable interaction parameters were found.
Change of phase boundary with pressure is not considered in calculation of partial molar volume.

mol2pp_h2s - calculates the partial pressure of H2S for a given H2S concentration in aqueous solution using Henry's law
The Henry constant for CO2 gas in water is calculated as a function of pressure, temperature and salinity from a multiparametric equation.

Usage: pp = mol2pp_h2s(p,T,S,m)

Input parameters (p,T,S: scalars or vectors; m: scalar/matrix of size P x T x S):
p - pressure [MPa] (0.1 < p < 20)
T - temperature [degC] (0 < T < 127)
S - practical salinity (0 < S < 350)
m - molal concentration of H2S [mol/kg]

Output parameter:
pp - partial pressure of H2S [MPa]

mol2pp_n2 - calculates the partial pressure of N2 for a given N2 concentration in aqueous solution using Henry's law
The Henry constant for CO2 gas in water is calculated as a function of pressure, temperature and salinity from a multiparametric equation.

Usage: pp = mol2pp_n2(p,T,S,m)

Input parameters (p,T,S: scalars or vectors; m: scalar/matrix of size P x T x S):
p - pressure [MPa] (0.1 < p < 35)
T - temperature [degC] (0 < T < 317)
S - practical salinity (S < 350)
m - molal concentration of N2 [mol/kg]

Output parameter:
pp - partial pressure of N2 [MPa]

mol2pp_o2 - calculates the partial pressure of O2 for a given O2 concentration in aqueous solution using Henry's law
The Henry constant for CO2 gas in water is calculated as a function of pressure, temperature and salinity from a multiparametric equation.

Usage: pp = mol2pp_o2(p,T,S,m)

Input parameters (p,T,S: scalars or vectors; m: scalar/matrix of size P x T x S):
p - pressure [MPa] (0.1 < P <20)
T - temperature [degC] (0 < T < 127)
S - practical salinity (0 < S < 350)
m - molal concentration of O2 [mol/kg]

Output parameter:
pp - partial pressure of O2 [MPa]

pp2pv_ch4 - converts the partial pressure of CH4 in a gas mixture into partial volume

Usage: pv = pp2pv_ch4(p,T,pp)

Input parameter (p, T: scalars or vectors; pp: scalar or vector of same size as p):
p - overall pressure [MPa] (0.012 < p < 1000)
T - temperature [degC] (-183 < T < 347)
pp - partial pressure of CH4 [MPa] (0 < pp < p)

Output parameter:
pv - partial volume of CH4 [ppmV]

pp2pv_co2 - converts the partial pressure of CO2 in a gas mixture into partial volume

Usage: pv = pp2pv_co2(p,T,pp)

Input parameter (p,T: scalars or vectors; pp: scalar or vector of same size as p):
p - overall pressure [MPa] (0.1 < p < 800)
T - temperature [degC] (-57 < T < 827)
pp - partial pressure of CO2 [MPa] (0 < pp < p)

Output parameter:
pv - partial volume of CO2 [ppmV]

Comments:
Equations are only valid for pressures below the vapor pressure of CO2.

pp2pv_h2s - converts the partial pressure of H2S in a gas mixture into partial volume

Usage: pv = pp2pv_h2s(p,T,pp)

Input parameter (p, T: scalars or vectors; pch2s: scalar or vector of same size as p):
p - overall pressure [MPa] (0.1 < p < 35)
T - temperature [degC] (0 < T < 137.7)
pp - partial pressure of H2S [MPa] (0 < pp < p)

Output parameter:
pv - partial volume of H2S [ppmV]

Comments:
Equations are only valid for pressures below the vapor pressure of H2S.

pp2pv_n2 - converts the partial pressure of N2 in a gas mixture into partial volume

Usage: pv = pp2pv_n2(p,T,pp)

Input parameter (p, T: scalars or vectors; pp: scalar or vector of same size as p):
p - overall pressure [MPa] (0 < p < 1000)
T - temperature [degC] (-73 < T < 727)
pp - partial pressure of N2 [MPa] (0 < pp < p)

Output parameter:
pv - partial volume of N2 [ppmV]

pp2pv_o2 - converts the partial pressure of O2 in a gas mixture into partial volume

Usage: pv = pp2pv_o2(p,T,pp)

Input parameter (p, T: scalars or vectors; pco2: scalar or vector of same size as p):
p - overall pressure [MPa] (0 < p < 81.8)
T - temperature [degC] (-219 < T < 127)
pp - partial pressure of O2 [MPa] (0 < pp < p)

Output parameter:
pv - partial volume of O2 [ppmV]

E.11. Auxiliary Functions

i_sw - calculates the ionic strength of seawater I = 0.5*sum(m_i*z_i^2)

Usage: I = i_sw(S)

Input parameter (scalars or vectors):
S - practical salinity

Output parameter:
I - ionic strength [mol/kg]

Comments:
For contribution of total borate (mTBOh4) and dissolved inorganic carbon (DIC) to the ionic strength, the composition at a pH of ~8 is assumed, where B(OH)4- is ~50% of the total borate, HCO3- is ~90% of the DIC and CO32- is ~5% of the DIC.

permeab - derives the permeability of the sediment from the porosity and the grain size

Usage: k = permeab(po,dp,'method')

Input parameters (poros, dp: scalars or vectors, method: string of SAME size):
po - porosity
dp - mean particle diameter [m]
'method' - choice of empirical relationship between porosity and permeability to be used.
The following 'methods' are included:
'ck' Carman-Kozeny: k= dp^2/180*(po^3/(1-po)^2))
'bk' Blake-Kozeny: k= dp^2/150*(po^3/(1-po)^2))
'rg' Rumpf-Gupte: k= dp^2*po^5.5/5.6
'hc' Hsu-Cheng: k= dp^2*po^2/(18*(1-po))
'bhc' blended H-C: k= dp^2*po^3/(180*(1-po)^2)*(1-exp(-10*(1-po)/po))

Output parameter:
k - permeability [m^2]

Default values:
A value for porosity has to be provided. The default value for dp is 1*10^(-6) m (the particle size in mud) and the default method is the blended Hsu-Cheng formula.

References:
Boudreau (1997) Diagenetic Models and Their Implementation, Springer Verlag.

seasalt - calculates the major salt concentrations in seawater based on its salinity

Usage: [mNa,mMg,mCa,mK,mSr,mLi,mCl,mBr,mF,mSO4,mTBOH4,mDIC,mOH] = seasalt(S)

Input parameters (scalar, vector or matrix):
S - practical salinity of seawater (absolute salinity = S*1.005 [g/kg])

Output parameters:
mI - molality of salt component I [mol/kg]

References:
Millero (2008) Deep-Sea Research I 55, 50–72.
Stoffyn-Egly & MacKenzie (1984) GCA 48, 859-872.

seasalt_molarity - calculates the major salt concentrations in seawater based on its salinity and density (which is also a function of pressure and temperature)

Usage: [cNa,cMg,cCa,cK,cSr,cLi,cCl,cBr,cF,cSO4,cTBOH4,cDIC,cOH] = seasalt_molarity(p,T,S)

Input parameters (scalar, vector or matrix):

p - pressure [MPa]
T - temeperature [degC]
S - practical salinity of seawater (absolute salinity = S*1.005 [g/kg])

Output parameters:
cl - molarity of salt component I [mol/l]

References:
Millero (2008) Deep-Sea Research I 55, 50–72.
Stoffyn-Egly & MacKenzie (1984) GCA 48, 859-872.

tortuos - calculates the tortuosity correction (to)^2 for diffusion coefficients in sediments
Ds = D0 / (to)^2 where D0 = molecular diffusion coefficient
to = tortuosity

Usage: tort2 = tortuos(poros,'method',aa)

Input parameters:
poros - porosity (scalar or vector)
aa - fitting parameter for equations (scalar)
recommended values are:
'wb': aa = 2.02
'ar': aa = 2.14
'bf': aa = 3.79
'method' - determines the empirical relationship between porosity and tortuosity to be used.
'bb' Boudreau: to^2 = 1-2*log(poros)
'wb' modified Weissberg: to^2 = 1-a*log(poros)
'ar' Archie: to^2 = poros^(1-a)
'bf' Buerger-Friecke: to^2 = poros+a*(1-poros)

Output parameter:
tort2 - squared tortuosity

Default values:
Porosity has to be provided at function call.
Default for aa is 0 and default for method is 'bb'.

References:
Boudreau (1997) Diagenetic Models and Their Implementation, Springer Verlag.

Appendix F: Nomenclature

a	activity
a	interaction parameter in EOS
b	finite molecule size parameter in EOS
c	concentration
c	specific heat capacity
d	diameter
d	half separation distance between bubbles
f	fugacity
g	gravitational acceleration
j	type of guest molecule
k	permeability
k	rate constant
k_B	Boltzmann constant
k_d	mass transfer coefficient
k_S	Setchenov constant
k_{sol}	dissolution rate
m	molarity
m	mass
n	number of moles
p	pressure
r	radius
t	time
u_t	terminal rise velocity
v	fluid advection velocity
v	reaction rate
x	mole fraction
x, y, z	cartesian coordinates
z	valency
z	film thickness

A	Helmholtz free energy
A	area
B_{ij}^{γ}	binary interaction parameters for species i and j
B_n	virial coefficients
C_{ijk}^{γ}	ternary interaction parameters for species i, j and k
C_{mj}	Langmuir constant
C	heat capacity
C_d	drag coefficient
D	diffusion coefficient
D_{eff}	effective diffusion coefficient
DH	Debye-Hückel limiting law
E	energy
F	Faraday constant
G	Gibbs energy
H	enthalpy
J	mass flux
J	nucleation rate
J_q	heat flux
K	equilibrium constant
K	hydraulic conductivity
K_H	Henry's law constant
L	length of shortest path
M	molar mass
P	probability
Q	thermal energy
R	gas constant
R_t	production rate of methane
Re	Reynold's number
S	entropy
T	temperature
U	internal energy
V	volume
V_m	molar volume
Z	compressibility factor

Greek characters

γ	activity coefficient
η	dynamic viscosity
θ	tortuosity
Θ	cage occupancy
κ	compressibility
λ	thermal conductivity
$\lambda_{Na/c}$	binary interaction parameter
Λ	equivalent ion conductivity
μ	chemical potential
v_m	number of cages of type m per water molecule in the hydrate lattice
v	kinematic viscosity
v_i	stoichiometric coefficient
ξ_{Nac}	tertiary interaction parameter
ρ	density
σ	surface tension
φ	particle size distribution
Φ	fugacity coefficient
Φ	porosity

superscripts

0	reference state
bub	bubble
bulk	bulk phase (water with dissolved gas)
DBL	diffusive boundary layer
drop	droplet
eq	equilibrium
g, G	vapour phase
h, H, hyd	hydrate phase
if	gas-liquid interface
l, L	liquid phase
n	hydration number
p	(gas hydrate) particle
pw	pore water
sfc	surface energy
v_i	stoichiometric coefficient

subscripts

0	reference state
3	gas hydrate liquid 3 phase boundary
a	anion
A	activation
B	gas hydrate formation
c	cation
C	carbon dioxide
CSW	seawater with carbon dioxide
d	diffusion
dis	dissociation
diss	dissolution
F	formation
i,j,k	gas species, component
ind	induction
L	pore fluid
m	type of hydrate cage (large or small)
m	molar
min	mineral
MH	methane hydrate
N	neutral species
p	particle
p	constant pressure
PF	pore fluid
r	reaction
sat	saturation
sol	solution, dissolution
S	sediment matrix
SW	seawater
v	vaporization
v	void
v	constant volume
vap	vaporization
W	water
β	hypothetical empty hydrate lattice
∞	infinite dilution

GEOMAR
Helmholtz-Zentrum für Ozeanforschung Kiel

GEOMAR Reports

No.	Title
1	FS POSEIDON Fahrtbericht / Cruise Report POS421, 08. – 18.11.2011, Kiel - Las Palmas, Ed.: T.J. Müller, 26 pp, DOI: 10.3289/GEOMAR_REP_NS_1_2012
2	Nitrous Oxide Time Series Measurements off Peru – A Collaboration between SFB 754 and IMARPE –, Annual Report 2011, Eds.: Baustian, T., M. Graco, H.W. Bange, G. Flores, J. Ledesma, M. Sarmiento, V. Leon, C. Robles, O. Moron, 20 pp, DOI: 10.3289/GEOMAR_REP_NS_2_2012
3	FS POSEIDON Fahrtbericht / Cruise Report POS427 – Fluid emissions from mud volcanoes, cold seeps and fluid circulation at the Don-_Kuban deep sea fan (Kerch peninsula, Crimea, Black Sea) – 23.02. – 19.03.2012, Burgas, Bulgaria - Heraklion, Greece, Ed.: J. Bialas, 32 pp, DOI: 10.3289/GEOMAR_REP_NS_3_2012
4	RV CELTIC EXPLORER EUROFLEETS Cruise Report, CE12010 – ECO2@NorthSea, 20.07. – 06.08.2012, Bremerhaven – Hamburg, Eds.: P. Linke et al., 65 pp, DOI: 10.3289/GEOMAR_REP_NS_4_2012
5	RV PELAGIA Fahrtbericht / Cruise Report 64PE350/64PE351 – JEDDAH-TRANSECT -, 08.03. – 05.04.2012, Jeddah – Jeddah, 06.04 - 22.04.2012, Jeddah – Duba, Eds.: M. Schmidt, R. Al-Farawati, A. Al-Aidaroos, B. Kurten and the shipboard scientific party, 154 pp, DOI: 10.3289/GEOMAR_REP_NS_5_2013
6	RV SONNE Fahrtbericht / Cruise Report SO225 - MANIHIKI II Leg 2 The Manihiki Plateau - Origin, Structure and Effects of Oceanic Plateaus and Pleistocene Dynamic of the West Pacific Warm Water Pool, 19.11.2012 - 06.01.2013 Suva / Fiji – Auckland / New Zealand, Eds.: R. Werner, D. Nürnberg, and F. Hauff and the shipboard scientific party, 176 pp, DOI: 10.3289/GEOMAR_REP_NS_6_2013
7	RV SONNE Fahrtbericht / Cruise Report SO226 – CHRIMP CHatham RIse Methane Pockmarks, 07.01. - 06.02.2013 / Auckland – Lyttleton & 07.02. – 01.03.2013 / Lyttleton – Wellington, Eds.: Jörg Bialas / Ingo Klaucke / Jasmin Mögeltönder, 126 pp, DOI: 10.3289/GEOMAR_REP_NS_7_2013

For GEOMAR Reports, please visit:
https://oceanrep.geomar.de/view/series/GEOMAR_Report.html

Reports of the former IFM-GEOMAR series can be found under:
https://oceanrep.geomar.de/view/series/IFM-GEOMAR_Report.html

GEOMAR
Helmholtz-Zentrum für Ozeanforschung Kiel

Das GEOMAR Helmholtz-Zentrum für Ozeanforschung Kiel
ist Mitglied der Helmholtz-Gemeinschaft
Deutscher Forschungszentren e.V.

The GEOMAR Helmholtz Centre for Ocean Research Kiel
is a member of the Helmholtz Association of
German Research Centres

Helmholtz-Zentrum für Ozeanforschung Kiel / Helmholtz Centre for Ocean Research Kiel
GEOMAR
Dienstgebäude Westufer / West Shore Building
Düsternbrooker Weg 20
D-24105 Kiel
Germany

Helmholtz-Zentrum für Ozeanforschung Kiel / Helmholtz Centre for Ocean Research Kiel
GEOMAR
Dienstgebäude Ostufer / East Shore Building
Wischhofstr. 1-3
D-24148 Kiel
Germany

Tel.: +49 431 600-0
Fax: +49 431 600-2805
www.geomar.de